

Ionophoric and Aptameric Recognition-Modulated Electroactive Polyaniline Films for the Determination of Tetrodotoxin



By

Gertrude Fomo

A thesis submitted in fulfilment of the requirements for the degree of

UNIVERSITY of the
WESTERN CAPE

Philosophiae Doctor

In the Department of Chemistry, Faculty of Science

University of the Western Cape

Bellville, Cape Town, South Africa

Supervisor: Prof. Emmanuel Iwuoha

Co-supervisor: Dr. Tesfaye Waryo

December 2014

Abstract

ABSTRACT

Tetrodotoxin (TTX) is a nonpeptidic neurotoxin with a high rate of food poisoning mortality (60%) that has been associated with the consumption of diets from puffer fish and mud snails harbouring TTX-producing bacteria. As this neurotoxin has no known antidote and could not be mitigated by cooking, the only way for safety appears to be the detection of TTX-contaminated fishes at the points of harvest and control. The overall aim of this study was to develop amperometric and impedimetric sensors for TTX based on ionophores and aptamer immobilised on the modified conducting electroactive polyaniline (PANI)/electrode. The undoped polyaniline and poly(4-styrenesulfonic acid) (PSSA) doped electroactive polyanilines were prepared in perchloric acid/acetonitrile and phosphoric acid respectively by electrochemical oxidative polymerisation. Two types of electropolymerisation were applied to prepare the neutral and p-doped PANI–PSSA films composites. The dynamic electroinactivity of TTX was studied which revealed that TTX is not electrochemically active on bare Au, GC, Pt, PG, Ni, Ti and BDD (Boron doped-diamond) electrodes in acetate buffer pH 4.8. Using ion transfer voltammetry and UV-Vis analysis, the complexation of TTX with two neutral ionophores (sodium ionophore X (NaX) and dibenzo-18-crown6 (B18C6)) was investigated. The cyclic voltammograms (CVs) recorded from ion transfer voltammetry presented no redox peak and no increasing/decreasing current was observed which indicates that no TTX ions transfer from the liquid to the organic phase. In addition, the absorption spectra of the mixture of TTX/NaX and TTX/B18C6 presented the same absorption bands recorded for NaX and B18C6 respectively. Three absorptions bands at 250.4, 278.3, and 370.6 nm for NaX and two at 222.03 and 274.10 nm for B18C6 were observed before and after mixing TTX with NaX and TTX with B18C6 separately. No chemical reaction occurred between the TTX and both ionophores, therefore, sodium ionophore X and dibenzo-18-crown-6 did not form

Abstract

a complex with TTX. Thus, TTX ion sensor cannot be developed based on these two neutral compounds. The electrodynamics of the PANI and PANI–PSSA films electropolymerised on the bare precious metal electrodes were also investigated through various electrochemical techniques. Cyclic voltammetry (CV) and electrochemical impedance spectroscopy (EIS) studies in sodium phosphate (SPB) and acetate (OAc) buffer revealed that both neutral and p-doped films synthesized were thin (thickness $L < 5$ nm in acetate buffer and $L < 10$ nm in sodium phosphate buffer) film polymers. In SPB pH 7.04, the CVs of both polymer films presented one redox couple which occurred at separation potentials $\Delta E_p > 200/n$ mV and the ratio $|i_{pa}/i_{pc}|$ was ≈ 1 which indicated a reversible electrode reaction system. In OAc buffer pH 4.8, CVs presented two redox couples which peaked at separation potentials and the ratio of current $|i_{pa(II)}/i_{pc(III)}| \approx 0.9$ for the second redox peak indicating the irreversibility of the reaction occurring at that specific potential. UV-Vis, FL and FTIR studies were used as spectroscopic signatures for the comparison of neutral and p-doped PANI–PSSA conductivity. Scanning electron microscopy (SEM) and transmission electron microscopy (TEM) images revealed an influence of the ending potential for electropolymerisation of the PSSA dope aniline. Biosensors containing p-doped PANI–PSSA were interrogated by CV and/or EIS in OAc buffer medium. P-doped PSSA–PANI/Glutaraldehyde/Aptamer biosensor gave rise to sensors for TTX which obeyed the absorption isotherm of BET (Brunauer Emmett Teller) with an estimated constant of BET c of 1.72 ng ml^{-1} and a concentration of TTX adsorbed by a monolayer of 0.002 ng ml^{-1} . The linear range of the biosensors for TTX detection was $0.06 - 0.74 \text{ ng ml}^{-1}$. The sensitivity of the biosensor for TTX was $226.4 \Omega \text{ ml ng}^{-1}$ and the limit of detection (LOD) was calculated to be 0.12 ng ml^{-1} .

KEYWORDS

Tetrodotoxin

Tetrodotoxin-aptamer

Cyclic voltammetry

Electrochemical impedance spectroscopy

Ionophores sensors

Ion transfer voltammetry

Aptasensor

p-doped and neutral polyaniline



Declaration

DECLARATION

I declare that this work entitled: **Ionophoric and aptameric recognition-modulated electroactive of polyaniline films for the determination of tetrodotoxin** is my own work, that it has not been submitted before for any degree or examination in any other university, and all sources I have used or quoted have been acknowledged as complete references.

Gertrude Fomo

November 2014

Signature.....



Supervisors: Prof. Emmanuel Iwuoha

Signature.....

Dr. Tesfaye Waryo

Signature.....

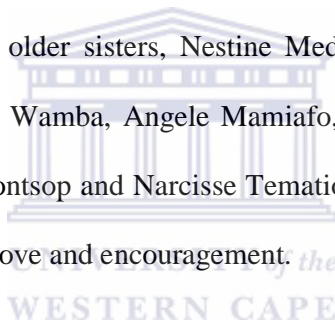
Acknowledgement

ACKNOWLEDGEMENT

I would like to thank the most High Almighty God, for his unconditional love and renewed strength for each day, which enabled me to complete this thesis.

Many thanks go to my supervisors, Professor Emmanuel Iwuoha and Dr. Tesfaye Waryo: indeed grateful for your excellent supervision, unlimited assistance, friendship and encouragement when things became difficult.

To my family, specially my older sisters, Nestine Medieu and Antoine Nkaze, Marie-Pascal Madjieugue and Piere Wamba, Angele Mamiafo, Sylviane Donchi Lemofack and Jean Teken, Linda Yrene Ndontsop and Narcisse Tematio, kwemo Alice sydie and all my nephews and nieces for your love and encouragement.



I also thank Professor Jean Ngoune of the University of Dschang-Cameroon for encouraging me to further my education. It was through your linkage and professional advice that I was motivated to further my studies. Thank you very much Professor.

Thanks a lot also to all my colleagues at the Sensor Research Laboratory and the Chemistry Department at large, for all their support during my stay at UWC. Special thanks also to Dr Chinwe Ikpo, Dr. Fanelwa Ngece, Anne Lutgarde Djoumessi Yonkeu, Sarre Kadia Myra Nzaba, Germaine Kemleu, and Emmanuel Ameh for all their support, friendship and encouragement. Thanks too to Dr. Franscious Cummings of Physics Department, UWC, for assistance with SEM and TEM analysis.

Acknowledgement

Finally, I sincerely thank the National Research Foundation (NRF) of South Africa for awarding me a PhD bursary. To all of you: may the Almighty God, the Creator of heaven and earth, and all that dwell in them, bless you all.



Dedication

DEDICATION

Every challenging work needs self-discipline as well as the guidance of elders, especially those who were very close to our heart.

My humble effort I dedicate to:

*My wonderful mother **Nguemo Marceline***



*My awesome sister **Mekeufouet Eveline***

WESTERN CAPE

*My lovely husband **Ghislain Blaise Voukeng***

Whose affection, love, encouragement and prayers both in the day and night enabled to attain such success and honour, along with all the hard work.

TABLE OF CONTENTS

ABSTRACT	i
KEYWORDS	iv
DECLARATION	v
ACKNOWLEDGEMENT	vi
DEDICATION	viii
TABLE OF CONTENTS	ix
LIST OF ABBREVIATION	xv
LIST OF SYMBOLS	xvii
LIST OF FIGURES	xix
LIST OF TABLES	xxvii
ACADEMIC OUTPUT	xxx
CHAPTER 1: INTRODUCTION	1
1.0 Background of this study	1
1.1 Scope of this study	8
1.2 Objectives of the study	10
1.3 Overview of the thesis	11
CHAPTER 2: ANALYSIS OF TETRODOTOXIN	14
2.0 Introduction	14
2.1 Chemistry of tetrodotoxin	14
2.2 Synthesis of tetrodotoxin	15
2.3 Structure of tetrodotoxin	16
2.4 Chemical reaction of tetrodotoxin	19
2.5 Some physico-chemical properties of tetrodotoxin	20
2.6 Analytical methods of detection of tetrodotoxin	22
2.6.1 Spectroscopy techniques for tetrodotoxin analysis	23
2.6.2 Immunoassay methods for tetrodotoxin analysis	30
2.7 Conclusion	32
CHAPTER 3: DOPED POLYANILINE FILMS ELECTROCHEMICAL ACTIVITIES AND REDOX PROBE APPLICATION	33
3.0 Introduction	33
3.1 Electrochemistry of conducting electroactive thin films polymers	34
3.1.1 Conducting electroactive polymers	34

Table of contents

3.1.2	The concept of doping	38
3.1.3	Polyaniline and its derivatives	40
3.1.4	Synthesis of polyaniline	41
3.2	Molecular recognition elements and their application in sensors and biosensors	48
3.2.1	Neutral ionophore compounds	48
3.2.2	Ionophore exchange kinetics.....	49
3.2.3	Application of ionophores in electrochemical sensors	53
3.2.4	Aptamer biomolecule	54
CHAPTER 4: PRINCIPLE OF SELECTIVE ANALYTICAL TECHNIQUES ...		67
4.0	Introduction	67
4.1	Electrochemical techniques	67
4.1.1	Cyclic voltammetry (CV)	67
4.1.2	Electrochemistry at liquid-liquid interface: theory and application.....	72
4.1.3	Linear sweep or scan voltammetry (LCV) and square waver voltammetry (SWV)	82
4.1.4	Electrochemical impedance spectroscopy (EIS)	85
4.2	Spectroscopy techniques	94
4.2.1	Proto nuclear magnetic resonance (¹ H.NMR) spectroscopy	94
4.2.2	Fourier transform infrared (FTIR) spectroscopy	98
4.2.3	Ultraviolet / Visible (UV/Vis) spectroscopy	105
4.2.4	Fluorescence (FL) spectroscopy.....	113
4.2.5	Atomic force microscopy (AFM)	116
4.3	Conclusion	119
CHAPTER 5: MATERIALS, REAGENTS AND EXPERIMENTAL METHODS.....		120
5.0	Introduction	120
5.1	Reagents and materials.....	120
5.1.1	Reagents	121
5.1.2	Materials.....	122
5.1.3	Ion selective electrode	123
5.2	General electronics instrumentation	123
5.3	Preparation of reagent solutions	124
5.3.1	Preparation of tetrodotoxin solution	124
5.3.2	Preparation of buffer solutions	125
5.3.3	Preparation of liquid phase solution	126

Table of contents

5.3.4	Preparation of organic phase solution	127
5.3.5	Preparation of standard solution	127
5.3.6	Preparation of aptamer solution	128
5.4	Electrodes preconditioned	129
5.5	Electro-inactivity of tetrodotoxin at solid electrodes	130
5.6	Electrokinetics of polymerisation of undoped and doped PANI films in perchloric acid/ acetonitrile.....	130
5.6.1	Electrosynthesis of undoped PANI films in perchloric acid/ acetonitrile	130
5.6.2	Electrosynthesis of PSSA doped PANI films in perchloric acid/ acetonitrile	132
5.7	Indirect detection of TTX at modified-NaX/PANI-PSSA films electrodes	132
5.8	Investigation of ionophore complexation with TTX using ion transfer voltammetry...	133
5.8.1	Choice of electrolyte solution.....	133
5.8.2	Ionophore complexation with TTX	134
5.9	Investigation of ionophore complexation with TTX using ultraviolet/visible absorption.....	135
5.9.1	NaX complexation with TTX.....	135
5.9.2	B18C6 complexation with TTX.....	135
5.10	Electrochemical synthesis of neutral and p-doped PANI-PSSA in phosphoric acid	136
5.10.1	Electrochemical polymerisation procedure using HClO_4/ACN and in H_3PO_4	136
5.11	Characterisation of neutral and p-doped PANI-PSSA in buffer solutions	137
5.12	Electrochemical impedance measurement of neutral and p-doped PANI-PSSA	137
5.13	Solubility test.....	138
5.14	Determination of absorption bands of neutral and p-doped PANI-PSSA	138
5.15	Emission wavelength of neutral and p-doped PANI-PSSA	139
5.16	FTIR measurement of neutral and p-doped PANI-PSSA composites	139
5.17	Characterisation of neutral and p-doped PANI-PSSA using SEM analysis	140
5.18	Characterisation of neutral and p-doped PANI-PSSA using TEM analysis	140
5.19	Application of p-doped PANI-PSSA films in the construction of electrochemical tetrodotoxin biosensors.....	141
5.19.1	The attachment of glutaraldehyde on the modified p-doped PSSA-PANI/GC	141
5.19.2	The immobilisation of aptamer on Glu/PANI-PSSA/GC electrode.....	141
5.20	The detection of TTX using the biosensor NH_2 -Aptamer/Glu/PANI-PSSA/GC	142
CHAPTER 6: INVESTIGATION OF ELECTROINACTIVITY OF TETRODOTOXIN AND ITS COMPLEXATION TO IONOPHORES		143
6.0	Introduction.....	143

Table of contents

6.1	Electro-inactivity of TTX	143
6.2	The electrokinetics of the electropolymerisation of undoped and doped PANI films in HClO ₄ /ACN	148
6.2.1	The electro-oxidation of aniline	148
6.2.2	Cyclic voltammograms of PANI in HClO ₄ / ACN	153
6.2.3	Stability of the modified-PANI electrodes and reversibility of the system	158
6.2.4	Electrochemical impedance spectroscopy (EIS) of PANI	161
6.2.5	Study of PANI films	167
6.2.6	Characterisation of electropolymerised PANI on PG and Pt electrode in acetate buffer pH 4.8.....	172
6.3	Indirect detection of TTX on modified-ionophore/PANI.....	173
6.3.1	Electrochemical synthesis of PSSA doped PANI in HClO ₄ /ACN.....	173
6.3.2	Sodium ion sensor based on NaX/PANI-PSSA/PG	175
6.4	Electrochemical tetrodotoxin sensor based on neutral selective NaX and B18C6 ionophores	178
6.4.1	Investigation of ionophore complexation of TTX using ion transfer voltammetry ...	179
6.4.2	Investigation of ionophore complexation of TTX using UV-Vis absorption.....	189
6.5	Conclusion	198
CHAPTER 7: APPLICATION OF ELECTROCHEMICALLY SYNTHESISED NEUTRAL AND P-DOPED PANI-PSSA FOR THE DETERMINATION OF TETRODOTOXIN		
7.0	Introduction.....	200
7.1	Electrosynthesis of neutral and p-doped PANI-PSSA films.....	201
7.2	Electrochemical active zone of neutral and p-doped PANI-PSSA in H ₃ PO ₄	203
7.3	Electrochemical activity of neutral and p-doped PANI-PSSA SPB	208
7.4	Characterisation of neutral and p-doped PANI-PSSA in SPB using EIS.....	222
7.5	The study of the electroactivity of neutral and p-doped PANI-PSSA films in acetate buffer pH 4.8	226
7.6	The study of R _{ct} for neutral and p-doped PANI-PSSA in acetate buffer pH 4.8.....	243
7.6.1	Charge transfer resistance (R _{ct}) of different bare electrode potentials	243
7.6.2	The determination of R _{ct} for the modified neutral and p-doped PANI-PSSA/GC	244
7.7	Effect of polarity of solvent on the solubility of neutral and p-doped PANI-PSSA.....	252
7.8	The characterisation of neutral and p-doped PANI-PSSA using UV-Vis absorption analysis.....	253
7.9	Emission wavelengths of neutral and p-doped PANI-PSSA	255
7.10	Characterisation of neutral and p-doped PANI-PSSA using FTIR analysis	258

Table of contents

7.11	Characterisation of neutral and p-doped PANI–PSSA using SEM analysis.....	260
7.12	Characterisation of neutral and p-doped PANI-PSSA using TEM analysis	264
7.13	Application of p-doped PANI–PSSA films on the construction of biosensor for the detection of tetrodotoxin	270
7.14	Detection of TTX based on PANI–PSSA, GLu/PANI–PSSA and NH ₂ –Atp/Glu/PANI–PSSA /Au sensors.....	270
7.15	Detection of TTX based on NH ₂ –Apt/Glu/PANI–PSSA/GC	273
7.16	Optimisation of glutaraldehyde concentration.....	279
7.17	Optimisation of aptamer concentration	282
7.18	UV/Vis absorption of the composite obtained for each detection step dispersed in DMF and DMSO	286
7.19	Scanning electron microscopy of each detection step on screen-printed electrode ...	288
7.20	Optimisation of aptasensor response	291
CHAPTER 8: CONCLUSION AND PERSPECTIVES.....		296
8.0	Conclusions.....	296
8.1	Perspectives	298
REFERENCES		299
ANNEX		335



List of abbreviation

LIST OF ABBREVIATION

	Atomic force microscopy
AFM:	
Apt	Aptamer
FTIR:	Fourier transform infrared
CPE:	Constant phase element
CV:	Cyclic voltammetry
CVs	Cyclic voltammograms
DNA:	Deoxyribonucleic acid
EB:	Emeraldine base
ES:	Emeraldine salt
EIS:	Electrochemical impedance spectroscopy
ELISA:	Enzyme linked Immunosorbent Assays.
FL:	Fluorescence
Glu	Glutaraldehyde
HOMO:	Highest occupied molecular orbital
HPLC:	High performance liquid chromatography.
HRSEM:	High resolution scanning electron microscopy
HRTEM:	High resolution transmission electron microscopy
LEB:	Leucoemeraldine state
LUMO:	Lowest unoccupied molecular orbital
PANI:	Polyaniline
PSSA	Poly(4-styrenesulfonic acid)

List of abbreviation

PNB:	Pernigraniline state
RE:	Reference electrode
SPR:	Surface plasmon resonance
SPE:	Screen-printed electrodes
UV-Vis	Ultraviolet-visible
WE:	Working electrode



LIST OF SYMBOLS

	Surface area of the electrode
$A:$	
$C^0:$	Bulk concentration
$D:$	Diffusion coefficient
$E_i:$	Initial potential
$E_\lambda:$	Switch potential
$E^0:$	Formal electrode potential
$E_p:$	Peak potential
$E_{pa}:$	Anodic peak potential
$E_{pc}:$	Cathodic peak potential
$\Delta E_p:$	Peak to peak separation
$i_p:$	Peak current
$i_{pa}:$	Anodic peak current
$i_{pc}:$	Cathodic peak current
i_0	Exchange current
$F:$	Frequency
$k^0:$	Standard rate constant
k_{app}	the apparent heterogeneous rate constant
$k_s:$	Rate constant of reaction
$n:$	Number of electron
$Q:$	Charge
$R:$	Gas constant
$\mu:$	Micro

List of symbols

ng	Nanogram
α :	Transfer coefficient
Ω :	Ohm
ν :	Scan rate
π :	Pi
λa :	Absorption Wavelength
λ_{em} :	Emission wavelength
ε_{λ} :	Molar extinction coefficient at wavelength λ
Γ^* :	Surface coverage
L :	Films thickness
ppm	Parts per million



LIST OF FIGURES

Figure 1.1: Sodium channel and TTX binding sites. [8]	4
Figure 1.2: Comparatively smaller hydrated sodium ions versus bulky TTX. [8].....	4
Figure 1.3: Example of a fugu fish containing tetrodotoxin.	5
Figure 2.1: The first Asymmetric synthetic tetrodotoxin produced in a laboratory in 2003.[37].....	16
Figure 2.2: Chemical structure of tetrodotoxin (TTX).	17
Figure 2.3: Guanidinium group.	17
Figure 2.4: (a) Equilibrium mixture, (b) The tautomer of TTX.....	18
Figure 2.5: Chemical structures of TTX analogues.[39].....	19
Figure 2.6: Chemical reaction of TTX.	20
Figure 2.7: ¹ H-NMR spectrum of tetrodotoxin.....	27
Figure 2.8: Infrared spectrum of tetrodotoxin.	29
Figure 2.9: The fragment ion spectrum of MH ⁺ of TTX. Volume of 100 to 200 pmol of TTX was injected into 0.05 ml min ⁻¹ of aqueous 50 % MeOH (v/v). Argon at a target thickness, 1,5 X 10 ¹⁴ molecules cm ⁻² ; collision energy, 49 eV. [70].	30
Figure 3.1: A schematic picture of a polymer film electrode.....	35
Figure 3.2: Schematic representation of n and p- doping processes respectively [102]....	39
Figure 3.3: Mechanism of polymerisation of aniline [92].....	42
Figure 3.4: Chain propagation state of aniline.....	44
Figure 3.5: SELEX technology aptamer screening process.[151].....	56
Figure 3.6: Biotin–streptavidin interaction. Biotin (green, red, and blue spheres) fits inside a pocket formed by the streptavidin protein (blue ribbon). [161].	59
Figure 3.7: (a) “Standard” Biotin (this version is used for addition to the 3’ end), (b) Biotin dT.	61
Figure 3.8: Standard nucleic acid modifications used for aptamer immobilisation [170].....	65
Figure 4.1: Cyclic Voltammogram: Excitation signal.....	69
Figure 4.2: Cyclic Voltammogram of a Single electron oxidation-reduction.....	69
Figure 4.3: Schematic of voltammetric experiments at (a) a macroscopic and microscopic ITIES supported at (c) a microhole and at (e) a micropipet.	

List of figures

<i>(b, d, and f) The corresponding cyclic voltammograms Adapted from Liu & Mirkin. [184].</i>	74
<i>Figure 4.4: Schematic diagram for the apparatus for cyclic voltammetry at the ITIES between water and nitrobenzene. Ref α and Ref β are reference electrodes, Wk α and Wk β are metal working electrodes. [185].</i>	76
<i>Figure 4.5: Ionic partition diagram showing transfer mechanisms of various forms of quinidine at the DCE/water interface.</i>	82
<i>Figure 4.6: Typical potential waveform for the cyclic voltammetry technique.</i>	84
<i>Figure 4.7: 1 mM Ferrocene in 0.1 M Bu_4NClO_4/CH_2Cl_2, 25 mV Square amplitude, 2 mV Square increment, 10 ms Square period, 1 ms Sample width.</i>	85
<i>Figure 4.8: The impedance Z plotted as a planar vector using rectangular and polar coordinates.</i>	87
<i>Figure 4.9: Electronic design used for electric measurements, dashed lines, - output signal routing, normal line – input signal routing.</i>	91
<i>Figure 4.10: General equivalent circuit element for a single cell fuel cell. Key: GDL = gas diffusion layer, dl = double layer, ct = charge transfer, a = anode, c = cathode.</i>	92
<i>Figure 4.11: Nyquist plot for mixed control circuit.</i>	93
<i>Figure 4.12: Illustration diagram of the principle 1H NMR.</i>	95
<i>Figure 4.13: Diagram showing the 1H NMR chemical shifts for common functional groups.</i>	96
<i>Figure 4.14: Pascal's triangle gives the intensity ratios between the split signals. 1 neighbor (doublet); 2 neighbors (triplet); 3 neighbors (quartet).</i>	97
<i>Figure 4.15: Electronic diagram used for a typical NMR spectrometer.</i>	98
<i>Figure 4.16: Electromagnetic spectrum. [202].</i>	100
<i>Figure 4.17: (a) Stretching and bending vibrational modes for H_2O. (b) Stretching and bending vibrational modes for CO_2.</i>	101
<i>Figure 4.18: The functioning principle of an infrared spectrophotometer.</i>	104
<i>Figure 4.19: Energy levels of electronic transitions.</i>	106
<i>Figure 4.20: Schematic of a dual-beam uv-vis spectrophotometer.</i>	110
<i>Figure 4.21: The Jablonski (electronic transition) diagram. E is the energy scale; S_0 is the ground singlet electronic state; S_1 and S_2 are the successively</i>	

List of figures

<i>higher energy excited singlet electronic states. T1 is the lowest energy triplet state.</i>	114
Figure 4.22: Schematic diagram of a spectrofluorometer. [209].	115
Figure 4.23: Typical force-separation curve.	117
Figure 4.24: Concept of AFM and the optical lever.	118
Figure 6.1: Cyclic voltammograms (CVs) of drop-coated TTX films on bare (a) Au, (b) GC, (c) BDD, (d) Ni, (e) PG, (f) Pt and (g) Ti electrodes in 10 ml acetate buffer, pH 4.8 at different concentrations at 100 mV s^{-1} .	144
Figure 6.2: CVs of drop-coated TTX films on bare electrodes in 1mL acetate buffer, (a) pH 4.10, (b) pH 5.01, (c) pH 6.03, (d) pH 7.02, (e) pH 8.03 at different concentrations.	146
Figure 6.3: SWVs of drop-coated TTX films on bare electrodes in 1 ml acetate buffer (a) pH 6.03, (b) pH 7.05, and (c) pH 8.03 at 100 mV s^{-1} .	147
Figure 6.4: Linear scan voltammograms of 50 mM aniline in 0.1 M HClO_4/ACN using (a) Pt, (b) PG, (c) Au, (d) GC electrode and silver wire reference electrode at 50 mV s^{-1} .	149
Figure 6.5: Dependence of open circuit voltage on the concentration of aniline in 0.1 M HClO_4/ACN .	150
Figure 6.6: Anodic Tafel plot.	151
Figure 6.7: Cyclic voltammograms (15 cycles) recorded during potentiodynamic growth of PANI films on (a) Au, (b) GC, (c) PG, and (d) Pt in 0.1 M HClO_4/ACN containing 0.05 M aniline at 50 mV s^{-1} scan rates.	155
Figure 6.8: The cathodic growth peak of PANI vs cycle number.	156
Figure 6.9: Overview of 3 cycles CVs of PANI films on Au, GC, PG and Pt electrode in 0.1 M HClO_4/ACN at a scan rate 50 mV s^{-1} .	160
Figure 6.10: Nyquist plots of PANI films prepared in 0.1M HClO_4/ACN on (a) Au, (b) GC, (c) PG, (d) Pt electrodes at different potential.	164
Figure 6.11: Bode plots of PANI films prepared in 0.1 M HClO_4/ACN on various electrodes at different potential.	165
Figure 6.12: Cyclic voltammograms of the PANI electrodeposited on (a) Au, (b) GC, (c) PG, and (d) Pt electrodes in 0.1 M HClO_4/ACN at different potential scan rates.	167

List of figures

Figure 6.13: (a) A plot of E_{p3} vs. $\log v$ and (b) plot of ΔE_{p3} vs. $\log v$ for the voltammograms of PANI films deposited on different electrode surface in 0.1 M $HClO_4/ACN$	168
Figure 6.14: The plot of logarithm of the growing PANI peak (i_{pc3}) vs. $\log v$	170
Figure 6.15: CVs of PANI in OAc buffer on Pt and PG electrode at 50 $mV s^{-1}$	172
Figure 6.16: CVs of polymerization of 25 mM PSSA doped 0.05 M aniline in 0.1 M $HClO_4/ACN$ at 50 $mV s^{-1}$, 15 cycles on PG electrode.....	174
Figure 6.17: Overview of 3 cycles CVs PANI-PSSA in 0.1 M $HClO_4/ACN$ at 50 $mV s^{-1}$ on PG electrode.....	175
Figure 6.18: CVs of different concentration of NaCl solution on NaX/PANI-PSSA/PG in 0.1 M OAc buffer pH 4.8 at 50 $mV s^{-1}$	177
Figure 6.19: Overview of 3 cycles CVs of different concentration of NaOAc in 0.1 M OAc buffer pH 4.8 at 50 $mV s^{-1}$ on PG electrode.....	178
Figure 6.20: Conventional scheme of electrochemical cell (I) used for the purpose of this study in ion transfer voltammetry.....	180
Figure 6.21: Overview 3 cycles background CVs of different electrolyte solutions obtained with NaX at the W 1,2-DCE interface, scan rate 0.01 $V s^{-1}$	181
Figure 6.22: Overview of 3 cycles of Cyclic voltammograms obtained for different concentrations of Na^+ ion transfer across the 0.05 M $MgSO_4$ 1,2-DCE/50 mM ETH 500 interface, using 10 mM NaX at 0.01 $V s^{-1}$	183
Figure 6.23: Overview of 3 cycles of CVs obtained for different concentrations of TTX^+ ion transfer across the 0.05 M $MgSO_4$ 1,2-DCE/50 mM ETH 500 interface, using 50 mM NaX at 0.01 $V s^{-1}$	184
Figure 6.24: Influence of K^+ ion peak on the CVs of different concentrations of TTX^+ and Na^+ ions transfer across the 0.05 M $MgSO_4$ /1,2-DCE/50 mM ETH 500 interface, using 50 mM NaX at 0.01 $V s^{-1}$	185
Figure 6.25: Conventional scheme of electrochemical cell (II) used for the purpose of this study in ion transfer voltammetry.....	186
Figure 6.26: Principle of the voltammetry Na^+ ion-selective electrode based on the facilitated transfer of Na^+ at the 1,2-DCE/ETH 500 /organic phase interface by B18C6.....	187

List of figures

Figure 6.27: Overview of 3 cycles CVs of different concentrations of Na^+ ion transfer across the 50 mM MgSO_4 /1,2-DCE/ 50 mM ETH 500 interface, using 50 mM B18C6 at 0.01 V s^{-1}	188
Figure 6.28: a) CV of different $[\text{TTX}^+]$ transferred across the 0.05 M MgSO_4 /1,2-DCE/ 50 mM ETH 500 without B18C6 , (b), (c) and (d) CV repetition at different $[\text{TTX}^+]$ ion transfer across the 0.05 M MgSO_4 /50 mM B18C6 interface at 0.01 V s^{-1}	189
Figure 6.29: $n \rightarrow \sigma^*$ electronic transition and band gap energy during the absorption of $-\text{C}-\text{O}-\text{H}$ and $=\text{C}-\text{N}-\text{H}$ chromophores in TTX molecule.	190
Figure 6.30: $n \rightarrow \pi^*$ electronic transition and band gap energy during the absorption of $-\text{N}=\text{C}-\text{N}-$ chromophores in TTX molecule.	191
Figure 6.31: $\pi \rightarrow \pi^*$ electronic transition and band gap energy during the absorption of $-\text{C}=\text{C}-$ chromophores in NaX molecule.	192
Figure 6.32: $n \rightarrow \pi^*$ electronic transition and band gap energy during the absorption of $=\text{C}-\text{O}-$ chromophores in NaX molecule.	192
Figure 6.33: $n \rightarrow \pi^*$ electronic transition and band gap energy during the absorption of $-\text{C}=\text{O}$ chromophores in NaX molecule.	193
Figure 6.34: UV-Vis absorption spectrum of 3.33 μM TTX (back line), 1000 μM NaX (red line) and TTX/ NaX (green line) in water.	194
Figure 6.35: UV-Vis absorption spectrum of 9.33 μM TTX (back line), 3330 μM B18C6 (red line) and TTX/B18C6 (green line) in water.	195
Figure 6.36: Chemical structure of (A) tetrodotoxin (TTX), (B) sodium ionophore X (NaX) and (C) Dibenzo-18-crown-6 (B18C6). Atoms: Hydrogen (white color), (carbon (cyan color), oxygen (red color), and nitrogen (blue color).	197
Figure 7.1: Cyclic voltammograms (15 cycles) recorded during potentiodynamic growth of PANI-PSSA films on Au, GC, PG, and Pt in 1 M H_3PO_4 containing 0.05 M aniline / 0.025 M PSSA at 0.050 V s^{-1} scan rates.	202
Figure 7.2: Electrochemical transitions between PSSA-PANI's base forms are shown vertically as a series of successive reduction reactions from LB to EB, and to PB. Transitions to the ES form of PANI are shown via diagonal and horizontal reactions.	203

List of figures

Figure 7.3: Overview of 3 cycles CVs of neutral and p-doped PSSA–PANI in 1 M H_3PO_4 on Au, GC, PG and Pt electrodes. Scan rates $0.050 V s^{-1}$	204
Figure 7.4: CVs of 5 cycles recorded during potentiodynamic growth of PANI–PSSA films on Au, GC, PG, and Pt in 1 M H_3PO_4 containing 0.05 M aniline / 0.025 M PSSA at $50 mV s^{-1}$ scan rates.	207
Figure 7.5: Cyclic voltammograms of the PANI–PSSA electrodeposited on Au, GC, PG, and Pt electrodes in 0.1 M PB pH 7.04 at different potential scan rates.	210
Figure 7.6: Electrode surface reactions during the cyclic voltammetry of neutral PANI–PSSA.	211
Figure 7.7: Electrode surface reactions during the cyclic voltammetry of p-doped PANI–PSSA.	211
Figure 7.8: A plot of E_p vs. $\log v$ for the voltammograms of neutral and p-doped PANI–PSSA films deposited on bare of different electrodes in 0.1 M sodium phosphate buffer pH 7.04.	214
Figure 7.9: A plot of ΔE_p vs. $\log v$ for the voltammograms of neutral and p-doped PANI–PSSA films deposited on bare of different electrodes in 0.1 M sodium phosphate buffer pH 7.04.	217
Figure 7.10: A typical Randles-Sevcik plot showing the peak current and square root of voltammograms scan rates for the neutral and p-doped PANI–PSSA films deposited on of different bare electrodes in 0.1 M PB pH 7.04.	218
Figure 7.11: Nyquist plot of neutral and p-doped modified-PANI–PSSA electrodes in 0.1 M sodium phosphate buffer pH 7.04 at a frequency range 100 mHz to 100 kHz.	223
Figure 7.12: Cyclic voltammograms of the PANI–PSSA electrodeposited on Au, GC, PG, and Pt electrodes in 0.1 acetate buffer pH 4.8 at different potential scan rates.	227
Figure 7.13: A plot of E_p vs. $\log v$ for the voltammograms of neutral and p-doped PANI–PSSA films deposited on different bare electrodes in 0.1 M acetate buffer pH 4.8.	233
Figure 7.14: A plot of ΔE_p vs. $\log v$ for the voltammograms of neutral and p-doped PANI–PSSA films deposited different bare electrodes in 0.1 M acetate buffer pH 4.8.	237

List of figures

Figure 7.15: A plot of i_p vs. square root v for the voltammograms of neutral and p-doped PANI–PSSA films deposited on different bare electrodes in 0.1 M acetate buffer pH 4.8.	241
Figure 7.16: Nyquist plot for bare Au, GC, PG, and Pt electrodes in 0.1 M acetate buffer pH 4.8.	244
Figure 7.17: Nyquist plot for neutral and p-doped PANI–PSSA in 0.1 M acetate buffer pH 4.8 on (a) and (a') Au, (b) and (b') GC, (c) and (c') PG, (d) and (d') Pt electrodes.	246
Figure 7.18: Equivalent circuit for neutral and p-doped PANI-PSSA electrode. R_s is the solution resistance, R_1 is the charge transfer resistance (R_{ct}), CPE1 denote constant-phase element.	247
Figure 7.19: Plot of charge transfer resistance (R_{ct}) versus potential.	249
Figure 7.20: Neutral and p-doped PANI–PSSA dispersed in DMF and DMSO.	253
Figure 7.21: UV-vis spectra of neutral PANI–PSSA and p-doped PANI–PSSA composites in DMF as solvent.	254
Figure 7.22: UV-vis spectra of neutral PANI-PSSA and p-doped PANI–PSSA composites in DMSO as solvent.	255
Figure 7.23: Emission spectra of neutral and p-doped obtained in DMF and DMSO solvent.	257
Figure 7.24: FT-IR spectra of neutral and p-doped PANI–PSSA composites in (a) DMF and (b) DMSO.	259
Figure 7.25: SEM images of bare screen-printed carbon electrode.	261
Figure 7.26: SEM images of neutral PANI-PSSA composites.	262
Figure 7.27: SEM images of p-doped PANI-PSSA composites.	263
Figure 7.28: TEM images of neutral PANI-PSSA composites.	265
Figure 7.29: TEM images of (b) p-doped PANI-PSSA composites.	266
Figure 7.30: Energy-dispersive X-ray spectrum (EDX) of neutral PANI–PSSA PANI–PSSA films in DMF.	268
Figure 7.31: Energy-dispersive X-ray spectrum (EDX) p-doped PANI–PSSA films in DMF.	269
Figure 7.32: Cyclic voltammograms for the detection of TTX based on (a) p-PANI–PSSA, (c) Glu/PANI–PSSA, (e) Apt/Glu/PANI–PSSA and EIS measurements for the detection based on (b) P-PANI–PSSA, (d)	

List of figures

<i>Glu/PANI–PSSA, (f) Apt/Glu/PANI–PSSA. (g) The bode plot of (h) which present together the three separated detections.</i>	272
<i>Figure 7.33: Overview of three cycles of cyclic voltammograms responses obtained after each in 0.1 M OAc buffer pH 4.8 with 0.02 mM glutaraldehyde (4 h incubation), 2 μM aptamer (4 h incubation), and 5μM TTX (30 mins incubation).</i>	274
<i>Figure 7.34: (a) Nyquist plot recorded after each step of TTX biosensor in 0.1 M acetate buffer pH 4.8 at formal potential. (b) An equivalent circuit model used in this biosensor analysis.</i>	277
<i>Figure 7.35: Bode plot of the overlay of each step of immobilization of glutaraldehyde, aptamer and TTX in 0.1 M acetate buffer pH 4.8 at formal potential.</i>	279
<i>Figure 7.36: (a) Nyquist plot of TTX aptasensor developed on seven different GC electrodes at different concentration of aldehyde and fixed concentration of aptamer, 2 μM, and 5 μM TTX. (b) Absolute value of the relative variation (%) of the charge transfer resistance as a function of concentration of glutaraldehyde.</i>	280
<i>Figure 7.37: EIS response of TTX biosensor (TTX/Apt/Glu/PANI–PSSA) at different concentration of aptamer in OAc buffer pH 4.8. Calibration curve for the TTX/Apt/Glu/PANI–PSSA biosensor response to different concentrations of aptamer.</i>	283
<i>Figure 7.38: Linear structure of the most stable NH₂-aptamer for TTX obtained from RNA Institution mfold (sequence: AAAAAATTCACACGGGTGCCTCGGCTGTCC).</i>	285
<i>Figure 7.39: UV-Vis spectra of TTX biosensor in DMF.</i>	287
<i>Figure 7.40: Scheme of the aptasensors: (a) electropolymerisation of PSSA dope aniline, (b) binding of glutaraldehyde on the modified-PANI–PSSA/GC surface, (c) immobilisation of NH₂-Aptamer on Glu/PANI–PSSA/GC, (d), binding of tetrodotoxin to aptamer, (e) Route for label-free TTX detection</i>	288
<i>Figure 7.41: Scanning electron micrographs of Glu/PANI–PSSA.</i>	289
<i>Figure 7.42: Scanning electron micrographs of Apt/Glu/PANI–PSSA.</i>	290
<i>Figure 7.43: Scanning electron micrographs of TTX/Apt/Glu/PANI–PSSA.</i>	291

List of figures

- Figure 7.44: Calibration curve for the PSSA–PANI/Glu/Aptamer biosensor response to different concentrations of tetrodotoxin. Inset analytical linear range of the biosensor from 0.3 to 1.0 ng ml⁻¹. 292*
- Figure 7.45: Calibration curve for the PSSA–PANI/Glu/Aptamer biosensor response to different concentrations of tetrodotoxin repeated three times at the range 0 to 0.2 ng ml⁻¹. 293*
- Figure 7.46: Calibration curve for the PSSA–PANI/Glu/Aptamer biosensor response to different concentrations of tetrodotoxin. Inset analytical linear range of the biosensor from 0 to 0.5 ng ml⁻¹. 294*



LIST OF TABLES

Table 1.1: Fish poisonings due to animal natural toxins (Total score from 2002–2006, Ministry of Health, Labour and Welfare Japan, Taiwan/China, Bangladesh, South Africa, Florida, Virginia, Asia).....	2
Table 2.1: Some physico-chemical properties of tetrodotoxin [8]	21
Table 2.2: Summary of different works done on analytical techniques for TTX detection	30
Table 3.1: Some example of conducting polymers [101]	37
Table 3.2a: Ions sensors and their selective ionophores [144].....	51
Table 4.1: Different diagrams with corresponding equivalent circuit	89
Table 4.2: Circuit elements used in the models.....	94
Table 4.3: Some selected bonds with their absorption regions [206]	102
Table 4.5: List of selected chromophores and their light absorption characteristics.....	108
Table 4.6: Solvent effect on wavelength in UV-Vis (for 1 cm cell).....	109
Table 5.1a: List of chemical reagents used in this study	121
Table 5.2: Working electrodes used to carry out the experiment.....	123
Table 5.3: Organic solutions used to carry out the ion transfer voltammetry experiment	127
Table 6.1: Kinetics parameters evaluated from the plot $\log i$ vs. E of linear sweep voltammogram data near to the E_{onset}	152
Table 6.2: Kinetic parameters of PANI from potentiodynamic process on various electrodes in 0.1 M HClO ₄ / ACN	157
Table 6.3: Parameters evaluated from CVs of PANI vs Ag wire electrode in HClO ₄ / ACN	161
Table 6.4: Comparison of impedimetric parameters of PANI modified-electrodes [220-221]	166
Table 6.5: Kinetic parameters of PANI films on various electrodes obtained from the plot $E_{\text{pc-growing}}$ versus logarithm of scan rate	169
Table 6.6: Data obtained from the plot ΔE_{pc3} vs. $\log v$	170
Table 6.7: Study of PANI films base on the slope (b) of the plot $\log i_{\text{pc-gr}}$ vs. $\log v$	171
Table 6.8: Kinetic parameters of the interfacial transfer reaction obtained from background CVs of different electrolytes solution	182

List of tables

Table 6.9: UV-Vis absorption data of TTX, NaX, B18C6 and TTX/B18C6	196
Table 6.10: Active site and distances between atoms responsible for complex formation	198
Table 7.1: Values of peak characteristics of electrodeposited PANI–PSSA films in 1 M H ₃ PO ₄ at three sweep cycles	206
Table 7.2: Values of peak characteristics of electrodeposited neutral PANI–PSSA films on various electrodes in 0.1 M PB pH 7.04 over three sweep cycles at different scan rates	212
Table 7.3: Values of peak characteristics of electrodeposited p-doped PANI–PSSA films on various electrodes in 0.1 M PB pH 7.04 over three sweep cycles at different scan rates	213
Table 7.4: Anodic and cathodic transfer coefficient of neutral and p-doped PANI–PSSA films on various electrodes obtained from the plot $E_{pa,c}$ versus logarithm of scan rate	215
Table 7.5: Electrode reaction rate constant of neutral and p-doped PANI–PSSA films on various electrodes obtained from the plot ΔE_p versus logarithm of scan rate.....	219
Table 7.6: Diffusion coefficient of neutral and p-doped PANI–PSSA films on various electrodes obtained from the plot i_p versus square root of scan rate.....	221
Table 7.7: Diagnostic parameters for neutral and p-doped-modified electrodes	225
Table 7.8: Electrochemical potential parameters of neutral PANI–PSSA films	229
Table 7.9: Electrochemical current parameters of neutral PANI–PSSA films	230
Table 7.10: Electrochemical potential parameters of p-doped PANI–PSSA films.....	231
Table 7.11: Electrochemical current parameters of p-doped PANI–PSSA films	232
Table 7.12: Anodic and cathodic transfer coefficient of neutral PANI–PSSA films.....	235
Table 7.13: Anodic and cathodic transfer coefficient of p-doped PANI–PSSA films.....	236
Table 7.14: Electrode reaction rate constant of neutral and p-doped PANI–PSSA film study in acetate buffer	239
Table 7.15: Electron transport diffusion coefficient of neutral and p-doped PANI–PSSA film study in acetate buffer.....	242
Table 7.16: Equivalent circuit resistance deduced by fitting Nyquist plots to circuit of neutral and p-doped PANI–PSSA	248

List of tables

Table 7.17: Electrochemical kinetic parameters of neutral and p-doped PANI–PSSA study in acetate buffer pH 4.8.....	250
Table 7.18: Nyquist plot parameters analysis for the detection of TTX.....	273
Table 7.19: Characteristic peaks obtained from the CVs of each step of TTX biosensor.....	275
Table 7.20: Values of the equivalent circuit parameters of the fitting curves	278
Table 7.21: EIS parameters determined form the equivalent circuit of the fitting curves	282
Table 7.22: Concentration of aptamer and charge transfert resistance recorded at two different formal potential.....	284
Table 7.23: The Gibbs free energy of five bases involved on the binding active site of the aptamer	286
Table 7.24: Comparison of different method of determination of tetrodotoxin.....	295



ACADEMIC OUTPUT

Christopher E. Sunday^a, Mawethu Bilibana^a, Sinazo Qakala^a, Oluwakemi Tovide^a, Kerileng M. Molapo^a, **Gertrude Fomo**^a, Chinwe O. Ikpo^a, Tesfaye Waryo^a, Gcineka Mbambisa^a, Bulelwa Mpushe^a, Avril Williams^{a,b}, Priscilla G.L. Baker^a, Sibulelo Vilakazi^c, Robert Tshikhudo^c, Emmanuel I. Iwuoha^a, Modulation of the matrix effect of nafion on tris(bipyridine) ruthenium(II) electrochemical probes by functionalisation with 4-nitrophenylazo graphene-gold nanocomposite. *Electrochimica Acta*, (2014) 128, 128-137 <http://dx.doi.org/10.1016/j.electacta.2013.12.143>).

Abd Almonam Baleg^a, Nazeem Jahed^a, Anne L. Djoumessi Yonkeu^{a,b}, Njagi Njomo^a, Gcineka Mbambisa^a, Kerileng M. Molapo^a, Xolile G. Fuku^a, **Gertrude Fomo**^a, Hlamulo Makelane^a, Abebaw Tsegaye^a, Tesfaye T. Waryo^a, Priscilla Baker^a, Sibulelo Vilakazi^b, Robert Tshikhudo^b, Emmanuel I. Iwuoha^a, Impedimetry and microscopy of electrosynthetic poly(propylene imine)-co-polypyrrole conducting dendrimeric star copolymers, *Electrochimica Acta*, (2014) 128, 448-457 (<http://dx.doi.org/10.1016/j.electacta.2013.12.138>).

Manuscript: **Gertrude Fomo**, Tesfaye T. Waryo, Priscilla G. Baker, Emmanuel I. Iwuoha, Differential electrode kinetics and electronics of electrosynthetic polyaniline on carbonaceous and precious metal systems in perchlorate/acetonitrile medium, submitted to *Electrochimica Acta*.

List of tables

Manuscript: Gertrude Fomo, Tesfaye T. Waryo, Emmanuel I. Iwuoha' Electroinactivity of tetrodotoxin studied on various metal electrode using cyclic voltammetry, submitted to Electrochemistry Communications.

Manuscript: Gertrude Fomo, Tesfaye T. Waryo, Emmanuel I. Iwuoha Complexation affinity of tetrodotoxin with sodium ionophore X and dibenzo-18-crown-6 using ion-transfer voltammetry and ultraviolet/visible absorption, submitted to Electrochimica Acta.

Conference: Attended the SACI National 2013 convention in East London Organised by the South African Chemical Institute during the period of 1 – 6 December 2013



INTRODUCTION

1.0 Background of this study

Fish such as shellfish are nutritionally and economically valuable, and million tonnes of protein consumed annually by humans worldwide comes from marine species. Looking at the entire international trade in fisheries' products where three-quarters are fish and a quarter is shellfish, the total value is estimated to be a billion dollars per annum [1]. Food poisoning occurs when contaminated food or water is ingested. The poison in fish firstly from bacteria can cause food poisoning, either directly or by the toxins they produce. Secondly, parasites such as giardia lamblia can also cause food poisoning through contaminated produce and water. Apart from the high quality protein, and essential amino acids, Omega-3 fatty acids are an unsaturated acid that is thought to reduce inflammation throughout the body as it lowers the cholesterol level, which reduces the risk of heart disease, particularly sudden cardiac death. According to Gallacher (2000) "people have been encouraged to choose seafood as healthy food, particularly important in northern Europe, where deaths from coronary heart disease in 1986 ranged from 245 to 625 annually per 100,000 men".[2]

The 1993 Chemical Weapons Convention defines "toxin," as "any chemical which through its chemical action on life processes can cause death, temporary incapacitation or permanent harm to humans or animals," regardless of its origin or method of production [3]. Certain types of fish and fish products contain naturally occurring marine biotoxins

Chapter 1: Introduction

(toxic substance produced by plants and animals) and when consumed, can produce illness in humans and in certain cases, death can follow. The literature shows that a large amount of research has been done on fish toxins and Table 1.1 presents some of the results obtained by different authors.

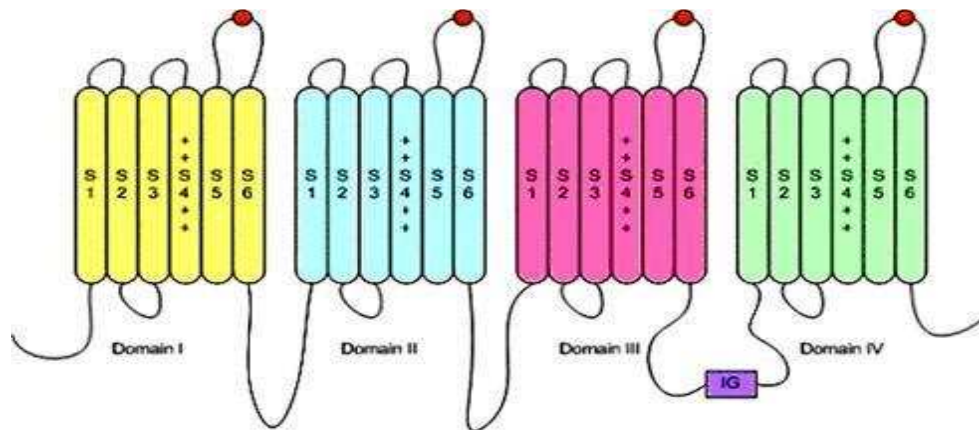
Table 1.1: Fish poisonings due to animal natural toxins (Total score from 2002–2006, Ministry of Health, Labour and Welfare Japan, Taiwan/China, Bangladesh, South Africa, Florida, Virginia, Asia)

Causative food	Causative toxin	Number of patients	Number of deaths	Refs
Puffer fish of tetraodontidae	Tetrodotoxin (TTX) and Saxitoxin (STX)	223	13	[4-5]
Ciguateric fish	Ciguateric toxins or Ciguatoxin	67	0	[4]
Scombroid fish poisoning (SFP)	Histamine	275	0	[6]
Diarrhetic shellfish poisoning (DSP)	Azaspiracid	8	0	[6]
Amnesic shellfish poisoning (ASP)	Domoic acid (DA)	107	3	[6]
Fish	Palytoxin (PTX)	4	2	[7]
Fish	Brevetoxin (PbTx)	59	0	[7]

From Table 1.1, it is noted that the most dangerous causative toxin is tetrodotoxin with a high number of patients and deaths. It is therefore important and necessary to conduct a thorough study on the analysis and detection of tetrodotoxin.

Chapter 1: Introduction

Tetrodotoxin is a potent neurotoxin with no known antidote which blocks the action of potentials in nerves by binding to the sodium voltage-gated. TTX is a nonpeptidic neurotoxin with a high rate of food poisoning mortality (60 %) that has been associated with the consumption of diets containing puffer fish and mud snails harbouring TTX-producing bacteria. Tetrodotoxin acts on the central and peripheral nervous system by blocking the sodium ion channels vital for signalling pathways (e.g. transmission of impulses and maintenance of cell functions), eventually leading to paralysis and even death. Tetrodotoxin binds specifically to sodium channels by mimicking the hydrated Na^+ ion and denying entry to Na^+ ions. Tetrodotoxin inhibits or reduces the chances of an action potential being produced. The binding site of this toxin is located at the pore opening of the voltage-gated Na^+ Channel (Fig.1.1 and 1.2). The diagram below shows the sodium channel with four repeating units. The TTX bind site is represented by the orange filled circles on the connecting segments between S5 and S6 [8]. It has been proposed that the binding between TTX and the Na channel results from the interaction between the positively charged guanidine group of TTX and the negatively charged carboxylate groups on the side chains at the mouth of the channels.



Chapter 1: Introduction

Figure 1.1: Sodium channel and TTX binding sites. [8]

It has been proposed that the binding between TTX and the sodium channel results from the interaction between the positive charge of the guanidinium group of TTX and the negative charge of carboxylate groups on the side chains at the mouth of the channel. Being much larger than the Na^+ ions, the bulk of the molecule blocks the entrance to the sodium channel, preventing the flow of Na^+ ions until it slowly diffuses off. With the multiple roles which sodium plays in the body, the detection of TTX in puffer fish has received much attention. Sodium plays an important role in cellular activity, the regulation of osmotic pressure and the regulation of the activity of the nervous and bloodstream systems. As a consequence of TTX blockage, sodium ion movement is effectively shut-down and the propagation of action potential ceases. The central and peripheral nervous systems are impaired, resulting in paralysis and death.

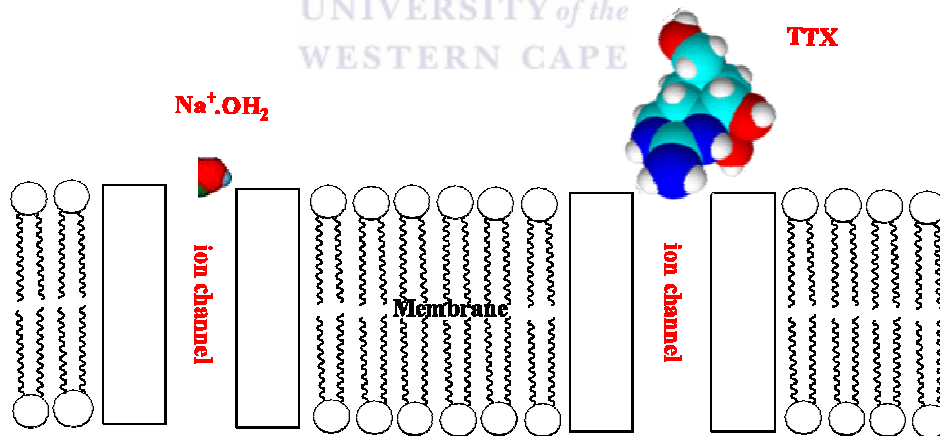


Figure 1.2: Comparatively smaller hydrated sodium ions versus bulky TTX. [8]

As mentioned previously, tetrodotoxin is a heat-stable neurotoxin that blocks sodium conductance and neuronal transmission in skeletal muscle, leading to weakness or

Chapter 1: Introduction

paralysis and potentially death if ingested in sufficient quantities [9]. There is no exact toxic dose of TTX because it is found in different concentrations in puffer fish. The minimum lethal dose in humans for tetrodotoxin is estimated to be 1-2 mg [10] and the minimum dose necessary to cause symptoms has been estimated to be 0.2 mg. This latter number can vary based on age, health, and sensitivity to the toxin. It is 100-fold more toxic than cyanide and, as such, it should be dubbed a “super-neurotoxin”. According to literature [10], TTX is among the most toxic substances known to man; death can occur within 30 minutes or less depending on the age of the victim. The minimum lethal dose is assumed to be 1000 micrograms for an adult human and LD50 for the mouse which is 10000 micrograms.

The blowfish, which is one type of puffer fish, has many parts (including the liver, muscles, skin, and ovaries) contain an extremely strong, paralyzing poison called tetrodotoxin.

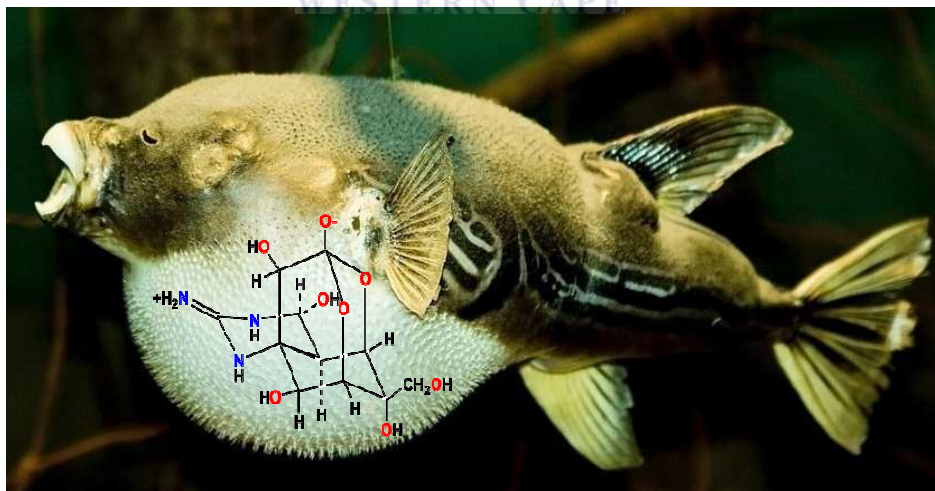


Figure 1.3: Example of a fugu fish containing tetrodotoxin.

Chapter 1: Introduction

Various organisms besides marine puffer fish contain TTX [11]. It is also found in organisms such as Gastropod mollusk, the eggs of horseshoe crabs [11], newts of the genus *Taricha*, the skin of *Ateloid frogs*, the skin and viscera of porcupine fish, globefish, balloon fish, sunfish, toadfish and the blue-ringed octopus. In Central America, species like the family *Salamandridae* and toads and harlequin frogs also contain the toxin.

Tetrodotoxin is one of the best known marine toxins that have been isolated predominantly in many species of puffer fish and the origin of the toxin is hypothetic. Indeed, since the discovery of TTX in 1995, three different hypotheses have been given as to where TTX might come from. The first option is that it is produced by bacteria which live within the organisms. The second one is based on something that the organisms eat or it is some sort of algae that they eat or another organism and that they can then accumulate the TTX and the third suggestion is that the organisms produce it themselves. The fact that the content of TTX in animals fluctuates according to regional, seasonal and individual differences, strengthens the suggestion that the toxin may not be genetically inherited. Those hypotheses mentioned above have been investigated and it has been found that bacteria are the primaries and good sources of TTX [11-12].

Tetrodotoxin is a real inhibitor of the regulation of osmotic pressure, the transmission of nerve impulses by mimicking the Na^+ ion and blocking the Na^+ ion channels, thus preventing the flow of Na^+ ions. The toxin is extremely dangerous through ingestion, inhalation, skin absorption, or if it enters the blood stream in any manner. The onset of symptoms of tetrodotoxin intoxication usually occurs from 10 to 45 minutes after ingestion, but may be delayed by three hours or more depending on the body. Paraesthesia

Chapter 1: Introduction

appears in the face and extremities, which may be followed by dizziness or numbness. Nausea, vomiting, diarrhoea and epigastric pain may also be present. Later, respiratory symptoms such as rapid breathing may follow. Low blood pressure, convulsions and irregular heart rate may occur. In most instances, the patients retain consciousness until shortly before death, which usually takes place within the first six hours.

Tetrodotoxin has a very important role in neurophysiology, and in other fields of study as a research reagent (a specific sodium channel blocker). In clinical medicine, it is used as an analgesic for terminal cancer (in China) and as an analgesic for neuralgia and rheumatism (in Japan) [13-14]. TTX finds an application in the production of non-toxic cultured pufferfish whose liver can be used as a poison-free food due to their biochemical properties and mechanism through the development of technology [15]. The guanidinium groups, being the active site of TTX, have different applications in addition to being central as a base of DNA. They are also applied for gas-proofing swim bladders and act as a reflector. People at greatest risk for food poisoning are seniors, pregnant women, young children and babies and people with chronic medical conditions (e.g., diabetes, AIDS, liver disease). A poison similar to that, naturally found in the puffer fish can also occur in many edible Caribbean and Pacific species. From January 2002 to May 2004, 28 pufferfish poisoning cases in Florida, New Jersey, Virginia, and New York were linked to River Lagoon in Florida [16]. To protect public health, monitoring programs for fish have been established in many countries, which often stipulate the use of animal models like mouse bioassay (MBA) and the rat bioassay (RBA), even the use of enzyme-linked immunosorbent assay (ELISA), high performance liquid chromatography (HPLC), liquid

Chapter 1: Introduction

chromatography-tandem mass spectrometry (LC-MS/MS) and a surface Plasmon resonance sensor, for detecting the presence of tetrodotoxin in fishes.

1.1 Scope of this study

Every year, a large number of people fall victim to some sort of poisoning induced after ingestion of Puffer fish (most cases are found in Japan, China, and Australia). That is why quality control is the key issue common to all horticultural products and with the high level of technology in the world, a huge number of techniques and methods are used for this purpose. The analytical methods mentioned in the previous paragraph allow the unequivocal identification of the toxins present in a sample and their quantification with high levels of sensitivity. For example, one common method of quantifying and analyzing TTX is high performance liquid chromatography (HPLC; as reviewed by [17]). HPLC is an effective means of measuring TTX but it is costly, time consuming and requires special training and expensive equipment. A major disadvantage of these methods is the need for certified standards for each known analogue of every group of toxins in order to evaluate total toxicity and in any case the contribution of unknown compounds to sample toxicity will not be considered. The problem of lack of standards is an important obstacle for the substitution of the mouse bioassay by other analytical methods. Biological methods are another group of alternative techniques that have been developed for most of the fish toxin groups with a great variety of designs, from immunoassays to biosensor techniques. These techniques vary in specificity and their practicality depends on the technological approach, as well as the cost. Biosensor or sensor technologies can offer good characteristics for tetrodotoxin detection solutions such as being cost-effective, specificity, sensitivity,

Chapter 1: Introduction

portability, repeatability and robustness. The research proposal deals with the development of such electrochemical biosensors for potential use in the fast and efficient control of quality fish in the market. This study thus intends to solve the main problem which is the monitoring and control of the quality of fish in the market through a novel aptasensor to reduce the death rate by limiting consumption of these poisonous fishes. The characteristics of biosensors (aptasensor) would support the use, not only to obtain more uniform results, but also to comply with the rapidly increasing demand for certification and the traceability of traded seafood. This project aims to carry out the first electrochemical study and the development of electrochemical aptasensor of tetrodotoxin, in particular those based on affinity interactions, by using bare electrodes or electrodes modified with selective-sodium ionophore and tetrodotoxin-aptamer immobilized on existing conducting polymer platforms based on PSSA doped aniline. Several types of conducting polymers based on derivatives of aniline monomer such as poly[(R)-(-)-3-(1-pyrrolyl)propyl-N-(3,5-dinitrobenzoyl)- α -phenylglycinate] [poly(DNBP)] [18] pentameric thiophene derivatives [19], alkyl polythiophenes [20], alkyl, halogens, aryl and nitro polyanilines [21-22] have been reported. In most cases these polymers are difficult to process because of lack of solubility in common solvents. It has been described to be 100-fold more toxic than cyanide and, as such, it should be dubbed a “super-neurotoxin”. As this neurotoxin has no known anti-dote and could not be mitigated by cooking, the only way to enforce safety appears to be abstinence from these food types or via the detection and screening of TTX-contaminated fishes at the points of harvest and control. On the other hand, due to the interesting molecular mechanism of action of TTX, it has found important applications in neurophysiology (as a specific sodium channel blocking agent) and as an analgesic (e.g., for neuralgia and rheumatism). Therefore, reliable, low-cost and

Chapter 1: Introduction

portable analytical devices and methods for detection of tetrodotoxin will be developed in this study.

1.2 Objectives of the study

The aim of the research project presented in this dissertation is to design and characterize a novel electrochemical sensor and biosensor that is highly specific and selective for the detection of tetrodotoxin in various aqueous mediums. The sensors are constructed by incorporating selective-sodium ionophores and tetrodotoxin-aptamer on the electroactive polymers-carbonaceous and precious metal systems on the working electrode. The biosensor reactivity is modelled using EIS, amperometry or direct potentiometry and CV techniques.

The following objectives highlighted will be achieved to fulfil the aim of this research work.

- i. The study of electroinactivity of tetrodotoxin at various electrodes (Pt, Ti, Ni, PG, Au, BDD, GC) in suitable electrolytes (citrate buffer, pH 4 to 8) and study its electrode kinetics at different pH and supporting electrolytes.
- ii. The study of electrochemical polymerization of aniline monomers and characterization of the PANI-modified electrode surfaces using electrochemical impedance spectroscopy and cyclic voltammetry techniques in organic medium.
- iii. The study of undoped PANI-modified electrode in buffer solution and evaluation of electroanalytical performance of PANI-modified electrodes in the detection of tetrodotoxin.

Chapter 1: Introduction

- iv. The attachment of selective-sodium ionophore X and dibenzo-18-crown-6 on the surface of doped PANI–PSSA-modified electrodes to develop the electrochemical tetrodotoxin ionophore sensor. This objective to be completed with the investigation of ionophore complexation of TTX using ion transfer voltammetry and ultraviolet/visible analysis.
- v. The electrochemical synthesis of neutral and p-doped PANI–PSSA films on bare electrodes and their characterizations using electrochemical impedance spectroscopy and cyclic voltammetry techniques in acetate and sodium phosphate buffers.
- vi. The application of the modified p-doped PANI–PSSA/electrode on the amperometric and impedimetric sensors for a tetrodotoxin based on aptamer.

1.3 Overview of the thesis



This thesis is composed eight chapters:

Chapter 2 reviews literature related to the analysis of tetrodotoxin with respect to its chemical synthesis and physico-chemical properties. The chapter also highlights some of the works reported on the quantification and qualification detection of tetrodotoxin using different techniques.

Chapter 3 reviews the literature related to conducting electroactive polymers with respect to their synthesis, the doping effect on their conductivity and activity and their application for electromediation roles in biosensors. The literature searches the media regarding the synthesis of conductive electroactive polymers, the synthetic routes for preparation of

Chapter 1: Introduction

doped polyanilines and the properties of the resultant composites. Some investigations which reported on the conducting of the electroactive PANI–PSSA composite are also reviewed.

Chapter 4 explains the principle of the selected techniques such as electrochemical techniques (CV, LCV, ISE, SWV and EIS) and spectroscopy techniques (IR, UV-Vis, FI and ^1H NMR) used in this thesis to develop the electrochemical tetrodotoxin sensors based on selective ionophores and aptamer.

In chapter 5, all the reagents and instruments are listed and the experimental methods that were employed for the electroactivity of TTX on bare electrodes are described for all measurements obtained in this work.

Chapter 6 on the one hand, thoroughly interprets and discusses results showing the development of the electrochemical tetrodotoxin based on ionophores. Firstly, the results on the electroactivity of TTX were presented and discussed. Then, the results obtained from the investigation of the polymerization medium of aniline were discussed. Additionally, the results for the complexation of TTX with selective ionophores using ions-transfer voltammetry and UV/Vis and the detection of TTX on modified ionophore/PANI-PSSA/electrode were then presented

Chapter 7 presents the characterization results of the electrochemical synthesised neutral and p-doped polyaniline and poly(4-styrenesulfonic acid) doping using CV, EIS, UV/Vis, FTIR, SEM and TEM. This is followed by a critical analysis of the resultant voltammograms and the extraction of suitable data which is then used for the estimated

Chapter 1: Introduction

important kinetic parameters describing the electrochemical behaviour of the doping polyanilines. Finally, the results of each step of electrochemical tetrodotoxin aptasensor using p-doped and PANI-PSSA films polymerized on the electrode surface are discussed.

Finally, Chapter 8 summarizes the major results for the synthesis, characterization and application of the undoped and doped polyaniline. The chapter also draws conclusions from the various results and this forms a basis for the suggested recommendations that follow.



ANALYSIS OF TETRODOTOXIN

2.0 Introduction

In this chapter, a review of tetrodotoxin based on the works which have been done before will be presented. This literature of the general view of tetrodotoxin focuses firstly on its synthesis and chemical reaction involved. Secondly the analytical studies using different analytical techniques which have been reported by different researchers on tetrodotoxin will also be highlighted.

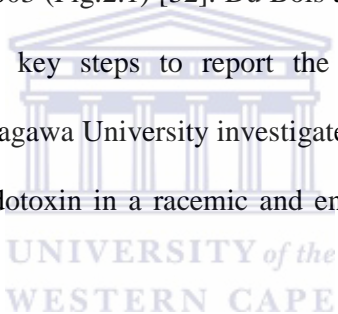
2.1 Chemistry of tetrodotoxin



Tetrodotoxin (TTX), known as puffer fish toxins, is one of the most potent non-peptidic neurotoxin because of its frequent involvement in fatal food poisoning, its unique chemical structure and its specific action of blocking sodium channels of excitable membranes [23]. Tetrodotoxin is a neurotoxin found in the toxic Pufferfish with low molecular weight, which was isolated for the first time in 1950. The pufferfish family tetraodontidea has revealed its wide distribution in both terrestrial and marine animal kingdoms such as vertebrate species inclusive of pufferfish, goby, newt and frog, invertebrates including octopus, gastropod mollusc, crab, starfish, nemertean and turbellarian [24-28]. The toxin is named after the tetraodon pufferfish which is the most commonly available source of TTX. Puffer fish can be found worldwide in warm seas from about 45° latitude north to 45° latitude south [29].

2.2 Synthesis of tetrodotoxin

The synthesis of tetrodotoxin is through the complex reaction that involves a series of 67 steps [30], including a ketalization, a Meenwein-Ponndorf Verley reduction, selenium oxidation and a Diels-Alder cycloaddition amongst other techniques [8]. Since 1964 when its structure was elucidated, TTX has received much attention from the synthetic community. Many synthetic efforts have been proved for the synthesis of TTX but, Kishi in 1972, synthesized the racemic tetrodotoxin and the unnatural analogue (-)-5,11-dideoxytetrodotoxin in 1999 [31] using analogues obtained from the first asymmetric total synthesis of tetrodotoxin in 2003 (Fig.2.1) [32]. Du Bois at Stanford University used C-H functionalisation reaction as key steps to report the asymmetric total synthesis of tetrodotoxin [33]. Sato at Kanagawa University investigated two total syntheses based on a sugar-based strategy of tetrodotoxin in a racemic and enantiomeric manner in 2005 and 2008 respectively [34-36].



Chapter 2: Analysis of tetrodotoxin

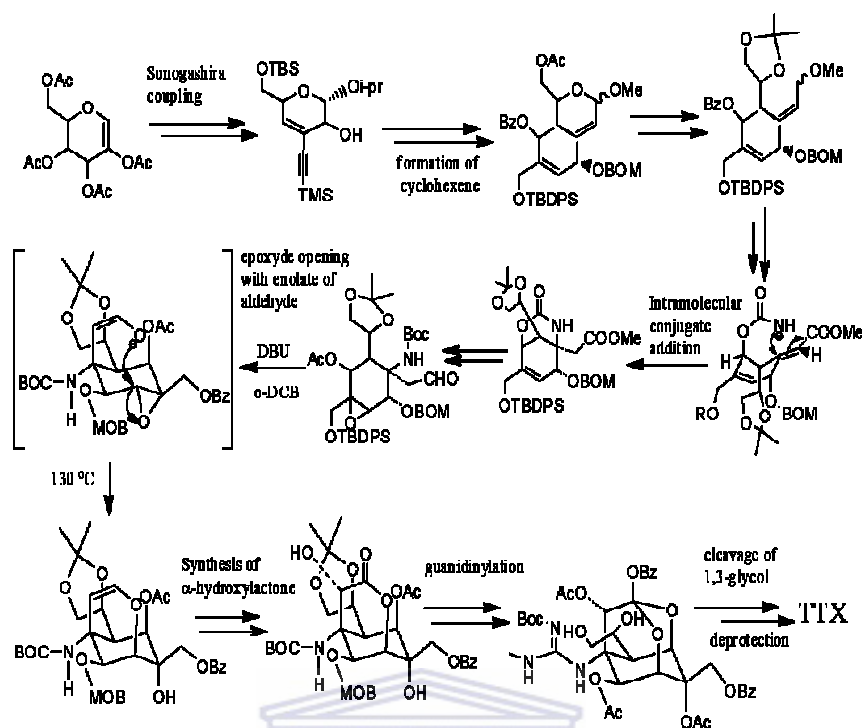


Figure 2.1: The first Asymmetric synthetic tetrodotoxin produced in a laboratory in 2003.[37]

2.3 Structure of tetrodotoxin

Tetrodotoxin as we mentioned above, is one of the most potent molecules that selectively blocks the voltage-sensitive sodium channels of excitable tissues. The structure of TTX is complex and contains an imidazole ring. The latter is likely the part of the molecule that lodges in the channel leaving the rest of the molecule blocking its outer mouth. Tetrodotoxin as said earlier on is one of the most potent neurotoxins and is known to block sodium ion channels responsible for nerve and muscle excitability [37]. The chemical structure of TTX has six hydroxyl residues at the C-4, C-6, C-8, C-9, C-10 and C-11 positions in addition to a guanidinium group (Fig.2.2), which is positively charged in the biological pH range. Although the hydroxyls at C-9 and C-10 are the most important,

Chapter 2: Analysis of tetrodotoxin

those at C-4, C-6 and C-11 also make significant contributions to the binding to the channel as hydrogen bond donors [38].

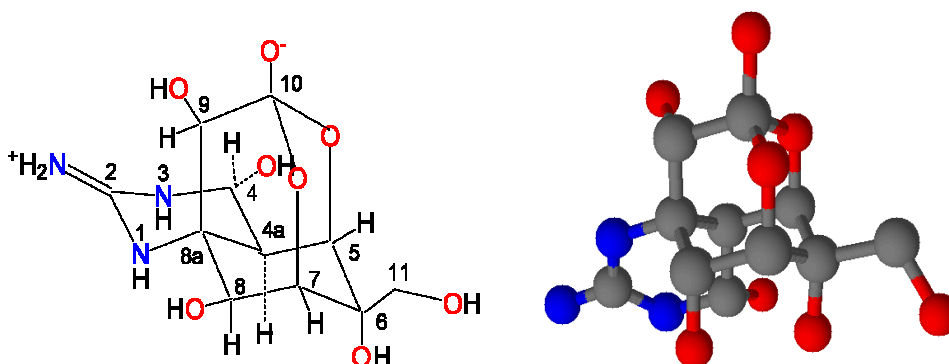


Figure 2.2: Chemical structure of tetrodotoxin (TTX).

The molecular structure of this alkaloid is relatively simple, forming a cyclic series of carbon atoms. The three nitrogen atoms make a positively charged guanidinium group (3 Nitrogen atoms) and the latter makes the molecule active. The resultant cation is stabilised by the resonance effect [8].

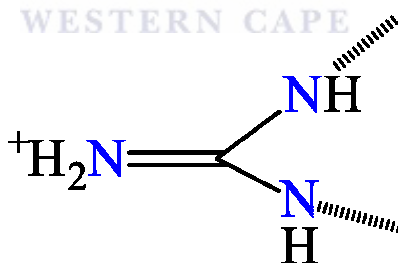


Figure 2.3: Guanidinium group.

Hydroxyl groups on the fused ring systems of the tetrodotoxin increase the stability and the ability of the toxin to react in an aqueous environment. Tetrodotoxin exists in an equilibrium mixture of its ortho ester, anhydride and lactone forms.

Chapter 2: Analysis of tetrodotoxin

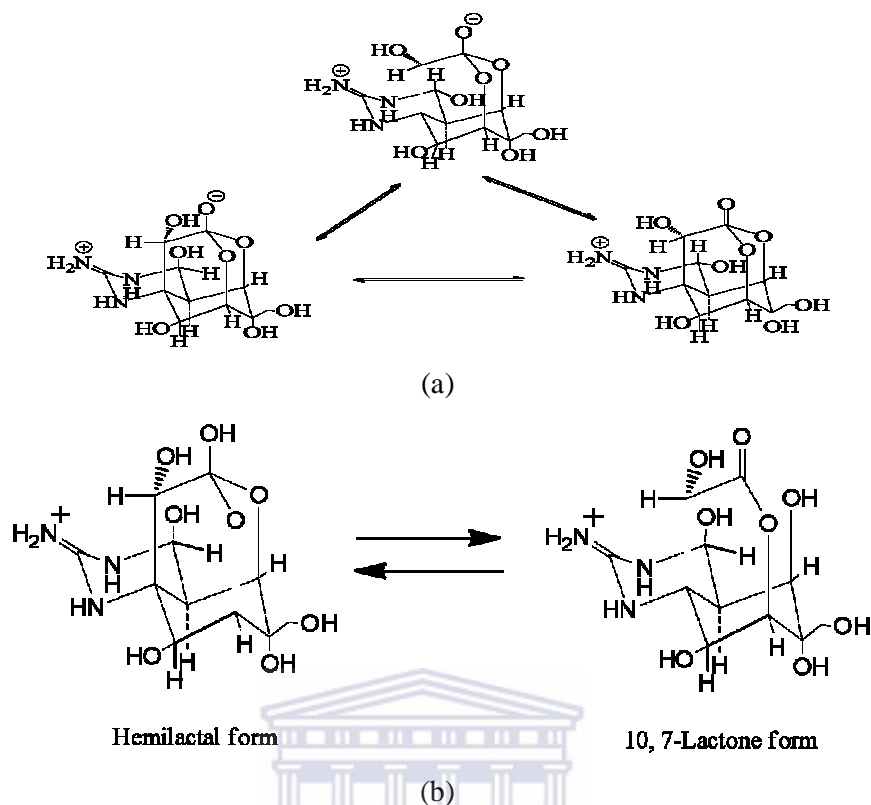


Figure 2.4: (a) Equilibrium mixture, (b) The tautomer of TTX.

In toxic puffer fish, TTX can co-exist with several of its analogues (Fig.2.5). Amongst them, 4-epiTTX and 4,9-anhydroTTX are the chemical equilibrium analogues of TTX [39]. Four deoxy analogues such as 5-deoxyTTX [40], 11-dexyTTX, [41] 6,11-dideoxyTTX [42], 5,6,11-trideoxyTTX [42] and two 11-nor analogues, 11-norTTX-6(R)-ol [43] and 11-norTTX-6(S)-ol [44], have also been isolated in the puffer fish and newts as the chemical non-equilibrium analogues.

Chapter 2: Analysis of tetrodotoxin

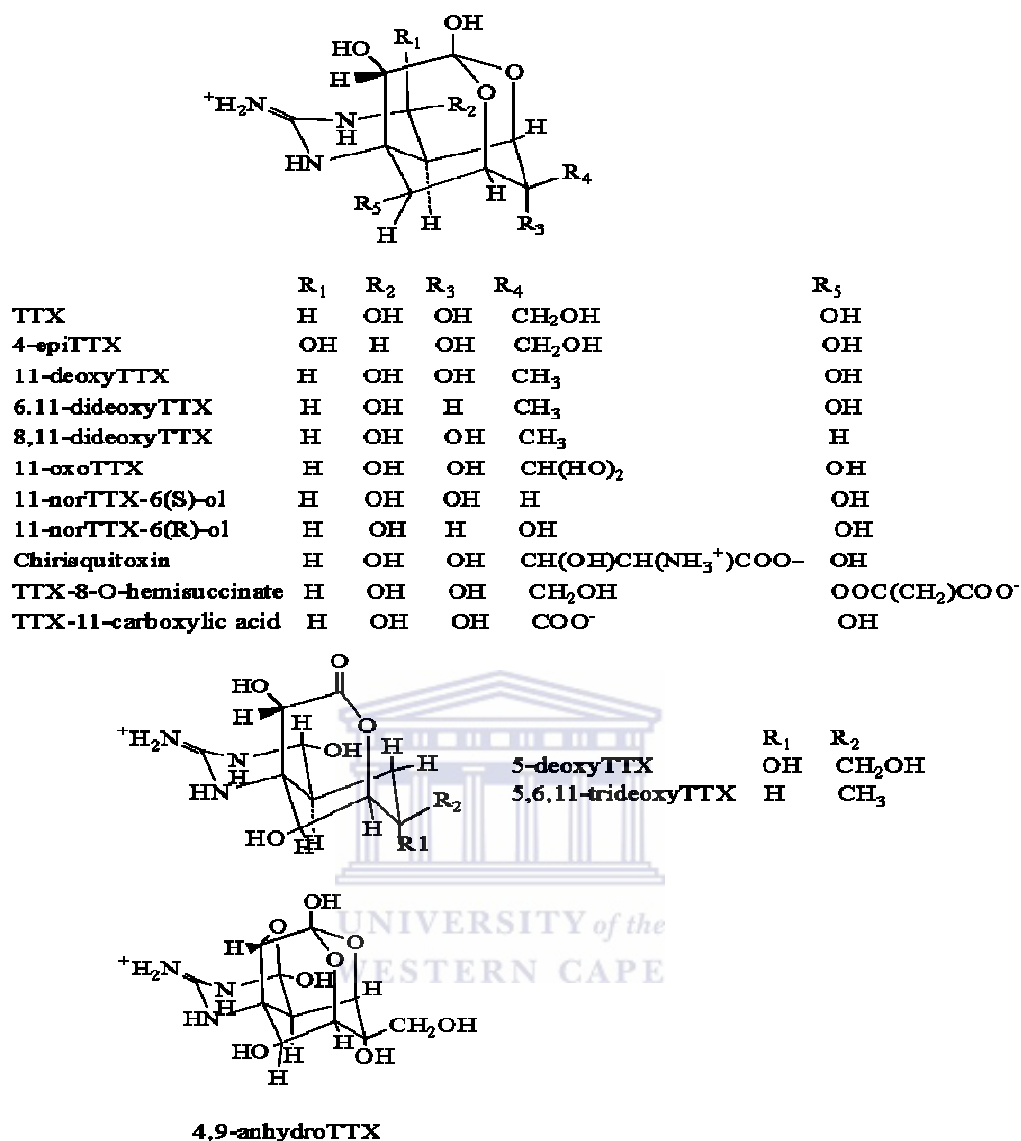


Figure 2.5: Chemical structures of TTX analogues.[39]

2.4 Chemical reaction of tetrodotoxin

Tetrodotoxin can be oxidized to give 11-oxo-TTX and the latter can be reduced to regenerate TTX [45]. During the oxidation reaction, the primary alcohol on C-11 was seen as a ready target for modification. Attempts at oxidizing this group ($-\text{CH}_2\text{OH}$) led to TTX, but a predicted aldehyde was never found.

Chapter 2: Analysis of tetrodotoxin

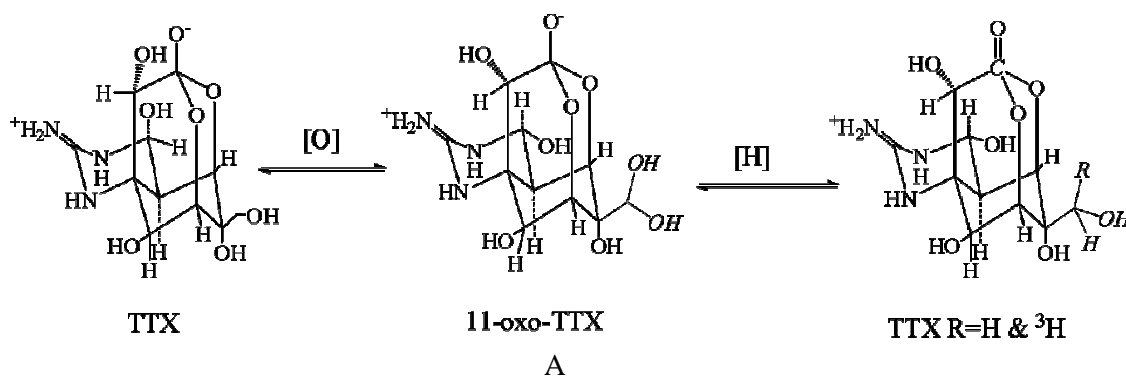


Figure 2.6: Chemical reaction of TTX.

2.5 Some physico-chemical properties of tetrodotoxin

Tetrodotoxin (Octahydro-12-(hydroxymethyl)-2-imino-5,9:7, 10a-dimethano-10aH-[1,3] dioxoci-no[6,5-d]pyrimidine-4,7,10,11,12-pentol, $C_{11}H_{17}N_3O_8$) is a low molecular weight, non-protein based small molecule with a unique cage structure. The toxin is odourless and stable by heating but unstable at pH levels above 8.5 and below 3.0.

Chapter 2: Analysis of tetrodotoxin

Table 2.1: Some physico-chemical properties of tetrodotoxin [8]

IUPAC name	Octahydro-12-(hydroxymethyl)-2-imino-5,9:7,10a-dimethano10aH-[1,3]dioxocino[6,5-d]pyrimidine-4,7,10,11,12-pentol
Empirical formula	C ₁₁ H ₁₇ N ₃ O ₈ , FW. 319.28 g.mol ⁻¹
Storage temperature	2-8 °C
Solubility	TTX can be soluble in water at neutral pH, in dilute acetic, dilute sulfuric acid and soluble in a dilute citrate but most soluble in water. It can be stored in citrate or acetate buffer for extended periods at -20°C without loss of efficacy.
Stability	TTX is unstable in strong acid, alkaline solutions, dilute hydrochloric and sulfuric acid, but it is relatively heat stable in neutral and organic acid solutions. It is rapidly destroyed by boiling at <i>pH</i> 2.
Pka	8.70
Boiling point	772.1°C
Melting point	Does not melt at 200°C, darkens and turns black with increasing temperature
Enthalpy of vaporization	128.15 KJ/mol
Form	powder
color	white
Toxicity (LD ₅₀)	mice (i.v.): 8.7µg kg ⁻¹ , mice (i.p.): 8 – 10 µg kg ⁻¹ , mice (s.c.): 11.5 µg kg ⁻¹

2.6 Analytical methods of detection of tetrodotoxin

Many diagnostic methods for quantifying [46], qualifying [47] and detecting [48-49] TTX have been investigated. The results of the investigation have been used to support clinical diagnoses of puffer fish poisoning toxins in Japan, Europe, Asia, Mexico, China and Australia. The standard mouse bioassay (MBA), receptor binding assay (RBA) and the mouse neuroblastoma cytotoxicity assay (MNCA) have been reported [50] and it is found that the standard/common method accepted worldwide for determining TTX toxicity in food matrices is the mouse bioassay [24]. Moreover, the use of an animal like the mouse for the experiment increases the resistance of the toxin.

Although several analytical methods for the analysis of TTX have been published: For quantitative analysis, gas chromatography-mass spectrometry (GC-MS) [51-52], immunoaffinity chromatography [52], high performance liquid chromatography with post-column derivatization and fluorescence detection (HPLC-FLD) [47], HPLC with ultra violet (UV) detection [53] and liquid chromatography-mass spectrometry (LC-MS) [54-55], most of them are for food tissue samples that were used. Unlike in food, the analysis of TTX in human urine and blood samples was analyzed by the mass spectrometry (MS) method because the amount of toxin is extremely low in the urine and blood of a patient [56].

In addition, the detection and qualification of TTX have been done through a biological test as an enzyme-linked immunosorbent assay (ELISA). Surface Plasmon resonance (SPR) biosensors were applied for detection using antibodies as a recognition element [57-58]. However, biological tests are not completely satisfactory due to their low sensitivity

Chapter 2: Analysis of tetrodotoxin

and the absence of specialized variations. It is also important to know that the bioassay is not relevant for analyzing TTX in a poisoned patient's urine or blood samples [56].

2.6.1 Spectroscopy techniques for tetrodotoxin analysis

2.6.1.1 Liquid chromatography-mass spectroscopy (LC-MS)

In 2001 in central Taiwan Strait, six fishermen developed the symptoms of tetrodotoxin which lead to one death after contracting food poisoning from an unknown fish on their boat. Without knowing what type of fish they had eaten, a new protocol of determination of TTX in the urine and blood of those victims was reported. The C18 Sep-Pak cartridge column with methanol as a solvent was used to extract the toxin from urine and blood samples. After cleaning the samples, the extract was filtered through a microcentrifuge filter and the filtrate was freeze-dried. The later was dissolved in distilled water and quantified by LC-MS with the recovery of 88.9% corresponding to the detection limit of 15.6 mM. This report had also proved the presence of TTX in the urine and blood of the victim with the linear curve obtained from the plot response again a concentration between 93.75 and 93.77 mM. In the blood, the range of TTX was 4.5 – 40.6 mM and 47–344 mM in the urine [54]. Hsiao-Chin *et al.* determined in 2008 the toxin in gastropod *Niothaclathrata* implicated food paralytic poisoning reported in Kaohsiung, Taiwan in 2006 [54]. The blood serum of the patient was analyzed using the LC-MS/MS method and the linearity in the serum was observed within a concentration ranged of 1 to 100 ng ml⁻¹. The limit of detection was evaluated to 0.1 ng ml⁻¹ and the limit of quantization (LOQ) was reproducible at 1000 µg ml⁻¹ in serum [54]. From the above reports, in 2001 and 2006,

Chapter 2: Analysis of tetrodotoxin

it appears that LC-MS/MS was lowering detectable for TTX determination than LC-MS. On the other hand, Horie *et al.* associated electrospray ionization-mass spectrometry with the liquid chromatography method to analyse the TTX in puffer fish. These authors extracted TTX in puffer fish using 0.1 % acetic acid by heating it in a boiling water bath and the extracts were cleaned up on a Bond Elut C18 (500 mg) cartridge. They determined that the detection limit of tetrodotoxin in puffer-fish was $1 \mu\text{g g}^{-1}$ [59]. At the same time, TTX in puffer fish tissues, in the serum and urine of humans poisoned after consuming puffer fish was also analyzed using the high-performance liquid chromatography with tandem mass spectrometry (LC/MS/MS). This method gave the detection limits of TTX was $0.01 \mu\text{g g}^{-1}$ in tissues of puffer fish and 0.1 ng ml^{-1} in human serum and urine. These authors extended the analysis to thirty samples of puffer-fish from wholesale markets, seven serum and five urine samples of humans poisoned after consuming puffer fish. The respective detection limit of TTX in all puffer fish tissues, all serum and urine samples at the which levels was equal to $40 - 140 \text{ ng ml}^{-1}$, $0.9 - 1.8 \text{ ng ml}^{-1}$ and $15 - 150 \text{ ng ml}^{-1}$ [60]. In addition, LC-MS method was used for the analysis of the chemically interchangeable analogues of TTX such as 4-epiTTX and 4, 9-an-hydroTTX. The analysis of TTX derivatives was done by optimizing the conditions for hydrophilic interaction liquid chromatography (HILC)-MS-MS to quantify TTX and its analogues via a good separation [59].

2.6.1.2 High performance liquid chromatography (HPLC)

Many works have been carried out on the determination of TTX with HPLC in gastropods, puffer fish and urine or blood serum [61]. Margaret *et al.* investigated the extraction or

Chapter 2: Analysis of tetrodotoxin

TTX in urine and serum samples using solid phase extraction cartridges from TTX-poisoned patients [62]. The TTX extraction sample was subsequently analysed by high performance liquid chromatography with post-column derivatisation and fluorescence detection. The quantity of TTX concentrations were 5 and 20 ng ml⁻¹ for serum and urine respectively. TTX was quantified in six samples of urine and six samples of serum from seven patients who ingested common toadfish and the standard curves were linear in the range of 20 – 300 ng ml⁻¹ for urine and 5 – 20 ng ml⁻¹ for serum [62]. Similarly, the urine and blood of six victims in Tungsha Island, Taiwan, in April 2004 who consumed both the digestive glands and muscles of the gastropod *Nassarius glans* in an incident of food paralytic poisoning were analysed. These tissues contained high concentrations of toxin and the quantitative analysis gives the highest toxicity scores at 2,048 and 2,992 MU g⁻¹ for glands and muscle respectively, based on the tetrodotoxin bioassay [63]. The purification of the toxin from these gastropods was done by HPLC, which revealed TTX and related analogue compounds 4-*epi* TTX and anhydro-TTX. Using liquid chromatography and mass spectrometry, this report obtained the detection limit for TTX to 1 ng ml⁻¹ with a linear range of 30 – 600 ng ml⁻¹ for urine and 1 – 30 ng ml⁻¹ for blood [64]. These previous works reviewed earlier shows that the urine of the victim of TTX-poisoning contains a higher concentration of toxin than the blood / serum. The HPLC is a simple and reproducible method but its limitation is that it is not portable and it is expensive.

Chapter 2: Analysis of tetrodotoxin

2.6.1.3 Solid-phase extraction (SPE) and gas chromatography/mass spectrometry (GC/MS)

This combination method has been used to determine tetrodotoxin in human plasma as well as in urine. The reference [65] described that using this GC/MS technique, TTX was first converted to 2-amino-6-hydroxymethyl-8-hydroxyquinazoline (C9-base) under alkaline conditions and extracted with the use of an OASIS HLB extraction cartridge. After the analysis of the C9-base the linear range was 0.5 – 10 ng ml⁻¹ and the detection limit was 100 µg ml⁻¹ [65]. The toxin from gastropods and the patient's blood serum was analyzed by a new developed method Solid-phase extraction and LC–MS/MS. The linear range determined was found within the concentration range of 1–100 ng ml⁻¹ and the limit of detection was 0.1 ng ml⁻¹ of TTX. The limit of quantification (LOQ) was reproducible at 1 ng ml⁻¹ in blood serum which showed that it contained TTX of 3.30 ± 0.08 ng ml⁻¹ [52]. Additional research was done on the double solid phase extraction (C18 and hydrophilic interaction liquid chromatography) by HPLC coupled with tandem mass spectrometry and was also used to determine TTX in urine and plasma matrices. This analysis has shown that the assay results were linear up to 500 ng ml⁻¹ for urine and 20 ng ml⁻¹ for plasma. The limit of detection and limit of quantification for both biological matrices were 0.13 ng ml⁻¹ and 2.5 ng ml⁻¹ respectively. The recoveries reported were in the range of 75 – 81 %. The analysis was extended to eight urine samples and seven plasma samples from eight patients suspected of having TTX poisoning. TTX was detected in all urine samples, with concentrations ranging from 17.6 – 460.5 ng ml⁻¹, but was not detected in any of the plasma samples [66].

Chapter 2: Analysis of tetrodotoxin

2.6.1.4 Proton nuclear magnetic resonance ($^1\text{H-NMR}$) spectroscopy of TTX

One of the techniques used to analyse TTX was $^1\text{H-NMR}$. Nowadays, many derivatives of TTX have been isolated [67] and their data have been reported using $^1\text{H-NMR}$ technique by various investigators [35, 68-69]. Yotsu-Yamashita *et al.* in 1995 carried out the $^1\text{H-NMR}$ method on 5 mg of TTX crystals dissolved in 0.5 ml of 1 % CD_3COOD in D_2O , which was placed in spectroscopy test tube [33]. Figure 2.7 shows the $^1\text{H-NMR}$ spectrum obtained with a 500 MHz JEOL JNM-500 spectrometer, using the methyl group protons of acetone as the internal standard [33]. Yotsu-Yamashita *et al.* reported that the $^1\text{H-NMR}$ spectrum presented a singlet at 2.20 ppm (CH_3COCH_3 formed in solution), a doublet centred at 2.33 ppm ($J = 10.0$ Hz), a large proton peak at 4.76 ppm (HDO) and a doublet centred at 5.48 ppm ($J = 10.0$ Hz) [42]. The pair of doublets around 2.33 and 5.48 ppm, which are the hallmarks of TTX and are assigned to H4a and H4 respectively, have been confirmed to be coupled with each other by double irradiation. These results agree well with the corresponding data of TTX. The signals at 4.24, 4.06, 4.28, 3.94, and 4.00/4.02 ppm are assigned to H5, H7, H8, H9, and H11 respectively [42].

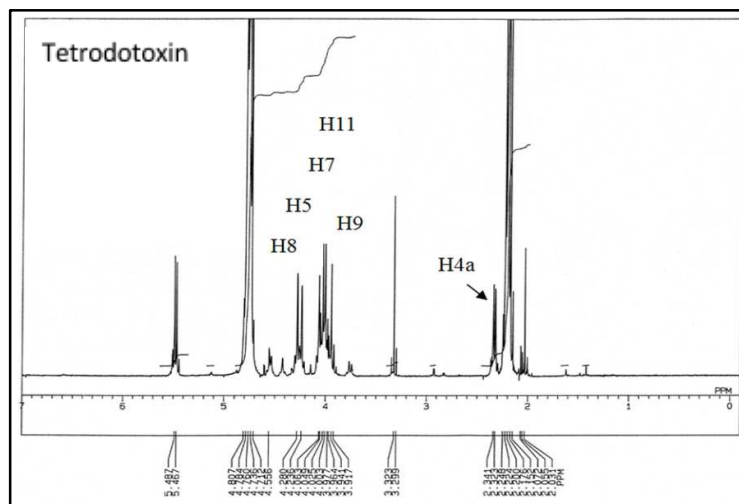


Figure 2.7: $^1\text{H-NMR}$ spectrum of tetrodotoxin.

Chapter 2: Analysis of tetrodotoxin

2.6.1.5 Fourier transform infrared spectroscopy (FT-IR) of TTX

The determination of functional groups in TTX was investigated by using FT-IR spectrometry which is the analytical technique for the determination of functional groups in the structure of compounds. Although the IR spectrum is a helpful tool to identify TTX in different species and is presumed to be complex. IR-spectra of KBr pellets were acquired using IR spectrophotometer, which was used on one hand by Asakawa *et al.* for determination of the IR spectrum of pufferfish toxin [70]. On the other hand, Tsuda *et al.* reported the IR spectrum of a TTX-HCl salt by the “Nujol” method [44]. A part of TTX synthesized crystals was analyzed by placing it on a small KBr plate and the IR spectrum was studied using a FT-IR spectrometer (Perkin Elmer, Spectrum 2000) equipped with an FT-IR microscope. Yotsu-Yamashita *et al.* discuss in Figure 2.2 the different absorption bands at 3353, 3235, 1688, 1612 and 1076 cm^{-1} were observed in the spectrum of TTX-HCl crystal [71]. They affirmed this spectrum as indistinguishable from that of the TTX they had reported on previously, showing characteristic absorptions for the functional groups OH, guanidinum, and COO- [71]. They also reported the absorption around 1700 cm^{-1} and in the range of 3600 – 4000 cm^{-1} was derived from H₂O in the air.

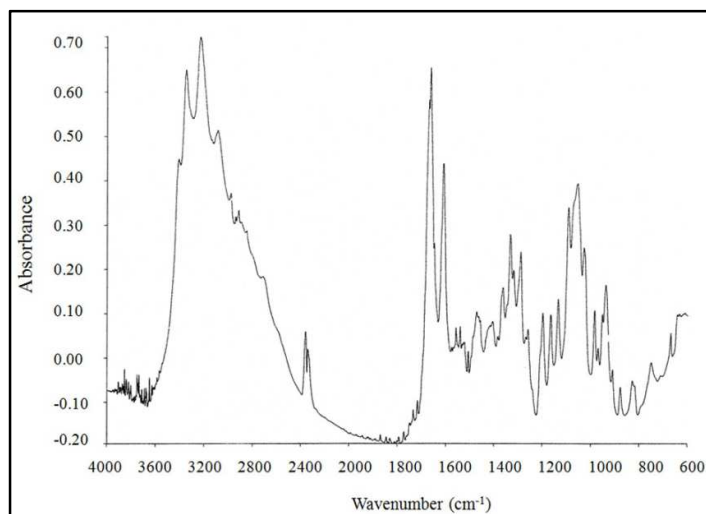


Figure 2.8: Infrared spectrum of tetrodotoxin.

2.6.1.6 Mass spectroscopy (MS) of TTX

Review of literature [8, 40] shows that the fragment ion spectrum of the molecular ion, MH^+ , for TTX (m/z 320) is obtained by the positive-ion ESI-MS/MS as shown in Figure.2.3. This result was compared with the one reported by Quilliam *et al.* [72] and it was almost identical to the ion-spray MS/MS of TTX. The spectrum presents the fragment ions due to the elimination of one or two water molecules. The minor ions at m/z 256 of TTX were probably generated with the loss of 28 mass units from the ion of $[MH-H_2O]^+$ or $[MH-2H_2O]^+$. This could be accounted by the elimination of CO at C10 as the result of the cleavage of the bonds between the C9 and C10, C10 and C5, C10 and C7, due to the α -hydroxy hemilactal structure. This explanation was supported by the fact that fragment ions similar to these were not detected on the spectra of the 10, 7-lactone-type analogues such as 5-deoxytetrodotoxin [70]. The intense fragment ions m/z 162 were shown on the spectra of TTX and because the generation of this ion did not depend on the structures of the substituent at C5, C6 and C10, the origin of this fragment ion was assumed to be a

Chapter 2: Analysis of tetrodotoxin

mixture of 2-aminohydroxyquinazolines [70] as the most probable fragment. These structures might occur due to the cleavage of the bonds between C8a and C9, and between C6 and C11, with the sequential elimination of water molecules. The origin of the fragment ion shown at m/z 178 corresponds to 2-aminodihydroxyquinazolines and 2-aminoquinazoline [70].

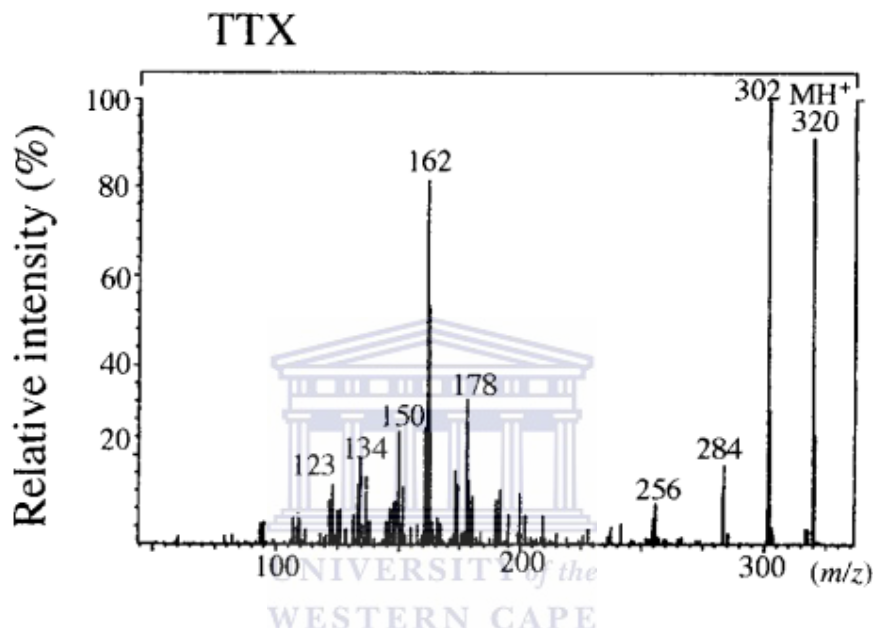


Figure 2.9: The fragment ion spectrum of MH^+ of TTX. Volume of 100 to 200 pmol of TTX was injected into 0.05 ml min^{-1} of aqueous 50 % MeOH (v/v). Argon at a target thickness, $1,5 \times 10^{14}$ molecules cm^{-2} ; collision energy, 49 eV. [70].

2.6.2 Immunoassay methods for tetrodotoxin analysis

2.6.2.1 Enzyme-linked immunosorbent assay (ELISA)

The direct competitive enzyme-linked immunosorbent assay (ELISA) kit was developed for detecting TTX. Neagu *et al.* used this technique to determine TTX and the method was adapted for an electrochemical assay device [73]. The antigen named alkaline phosphate

Chapter 2: Analysis of tetrodotoxin

(AP) was used and the conjugate (antibody) was synthesized in vitro. The dynamic range was 4 – 15 ng ml⁻¹ with a limit of detection of 2 ng ml⁻¹ ($R^2 = 0.9247$) for the spectrophotometric method, while the dynamic range was 2 – 50 ng ml⁻¹ and the LOD was 1 ng ml⁻¹ for the electrochemical protocol [73]. Wang *et al.* have been interested in the homogenization of the tissue samples of puffer fish where TTX was extracted with boiling 0.1 % acetic acid solution [74]. Then the water phase was diluted with 0.05 mol l⁻¹ phosphate buffer saline for ELISA determination. The results showed that the linear range of 0.1 – 1.0 mg ml⁻¹ was used and the minimum detectable concentration of tetrodotoxin was 1.0 mg ml⁻¹. The recovery rates from tetrodotoxin spiked samples used in this method were 73.8 % ~ 117.4 % [74]. On the other hand, tetrodotoxin was determined in a puffer fish sample using an anti-tetrodotoxin monoclonal antibody with the ELISA test by Rong *et al.* the range of standard curve was between 5 – 500 ng ml⁻¹ and the detection limit concentration of tetrodotoxin was 0.1 ng ml⁻¹. The TTX sample was spiked and the recoveries of the method were 73.0 % ~ 118.0 % [74]. A group of researchers investigated the analysis of 17 livers and 20 muscle samples of puffer fishes for the detection of the concentration of TTX using the mouse bioassay and indirect competitive inhibition enzyme-linked immunosorbent assay respectively. This research demonstrated that ELISA was remarkably correlated to mouse bioassay. It was also found that because of the easy-handle, rapid and highly sensitivity of the ELISA method, it is suitable for quantitatively detecting tetrodotoxin and effectively regulating poisonous puffer fishes [75]. Yu Zhou *et al.* in 2010 investigated the detection of tetrodotoxin in puffer fish using immunoassay based on a gold nanoparticle labelled monoclonal antibody (Mab) [76]. Two antibodies were relevant for the assay, the first one was as detector reagent supplied in sample pad and the second was as capture reagent immobilized on a diagnostic cellulose

Chapter 2: Analysis of tetrodotoxin

nitrate membrane. After the binding of immobilized TTX-BSA (bovine serum albumin) to a gold nanoparticle labelled Mab, the complex gold nanoparticle-Mab-TTX can be captured by the second antibody but cannot capture TTX-BSA. It was evaluated from the calibration curve that the concentration of TTX ranged from 40 – 8000 ng ml⁻¹ and the detection limit of TTX-spiked samples was equal to 40 ng ml⁻¹ with a very short time for detection, less than 10 minutes [76].

2.6.2.2 Surface plasmon resonance (SPR) sensor

Taylor *et al.* have developed the quantitative detection of TTX by an inhibition assay with a SPR sensor. They used a custom-built SPR sensor developed at the Institute of Photonics and Electronics, Academy of Sciences (Prague, Czech Republic). They reported the quantitative antibody-based detection of a low-molecular weight molecule, tetrodotoxin (TTX) (~319 Da) by an inhibition assay with a SPR sensor. The covalent binding method was used to immobilise the anti-TTX antibody on gold film with a mixed self-assembled monolayer (SAM) consisting of amine terminated oligo ethylene glycol (OEG) alkanethiol and a hydroxyl terminated OEG alkanethiol to develop a sensing surface of TTX. Both components of the mixed SAM contain ethylene glycol units used for this analysis minimized the non-specific protein adsorption [9, 77]. The amine groups on NH₂-OEG-AT can be functionalized by covalently linking TTX to the surface with formaldehyde [78]. These researchers found that from the calibration curves, two antibody concentrations incubated with samples of varying TTX concentrations ranging from 0.01 – 10 ng ml⁻¹. The detection limit for TTX was defined as IC₂₀ (20% inhibitory concentration), which was ~ 0.3 ng ml⁻¹. The corresponding calibration curve had a characteristic IC₅₀ (50%

Chapter 2: Analysis of tetrodotoxin

inhibitory concentration) of $\sim 6 \text{ ng ml}^{-1}$. They also showed that the TTX-immobilized surface which developed had the ability to be reproducibly regenerated [79].



Chapter 2: Analysis of tetrodotoxin

Table 2.2: Summary of different works done on analytical techniques for TTX detection

Method	Analytical column	Reagents	Sample	LOD [ng ml ⁻¹]	range [ng ml ⁻¹]	Refs
ELISA	-	-	Urine	N/A		
SPR	-	Amine terminated oligo-ethylene glycol (OEG) alkanethiol and a hydroxyl terminated OEG alkanethiol	Synthetic sample from Sankyo Co., Ltd. (Tokyo, Japan)	0.3	0.01 - 10,000	[80]
HPLC	ODS reversed-phase, YMC-pack ODS-Aq, YMC, 6.0 mm id x 300 mm	Heptafluorobutyric acid, sodium hydroxide	Urine	2	6 - 102	[81]
HPLC	Cosmosil 5C18-AR column, 250 x 4.6 mm	Heptanesulfonic acid, potassium phosphate buffer, sodium hydroxide	Gastropods and puffer fishes		10 - 2000	[82]
LC/ESI-MS/MS	HILIC (phosphorylcholine hydrophilic interaction liquid chromatography) column (150 mm ×	Methanol, acetic acid, acetonitrile	Blood/serum	0.32	2 - 1200	[81]

Chapter 2: Analysis of tetrodotoxin

Table 2.2: Summary of different works done on analytical techniques for TTX detection

Method	Analytical column	Reagents	Sample	LOD	range	Refs
				[ng ml ⁻¹]	[ng ml ⁻¹]	
LC-UV	Allsphere ODS-2, 5 μm, 250 x 4.6 mm	1-heptanesulfonic acid sodium salt monohydrate, sodium dihydrogen phosphate anhydrous, methanol	Urine	10		[83]
LC-FLD	Nova-pack C18, 4 μm, 100 x 8 mm	Hetonitrileptanesulfonic acid, ace	Urine and serum	u: 20; s: 5		[47]
GC-MS	DB-5 fusedsilica capillary colum, 30 m x 0.25 mm i.d.film thickness 5	-	Urine and serum	u: 0.5, s:1		[84]
LC-MS/MS	Atlantics dCl18, 5 μm, 150 x 2.1 mm	Heptanesulfonic acid, ammonium formate with formic acid, acetonitrile	Urine	0.13		[85]
LC-MS	Zorax 300SB-C3, 150 x 4.6 mm	Trimethylamine, ammonium formate, acetonitrile	Urine	4.97		[54]
LC-MS/MS	Zorbax 300SB-C3, 150 x 4,6 mm	Trimethylamine, ammonium formate, acetonitrile	Urine	1		[86]

2.7 Conclusion

As earlier highlighted tetrodotoxin is one of the most potent nonpeptidic neurotoxins because of its frequent involvement in fatal food poisoning, its unique chemical structure, and its specific action of blocking the sodium channels of excitable membranes. The flow of sodium ions into nerve cells is a necessary step in the conduction of nerve impulses in excitable nerve fibres and along axons. The victim of TTX poisoning is paralyzed and death can follow almost immediately. The minimum lethal dose in humans for tetrodotoxin is estimated to be 1-2 mg [10] and the minimum dose necessary to cause symptoms has been estimated to be 0.2 mg. From the various statistics reported in different countries, TTX generates interest in many research areas. Several researchers have investigated the quantification (determination) of TTX using HPLC, ¹H-NMR, FT-IR, MS/MS, LC/MS, LC/ESI-MS and the qualification (detection) using several analytical techniques such as LC-FLD, ELISA and SRP [70]. Amongst these analyses, it was found that, no electrochemical technique has ever been used to analyze TTX. Indeed, this being one of our first motivations, this research study will therefore be investigating for the first time the detection of TTX using unique techniques involving electrochemical analysis such as CV, SWV and EIS based on electrochemical biosensors. The next chapter (chapter 3) discusses a literature review of the electroactive compounds and the biomolecules needed for developing the electrochemical platforms which will be employed to achieve set objectives.

DOPED POLYANILINE FILMS ELECTROCHEMICAL ACTIVITIES AND REDOX PROBE APPLICATION

3.0 Introduction

Since the discovery of conducting polymer in the mid 1970's, the study of these materials has been a hot research area for many academic institutions. The conducting electroactive polymers (CEPs) such as polyaniline, polypyrrole, polythiophene, and polyacetylene are classified as electronic polymers which are driven by electric field or coulomb forces or ionic CEPs which change shape by mobility or diffusion of ions and their conjugated substances. A varied domain of applications of CEPs has been reported in electrochemical sensors and biosensors [87], actuators, artificial muscles [88], corrosion control [89-90] and batteries [91]. In the field of the sensor as an application, the CEPs provide a means for the direct or indirect entrapment of the specific agent as enzyme, antibody, ionophore and aptamer. Indeed, ionophores are chemical compounds that bind to a particular ion, shielding its charge from the surrounding environment and thus facilitating its crossing of the hydrophobic interior of the lipid membrane.

This work is based on the development of the electrochemical sensor of tetrodotoxin by modifying the electrode surface with electronic electroactive polymers using the immobilising agent to develop an electrochemical platform for detecting the tetrodotoxin.

Chapter 3: Doped polyaniline films electrochemical activity and redox probe application

Indeed, the electroactive polymers are used in electrochemical sensors and biosensors to enable the immobilisation of a specific agent or biomolecule (antibody, aptamer, enzyme, ionophores) on the electrode surface. The focus of this chapter however is on the study of electroactive undoped and doped polyaniline films and their application in sensors and biosensors based on ionophores and aptamer respectively.

3.1 Electrochemistry of conducting electroactive thin films polymers

3.1.1 Conducting electroactive polymers

Conducting polymers (CPs) are large organics conjugated electroactive polymers, capable of undergoing oxidation/reduction themselves [92]. We generally distinguish four groups of polymers. The first and most widely used commercial conducting polymers are composites in which an originally non-conducting polymer matrix is filled with a powdered conductive medium such as carbon or metal to give rise to its conductivity. Applications for such composites are varied and could be used for solder substitutes and antiseptics. The second group of polymers is called ionically conducting polymers. Here, electrical conductivity is as a result of the movement of ions. An example of such a polymer is polyethylene oxide, in which lithium ions are mobile. These kinds of polymers find various applications in industry and medicine [93], artificial muscles and robotics [94]. The third group of polymers is called redox polymers. These contain immobilized redox centres (electroactive centres). These centres are in contact with one another, but can conduct charge by electron transfer from one centre to another via a “hopping” mechanism [95]. In this mechanism, electrons transfer from one redox centre to another through an

Chapter 3: Doped polyaniline films electrochemical activity and redox probe application

insulating barrier. Due to this mechanism, redox polymers have been shown to be the most effective mediators in amperometric biosensors [95]. The fourth group is conjugated polymers which are polymers that consist of alternating single and double bonds, creating an extended π -network. They have attracted a great deal of attention lately, as materials for possible applications in micro-electronic devices, analytical chemistry and biosensor devices [96]. A simple model of the charge transfer and transport processes in a polymer film electrode is shown in Figure 3.1.

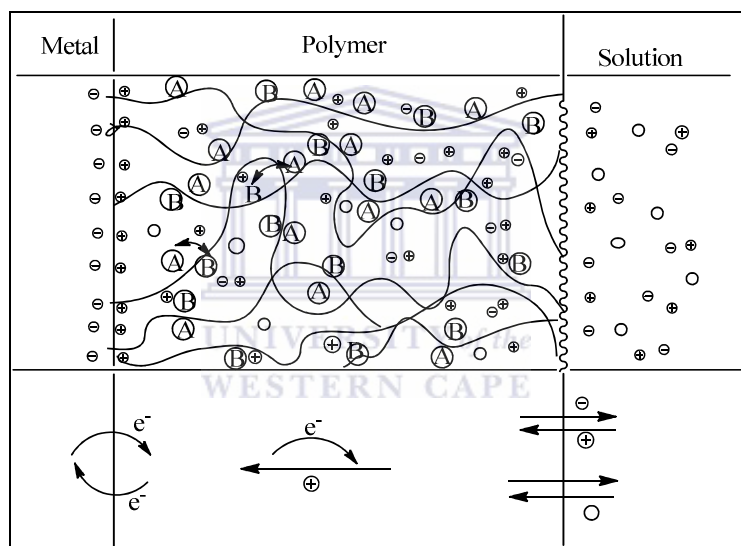


Figure 3.1: A schematic picture of a polymer film electrode.

In an electrochemical experiment, electron transfer occurs at the metal|polymer interface that initiates the electron propagation through the film via an electron exchange reaction between redox couples A and B via electronic conduction by the polymer backbone ie when the polymer reacts with an oxidant or reductant (added to the solution), the electron transfer starts at the polymer|solution interface. Ion-exchange processes take place at the

Chapter 3: Doped polyaniline films electrochemical activity and redox probe application

polymer|solution interface; in the simplest case, counter ions enter the film and compensate for the excess charge of the polymer. Neutral (solvent) molecules (O) may also be incorporated into the film (resulting in swelling) or may leave the polymer layer.

Since the discovery of polythiazyl, the first conjugated polymer [97], the idea of using polymers for their electrical conducting properties has generated much interest. Electron movement within this π -framework is the source of conductivity. The model of conductivity in a polymer is translated from the reduced to oxidised form. This means that, electrons move from cathode to anode, so the polymer obtained in the oxidised form is more conducted than the one obtained in the reduced form. For example, with polyanilines as shown in Figure 3.4, the pernigraniline, which is fully oxidised, is more conducting than the leucoemeraldine which is fully reduced. Other conducting polymers containing conjugated π bonds such as polyaniline (PANI), polypyrrole (PPY), polythiophene (PT), polyfuran (PFU), poly(*p*-phenylene) (PPN) and polycarbazole (PCB), have been synthesised for possible applications [98-99]. Amongst all the conducting polymers stated above, this study is focused on polyanilines because of their properties and application in electrochemical sensors. Polymers have been used to immobilize biomolecule onto the electrode surface almost from the birth of biosensor research, but recently they have been used to fulfil a number of diverse roles. A large number of polymers have been used in the production of biomolecule sensors especially polymers that are capable of electrochemical polymerisation. For electrochemical sensors as said earlier, the polymer can be doped to increase its stability and the conductivity [100] when the polymer is studied in an alkaline medium.

Chapter 3: Doped polyaniline films electrochemical activity and redox probe application

Table 3.1: Some example of conducting polymers [101]

Structure	Name	Structure	Name	Structure	Name	Structure	Name
	Polyacetylene (PAC)		Poly(para-phenylene) (PPP)		poly(Thienylene-Vinylene) (PTV)		Polycarbazole
	Polypyrrole (PPy)		Poly(phenylene ethynylene) (PPE)		Poly(Furylene vinylene) (PFV)		Poly(thieno[3,2-b]pyrrole)
	polythiophene (PTh)		Poly(phenylene sulfide) (PPS)		Polyaniline (Pan)		Poly(thieno[3,2-b]thiophene)
	Poly(ethylene dioxythiophene) (PEDOT)		Poly(phenylene ethynylene) (PPE)		Polydiphenylamine		Poly(fluorene)
	polyselenophene (X=Se) Polyfuran (X=O)		Poly(indole)		Polypyridine		Polycarbazole

Chapter 3: Doped polyaniline films electrochemical activity and redox probe application

3.1.2 The concept of doping

Doping is the process of introducing a controlled quantity of impurities (non-stoichiometric) into a semiconductor material to enhance the electronic, magnetic, optical and structural properties [100] of the polymer. Conjugated polymers can be oxidised or reduced chemically or electrochemically, accompanied by an insertion of counter-ions. Conducting polymers can be doped by adding chemical reactants to oxidise or to reduce the system so that electrons are pushed into the conducting orbital within the already potentially conducting system. There are two primary methods of doping a conductive polymer, both of which use a redox process (oxidation-reduction).

1. Chemical doping which involves exposing the polymer (thin film) to an oxidant such as iodine or bromine. Alternatively, the polymer can be exposed to a reductant; this method is far less common and typically involves alkali metals.
2. Electrochemical doping involves suspending a polymer film on the working metal electrode in an electrolyte solution in which the polymer is insoluble along with separate counter and reference electrode. An electric potential difference is created between the electrode that causes a charge and the appropriate counter ion from the electrolyte to enter the polymer in the form of electron addition (i.e. n-doping) or removal (i.e. p-doping).

An electron-rich, n-doped polymer will react immediately with elemental oxygen to dedope the polymer (i.e. reoxidise to the neutral state). Thus, chemical n-doping must be performed in an environment of inert gas such as argon. Electrochemical n-doping is far more common in research, because it is easier to exclude oxygen from a solvent in a sealed

Chapter 3: Doped polyaniline films electrochemical activity and redox probe application

flask. Oxidative doping refers to the partial oxidation of the organic polymer π -backbone through the interaction between the polymer and the p-type dopant. The flow of electrons from the valence band to the acceptor dopant leads to the delocalisation of holes within the polymer backbone which enhances the conductivity of the polymer [102]. On the contrary, during reductive doping (n-type), there is a partial introduction of mobile electrons into the π system. The illustration of the concept of n- and p-doping is as follows:

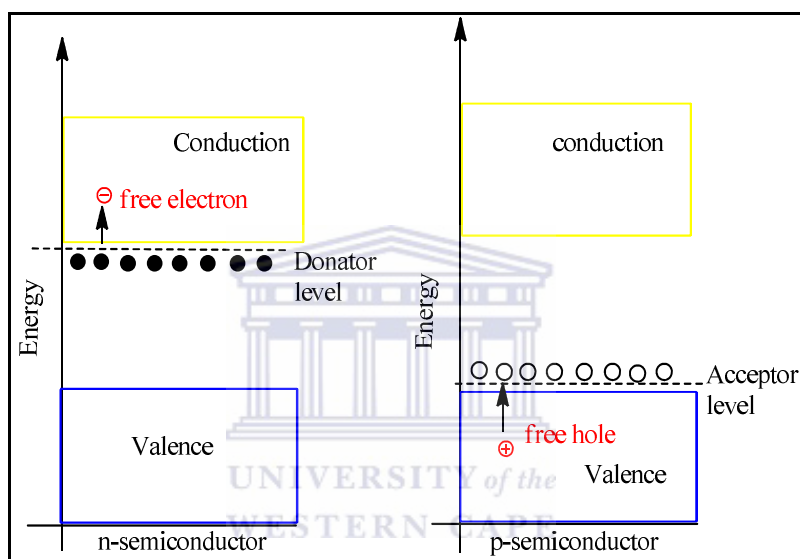
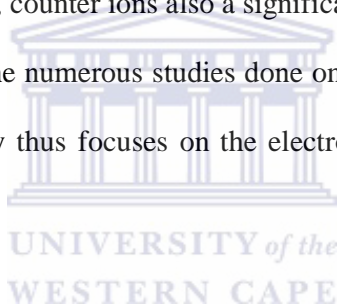


Figure 3.2: Schematic representation of n and p- doping processes respectively [102]

Numerous studies had been performed to dope PANI and its derivatives with various dopants to enhance their stability and conductivity [103]. Indeed, Yanyan and Kalle have doped PANI with different dopants such as hydrochloric acid, perchloric acid, sulfuric acid, methanesulfonic acid, benzene sulfonic acid, p-toluenesulfonic acid, poly(4-styrenesulfonic acid) (PSSA), poly(vinylsulfonic acid), poly (acrylic acid) and poly(anilinesulfonic acid) for studies in alkaline and neutral media [103]. These authors reported that the stabilizing effect dopants have on polymers as it increases with the large

Chapter 3: Doped polyaniline films electrochemical activity and redox probe application

macromolecular counter ions. It was also demonstrated that amongst these dopants, PSSA was the one that can effectively enhance the electroactivity of PANI in neutral and alkaline media. Elsewhere, the PANI was doped with different anions including the chloride, methane sulphonic acid, benzene sulphonic acid and dibenzenesulphonic acid, this time to study the effect of pH composite [104]. Not only PANI can be doped, but its derivatives as well. PANI derivatives like poly-N-methylaniline, poly-o-methoxyaniline and poly-2,5-dimethoxyaniline separately doped with PSSA, naphthalenesulphonic acid and anthracene sulfonic acid and the polymer composites have been applied on the detection of diazinon [102]. The importance of doping is that besides the enhancement of conductivity and electroactivity of the polymer, counter ions also a significant effect on polymer growth rate and redox behaviour. From the numerous studies done on the doping process as presented earlier on, this research study thus focuses on the electrochemical doping of PSSA with PANI.



3.1.3 Polyaniline and its derivatives

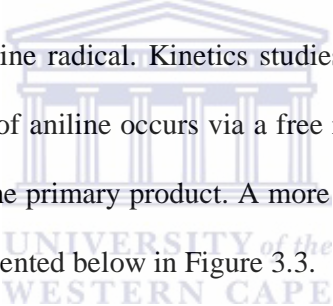
Polyaniline is a special of kind of conducting electroactive organic polymer which shows many interesting properties such as electrochemical redox behavior, electrochromic [105] and catalytic activities [106-108]. The specificity of the PANI is that besides redox doping it also undergoes protonic doping. Protonic doping differs from redox doping in that in the former case, the number of electrons associated with polymer backbone does not change during the doping process but instead a re-arrangement of the polymer energy levels occurs [109]. Protonic doping in polyaniline has been achieved through the protonation of imine nitrogens of the polyleucoemeraldine (PLE) form of PANI using strong acids [110].

Chapter 3: Doped polyaniline films electrochemical activity and redox probe application

This leads to the production of a highly conductive, delocalised, stable polysemiquinone radical cation and the PANI polyemeraldine salt form (PES) [104, 109].

3.1.4 Synthesis of polyaniline

Two common methods have been used for the synthesis of polyaniline. The aniline monomer can be polymerised chemically (chemical synthesis) or electrochemically (electrochemical synthesis) to prepare the powder or the films polyaniline respectively [102, 111-112]. As early as in 1962, Mohilner *et al.* [92] investigated the kinetics of the electrochemical oxidation of aniline in sulfuric acid and deduced that the initial oxidation requires the formation of aniline radical. Kinetics studies led Mohilner *et al.* [92] to the conclusion that the oxidation of aniline occurs via a free radical mechanism that produces the emeraldine (octamer) as the primary product. A more detailed mechanism as proposed by Wei and co-workers is presented below in Figure 3.3.



Chapter 3: Doped polyaniline films electrochemical activity and redox probe application

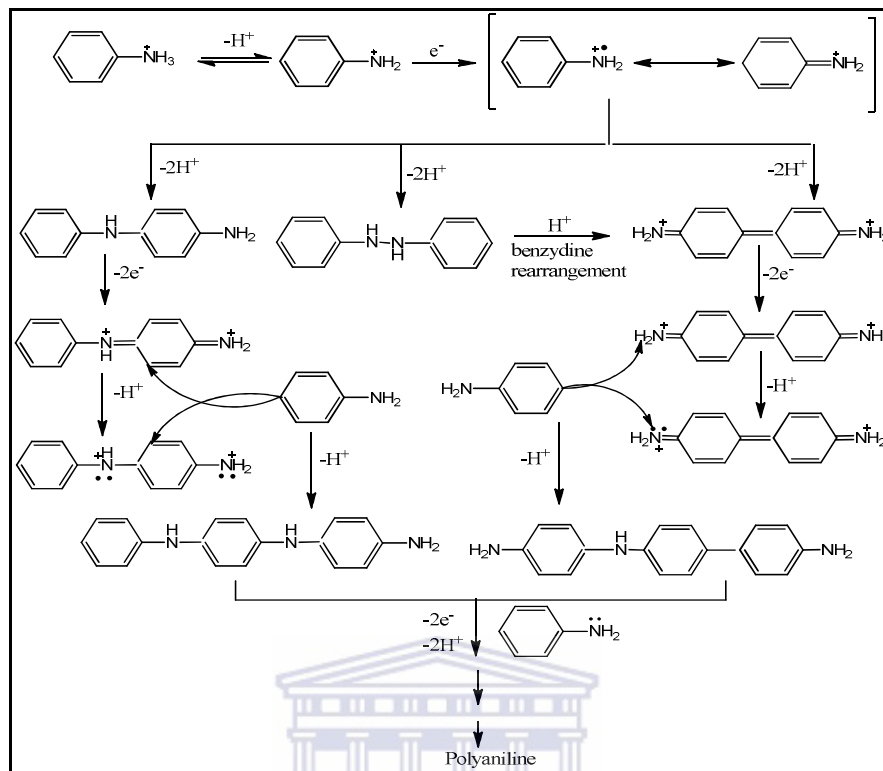


Figure 3.3: Mechanism of polymerisation of aniline [92]

3.1.4.1 Chemical synthesis of polyanilines

The chemical oxidation polymerisation process is particularly important because this synthesis is the most feasible method for producing PANI powder on a large scale. The chemical synthesis entails the oxidative polymerisation of the requisite monomers in an acidic media using strong oxidants such as ammonium persulfate or sodium metavanadate [113], ammonium peroxydisulfate [114], potassium persulfate or dichromate and ferric ions or hydrogen peroxide in the presence or absence of templates. These oxidants in solution oxidise the monomers creating the electron deficient site with chemically active cationic radicals of the respective monomers. Then, the cationic radicals formed react with

Chapter 3: Doped polyaniline films electrochemical activity and redox probe application

more monomer molecules yielding oligomers or insoluble polymers [102]. The polymerisation occurs in the bulk during the chemical synthesis and the resultant polymers precipitate as insoluble solids.

3.1.4.2 Electrochemical synthesis of polyaniline

Electrochemical polymerisation also called electropolymerisation is a typical method generally used for the synthesis of PANI coating because of its simplicity and reproducibility. In general, this method consists of applying an opportune potential to a working electrode immersed in an electrolyte solution. The monomer is thus electrochemically oxidised and polymerisation occurs at the electrode surface with deposition of the polymer film. Since then the nature of the intermediates of PANI synthesis have been proposed based on cyclic voltammograms. The first stage of the PANI synthesis was found to be the formation of $C_6H_5-NH_2^+$ cation radical through the transfer of an electron from a sp^3 orbital of nitrogen atom to the electrode during electrochemical oxidation. During polymerisation, the PANI chain propagation starts with the formation of non-conducting PANI, leucoemeraldine (oxidation state $n = 1$) complete reduction state and terminates with the formation of the most conductive PANI form, the emeraldine ($n = 0.5$) oxidation state. In some cases, when using this method, the intermediate process occurs, and it forms the pernigraniline ($n = 0$) fully oxidized state. This can be illustrated by Figure 3.4 [115]

Chapter 3: Doped polyaniline films electrochemical activity and redox probe application

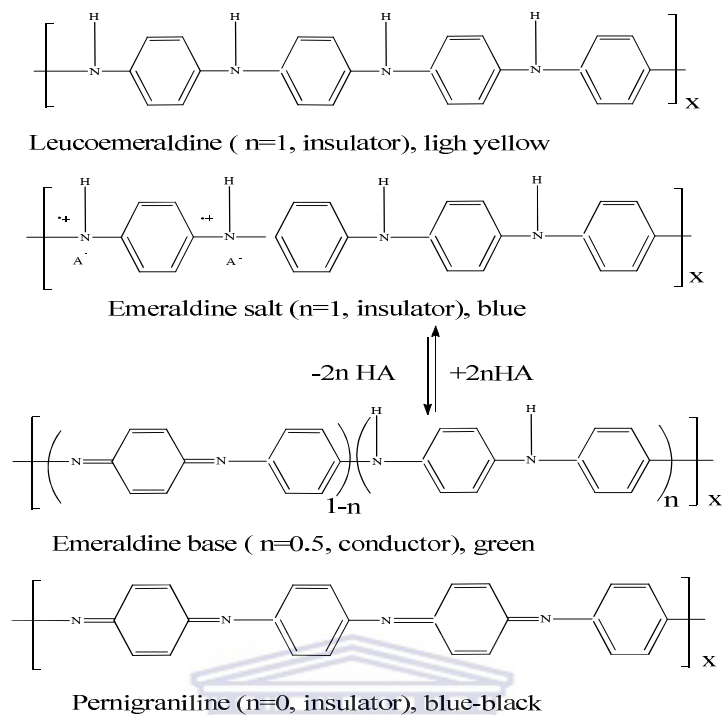


Figure 3.4: Chain propagation state of aniline.

This technique presents many advantages over the more traditional dip-coating procedures such as greater simplicity, reproducibility, completed coverage of the active surface, greater control over film thickness and perhaps provide a means for the entrapment of both the specific agent and a suitable mediator. One of the advantages of electrochemical polymerisation is that the reactions can be carried out at room temperature by varying either the potential or current with time to control the thickness of the film. Moreover, electropolymerisation is a cheap technique and polymerisation media can be used repeatedly. On the other hand, the possibility of a polymer film formation directly on the electrode surface is also a big advantage. Most electrochemical syntheses proceed through radical coupling polymerisations, while chemical syntheses are condensation polymerisations. Condensation polymerisation generally involves loss or elimination of a

Chapter 3: Doped polyaniline films electrochemical activity and redox probe application

chemical species resulting from the reaction of end groups on monomer molecules. The electrochemical synthesis, which is used in this study, is a more preferred method due to its reproducibility and simplicity. Polyaniline films are obtained by electrochemical deposition onto certain surfaces. This deposition leads to the preparation of thin films or thick films at a well-defined redox potential in the presence of a given counter ion, which in turn defines the level and characteristics of the doping reaction [116-119]. For electrochemical methods, potentiostatic, galvanostatic and potential sweep methods are usually used for electropolymerisation of PANI and its derivatives. Standard electrochemical techniques, which employ a divided cell containing a working electrode, a counter electrode and a reference electrode generally, produce the required films. The commonly used working electrodes are conducting substrates such as gold, carbon, platinum and indium-tin oxide coated glass plates. Semi-conducting materials including n-doped silicon, gallium arsenide, cadmium sulphide and semi-metal graphite, are also employed for the growth of polymer films. It is important to remember that many CPs synthesised by electrochemical methods are oligomers, with chain lengths ranging from about eight monomer units to 50 units, which is much less than the typically portrayed 100,000 units of some anilines [92].

3.1.4.3 Medium of polymerization

The synthesis of PANI is performed generally in aqueous acid solutions [120] and neutral aqueous media [121], either chemically or electrochemically. But in the case of organic media, it was considered that good quality of PANI films cannot be obtained. The properties and several applications of PANI obtained depend on synthesis parameters such

Chapter 3: Doped polyaniline films electrochemical activity and redox probe application

as the technique of electrosynthesis and the composition of the polymerisation solution. Examples of electrolytes which have been used to this end include aqueous acids [122-124] (hydrochloric acid, sulfuric acid, oxalic acid, nitric acid) and salts [125-129] (copper (II) nitrate, sodium sulfate, sodium sulfate/sodium perchlorate, lithium perchlorate), organic [130-131] electrolytes (tetramethylammonium trifluoromethane-sulfonate /acetonitrile, periodic acid/tetraethylammonium tetrafluoroborate/acetonitrile, trichloromethane, tetrabutylammonium perchlorate/acetonitrile, perchloric acid/benzenesulfonic acids), ionic liquids [132-135] (1-methyl-3-butylimidazolium tetrafluoroborate) and fluoride medium (ammonium fluoride, hydrofluoric Acid) [136].

From these previous studies done on the synthesis of polyaniline in different media, some of them have shown that the medium of the polymerisation affects the properties of the polyaniline. The yield and electrical conductivity of emeraldine salt-form PANI prepared in acid medium is increased by decreasing the ionic strength of the acid [111]. The stability of polyaniline is an important property in most of its applications and can be accessed from various viewpoints [137]. However, Brozova *et al.* investigated the stability of chemical synthesised PANI in a strongly alkaline and acidic aqueous medium and it was found that PANI is more stable in alkaline medium than acidic medium at the temperature range of 250 – 350 °C [138]. On the other hand, this research study intends to prove that PANI can be electrochemically synthesised on a precious metal system in an organic medium (Perchloric acid/acetonitrile), possess a higher stability at room temperature and does not deteriorate on scanning and will therefore find applications in electrochromic tetrodotxin devices.

Chapter 3: Doped polyaniline films electrochemical activity and redox probe application

3.1.4.4 Properties and application of conducting electroactive thin films polymers

Nowadays, conducting polymers are synthesised in the form of nanomaterials. These nanomaterials have the properties of polymeric materials with high strength, flexibility, elasticity, stability and ease of handling. These physical properties give a particular interest to conducting polymers which significantly change as compared to the properties of their bulk counterpart. For the usual electronic properties like electrical conductivity, this is due to the π -conjugated electron contained in conducting polymers chain. The conductivity properties are responsible to low energy optical transitions, low ionisation potential and high electron affinity. This property results in conducting polymers to be employed as charge storage materials for rechargeable batteries and used in the fabrication of biosensors in various fields such as

- Healthcare which is applied in medical diagnosis (glucose, fructose, lactate, ethanol, cholesterol, urea etc.)
- Immunosensors that can be used in medical diagnostics and environmental sensors
- DNA sensors for the detection of various genetic disorders.
- Environmental monitoring for quality control of pollution and detection of hazardous chemicals in biosensors (polyphenols, sulfites, peroxides, formaldehyde etc.)
- Food analysis for detecting the glucose, fructose, ethanol, sucrose, lactate, malate, galactose, citrate, lactose, urea and starch in food industries.

Conducting electroactive polymers have received considerable attention from both academia and industry because of their many potential applications such as artificial

Chapter 3: Doped polyaniline films electrochemical activity and redox probe application

muscles and sensors [139]. The application of conducting polymers to electrochemical biosensors is mainly based on the idea that they can improve direct electron transport between oxidoreductase enzymes and electrode surface in amperometric biosensors [140]. Regarding these properties and the application of conductive electroactive polymers, an increasing number of academics, governmental and industrial laboratories throughout the world that are involved in basic research show that this area is interdisciplinary in nature. The aim of the present research is to exploit the stability and the conductivity properties of conducting electroactive polyaniline as a probe to develop the electrochemical sensor and biosensor for the detection of tetrodotoxin. One of the motivations is to choose the a conducting polymer to construct novel sensor that improves the detection limit and smaller potential drift [141].

3.2 Molecular recognition elements and their application in sensors and biosensors

3.2.1 Neutral ionophore compounds

Ionophores are a type of chemical compound which can be called ion carriers because of the capability of binding ions reversibly and transporting them across organic membranes by carrier translocation. They are lipophilic complexing agents [142]. Since the late 1960's, a large number of electrically neutral carriers with high selectivity for specific cations have been developed and have found applications in potentiometric sensors (ion-selective electrodes (ISE)) or in optical sensors (ion-selective optodes) for the measurement of the respective ion activities in different sample environments [80].

Chapter 3: Doped polyaniline films electrochemical activity and redox probe application

Ionophores have been shown to form inclusion complexes with different ion molecules in various environments [143]. Their functions as ion carriers for active substances have important applications in biology, drug research, electrochemistry and the food industry.

Lipophilicity of ionophores: The lifetime of a chemical sensor based on a carrier doped solvent polymeric membrane is limited by substantial and irreversible changes in the membrane composition. To assure reproducible sensor behaviour, all the membrane components have to be confined to the membrane phase over an analytically relevant time period. Depending on the geometry of the sensor, the type of sample and the technique of sensor use, widely different lipophilicities.

3.2.2 Ionophore exchange kinetics

The ionophores should form relatively stable complexes with the primary ion I (ion I to be sensed with high selectivity) but on the other hand, the exchange reaction of the selected ions at the membrane/solution interface must be sufficiently reversible. Therefore, the free energy of activation of the ligand exchange reaction can be represented by the Equation 3.1 below

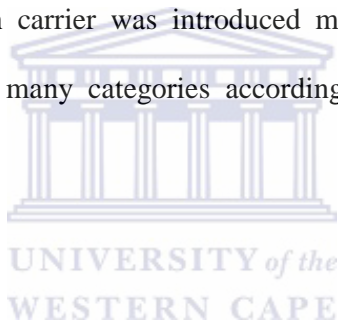


where S and S' are relatively low ionophores. The limit for the free energy of activation of the ligand exchange reaction is probably around 45-65 kJ mol⁻¹.

The requirement that a sufficiently high and constant concentration of ionophore should be present in the membrane phase in unloaded form is theoretically related. If a cation

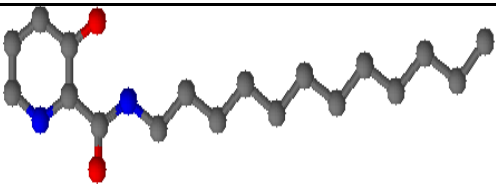
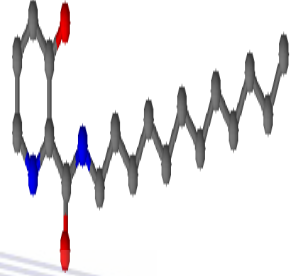
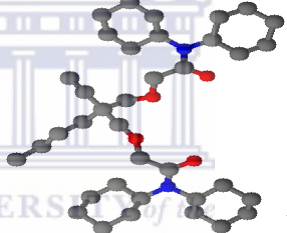
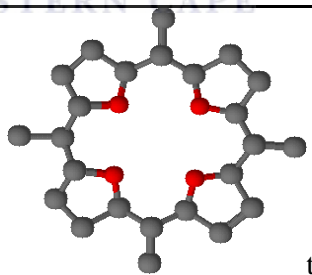
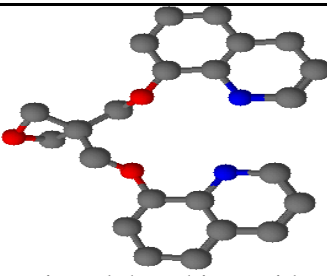
Chapter 3: Doped polyaniline films electrochemical activity and redox probe application

ionophore is predominantly present within the membrane phase in the loaded form, anion-selectivity is induced. These findings are in agreement with the experimental evidence that the transport rate of ionophores passes a maximum when increasing the stability constant of the ionophore/ion interaction. In order to keep the free energy of activation of the ligand exchange reaction sufficiently small, we have been focusing our design of the ionophore on non-macrocyclic structures. Numerous studies on sensors have been carried out based on neutral ionophores or neutral carriers. The sensors based on selective ionophores are usually called ion-selective electrodes, using the technique of liquid-liquid interface which is developed in Chapter 4. The first ion-selective electrodes (ISEs) based on bulk membrane containing an ion carrier was introduced more than 50 years ago. Neutral ionophores are divided into many categories according to ion-exchange molecules as shown in Table.3.2.



Chapter 3: Doped polyaniline films electrochemical activity and redox probe application

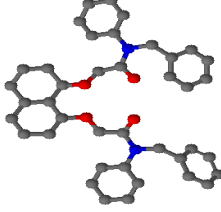
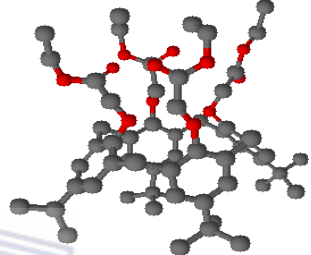
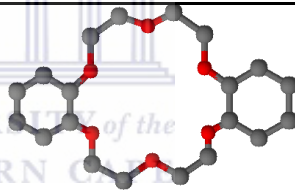
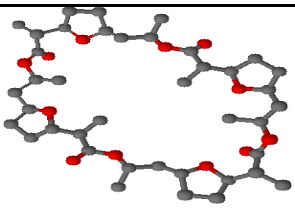
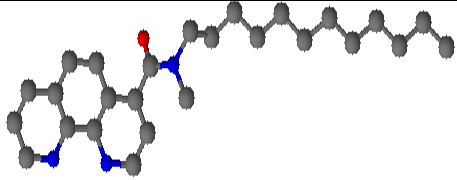
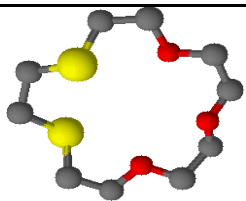
Table 3.2a: Ions sensors and their selective ionophores [144]

Ions sensor	Name ionophores	Structure of selective ionophore
H ⁺	3-hydroxy-N-dodecylpicolinamide	
	Octaphenylcyclotetrasiloxane	
Li ⁺	Di- or triamide ionophores	 ETH 2137
	Natural carboxylic polyether	 tetrahydrofuran
	Heteroaromatic ionophores	 trioctylphosphine oxide

C (gray), S (yellow), O (red), N (blue)

Chapter 3: Doped polyaniline films electrochemical activity and redox probe application

Table 3.2b: Ions sensors and their selective ionophores:

Ions sensors	Name ionophores	Structure of selective ionophore
Na ⁺	Noncyclic amide ionophores	 1,8-naphthalenediol
	Calixarene ionophores	 4-tert-Butylcalix[4]arene-tetraacetic acid tetraethyl ester
Na ⁺ and K ⁺	Crown ether ionophores	 Dibenzo-18-crown-6
NH ₄ ⁺	antibiotics nonactin	
Mg ²⁺	1,10-Phenanthroline ionophores	
Ag ⁺	1,4-dithia-15-crown-5	

Chapter 3: Doped polyaniline films electrochemical activity and redox probe application

3.2.3 Application of ionophores in electrochemical sensors

A characteristic property of all the ionophores is their ability to adopt a cyclic ring formation by concentrating on all the heteroatom functions at the centre of the structure where they are available for complexing mono- or divalent cations. Crown ethers have been reported to be inexpensive neutral carriers in the construction of ISEs. Additionally, these carriers have the option of covalently attaching the desired molecule for electroanalytical applications. It is proposed to study the ion-sensing response of the dibenzo-18-crown-6 (B18C6). The resulting ISEs result in a highly sensitive response with extended linearity to a potassium impregnated polyvinyl chloride matrix membrane laid down on the surface of a polyindole modified electrode. The use of an ionophore-impregnated plasticised PVC matrix membrane in developing a solid-state configuration of an ion-selective electrode is an attractive requirement and we have made efforts using polyindole and polycarbazole synthesised in dichloromethane which contains tetrabutylammonium perchlorate as a bathing electrolyte [145]. The crown ether ionophore was used to the serum Li^+ assay by voltammetric measurements with artificial serum under quiescent conditions (i.e. in batch measurement) [146]. This ionophore was also used in the determination of a thallium (I)-selective electrode based on dibenzylidiaz-18-crown-6 by potentiometric titration over a wide concentration range of Thallium ions [147]. The ISE measurement of Mg^{2+} , Na^+ , K^+ and Ca^{2+} ions based on ionophore ETH 5220 has been reported by Malon and Maj-Zurawska [148].

Chapter 3: Doped polyaniline films electrochemical activity and redox probe application

3.2.4 Aptamer biomolecule

Aptamers are short synthetic single-stranded oligonucleotides that specifically bind to various molecular targets such as small molecules, proteins, nucleic acids, cells and tissues [149]. This new class of oligonucleotide-based molecular recognition elements has more recently emerged as a rival of enzyme and antibody-based methods. This name ‘‘aptamer’’, is derived from a linguistic chimera composed of the Latin word *aptus* (meaning ‘‘to fit’’) and the Greek suffix ‘‘-mer’’ [150-151]. Aptamers can bind to a wide range of target molecules that include proteins, peptides, nucleotides, amino acids, antibiotics, low-molecular organic or inorganic compounds and whole cells with high affinity and specificity [152]. However, like proteins, nucleic acids are able to fold into intricate tertiary structures that have the potential to perform a variety of functions including gene-regulation, catalytic activity and ligand-binding [153]. Two decades ago, several researchers revolutionised molecular recognition by developing synthetic RNA motifs that bound specifically to molecular targets [153]. These RNA structures, called aptamers, were developed in an in-vitro selection procedure by the systematic evolution of ligands by exponential enrichment (SELEX) [151, 153]. This technique makes it possible to isolate functional oligonucleotides against a specific target from a random single strand of ssDNA or RNA library (usually in 10^{15} different sequences).

Chapter 3: Doped polyaniline films electrochemical activity and redox probe application

3.2.4.1 Systematic evolution of ligands by exponential enrichment (SELEX) for general process of aptamer synthesis

Cell-SELEX enabled the isolation of many aptamers by recognising particular cell types. In 1990, three independent research groups reported an in-vitro technique for the isolation of functional oligonucleotides [151, 153]. Fitted with this modern technique, SELEX has become a general and powerful method for isolating nucleic acid aptamers. Since the introduction of aptamers and the SELEX process, several works have improved the aptamer selection and isolation acids process with a wide variety of application fields. Tuerk and Gold used the term SELEX for their process of selecting RNA ligands against T4 DNA polymerase; Ellington and Szostak performed in-vitro selection to select RNA ligands (for which they coined the term “aptamers”) against various organic dyes; while Robertson and Joyce evolved the tetrahymen a self-splicing intron to perform out a DNA cleavage reaction [153]. Some changes of the SELEX process have been reported by various researchers but its invention in general remains the same. Figure 3.5 is a schematic depicting the basic SELEX process that includes repeated cycles of selection and amplification. This aptamer screening process is influenced by many parameters such as target features, design of the random DNA library, selection condition and the efficiency of partitioning methods.

Chapter 3: Doped polyaniline films electrochemical activity and redox probe application

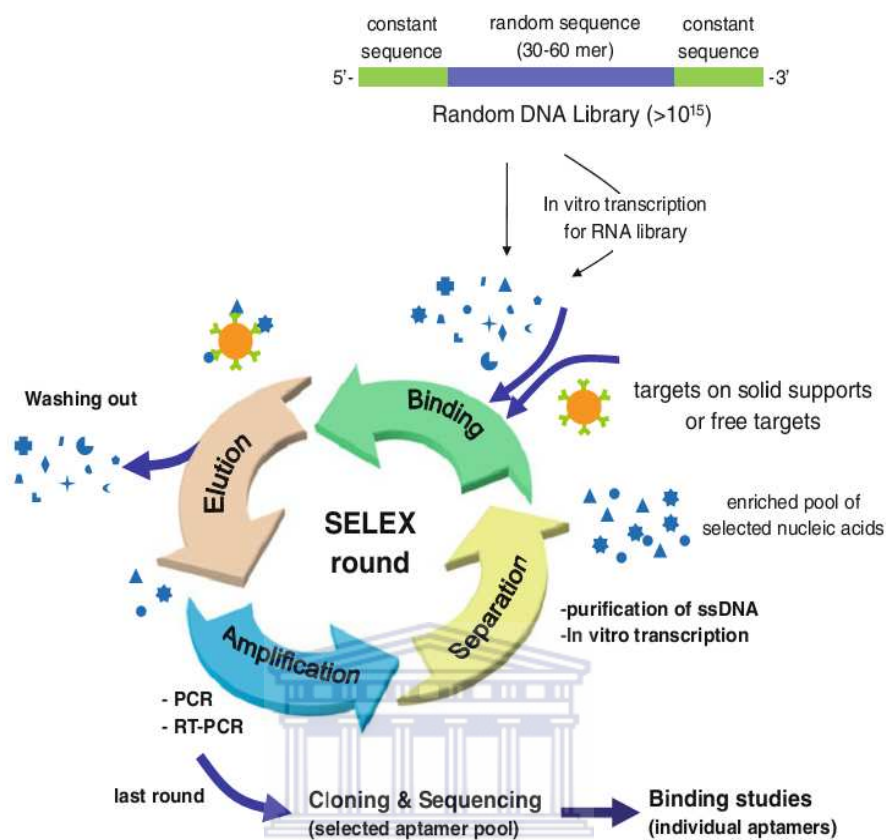


Figure 3.5: SELEX technology aptamer screening process.[151]

Typically, SELEX begins with an initial library (often referred to as “a pool”) of random nucleic acid sequences (either RNA or DNA depending on the nature of the research). SELEX libraries ideally consist of 30–80 random nucleotide positions flanked by primer-binding sites necessary for polymerase chain reaction (PCR) amplification [154]. Four essential steps for the normal SELEX process can be stated; these binding, selection, amplification and partitioning. Out of all these steps, the most critical one is the selection step. In the first step of SELEX, the random sequence of the DNA or RNA library is incubated with the target. This is one of the most critical steps to isolate high affinity and specificity aptamers among the extremely diverse oligonucleotide library. Afterwards, the

Chapter 3: Doped polyaniline films electrochemical activity and redox probe application

selection steps based on the filtrations uses a nitrocellulose membrane or affinity chromatography column containing the target immobilized beads for partitioning in the SELEX process [155-156]. In the filtration method, oligonucleotides not bound to the targets are removed from aptamer–target complexes based on the molecular weight difference between nucleic acids and the oligo-nucleotide–target complex. However, it is very difficult or impossible to separate these from a library readily at any time, due to the low partitioning coefficient of normal separation techniques. Therefore, the repetition of the selection step is required in practical protocols of aptamer screening. To perform this repeated selection, the oligonucleotides bound to the targets should be amplified by reverse transcription (RT)-PCR for a RNA library or PCR for a DNA library, which generates a new population of oligonucleotides for the next round of SELEX. Normally, 10–20 amplifications are sufficient within 10–20 cycles [157] for the next round of selection. Finally, after PCR amplification, the enriched oligonucleotide pool exists as double-stranded DNAs. This dsDNA pool is separated to individual ssDNAs and then a forward strand DNA pool is incubated with targets as the next round of SELEX.

3.2.4.2 Strategies for attaching of the solid support

Many important molecular applications of DNA oligonucleotide arrays utilise synthetic oligonucleotides attached to the surface (solid support). The most accessible approach for producing an oligonucleotide microarray is to synthesise individual oligonucleotides and subsequently immobilise them to a solid surface. For this immobilisation to take place, the oligonucleotides must be modified with a functional group in order to have attachment to a reactive group on a solid surface. Different modifications allow immobilisation onto

Chapter 3: Doped polyaniline films electrochemical activity and redox probe application

different surfaces. Some of the modifications routinely used to construct oligonucleotide arrays are reviewed below including the attachments:

- Amine-modified oligos covalently linked to an activated carboxylate group or succinimidyl ester.
- Thiol-modified oligos covalently linked via an alkylating reagent such as an iodoacetamide or maleimide.
- Biotin-modified oligos captured by immobilized streptavidin.

a) Amino-modified oligonucleotides

Generally, the amine-terminated aptamers are prepared with a primary amine link to a biomolecule of interest with a functional group that allows covalent attachment to a reactive group on the surface [158]. Amine-terminated aptamer used in the preparation of self-assembled monolayers (SAMs) can be reacted with sulfosuccinimidyl 4-(N-maleimidomethyl cyclohexane)-1-carboxylate (SSMCC) to create a male-imide-terminated surface, which can in turn react with thiol-containing biomolecules [159]. An amino modified can be placed at the 5'-end, 3'-end or internally using an amino-deoxycytidine or amino-deoxythymidine modified base.

b) Thiol-modified Oligonucleotides

Amine and thiol modifications of synthetic oligonucleotides are also readily available. The thiol (SH) modifier enables covalent attachment of an oligo to a variety of ligands. A SH-modifier can be placed at either the 5'-end or 3'-end of an oligo. It can be used to form reversible disulfide bonds (ligand-S-S-oligo) or irreversible bonds with a variety of activated accepting groups. Thiol-modifiers can be incorporated at the start of synthesis by

Chapter 3: Doped polyaniline films electrochemical activity and redox probe application

placing the reactive SH-group at the 3'-end using cordycepin residue, thiol- CPG and can also be incorporated as the last step of synthesis using a thiol-phosphoramidite which places the reactive SH-group at the 5'-end of the oligo. The incorporation of a thiol group at the 5' end of an oligo is achieved with S-trityl-6-mercaptohexyl derivatives [158].

c) Biotin modified oligonucleotides

Biotin is an important molecule in molecular biology applications, in part due to its very high affinity for streptavidin and avidin. It is used in mobility shift assays and for enrichment, purification and attachment to solid surfaces. Biotin can also be used for tagging target molecules with dye- or enzyme-labelled streptavidin. The affinity of the biotin–streptavidin interaction is extremely strong, with a disassociation constant (K_d) of 10–15 M. Biotin fits inside a ‘pocket’ (Fig.3.6) of the streptavidin protein [160], creating an enveloping effect which supplements the binding interaction. It is this binding strength that makes biotin a very useful tool for molecular and biomedical research.

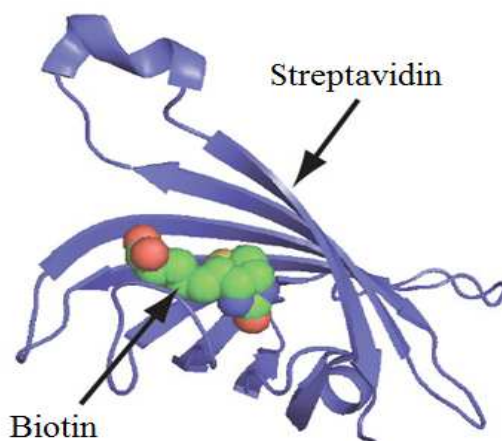
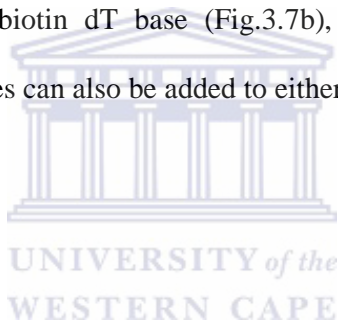


Figure 3.6: Biotin–streptavidin interaction. Biotin (green, red, and blue spheres) fits inside a pocket formed by the streptavidin protein (blue ribbon). [161].

Chapter 3: Doped polyaniline films electrochemical activity and redox probe application

Biotin can be added to oligonucleotides on either terminus (“standard” Biotin), or internally through a modified thymidine residue (Biotin-dT). There are several types of biotin modifications, each with their own benefits. However, it is important to note that each of the different biotin modifications contains the same functional biotin group. Biotin can be added to the 5'- or 3'-ends of an oligo using either a C6 (standard) (Fig.3.7a) or TEG (tetra-ethyleneglycol). Biotin-TEG increases the oligo–biotin distance to 15 atoms using a triethyleneglycol (TEG) spacer arm. Biotin-TEG is commonly used to avoid hindrance issues and can be beneficial for attaching oligonucleotides to nanospheres or magnetic beads. For 5' Biotin-TEG, purification is required. Internal biotin modification can be introduced using a biotin dT base (Fig.3.7b), which also requires additional purification. Biotin dT residues can also be added to either end of an oligo.



Chapter 3: Doped polyaniline films electrochemical activity and redox probe application

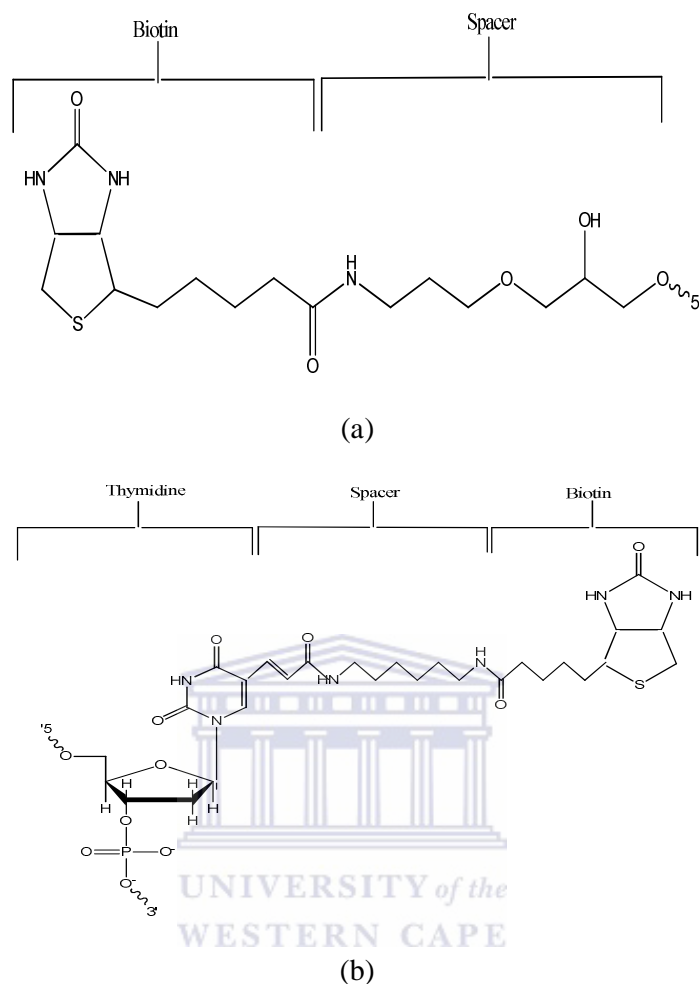


Figure 3.7: (a) “Standard” Biotin (this version is used for addition to the 3' end), (b) Biotin dT.

3.2.4.3 Immobilisation method of aptamer

Construction of arrays involves a number of parameters each of which must be optimised for efficient and effective experimental design. One important parameter is the method of choice for attachment of the synthetic oligonucleotides. Some of the issues to be considered in choosing an appropriate support and the associated attachment chemistry include: the level of scattering and fluorescent background inherent in the support material

Chapter 3: Doped polyaniline films electrochemical activity and redox probe application

and added chemical groups; the chemical stability, binding affinity, selectivity and complexity of the construct [162]; the amenability to chemical modification; surface area; loading capacity and the degree of non-specific binding of the final product [158]. The method of immobilization of aptamer to a solid support affects the sensitivity of the aptamer to the target molecule. As well as the immobilisation of enzyme, peptides, ligands or other biomolecules, DNA or RNA oligonucleotides (aptamer) have the same method for immobilisation since there is no general universally applicable method of certain particular molecule immobilisation [163]. The solid surface material and the method of immobilisation are key parameters in biomolecule immobilisation. However, three principal methods can be used for immobilisation of aptamers and cells such as adsorption, covalence and the cross-linking method.

a) Adsorption

Physical adsorption of an aptamer onto a solid surface is probably the simplest way of preparing an immobilised aptamer. The adsorption process is a mixture of a biomolecule and a solid surface support with adsorption properties under defined condition of pH and ionic strength for a period of incubation, followed by a collection of immobilised material and extensive washing to remove the unbound biological components. The many advantages of this technique include; the reversibility of the system, the simplicity of the operation under mild conditions, the possible high retention of activity (no chemical modification) [164], cheap and quick method as well as rigidity of the properties of the support surface and aptamer. The limitations of this method are the non-specific interaction between the aptamer and the surface of the matrix, the contamination of the product and the steric hindrance by the support.

Chapter 3: Doped polyaniline films electrochemical activity and redox probe application

b) Covalent binding method

Covalent binding is the procedure mostly studied for insolubilisation techniques in the formation of covalent bonds between the biomolecule and the support matrix. The functional groups of proteins involved in the covalent binding process under mild conditions include (i) the alpha amino groups of the chain and the epsilon amino groups of lysine and arginine, (ii) the alpha carboxyl group of the chain end and the beta and gamma carboxyl groups of aspartic and glutamic acids, (iii) the phenol ring of tyrosine, (iv) the thiol group of cysteine, (v) the hydroxyl groups of serine and threonine, (vi) the imidazole group of histidine, and (vii) the indole group of tryptophan [165]. The bond is normally formed between functional groups present on the surface of the support matrix and functional groups belonging to the biomolecule (aptamer). Advantages of enzymes immobilised using the covalent technique are that the aptamer can be easily in contact with the substrate due to the localisation of the aptamer on support materials. Both absorption and covalent binding techniques were compared in the immobilisation of the cellulase enzyme mixture [166].

c) Cross-linking method

Immobilisation of an aptamer has been achieved by intermolecular cross-linking of the protein, either to other protein molecules or to functional groups on an insoluble support matrix. This type of immobilisation can be achieved by chemical or physical methods [167]. Chemical methods of cross-linking normally involve covalent bond formation between the enzymes by means of a bi- or multifunctional reagent such as glutaraldehyde, dicarboxylic acid or toluene diisocyanate [163]. For the physical method, flocculating

Chapter 3: Doped polyaniline films electrochemical activity and redox probe application

agents such as polyamines, polyethyleneimine, polystyrene sulfonates and various phosphates have been used extensively to cross-link cells to form physical bonds. This technique has an advantage in that the cross-linking between the same aptamer molecules enhances the stability of the aptamer and therefore increases the rigidity of the structure.

Aptamers can be attached to the solid support at either the 5'-end or the 3' end. Both positions have been reported as being used to develop the aptasensor. Cho *et al.* suggested that depending on the particular aptamer, the 3' end is more suitable for biological targeting since the 3' end is the primary target for exonucleases, thus its coupling to the solid surface would simultaneously confer resistance to nucleases [168].

For direct attachment of a thiol-aptamer, a gold surface is commonly used for many electrochemical measurements using thiol-alkane linked to the aptamer sequence. The gold surface could be functionalised with self-assembled monolayers (SAMs) with selective chemistry depending on the type of terminal functional group (amine, thiol or biotin) linked to the aptamer (Fig.3.7). The disadvantage of functionalising the gold surface with self-assembled monolayers (SAMs) for long oligonucleotides with larger numbers of amine groups is the nonspecific adsorption of aptamer to the functionalised surface [169].

For biotin aptamer immobilisation, avidin-biotin technology has also been exploited. Streptavidin is more suitable for physically adsorbed or covalent immobilisation of biotin-aptamer onto the support and the method mainly requires incubation of the biotin-tethered aptamer with the modified substrate. For the application of this avidin-biotin method, the anti-thrombin aptamer was used to detect thrombin and it gives best results regarding sensitivity compared to other immobilisation strategies by Hianik *et al.* [170].

Chapter 3: Doped polyaniline films electrochemical activity and redox probe application

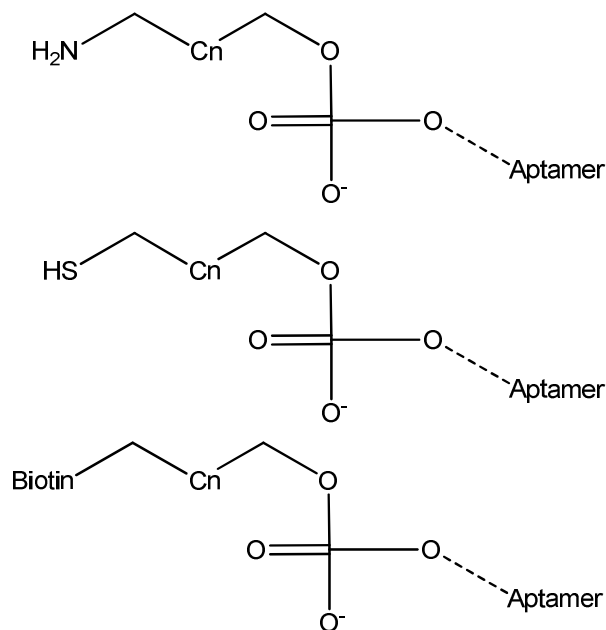


Figure 3.8: Standard nucleic acid modifications used for aptamer immobilisation [170]

3.2.4.4 Application of aptamer on electrochemical biosensors

Due to their easy and quick preparation, cost-effectiveness, small size and versatility, aptamers have become useful tools for the validation of intracellular and extracellular targets. A continuously growing number of nucleic acid aptamers are used as research tools to study specific protein functions and interactions [171-172]. After the synthesis of a DNA or RNA aptamer, the first and common application is in the study of the streptavidin/biotin interaction. In this method, a biotin molecule is incorporated into the unwanted strands during PCR amplification with biotinylated reverse primer. Gonzalez-Garcia *et al.* investigated the new electrochemical method to monitor the biotin – streptavidin interaction based on the use of colloidal gold as an electrochemical label which absorbs the biotinylated albumin on the pretreated surface of a carbon paste

Chapter 3: Doped polyaniline films electrochemical activity and redox probe application

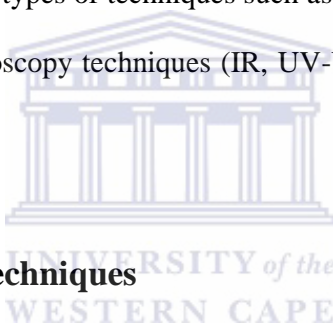
electrode (CPE) recording a detection limit of 7.3 nM [173]. On the other hand, hybridization of a biotinylated target DNA to streptavidin coated magnetic bead-binding biotinylated probe and followed by the binding of streptavidin-coated AuNPs to the target-DNA was published. In the same work the dissolution of the AuNPs and electrochemical detection using potentiometric stripping analysis (PSA) of the dissolved gold tag at single DNA use thick film carbon electrodes and a detection limit was 4 nM [174].

The high affinity and specificity of aptamer make them ideal diagnostic reagents. In research, an aptamer can be also used as a molecular recognition element in food control and environmental analytical chemistry [175-176]. In this research application field, many studies have been carried out. Recently, Lifang *et al.* used the thiolated DNA aptamer for sensitive and selective detection of acetamiprid based on an electrochemical impedance spectroscopy and a detection limit of 1 nM [177]. Zhengbo *et al.* developed a simple, sensitive and label-free EIS using the thiolated DNA aptamer for the detection of lysozyme, recording a very low detection limit of 0.01 pM [178].

PRINCIPLE OF SELECTIVE ANALYTICAL TECHNIQUES

4.0 Introduction

Analytical techniques are methods that are used for detecting, measuring, separating, and monitoring the concentration of a chemical compound or chemical element. This chapter set to identify well-established methods used as standard methods of analysis. Depending on the investigation, different types of techniques such as electrochemical techniques (CV, LCV, SWV, EIS) and spectroscopy techniques (IR, UV-Vis absorption, FI, ^1H NMR) are consider in this chapter.



4.1 Electrochemical techniques

Electrochemical techniques employed in this study gives information on the processes involved when an electric potential is applied to the system under investigation. Electrochemical techniques such as CV, SWV, EIS and linear scan voltammetry (LSV) have been powerful tools for analytical purposes during this research study..

4.1.1 Cyclic voltammetry (CV)

Cyclic voltammetry is the most common type of electroanalytical measurement used for obtaining substantial information about the electrochemical processes and for probing

Chapter 4: Principle of secretive analytical techniques

kinetic and thermodynamic properties of the compound studied. CV is an electrochemical technique which measures the current that develops in an electrochemical cell under conditions where voltage is in excess of that predicted by the Nernst equation. CV is performed by cycling the potential window of a working electrode at a certain scan rate, and measuring the resulting current.

Principle: The CV involves the potential and current as mentioned in the previous paragraph. The potential of the analyte is measured with the reference electrode and the resulting applied potential produces an excitation signal as shown in Figure 4.1. The current is measured with the working electrode and the resulting current produces an excitation peak as shown in Figure 3.2 [179]. The potential can be scanned negatively or positively as shown in Figure 4.1, depending on the analyte. When the potential is scanned positively, the scan starts from a high potential (a) and ends at a lower potential (b) for one scan (one cycle). The potential extremum (b) is called the switching potential and is the point where the voltage is sufficient enough to oxidise or reduce the analyte in the electrolyte cell solution. When the potential is scanned negatively, the reverse scan occurs from (b) to (c), see Figure 4.1 and this figure shows the reduction occurring from (a) to (b) and an oxidation occurring from (b) to (c).

Chapter 4: Principle of secretive analytical techniques

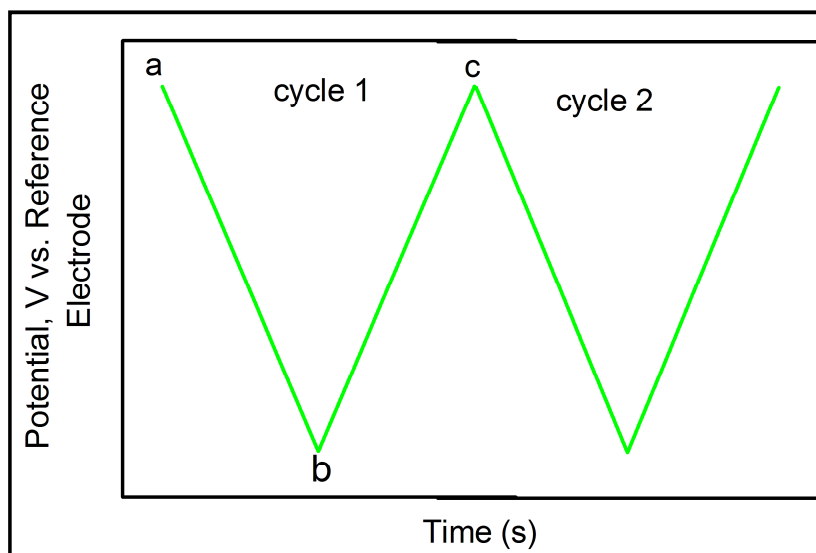


Figure 4.1: Cyclic Voltammogram: Excitation signal.

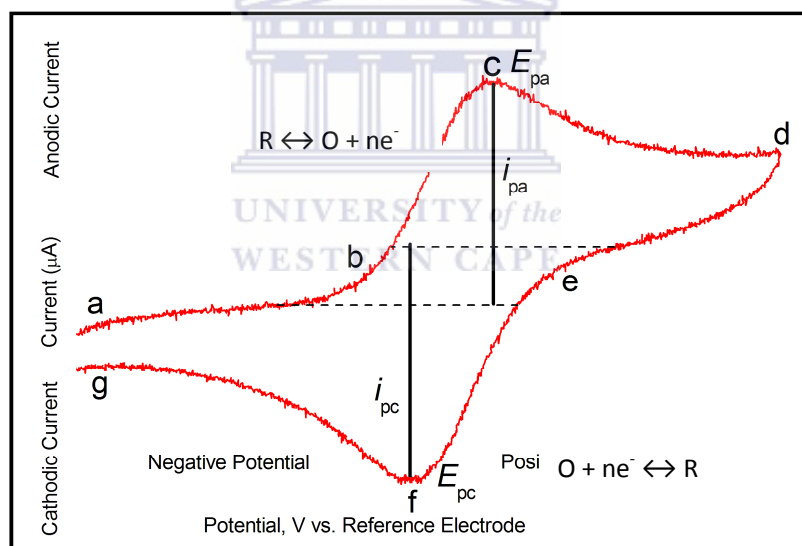
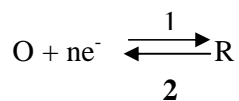


Figure 4.2: Cyclic Voltammogram of a Single electron oxidation-reduction.

The following reversible equation



Equation 4.1

Chapter 4: Principle of secretive analytical techniques

is the reaction that takes place on the electrode surface during cyclic voltammetry analysis which is responsible for the signal shown in Figure 4.2. The reversible reaction (Eq.4.1) can be explained using the cyclic voltammogram response. In Figure 4.2, the oxidation process (2) occurs from (a) the initial potential to the switching potential (d). In this region the potential is scanned positively to produce an oxidation. The resulting current is called anodic current (i_{pa}). The corresponding peak potential occurs at (c) and is called the anodic peak potential (E_{pa}). When all the substrate is reached at the surface of the electrode and oxidised to (O), process (2), the E_{pa} is measured. After the switching potential has been reached (d), the potential scans negatively from (d) to (g). This results in a cathodic current (i_{pc}) and the reduction process (1) occurs to give the product (R). The peak potential at (f) is called the cathodic peak potential (E_{pc}) and is reached when all of the substrate at the surface of the electrode has been reduced.

The potential of electrode (E) is calculated by using the equation:

$$E = E_i + vt$$

Equation 4.2

where (E_i) is the initial potential in volts, (v) is the sweep rate in volts s^{-1} , and t is the time in seconds. When the direction of the potential sweep is switched, the equation becomes,

$$E = E_s - vt$$

Equation 4.3

where (E_s) is the potential at the switching point (d). When the system is reversible, electron stoichiometry (n) [180]

$$E_p - E_{p/2} > \frac{0.0565}{n}$$

Equation 4.4

Where n is the number of electrons participating in the redox reactions.

Chapter 4: Principle of secretive analytical techniques

Formal Reduction Potential (E°) which can be called the standard electrode potential at 298 K is the mean of the E_{pc} and E_{pa} values: $E^{\circ} = (E_{pa} + E_{pc})/2$.

When no current passes through the cell during an equilibrium electrochemical experiment, the activities of the electroactive species in the solution will obey the Nernst equation:

$$E_{working\ electrode} = E_{0,R}^{\circ} + \frac{RT}{nF} \ln \frac{a(O)_{surface}}{a(R)_{surface}} \quad \text{Equation 4.5}$$

where ‘surface’ is the surface of the working electrode, E° is the formal electrode potential, “a” is the activity of the oxidizing (O) and reducing (R) species

Instrumentation: A CV system consists of an electrolysis cell, a potentiostat, a current-to-voltage converter and a data acquisition system. The electrolysis cell consists of a working electrode (WE), counter electrode (CE), reference electrode (RE), and electrolytic solution. The working electrode’s potential is varied linearly with time, while the reference electrode maintains a constant potential. The counter electrode conducts electricity from the signal source to the working electrode. The electrolytic solution is a solution that generally contains ions, atoms or molecules that have lost or gained electrons and is electrically conductive. The role of this electrolytic solution in the electrolysis cell is to provide ions to the electrodes during the oxidation and reduction process. A potentiostat, also called a “Patch Clamp Amplifier” is an electronic device used to keep a working electrode at desired potential with respect to a reference electrode. The potentiostat uses a dc power source to produce the potential while allowing small current to be drawn into the system without changing the voltage. The resulting current is measured with the current-to-voltage converter and the data acquisition system produces the resulting voltammogram.

Chapter 4: Principle of secretive analytical techniques

Applications: CV is an important analytical technique in chemistry. It is used to study a variety of redox processes under various conditions such as the presence of intermediates in oxidation-reduction reactions, the reversibility of a reaction [181], reaction and electron transfer kinetics [182] and the stability of the electrode vis-à-vis a electroactive compound. CV can also be used to determine the electron stoichiometry of a system [181], the diffusion coefficient of an analyte [182-183] and the formal reduction potential. In addition, by generating a calibration curve of current vs. concentration, the concentration of unknown solution can be determined and it can be seen that the concentration is proportional to current in a reversible nernstian system.

4.1.2 Electrochemistry at liquid-liquid interface: theory and application

An electrochemical setup without a working electrode will look strange to the traditional electrochemist; nevertheless several laboratories are doing just that by running their experiments at the interface between two immiscible electrolyte solutions (ITIES). Moreover, literature increasingly shows that this can be a valuable technique [184] In a conventional (potentiostatic) electrochemical experiment, the potential of the working electrode is controlled with respect to a reference electrode. The applied potential drives an electron transfer (ET) reaction, which occurs at the working electrode/solution interface [184]. In the ITIES experiment, voltage is applied between two reference electrodes positioned on opposite sides of the interfacial boundary and the current flows between two counter electrodes, one in an aqueous phase, the other in an organic phase (Fig.4.3a). The reaction is driven by the voltage applied across the liquid interface and the measured current arises from ET or ion transfer (IT) at the ITIES. An ET reaction at the ITIES can

Chapter 4: Principle of secretive analytical techniques

be represented as in which Ox1/Red1 and Ox2/Red2 are the aqueous and organic redox couples respectively. A simple IT reaction involves reversible transfer of a cation or anion between two immiscible liquid phases. If it happens in one of the two phases typically, that the organic solvent contains a ligand (L) that can react with ion (X) to form a complex (LX), such a reaction can assist the transfer of X.



Assisted IT reactions usually require less driving force (i.e. lower external voltage) than the simple transfer of the same ion. When the interfacial area is large (e.g. mm²), a four-electrode setup (Fig.4.3a) is necessary to minimise the potential drop in a resistive organic solvent.



Chapter 4: Principle of secretive analytical techniques

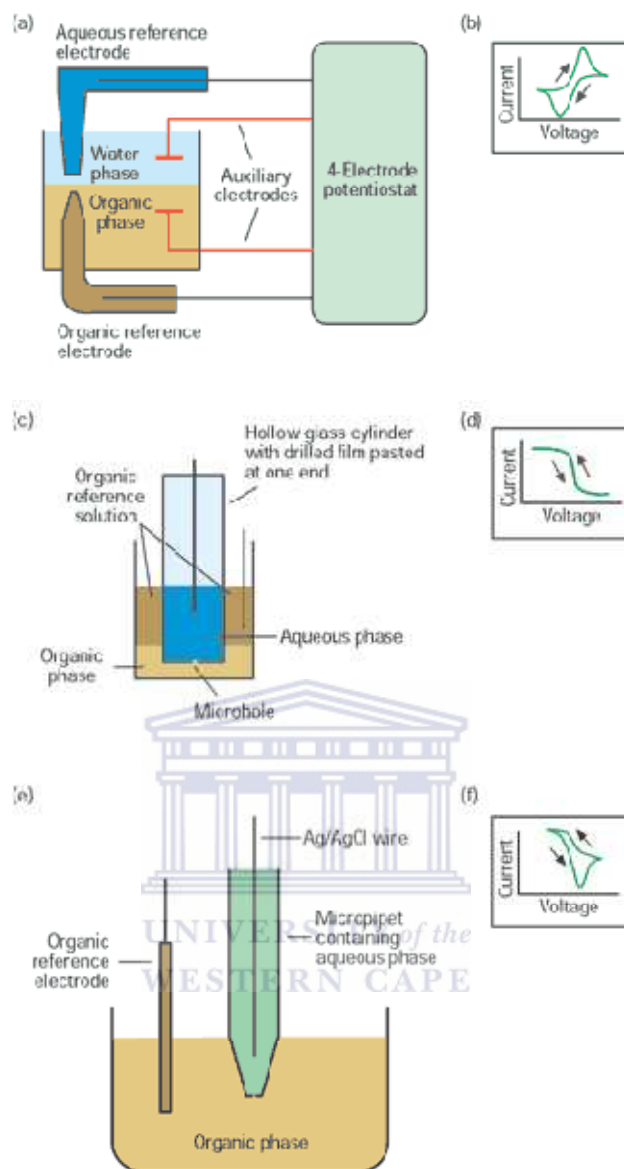
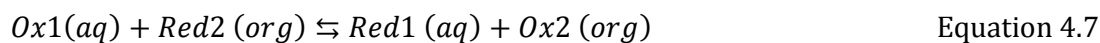


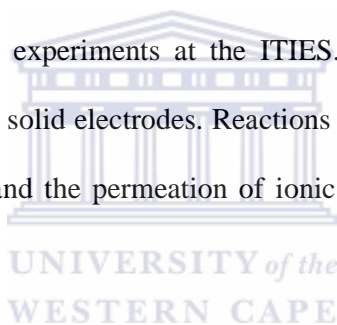
Figure 4.3: Schematic of voltammetric experiments at (a) a macroscopic and microscopic ITIES supported at (c) a microhole and at (e) a micropipet. (b, d, and f) The corresponding cyclic voltammograms Adapted from Liu & Mirkin. [184].



Cyclic voltammograms of IT and ET reactions at the macro-ITIES (Fig. 4.3b) look similar to conventional voltammograms obtained at metal electrodes. The height of a

Chapter 4: Principle of secretive analytical techniques

voltammetric peak is still proportional to the concentration of one of the reactants, whose diffusion is rate-limiting and to the square root of the potential sweep rate. For a micrometer-sized interface (micro-ITIES), the resistive effect is less important and the simpler, two-electrode setup shown in Figures 4.5c and 4e can be used [31]. The current is limited by the spherical diffusion of a reagent to a micrometer-sized orifice of a microhole (Fig. 4.3.c) or a micropipet (Fig.4.3e) and sigmoidal steady-state voltammograms are obtained (Fig.4.3.d and f). The diffusion limiting current is proportional to the reagent concentration and independent of the potential sweep rate. With micropipets, peak-shaped voltammograms are obtained when the linear diffusion of ions inside the narrow shaft of a pipet is rate-limiting (Fig.4.3f) [184]. The presence of the second liquid phase adds versatility to electrochemical experiments at the ITIES. A large group of IT reactions occurs at the ITIES but not at solid electrodes. Reactions involving substances of different polarities can be conducted and the permeation of ionic species through bio-membranes can be modelled.



Amperometric sensors and detectors: Similar to potentiometric ion-selective electrodes (ISEs), the equilibrium potential difference at the ITIES is determined by the activities of the common ion when it is present in both liquid phases. Moreover, the diffusion-controlled IT current at the ITIES is proportional to the concentration of the transferred ion. Therefore, the ITIES can also be used as an amperometric ISE. An amperometric system has an advantage over a potentiometric ISE because its selectivity may be tailored by the polarisation potential. Therefore, two or more ions can be determined simultaneously if their half-wave potentials are reasonably well separated. For instance, an amperometric ISE using a nitrobenzene/water ITIES determined K^+ and Na^+ in drinking

Chapter 4: Principle of secretive analytical techniques

water. A number of such devices have been used for measuring various analytes in food, pharmaceutical products, toxic water and industrial samples [185]. Unfortunately, broader development of transducers based on ITIES has been hindered by the use of toxic and high-electrical resistive organic solvents and by the mechanical instability of liquid/liquid interfaces. To tackle the toxicity problem, less toxic solvents such as 2-nitrophenyloctylether are replacing traditional media as nitrobenzene or 1,2-dichloroethane [185].

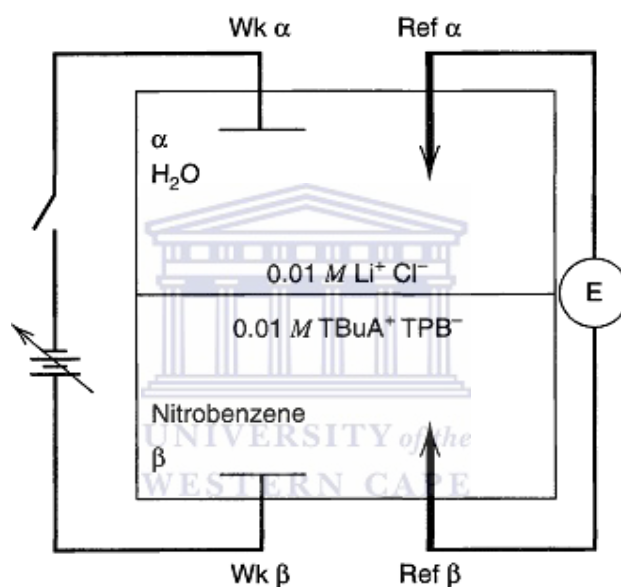


Figure 4.4: Schematic diagram for the apparatus for cyclic voltammetry at the ITIES between water and nitrobenzene. $\text{Ref } \alpha$ and $\text{Ref } \beta$ are reference electrodes, $\text{Wk } \alpha$ and $\text{Wk } \beta$ are metal working electrodes. [185]

Micro-ITIES can be used to minimize the ohmic potential drop problem and analyze small samples. For example, Osborne *et al.* used a microhole-based ITIES (Figure 4.3c) to determine aqueous NH_4^+ at the water/1,2-dichloroethane (DCE) interface [186]. The ammonium's transfer was assisted with dibenzo-18-crown-6 (DB18C6). Because the ionophore concentration in the organic phase was high, the measured steady-state current

Chapter 4: Principle of secretive analytical techniques

was proportional to the concentration of NH_4^+ in the aqueous phase. The time required to reach steady state was relatively short (e.g. 5 s for an 11- μm hole) and the relationship between the steady-state plateau current and the NH_4^+ concentration was linear over the range 1–500 μM . A microhole-based ITIES has also been used as an enzymatic urea detector at concentrations from 200 μM to 4 mM [187].

A lot of research work has been done to increase the mechanical stability of liquid/liquid systems by gelling the organic or aqueous phase [186]. Typically, the organic phase has been solidified by adding polyvinylchloride (PVC) and the aqueous phase has been solidified by adding agar. Different gelling agents such as 1,3:2,4-dibenzylidene sorbitol, have also been used to prepare organic gels with ionic conductivities similar to electrolyte solutions [188]. Although the diffusion coefficients of ions in gels are significantly reduced, the IT processes could still be used for amperometric detection. The gelation of the organic phase often increases resistivity, which impedes amperometric determination. Using arrays of liquid/liquid microinterfaces could lessen this problem [189]. Urea and creatinine sensors based on the amperometric detection of NH_4^+ were fabricated using this approach. Recently, Lee *et al.* prepared microfabricated composite polymer membranes, which combine the advantages of the gelled organic phase and micro-ITIES [190]. The composite membrane consists of a thin, inert and microperforated polymer layer which is covered by PVC-2- nitrophenyloctylether (PVC-NPOE) electrolyte gel. The composite membrane electrode can be incorporated into a flow cell. The IT behavior of the microhole array interface between an analyte solution and a PVC gel electrolyte was similar to that of a conventional micro-ITIES. When the composite polymer membrane was used for the amperometric sensing of choline, the plot of the diffusion-limiting current against the

Chapter 4: Principle of secretive analytical techniques

concentration was linear over the range 0.1– 0.9 mM [191]. Sensors for alkali metal ions were produced by adding ionophores (e.g. DB18C6, valinomycin) to the PVC membrane [192].

Another approach to stabilising the liquid/liquid interface is to insert a thin, porous, hydrophilic or hydrophobic membrane between the two phases. Such a membrane-stabilised ITIES and was used as an amperometric sensor for the flow-injection analysis (FIA) of alkali metal ions, halides and other anions. A successful simultaneous determination of K^+ and Na^+ in blood serum suggests promising applications of this approach for clinical analysis. The ITIES can be used to detect ionic solutes in FIA, HPLC and CE. In ion-exchange chromatography, a composite polymer membrane showed detection limits similar to those of a conventional conductivity detector [193]. However, an amperometric detector based on a micro-ITIES can offer even higher selectivity by choosing the proper ionophore. For example, introducing an NH_4^+ -selective ionophore such as valinomycin into the gel membrane substantially increases the selectivity of the detector toward NH_4^+ in the presence of excess Na^+ [193]. A composite polymer membrane detector has been used for the FIA of halides, NO_3^- and SO_4^{2-} [194]. By using the dual-potential-pulse mode and pure water as an eluent, the detection limit for the anions could be lowered to the parts-per-trillion level. More recently, a microhole based ITIES amperometric detector for capillary zone electrophoresis determined choline and Ach^+ , aryl sulfate and sulfonate anions in four different determinations [195]. The detection limit in all cases was $\sim 1 \mu M$. An ITIES supported at a dual pipet consisting of two closely spaced pipets filled with aqueous solutions and separated by a submicrometer wide band of glass was used as a gas sensor [196]. When the outer glass surface is not

Chapter 4: Principle of secretive analytical techniques

silanised, the pipet orifices are linked by a thin aqueous film on the outer pipet wall. Such film can be sufficiently thick and conductive to yield reasonable quality voltammetric responses that are suitable for qualitative and quantitative analytical determinations. The response of a dual pipet is largely determined by the properties of the aqueous surface layer and is very sensitive to changes in film composition. Such changes occur when the pipet is exposed to a soluble gas.

Ion partitioning and drug delivery testing: The pharmacological activity of a drug is largely determined by its ability to permeate lipid cell membranes. Permeation depends on the physicochemical properties of the drug particularly its lipophilicity which is conventionally evaluated from the drug partitioning between water and octanol [191]. Because octanol can form hydrogen bonds, the water–octanol partitioning of a polar substance may not always be a good measure of lipophilicity. Hence, a drug’s ability to permeate cell membranes or cross the blood–brain barrier does not always correlate well with its water-octanol partition coefficient [185]. The partition coefficient, P , of an ion species, i , in a biphasic system is defined as:

$$P_i = \frac{a_i^o}{a_i^w} \quad \text{Equation 4.8}$$

In which “ a ” is the activity of the ion in the organic, o , and aqueous, w , phases. At thermodynamic equilibrium, the partition of an ionic species is described by the Nernst equation:

$$\Delta_o^w \phi = \Delta_o^w \phi_i^o + \frac{RT}{z_i F} \ln \left(\frac{a_i^o}{a_i^w} \right) \quad \text{Equation 4.9}$$

Chapter 4: Principle of secretive analytical techniques

In which $\Delta_o^w \phi$ is the interfacial voltage, $\Delta_o^w \phi_i^o$ is the standard IT potential, and z_i is the charge of the ion. When equations 4.8 and 4.9 are combined and rearranged, lipophilicity can be measured directly by:

$$\ln P_i^o = - \frac{z_i F}{RT} \Delta_o^w \phi_i^o \quad \text{Equation 4.10}$$

In which $\ln p_i^o$ is the partition coefficient when the interface is not polarised (i.e. $\Delta_o^w \phi = 0$).

For a reversible transfer of a simple ion, $\Delta_o^w \phi_i^o$ is related to the half-wave potential by:

$$\Delta_o^w \phi_i^o = \Delta_o^w \phi_{1/2} - \frac{RT}{2z_i F} \ln \left(\frac{D_i^w}{D_i^o} \right) \quad \text{Equation 4.11}$$

Thus, the partition coefficient of an ion can be accessed from cyclic voltammograms and the half-wave transfer potential of an ionisable compound can be used to characterise its lipophilicity. The value of $\Delta_o^w \phi_{1/2}$ can be easily found from an experimental voltammogram because it is equal to the mid peak potential, $(\Delta \phi_{pa} + \Delta \phi_{pc})/2$, in which $\Delta \phi_{pa}$ and $\Delta \phi_{pc}$ are the anodic and cathodic peak potentials respectively. Hence, IT voltammetry at the ITIES is a suitable technique for evaluating the lipophilicity of ionic drugs [197]. Extensive voltammetric studies of local anaesthetics such as procaine; antihistamines for example, doxylamine and uncouplers such as 2,4-dinitrophenol have been reported [198]. Assuming that the transfers of all relevant species across the ITIES are diffusion-controlled, theoretical $\Delta_o^w \phi_{1/2}$ versus pH dependences were obtained and used to evaluate the physicochemical properties of drugs. Reversible Nernstian behaviour was demonstrated for different types of drugs.

Chapter 4: Principle of secretive analytical techniques

For example, in cyclic voltammograms of procaine at the interface between nitrobenzene and 10 mM aqueous acetate buffer, the anodic peak height was proportional to the square root of the potential scan rate within the range 5 to 100 mV s^{-1} and the peak potential separation was close to the 58 mV value, which is characteristic of the reversible univalent ion transferred. The partition coefficient of procaine, the formal transfer potential of protonated procaine and the dissociation constants of the first and second protonation-deprotonation reactions were obtained from the half-wave potential versus pH dependence. The relationship between pharmacological activity and half-wave transfer potential has been established for a number of ionisable drugs [185]. For example, many barbiturate derivatives are weak acids and are transferred across the ITIES as anions. The $\Delta_o^w \phi_{1/2}$ of these ions becomes more positive with an increase in lipophilicity. Conversely, $\Delta_o^w \phi_{1/2}$ of some cationic anesthetic drugs becomes more negative with increasing lipophilicity. In either case, the higher lipophilicity corresponds to greater pharmacological activity. A strong correlation between the pharmacological activity and the half-wave potential was found for the families of hypnotic, anesthetic, cholinergic, and adrenergic drugs [185].

Many drugs are weak electrolytes that can undergo protonation-deprotonation reactions. The transfer of such species across the ITIES depends on the interfacial potential drop, the pH of the aqueous phase and the drug's dissociation constant. Lee *et al.* constructed ionic partition diagrams (Fig. 4.5) that define the domains of predominance for all the species present in the aqueous and organic phases as a function of interfacial voltage and aqueous pH. Partition diagrams offer a simple way to visualise all species at the ITIES predict the nature of the transferring species and describe the transfer mechanism of ionisable solutes. Such information can greatly improve our understanding of how drugs cross cellular membranes to reach their biological targets.

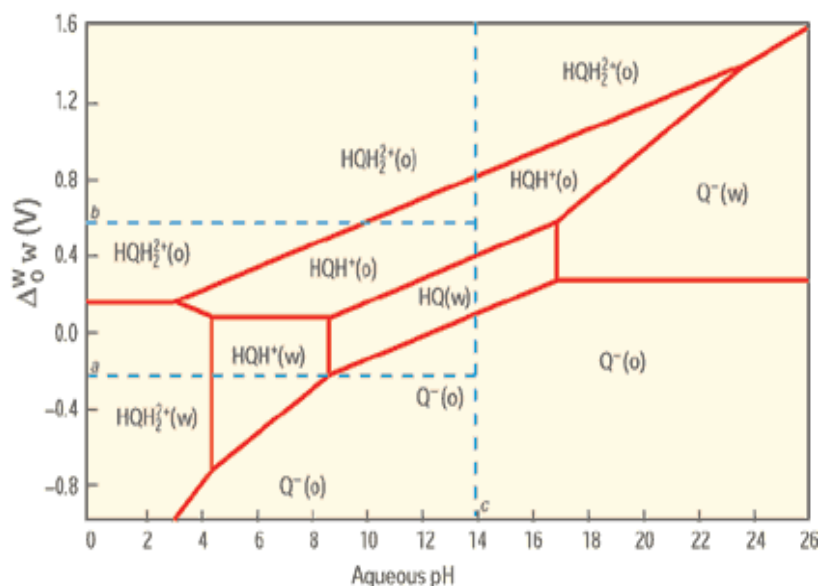


Figure 4.5: Ionic partition diagram showing transfer mechanisms of various forms of quinidine at the DCE/water interface.

HQH₂²⁺, HQH⁺, HQ, and Q⁻ stand for the doubly protonated, singly protonated, neutral and deprotonated species respectively. The solid red lines are the theoretical equi-concentration lines between two adjacent species. Blue lines *a* and *b* define the potential limits beyond which Li⁺ and TBA⁺ transfer preferentially. The domain above pH 14 (blue line *c*) is beyond experimental.

4.1.3 Linear sweep or scan voltammetry (LCV) and square waver voltammetry (SWV)

Linear potential sweep voltammetry (LSW) is one of the simplest voltammetric techniques which involve sweeping the electrode potential between limits E_1 and E_2 at a constant scan rate (v).

Chapter 4: Principle of secretive analytical techniques

$$E = E_1 + vt \text{ with } E \leq E_2 \quad \text{Equation 4.12}$$

The peak current, i_p , for a charge-transfer electrode reaction, is proportional to the concentration (C_0) of an electroactive analyte

$$i_p = 0.4463nFAC_0 \left(\frac{nF}{RT} \right) v^{1/2} D^{1/2} \quad \text{Equation 4.13}$$

where n is the number of electrons, v is the potential scan rate, A is the electrode surface area and D is the diffusion coefficient and F is the faraday's constant.

The derivative of LSV is the cyclic voltammetry technique. In this technique, the waveform is initially the same as in LSV at the difference that on reaching the potential E_2 the scan is reversed rather than terminated and again reaches the initial potential E_1 (Fig. 4.6). Depending on the aim of the study, single or multiple cycles can be used. During the potential scan, the applied potential results in the current measured by a current transducer. The position of the peaks is related to formal potential, E_0 , of the redox process, which is,

$$E_0 = \frac{E_p^{anodic} - E_p^{cathodic}}{2} \quad \text{Equation 4.14}$$

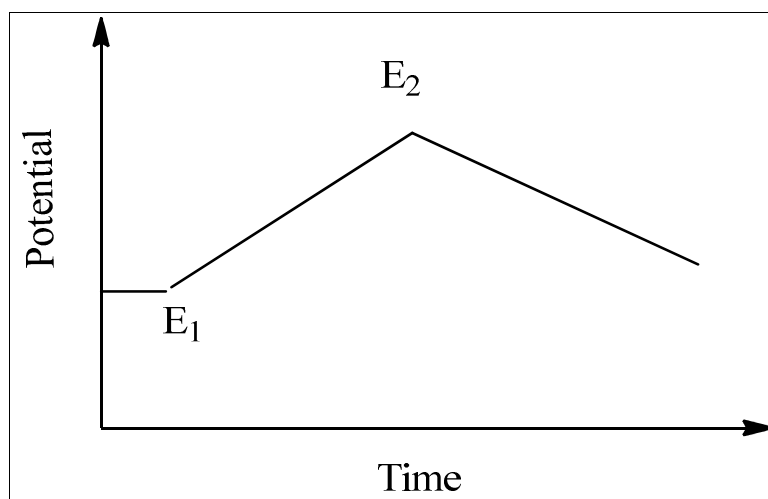


Figure 4.6: Typical potential waveform for the cyclic voltammetry technique.

Square-wave voltammetry is a large amplitude differential technique in which a waveform composed of an asymmetrical square wave superimposed on a base staircase potential applied to the working electrode. In fact, SWV is a small amplitude differential pulse technique in which a potential waveform composed of a symmetrical square wave is superimposed on a base-staircase potential [199]. The difference in current between the forward and reverse pulses is plotted as a function of the potential applied to the working electrode resulting in a voltammogram. Figure 4.7 illustrates the typical results of a 1 mM solution of ferrocene in 0.1 M $\text{Bu}_4\text{NClO}_4/\text{CH}_2\text{Cl}_2$ scan from lower potential to upper potential (oxidation process).

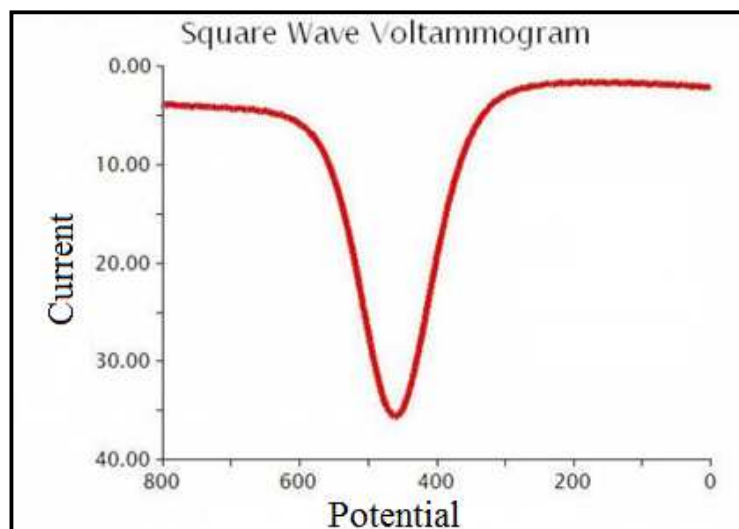


Figure 4.7: 1 mM Ferrocene in 0.1 M Bu_4NClO_4/CH_2Cl_2 , 25 mV Square amplitude, 2 mV Square increment, 10 ms Square period, 1 ms Sample width.

Applications: The advantages of square-wave voltammetry such as fast scan rate, large frequency, large amplitude and short time required for measurements as well as the specific approach in the current sampling procedure make this technique one of the most applicable among the pulse voltammetric techniques. This unique advantage makes the SWV useful in analytical applications as well as in fundamental studies of electrode mechanisms.

4.1.4 Electrochemical impedance spectroscopy (EIS)

Impedance spectroscopy (IS) is a relatively new and powerful method of characterization of electrical behaviour of material systems and their interfaces with electronically conducting electrodes.

Chapter 4: Principle of secretive analytical techniques

Principle: EIS is particularly characterised by the measurement and analysis of some or all of the four impedance-related functions Z , Y , M , and ϵ and the plotting of these functions in the complex plane. Where Z is frequency-dependent, Y is the admittance, $M = j\omega CZ$ is the modulus function and $\epsilon = M^{-1}$ is the complex dielectric constant or dielectric permittivity. The magnitude and direction of a planar vector in a right-hand orthogonal system of axes can be expressed by the vector sum of the components a and b along the axes that is by the complex number $Z = a + jb$. The imaginary number

$$j \equiv \sqrt{-1} \equiv \exp(j\pi/2) \quad \text{Equation 4.15}$$

indicates an anticlockwise rotation by $\pi/2$ relative to the X axis. Thus, the real part of Z , a , is in the direction of the real axis x , and the imaginary part b is along the Y axis. An impedance $Z(\omega) = Z' + jZ''$ is such a vector quantity and may be plotted in the plane with either rectangular or polar coordinates as shown in Figure 4.8 here the two rectangular coordinate values are clearly described in Equation 4.16.

$$R_e(Z) \equiv Z' = |Z|\cos(\theta) \text{ and } Im(Z) \equiv Z'' = |Z|\sin(\theta) \quad \text{Equation 4.16}$$

With the phase angle

$$\theta = \tan^{-1}(Z''/Z') \quad \text{Equation 4.17}$$

And the Modulus

$$|Z| = [(Z')^2 + (Z'')^2]^{1/2} \quad \text{Equation 4.18}$$

The plotting of these functions can be used to interpret the small-signal ac response of the electrode-material system being investigated.

Chapter 4: Principle of secretive analytical techniques

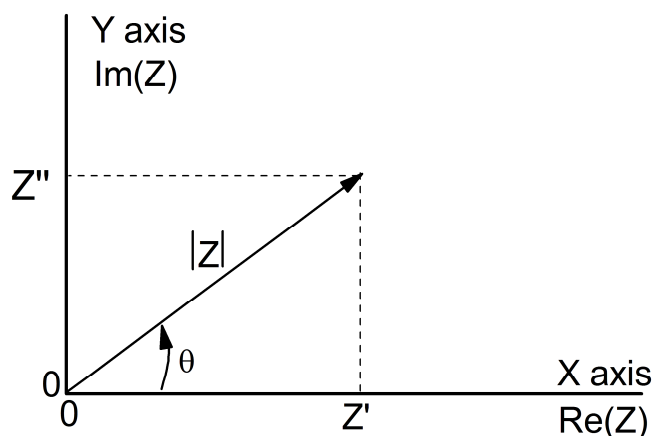


Figure 4.8: The impedance Z plotted as a planar vector using rectangular and polar coordinates.

In general, Z is frequency-dependent, as defined above. Conventional IS consists of the (nowadays often automated) measurement of Z as a function of the single frequency $\nu = \omega/2\pi$ or ω over a wide frequency range. It is from the resulting structure of the $Z(\omega)$ vs. ω response that one derives information about the electrical properties of the full electrode–material system. The early history of IS shows that the use of Z and Y in analyzing the response of electrical circuits is made up of ideal elements (R a resistor of resistance), L (inductor), and C (capacitor of capacitance)) and goes back to the beginning of the discipline of electrical engineering. These lumped elements are used on the equivalent circuit modelling of EIS data to physically extract properties of the electrochemical system by modelling the impedance data in terms of an electrical circuit. Z and/or Y have been widely used in theoretical treatments of semiconductor and ionic systems and devices since at least 1947 [200]. The complex plane plots have sometimes been called Nyquist diagrams or Bode diagrams. However, since Nyquist diagrams or Nyquist Plots are ways of showing frequency responses of linear systems, this refers to transfer function (three- or four-terminal) response. Nyquist plots display both the

Chapter 4: Principle of secretive analytical techniques

amplitude and phase angle on a single plot, using frequency as a parameter in the plot. Nyquist plots have properties that allow you to see whether a system is stable or unstable. It will take considerable mathematical development to see that, but it's the most useful property of Nyquist plots.

Bode diagrams or Bode' plots use frequency as the horizontal axis and use two separate plots to display amplitude and phase of the frequency response. A transfer function (T.F) can be represented by two separate plots, one giving the magnitude (in dBs) versus frequency and the other the phase angle (in degrees) versus frequency. A Bode diagram consists of two graphs: one is a plot of the logarithm of the magnitude of a transfer function, the other is a plot of the phase angle and both are plotted against frequency.



Chapter 4: Principle of secretive analytical techniques

Table 4.1: Different diagrams with corresponding equivalent circuit

Nyquist diagram						
Bode diagram						
Randles cell modelling						

Chapter 4: Principle of secretive analytical techniques

Experiment: On the experimental side, one should mention the early work of Randles and Somerton [200] on fast reactions in supported electrolytes; no complex plane plotting appeared here. Apparently the first plotting of impedance in the impedance plane for aqueous electrolytes was that of Sluyters (theory) and Sluyters and Oomen (experiment) [200]. Since then, there have been many pertinent theoretical and experimental papers dealing with IS and complex plane plots.

Electrochemical measurements are investigated to evaluate the electrochemical behaviour of an electrode and/or electrolyte materials that are usually made with cells which have two identical electrodes applied to the faces of a sample in the form of a circular cylinder or rectangular parallel pipe. However, if devices such as chemical sensors or living cells are investigated, this simple symmetrical geometry is often not feasible. Vacuum, a neutral atmosphere such as argon, or an oxidizing atmosphere is variously used. The general approach is to apply a voltage to the electrodes and observe the resulting current response.

During an impedance measurement, a frequency response analyser (FRA) is used to impose a small amplitude AC signal to the fuel cell via the load. The AC voltage and current response of the electrochemical cell is analysed by the FRA to determine the resistive, capacitive and the impedance which tell us about the inductive behaviour of the cell at that particular frequency. Many physicochemical processes occur within the cell such as the electron and ion transport, gas and solid phase reactant transport, heterogeneous reactions, etc. Also, these physico-chemical processes have a different characteristic time, and constants and therefore are exhibited at different AC frequencies.

Chapter 4: Principle of secretive analytical techniques

When conducted over a broad range of frequencies, impedance spectroscopy can be used to identify and quantify the impedance associated with these various processes.

Electronic equipment

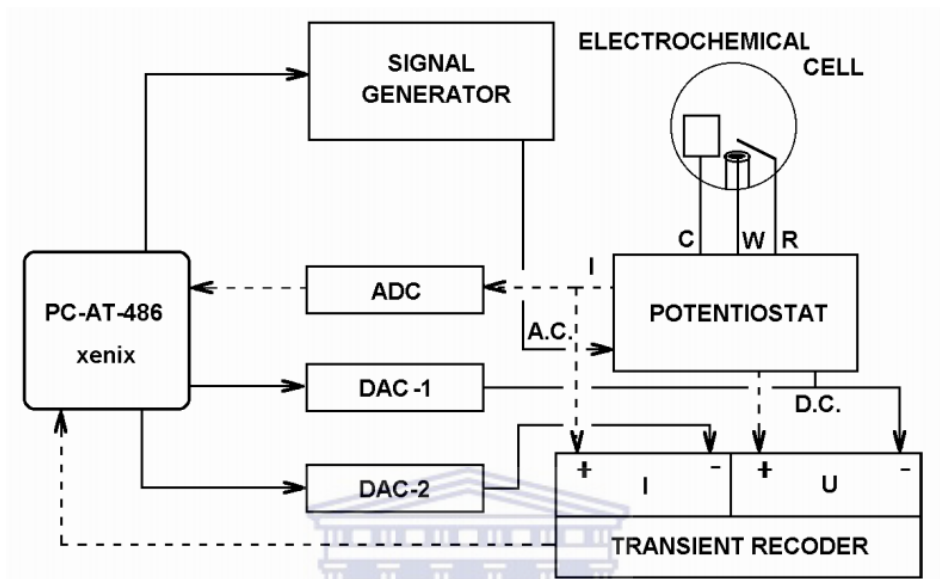


Figure 4.9: Electronic design used for electric measurements, dashed lines, - output signal routing, normal line – input signal routing.

Applications: Impedance spectroscopy (IS) appears destined to play an important role in fundamental and applied electrochemistry and materials science in the coming years. In this section two applications will be presented which illustrate the power of the IS technique when it is applied to two very diverse areas, aqueous electrochemistry and fast ion transport in solids. These particular examples were chosen because of their historical importance and because the analysis in each case is particularly simple. For the aqueous electrochemistry which is electrochemical impedance application, because we are dealing with real systems that do not necessarily behave ideally with processes that occur distributed in time and space, we often use specialised circuit elements (CPE and Z_W). The Warburg element (Z_W) is used to represent the diffusion or mass transport impedances of

Chapter 4: Principle of secretive analytical techniques

the cell. The electrochemical impedance is the response of the electrode chemical system (cell) to an applied potential. The electrochemical impedance spectroscopy (EIS) is used for diagnostic purpose to characterise changes at a surface. The EIS is also used for application purpose to know the effect of the materials on an electrode surface. An example of a generalised equivalent circuit element for a single cell fuel cell is shown below.

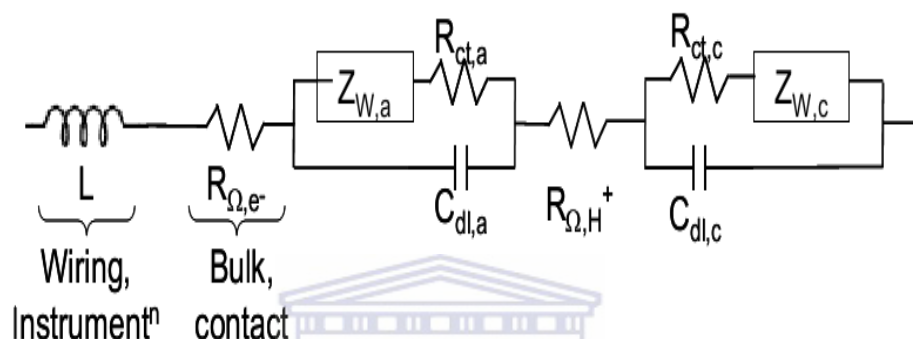


Figure 4.10: General equivalent circuit element for a single cell fuel cell. Key: GDL = gas diffusion layer, dl = double layer, ct = charge transfer, a = anode, c = cathode.

Figure 4.10 represents the general equivalent circuit analogue parameters. The resistors (R_{Ω,e^-} , $R_{ct,a}$, $R_{ct,c}$, and R_{Ω,H^+}) represent conductive pathways for ion and electron transfer. As such, they represent the bulk resistance of a material to charge transport such as the resistance of the electrolyte to ion transport or the resistance of a conductor to electron transport. Resistors are also used to represent the resistance to the charge-transfer process at the electrode surface. Capacitors ($C_{dl,a}$, $C_{dl,c}$) and inductors (L) are associated with space-charge polarisation regions such as the electrochemical double layer and adsorption/desorption processes at an electrode respectively. The impedance spectroscopy is applied in electrochemistry to determine the charge transfer resistance R_{ct} , the double

Chapter 4: Principle of secretive analytical techniques

layer capacitor C_{dl} the warburg impedance Z_w . Figure 4.11 shows how the later parameters can be graphically determined using Nyquist plot.

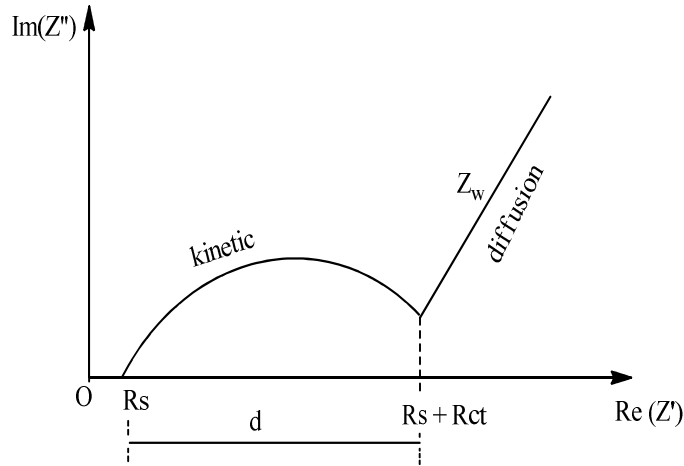


Figure 4.11: Nyquist plot for mixed control circuit.

$d = R_s + R_{ct}$ so, $R_{ct} = d - R_s$ where d is the diameter of the semi-circle, R_s (R_{Ω, H^+}) is for the resistance is the electrolyte solution. The equation of the above curve is

$$R_s(Z) = R_s + R_{ct} \left(1 + \frac{\lambda}{\sqrt{2\omega}} \right) \quad \text{Equation 4.19}$$

Where $\lambda = \frac{k}{\sqrt{D}}$, k is the chemical reaction rate, D is the diffusion coefficient

The Warburg impedance (Z_w) is created by diffusion within the cell and represented by the semi-infinite linear diffusion within the solution. As is shown in Figure 4.11, at high frequency, small Warburg impedance results and at low frequency, higher Warburg impedance is generated. The Equation 4.19 is used to determine the Warburg impedance

$$Z_w = \frac{R_{ct} \lambda}{\sqrt{2\omega}} \quad \text{Equation 4.20}$$

Chapter 4: Principle of secretive analytical techniques

Table 4.2: Circuit elements used in the models

Equivalent Element	Admittance	Impedance
R	$1/R$	R
C	$j\omega C$	$1/j\omega C$
L	$1/j\omega L$	$j\omega L$
W (Warburg)	$Y_0\sqrt{j\omega}$	$1/Y_0\sqrt{j\omega}$

4.2 Spectroscopy techniques

4.2.1 Proto nuclear magnetic resonance (^1H .NMR) spectroscopy

Proton nuclear magnetic resonance spectroscopy is the most powerful analytical technique appropriate for determination of the structure of organic compounds. NMR was first developed in 1946 by research groups at Stanford and M.I.T. in the USA [201].

Nowadays, NMR is an analytical technique used in advanced research and studied in basic undergraduate courses in many fields like chemistry, physics, biology, food sciences, medicine and material sciences. However, since it is half a century old, NMR was developed into the first organic spectroscopy available to chemists to determine the detailed chemical structure of the chemicals they were synthesising.

Principle: The ^1H NMR principle is based on the fact that the cores of atoms have magnetic properties that can be used to yield of chemical study. This principle is explained when the proton is placed in an external magnetic field, the proton's magnetic moment of the nuclei orient themselves with the external field (lower energy) or against it (higher

Chapter 4: Principle of secretive analytical techniques

energy). NMR is applied on the quantum subatomic particles which have spin such as proton, neutrons and electrons. The spin number can be paired in some atoms (eg ^{12}C , ^{16}O , ^{32}S) and cancel each other out so that the nucleus of the atom has no overall spin. However, in other atoms (eg ^1H , ^{13}C , ^{31}P , ^{15}N , ^{19}F), the spin number is unpaired and the nucleus does possess an overall spin. The spin of the given nucleus is determined by using the following rules:

- The spin is equal to zero if the number of nuclei and the number of protons of the atom are both even.
- The spin is equal to a half-integer (i.e. $\frac{1}{2}$, $\frac{3}{2}$, $\frac{5}{2}$) if the number of neutrons plus the number of protons is odd.
- The spin of the nucleus is equal to the integer spin (i.e. 1, 2, 3).

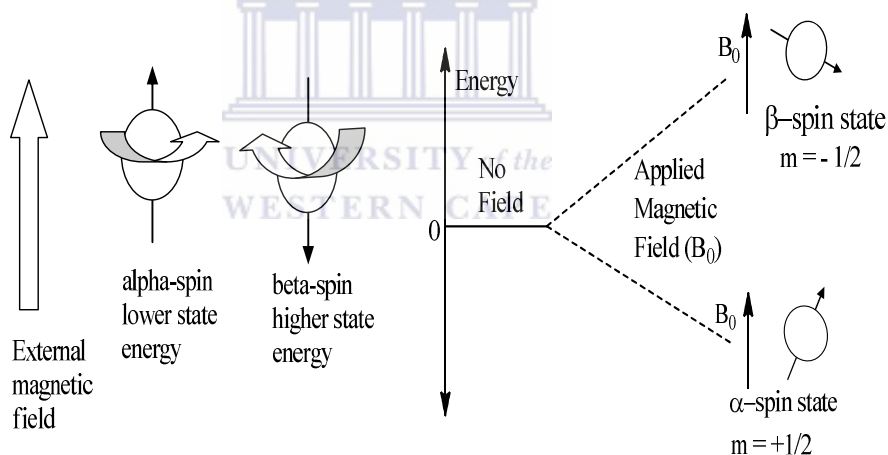


Figure 4.12: Illustration diagram of the principle ^1H NMR.

Chemical shift: It is the difference between the field strength at which the equivalent proton absorbs and the field strength at which the TMS proton absorbs when each proton is chemically shifted to a standard. It can be calculated using the relation:

Chapter 4: Principle of secretive analytical techniques

$$\delta(\text{delta}) = \frac{\text{observed chemical shift (Hz)} \times 10^6}{\text{Spectrometer frequencu (Hz)}} \text{ ppm} \quad \text{Equation 4.21}$$

When the chemical shift moves to the downfield, high magnetic field results and when the chemical shift moves to the upfield, low magnetic field strength is produced. Tetramethylsilane (TMS) is the reference compound used in order to standardise the NMR spectra. Tetramethylsilane, $(\text{CH}_3)_4\text{Si}$, is the standard and the reference compound for ^1H NMR because of its inert quality that prevents it from reacting with the sample as shown in the Figure 4.13 and its highly volatility property that makes it easy to evaporate out of samples. Figure 4.14 shows that when the chemical shift (δ) appeared on the downfield zone, high magnetic field strength results and when the chemical shift appeared in the upfield zone, low magnetic field strength is obtained. Some factors can affect the chemical shift like the shielding effects by decreasing the applied magnetic field (increasing the δ) and the electronegativity and deshielding by increasing δ .

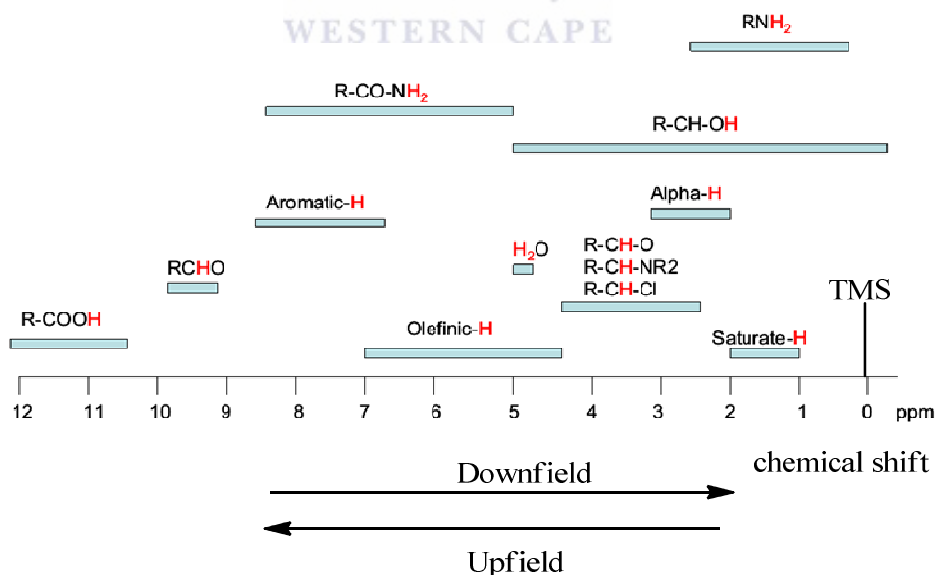


Figure 4.13: Diagram showing the ^1H NMR chemical shifts for common functional groups.

Chapter 4: Principle of secretive analytical techniques

Intensity and splitting of signals: The intensity of the signal is the area under the signals (integration) corresponding to the number responsible for that specific signal. Therefore, the signal is proportional to the number of protons, when the number of proton increases, the signal increases as well. The splitting of signal or spin-spin couple or multiplicity is the phenomenon where the spin of the nucleus of one proton is close enough to affect the spin of another (neighbors). The NMR signals are not always single but depending on the neighbors of a proton within the molecule, the split triangle can result in doublet (2 signals or peaks), triplets (3 signals) and quartets (4 signals). The distance between the split peaks are called coupling constants (J^{13}). The multiplicity is the number of protons bonded to the immediately adjacent carbon. The splitting of the signal is calculated using the $N + 1$ rule where N is the number of equivalent protons that are bonded to the adjacent carbons (neighbors).

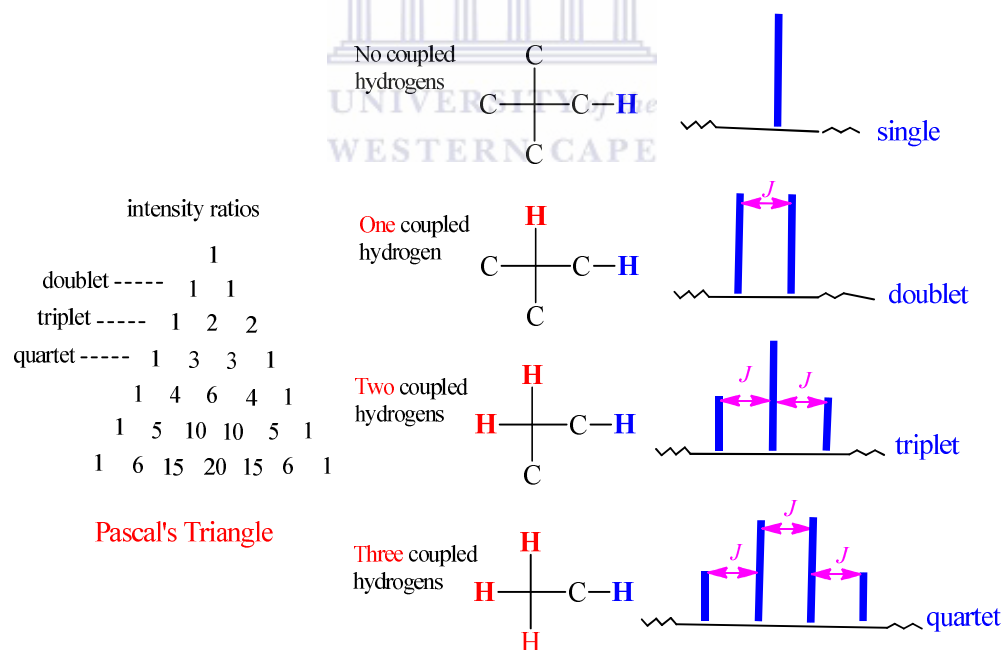


Figure 4.14: Pascal's triangle gives the intensity ratios between the split signals. 1 neighbor (doublet); 2 neighbors (triplet); 3 neighbors (quartet).

Chapter 4: Principle of secretive analytical techniques

Instrumentation

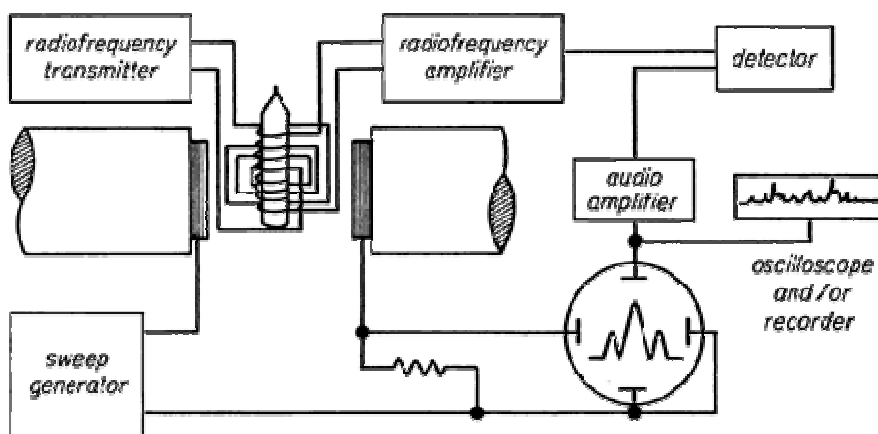


Figure 4.15: Electronic diagram used for a typical NMR spectrometer.

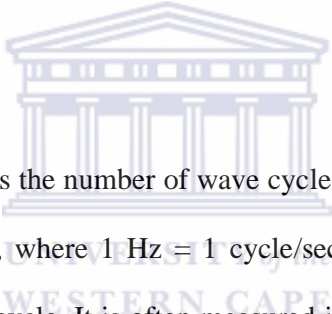
Applications: According to many studies carried out based on an NMR spectroscopy, this technique becomes a sophisticated and powerful analytical technology that found its applications in various disciplines of scientific research, medicine and various industries. In chemistry, the versatility of NMR spectroscopy has made it a widespread tool for the study of chemical structure. Similarly, NMR is used to study chemical bonds and to determine the structure of complex molecules like proteins. In addition, NMR of solid samples can help determine molecular structures in chemistry. For chemical kinetics, NMR spectroscopy is used to study molecular dynamics in solutions and to measure the diffusion coefficients.

4.2.2 Fourier transform infrared (FTIR) spectroscopy

The infrared spectroscopy is a chemical analysis technique used by organic and inorganic chemists to characterise functional groups present in a material. It provides mostly

Chapter 4: Principle of secretive analytical techniques

information about the presence or absence of certain chemical functional groups. Thus, the IR spectroscopy is a popular and important tool for structural elucidation and compound identification. This technique gives the band of frequencies between 4000 and 200 cm^{-1} beyond the red end of the visible spectrum. In a “classic” infrared spectrophotometer, an infrared light ray is produced and separated into two beams. One passes through a sample, another through a reference which is sometimes the compound in which the sample has been dissolved. Beams are then reflected until a detector, after being quickly alternated, enters beams into the detector. The two signals are compared and the spectrum obtained is registered. One of the great advantages of infrared spectroscopy is that we can study virtually any sample in virtually any state such as liquids, solutions, pastes, powders, films, fibres, gases and surfaces.



Principle: Frequency ν (nu), is the number of wave cycles that pass through a point in one second. It is measured in Hz, where 1 Hz = 1 cycle/sec. Wavelength λ (lambda) is the length of one complete wave cycle. It is often measured in cm (centimeters). Wave-length and frequency are inversely related:

$$\nu = \frac{c}{\lambda} \text{ and } \lambda = \frac{c}{\nu} \qquad \text{Equation 4.22}$$

Energy is related to wavelength and frequency by the following equation

$$E = h\nu = \frac{hc}{\lambda} \qquad \text{Equation 4.23}$$

Where c is the speed of light, h is Planck's constant, ν is the frequency and λ is the wavelength.

Chapter 4: Principle of secretive analytical techniques

That energy is directly proportional to frequency and inversely proportional to wavelength. The interpretation of an IR spectroscopy involves a new unit of measurement called the wavenumber ($\bar{\nu}$) which is the number of waves in one centimeter and has the unit of reciprocal centimetres (cm^{-1}). The wavenumber is inversely proportional to wavelength and directly proportional to frequency and energy which makes it more convenient to use. The IR region is divided into three regions: the near, mid and far IR (Fig. 4.16). The mid IR region is of greatest practical use to the organic chemist. This is the region of wavelengths between 3×10^{-4} and 3×10^{-3} cm. The energy of the IR photon, being insufficient to cause electronic excitation, can only cause vibration or rotation excitation.

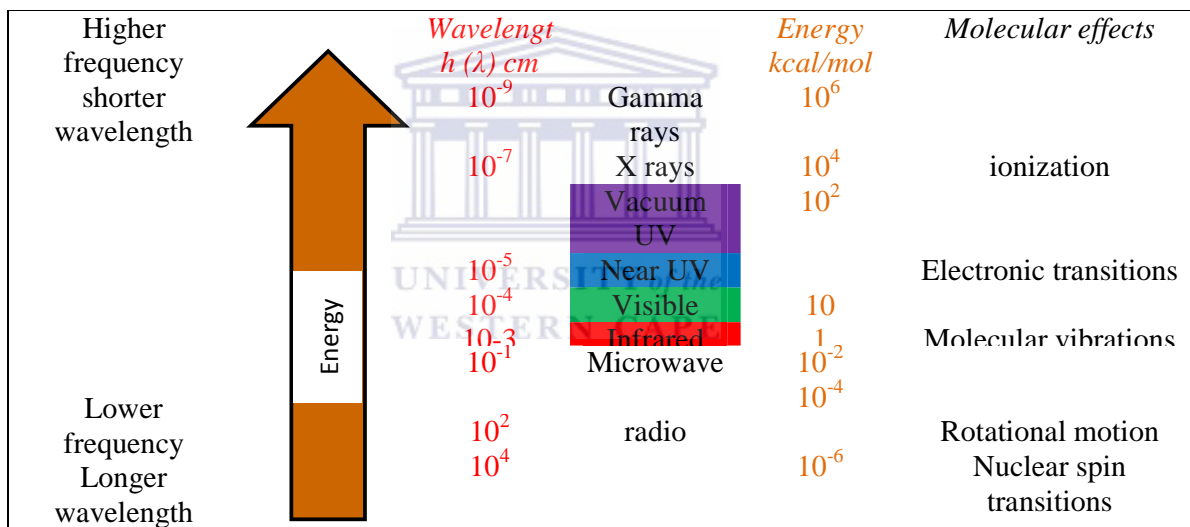


Figure 4.16: Electromagnetic spectrum. [202]

Molecular vibration [203]: The molecule can vibrate in two different ways, stretching and bending. A molecule containing N atoms has a total of $3N$ of degrees of vibrational modes (vibrational degrees of freedom) corresponding to the Cartesian coordinates of each atom in the molecule. The linear molecules have $3N - 5$ of vibrational degrees of freedom,

Chapter 4: Principle of secretive analytical techniques

whereas nonlinear molecules have $3N - 6$ degrees of vibrational modes. In nonlinear molecules, three of these degrees are rotational three are translational and the remaining correspond to fundamental vibrations while in linear molecules, two degrees are rotational three are translational [204-205]. The fundamental vibrations for water, H_2O and CO_2 which are nonlinear and linear molecules respectively are given by the Figure 4.17.

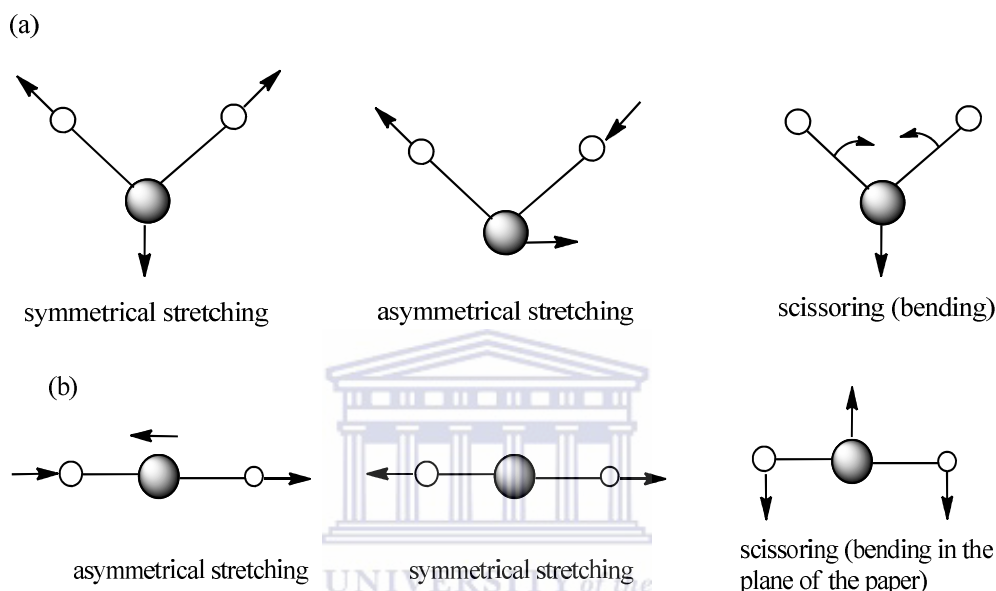


Figure 4.17: (a) Stretching and bending vibrational modes for H_2O . (b) Stretching and bending vibrational modes for CO_2 .

Chapter 4: Principle of secretive analytical techniques

Table 4.3: Some selected bonds with their absorption regions [206]

Functional class	Stretching vibrations		Bending vibrations	
	assignment	range [cm ⁻¹]	assignment	range [cm ⁻¹]
Alkanes	CH ₃ , CH ₂ & CH	2850-3000 str	CH ₂ & CH ₃ defor	1350-1470
	2 or 3 bands		CH ₃ defor	med
			CH ₂ rocking	1370-1390 med 720-725 wk
Alkenes	=C-H & =CH ₂	3020-3100 med	=C-H & =CH ₂	880-995 str
	C=C (symmetry)	1630-1680 var	(out-	780-850 med
	C=C (asymmetric stretch)	1900-2000 str	of-plane bending)	675-730 med
alkynes	C-H (sharp)	3300 str	Cis-RCH=CHR	
	C≡C (symmetry)	2100-2250 var	C-H defor	600-700 str
Arenes	C-H (several bands)	3030 var	C-H bending &	690-900 str-
	C=C (in ring)(2 or 3 bands)	1600 & 1500 med-wk	ring puckering	med
Alcohols & phenols	O-H (free, shp)	3580-3650 var	O-H bend (in-	1330-1430
	O-H (H-bonded, broad)	3200-3550 str	plane	med
			O-H bend (out-	650-770
	C-O	970-1250 str	of-plane	
Amines	N-H (1°-amines), 2 bands	3400-3500 wk	NH ₂ scissoring (1550-1650
	N-H (2°-amines)	3300-3400 wk	1°-amines)	med-str
	C-N	1000-1250	NH ₂ & N-H wagging (shifts on H-bonding)	660-900 var

Chapter 4: Principle of secretive analytical techniques

Table 4.3: Some selected bonds with their absorption regions [206]

Functional class	Stretching vibrations		Bending vibrations	
	assignment	range [cm ⁻¹]	assignment	range [cm ⁻¹]
Aldehydes & ketones	C-H (aldehyde)	2690-2840 (2 bands)		
		med	α -CH ₃	1350-1360
	C=O (saturated aldehyde)	1720-1740 str	bending	str
			α -CH ₂	1400-1450
	C=O (saturated ketone)	1710-1720 str	bending	str
			C-C-C	1100 med
	Aryl ketone	1690 str	bending	
α,β -unsaturation	1675 str			
cyclopentanone	1745 str			
cyclobutanone	1780 str			
Carboxylic acids & derivatives	O-H (very brd)	2500-3300(acids)	C-O-H	1395-144
	C=O (H-bonded)	1705-1720(acids)	bending	
	O-C (sometimes 2 peaks)	1210-1320(acids) med-str		
	C=O	1785-1815 (acyl halides)		
		str		
	C=O (2-bands)	1750 & 1820 (anhydrides) str		
	O-C	1040-1100 str		
	C=O	1735-1750 (esters) str		
	O-C (2-bands)	1000-1300 str	N-H (1i- amide) II band	1590-1650 med
	C=O(amide 1 band)	1630-1695 (amides) str	N-H (2i- amide) II band	1500-1560
Nitriles	C \equiv N (shp)	2240-2260 med		
Isocyanates,	-N=C=O,	2100-2270 med		
isothiocyanates,	-N=C=S,			
Diimides,	-N=C=N-,			
ketenes	C=C=O			

Chapter 4: Principle of secretive analytical techniques

Most of the absorptions cited are associated with stretching vibrations. Standard abbreviations (str = strong, wk = weak, brd = broad & shp = sharp, defor = deformation) are used to describe the absorption bands. Some of the functional groups in infrared absorption which are listed in the preceding table are given above [206].

Instrumentations: In a “classic” infrared spectrophotometer, an infrared light ray is produced and separated into two beams. One passes through a sample, another through a reference which is sometimes the compound in which the sample has been dissolved. Beams are then reflected until a detector after being quickly alternated, enters beams into the detector.

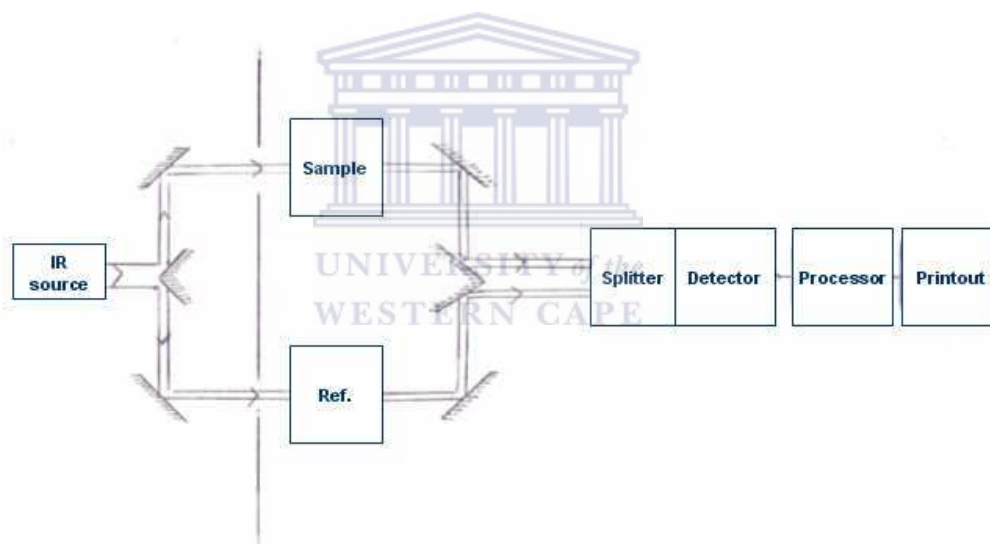


Figure 4.18: The functioning principle of an infrared spectrophotometer.

FTIR spectrometers are widely used in organic synthesis, polymer science, petrochemical engineering, pharmaceutical industry and food analysis. In addition, since FTIR spectrometers can be hyphenated to chromatography, the mechanism of chemical reactions and the detection of unstable substances can be investigated using such instruments.

Chapter 4: Principle of secretive analytical techniques

Applications: A spectroscopy in the IR region determines the frequency specific for a specific bonds such as C=C, C≡C, C=O and intensity of absorption. So the IR absorption data is very useful in structure determination. IR is useful for quantitative estimation and for identification of a functional group of molecules. IR analysis can be used to determine the identities of polymer materials in a multilayered film.

4.2.3 Ultraviolet / Visible (UV/Vis) spectroscopy

Ultraviolet and visible absorption spectroscopy is a very useful technique in analytical chemistry for the quantitative measurement of the attenuation of a beam of light after it passes through a sample or after reflection from a sample surface in solutions of transition metal ions and organic compounds.

Principle: A UV-Vis spectroscopy involves the absorption of ultraviolet light by a molecule causing the promotion of an electron from a ground electronic state to an excited electronic state. Electronic transition: it occurs when the electrons in the molecule move from a lower energy level to a high energy level in a few limited seconds. The electronic transition level stated that when σ , π and n electrons are present in a molecule, it can be excited from the ground state to excited state by the absorption of UV radiation. The various transitions levels are $n \rightarrow \pi^*$, $\pi \rightarrow \pi^*$, $n \rightarrow \sigma^*$ and $\sigma \rightarrow \sigma^*$ and can be represented using the diagram as follows:

Chapter 4: Principle of secretive analytical techniques

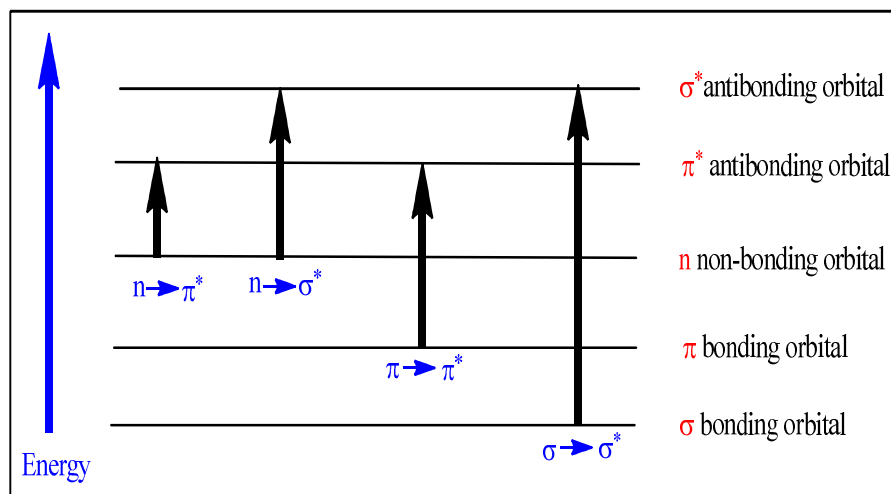
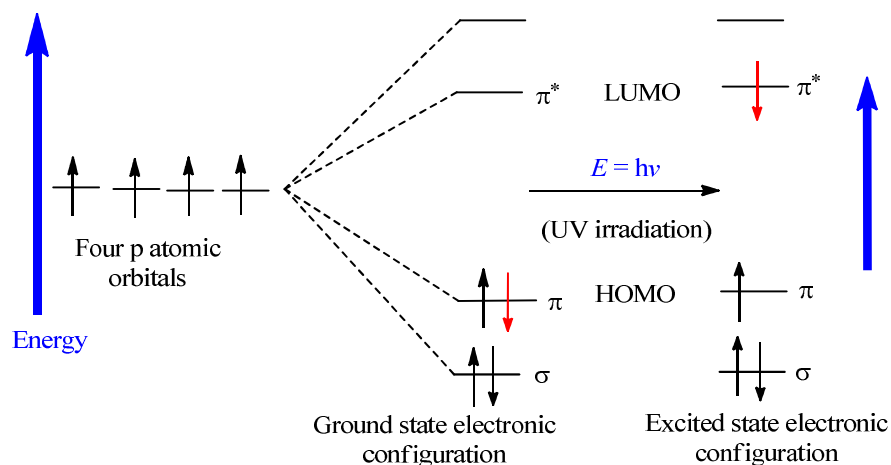


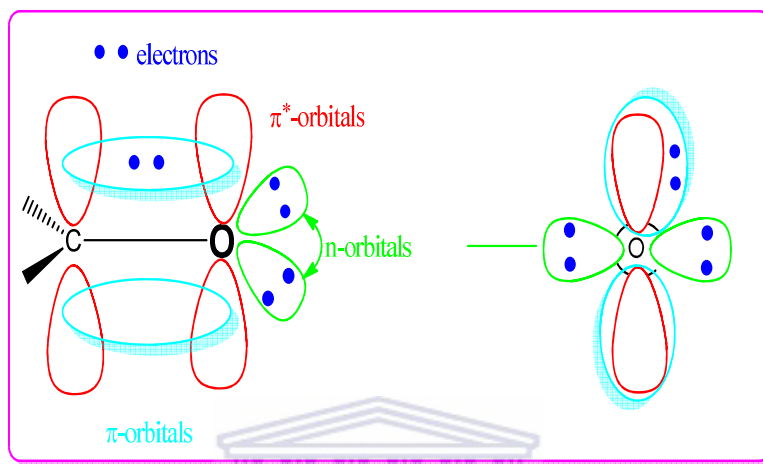
Figure 4.19: Energy levels of electronic transitions.

The transitions between the electronic states are governed by Selection Rules which states that allowed transitions means that a ground and excited state for a possible transition possess the required characteristics and forbidden transitions means ground and excited state do not meet the characteristics. Some transitions are “allowed” and others may be “forbidden”. Allowedness is associated with the geometries of HOMO and LUMO and the symmetry of the molecule as a whole.



Chapter 4: Principle of secretive analytical techniques

The common examples of transitions of an isolated carbonyl group are $n \rightarrow \pi^*$ transition which is lower in energy where ($\lambda_{\max} = 290 \text{ nm}$) is the forbidden transition and $\pi \rightarrow \pi^*$ transition which is higher in energy ($\lambda_{\max} = 180 \text{ nm}$) is an allowed transition. This can be explained on the basis of the spatial distribution of these orbitals.



The n -orbitals do not overlap at all well with the π^* orbital, so the probability of this excitation is small. The $\pi \rightarrow \pi^*$ transition, on the other hand, involves orbitals that have significant overlap and the probability is near 1.0. Allowed transitions have higher ϵ_{\max} values than the forbidden transitions.

Chromophores: There are a group of atoms and electrons within a chemical molecule which are responsible for the color which arises when the molecule absorbs certain wavelengths of visible light and transmits or reflects others. The bonds between the atoms in a chromophore group are responsible for the selective absorption of visible light while reflecting other light and lend color to the molecule. The presence of an absorbance band at a particular wavelength often is a good indicator of the presence of a chromophore. However, the position of the absorbance maximum is not fixed but depends partially on the molecular environment of the chromophore and on the solvent in which the sample

Chapter 4: Principle of secretive analytical techniques

may be dissolved. Other parameters such as pH and temperature also may cause changes in both the intensity and the wavelength of the absorbance maxima.

Table 4.4: List of selected chromophores and their light absorption characteristics

Chromophores	Electronic Transition	Molecules	λ_{\max} (nm)	ϵ_{\max} ($\text{cm}^2 \cdot \text{mmol}^{-1}$)
$\text{C}-\text{H}$	$\sigma \rightarrow \sigma^*$	CH_4	122	intensive
$\text{C}-\text{C}$	$\sigma \rightarrow \sigma^*$	$\text{H}_3\text{C}-\text{CH}_3$	135	intensive
O	$n \rightarrow \sigma^*$	H_2O	167	1 500
	$n \rightarrow \sigma^*$	$\text{H}_3\text{C}-\text{OH}$	183	200
	$n \rightarrow \sigma^*$	$\text{C}_2\text{H}_5-\text{O}-\text{C}_2\text{H}_5$	189	2 000
S	$n \rightarrow \sigma^*$	$\text{H}_3\text{C}-\text{SH}$	235	180
	$n \rightarrow \sigma^*$	$\text{CH}_3-\text{S}-\text{CH}_3$	228	620
	$n \rightarrow \sigma^*$	$\text{C}_2\text{H}_5-\text{S}-\text{S}-\text{C}_2\text{H}_5$	250	380
N	$n \rightarrow \sigma^*$	$\text{C}_2\text{H}_5-\text{NH}_2$	210	800
	$n \rightarrow \sigma^*$	$\text{C}_2\text{H}_5-\text{N}-\text{C}_2\text{H}_5$	193	3 000
	$n \rightarrow \sigma^*$	$(\text{C}_2\text{H}_5)_3\text{N}$	213	6 000
Hal	$n \rightarrow \sigma^*$	$\text{H}_3\text{C}-\text{Cl}$	173	200
	$n \rightarrow \sigma^*$	$\text{H}_3\text{C}-\text{Br}$	204	260
	$n \rightarrow \sigma^*$	$\text{H}_3\text{C}-\text{I}$	193	380
$\text{C}=\text{C}$	$\pi \rightarrow \pi^*$	$\text{H}_2\text{C}=\text{CH}_2$	165	16 000
	$\pi \rightarrow \pi^*$	$\text{C}_2\text{H}_5-\text{C}(\text{H})=\text{C}(\text{H})-\text{C}_2\text{H}_5$	185	7 940
$\text{C}\equiv\text{C}$	$\pi \rightarrow \pi^*$	$\text{HC}\equiv\text{CH}$	173	6 000
	$\pi \rightarrow \pi^*$	$\text{H}-\text{C}\equiv\text{C}-\text{C}_2\text{H}_5$	172	2 500
$\text{C}=\text{O}$	$n \rightarrow \pi^*$	$\text{H}_3\text{C}-\text{C}(\text{H})=\text{O}$	293	12
	$\pi \rightarrow \pi^*$	$\text{CH}_3-\text{C}(\text{O})-\text{CH}_3$	187	950
	$n \rightarrow \pi^*$	$\text{CH}_3-\text{C}(\text{O})-\text{CH}_3$	273	14
$\text{C}=\text{S}$	$n \rightarrow \pi^*$	$\text{CH}_3-\text{C}(\text{S})-\text{CH}_3$	460	weak
$\text{N}=\text{N}$	$n \rightarrow \pi^*$	$\text{H}_3\text{C}-\text{N}(\text{CH}_3)=\text{N}(\text{CH}_3)$	353	240
$\text{N}=\text{O}$	$n \rightarrow \pi^*$	$(\text{H}_3\text{C})_3\text{C}-\text{NO}$	300	100
		$(\text{H}_2\text{C})_3\text{C}-\text{NO}$	665	20

Chapter 4: Principle of secretive analytical techniques

Solvent effects: The electrostatic interaction between polar solvents and polar chromophores tend to stabilise both the non-bonding electronic ground states and the π^* excited states. This interaction causes the $n \rightarrow \pi^*$ transitions, which usually occur at lower energy and $\pi \rightarrow \pi^*$ transitions to move to lower energy. Thus, the $\pi \rightarrow \pi^*$ and $n \rightarrow \pi^*$ transitions for polar chromophores move closer to each other which increase the polarity of the solvent. An example of this phenomenon is the solvent shift of the $n \rightarrow \pi^*$ transition to lower energy in the ultraviolet spectrum of N-nitrosodimethylamine. For various solvents, the order for decreasing energy is given by the Table 3.4 [207].

Table 4.5: Solvent effect on wavelength in UV-Vis (for 1 cm cell)

Solvent	Approximate wavelength (nm)
Water	190
Ethanol	210
n-Hexane	195
Cyclohexane	210
Benzene	280
Diethyl ether	210
Acetone	330
1,4-Dioxane	220

Instrumentation: Currently, most of the work has been reported on the absorption spectra range of 200 to 1000 nm of organic molecules in diluted solutions as defined by typical commercial UV-Vis spectrophotometers. But the simple UV-Vis spectrometers can absorb the ultraviolet wavelengths less than 180 nm by atmospheric gases which are the short-wavelengths. The long-wavelength limit is usually determined by the wavelength response of the detector in the spectrometer. In a standard UV-Vis spectrophotometer, a beam of

Chapter 4: Principle of secretive analytical techniques

light is split; one half of the beam (the sample beam) is directed through a transparent cell containing a solution of the compound being analysed and one half (the reference beam) is directed through an identical cell that does not contain the compound but contains the solvent. The instruments for measuring the absorption of UV-Vis radiation are made up of the sources (UV and visible), filter or monochromator, sample container or sample cells and the detector. For the sources of radiation in the UV zone, hydrogen, xenon and mercury lamps are used and the deuterium and tungsten lamp are mostly used because they emit radiation in the range of 160 – 375 nm. In a visible zone, mercury vapour and carbon lamps are used and added to tungsten. The light source is either a diffraction grating or a monochromator. The detector can either be a photodiode (used with a monochromator) or a CCD (used with diffraction gratings).

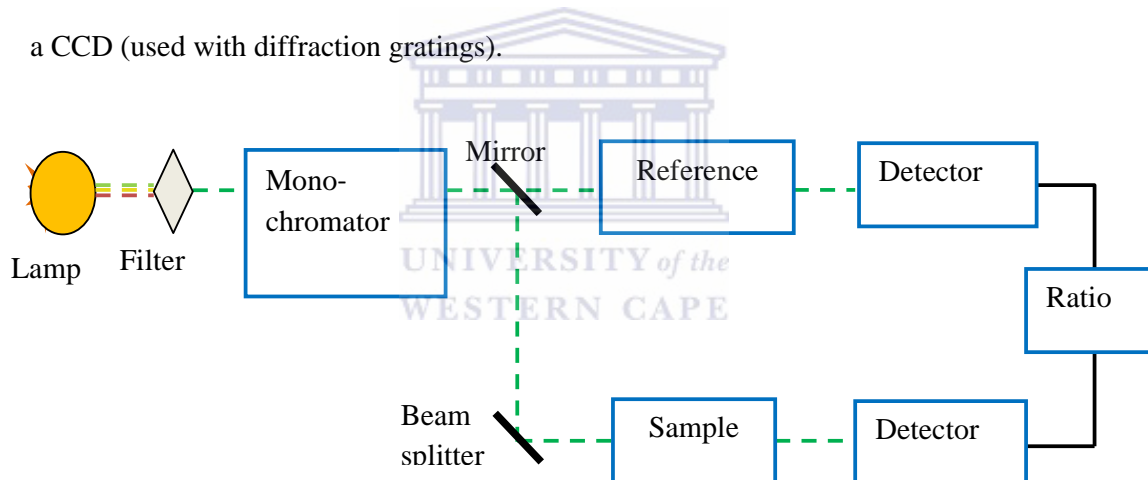


Figure 4.20: Schematic of a dual-beam uv-vis spectrophotometer.

This analytical method is most often used in a quantitative way to determine concentrations of an absorbing analyte in solution using the Beer-Lambert law. The Beer-Lambert Law states that the concentration of a substance in solution is directly proportional to the absorbance of the solution.

$$A = \log_{10}(I_0/I) = \log_{10}1/T = -\log_{10}T = \varepsilon \cdot c \cdot l$$

Equation 4.24

Chapter 4: Principle of secretive analytical techniques

where A is the measured absorbance, in Absorbance Units (AU), I_0 is the intensity of the incident light at a given wavelength, I is the intensity of the light transmitted through the sample, T is the transmittancy, l the path length (cm), ϵ is the molar absorptivity ($\text{L mol}^{-1} \text{cm}^{-1}$) and c is the concentration of the absorbing species (mol L^{-1}). This law is only true for monochromatic light, which is the light of a single wavelength or a narrow band of wavelengths and provided that the physical or chemical properties of the substance do not change with concentration.

Application: UV spectroscopy is used for measuring the absorption, emission and transmission of the ultraviolet and the visible wavelengths by matter. This technique is complementary to the fluorescence spectroscopy. Absorption of radiation by a sample is measured at various wavelengths and plotted by a recorder to give the spectrum which is a plot of the wavelength of the entire region versus the absorption (A) of light at each wavelength. A UV-Vis spectroscopy is routinely used in different ways. For detection of impurities: a UV absorption spectroscopy is one of the best methods use to determine the impurities in organic molecules. The spectral of the organic molecules shows additional peaks due to impurities in the sample and it can be compared with that of standard raw material. The absorbance measurement at a specific wavelength can be used to detect the impurities. For example, benzene appears as a common impurity in cyclohexane and its presence can be easily detected by its absorption at 255 nm. For structure elucidation of organic compounds: In organic molecules structure, the presence or absence of unsaturation and the presence of hetero atoms can be determined using the UV spectroscopy. From the location of peaks and the combination of peak absorption and referring to Table 3.3, it can be concluded whether the compound is saturated or

Chapter 4: Principle of secretive analytical techniques

unsaturated or contained hetero atoms or not. For quantitative analysis, the quantification of compounds that absorb UV radiation in analytical chemistry can also be done using UV absorption spectroscopy. Many other methods for quantitative analysis can be elucidated such as the calibration curve method; the simultaneous multicomponent method; the difference spectrophotometric method; and the derivative spectrophotometric method. For qualitative analysis, UV absorption spectroscopy can be used to characterise those types of compounds which absorb UV radiation with the spectra applied on the characterisation of aromatic compounds and aromatic olefins. Using the Equation 5.1, the PKa value can be calculated if the ratio of $[A^-] / [HA]$ is known at a particular PH. and the ratio of $[A^-] / [HA]$ can be determined spectrophotometrically from the graph plotted between absorbance and wavelength at different PH values. For chemical kinetics, the kinetics of reaction is very important in analytical chemistry and can also be studied using UV spectroscopy. It can be observed that the UV radiation passing through the reaction cell and the absorbance changes as well. For quantitative analysis of pharmaceutical substances, the pharmaceutical compounds (drugs) are either in the form of raw material or in the form of formulation. After assayed drugs are made into a suitable solution in a solvent, the absorbance at specific wavelength can be measured. For example, a diazepam tablet can be analyzed by 0.5% H_2SO_4 in methanol at the wavelength 284 nm. For molecular weight determination: In this case, the spectrophotometry is used to determine the molecular weights of compounds by preparing the suitable derivatives of these compounds. For example, if we want to determine the molecular weight of amine then it is converted in to amine picrate. Then a known concentration of amine picrate is dissolved in a liter of solution and its optical density is measured at $\lambda_{max} = 380$ nm. After this the

Chapter 4: Principle of secretive analytical techniques

concentration of the solution in moles per litre can be calculated by using the following formula.

$$c = \frac{\log_{10} I_0/I}{\varepsilon_{max} \times l} \quad \text{Equation 4.25}$$

Where the weight "w" of amine picrate is known so from "c" and "w", the molecular weight of amine picrate can be calculated. The molecular weight of picrate can be calculated using the molecular weight of amine picrate. As an HPLC detector, a UV/Vis spectrophotometer may be used as a detector for HPLC. The presence of an analyte gives a response which can be assumed to be proportional to the concentration. For more accurate results, the instrument's response to the analyte in the unknown should be compared with the response to a standard; as in the case of a calibration curve.

4.2.4 Fluorescence (FL) spectroscopy

Fluorescence spectroscopy perhaps is the photonic process that is opposite to UV-Vis spectroscopy as fluorescence allowed transitions with a lifetime in the nanosecond range from a higher to a lower excited singlet state of molecules. After photon is absorbed, FL is used to measure the intensity of photons emitted from a molecule. In UV-Vis spectroscopy, the component responsible for the electronic transition at the specific wavelength is called chromophore while in fluorescence, this component is named fluorophore [208]. Indeed, the theme chromophore implies that the molecule absorbs light while fluorophore means that the molecule, likewise, emits light. At room temperature most molecules occupy the lowest vibrational level of the ground electronic state and on absorption of light they are elevated to produce excited states. The simplified diagram

Chapter 4: Principle of secretive analytical techniques

below shows absorption by molecules from ground state to produce either the first, S1, or second S2, excited state (Fig 4.21).

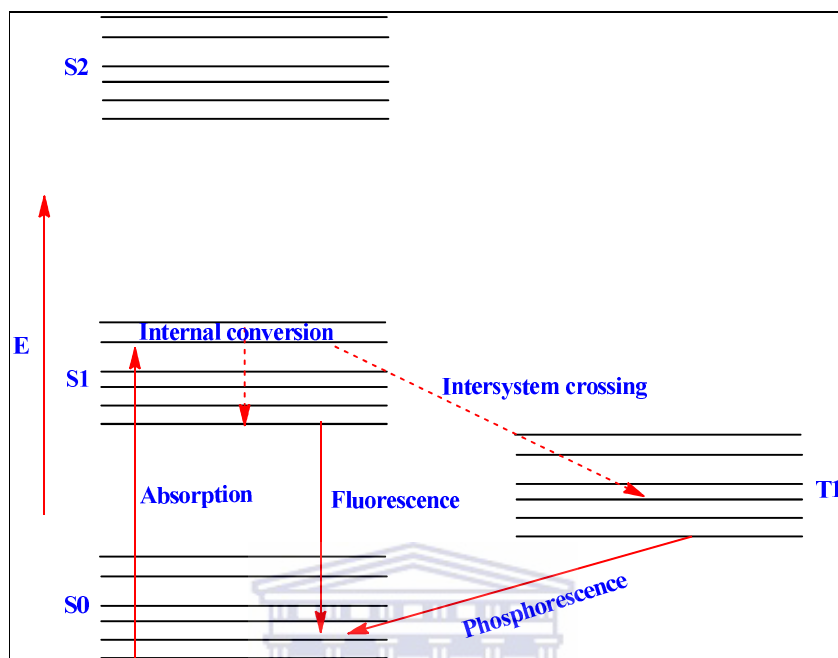


Figure 4.21: The Jablonski (electronic transition) diagram. *E* is the energy scale; *S0* is the ground singlet electronic state; *S1* and *S2* are the successively higher energy excited singlet electronic states. *T1* is the lowest energy triplet state.

Figure 4.21 is called the Jablonski diagram or the electronic transitions diagram, because electrons of chromophores and/or fluorophores are responsible for the different described transitions [209]. Fluorescence emission occurs as the fluorophore decays from the singlet electronic excited states to an allowable vibrational level in the electronic ground state.

Principle: Emission spectra are recorded by choosing an appropriate excitation wavelength and scanning wavelength with the emission monochromator. When we want to record the fluorescence emission spectrum, the excitation wavelength is kept fixed and the emission monochromator is run.

Chapter 4: Principle of secretive analytical techniques

Instrumentation

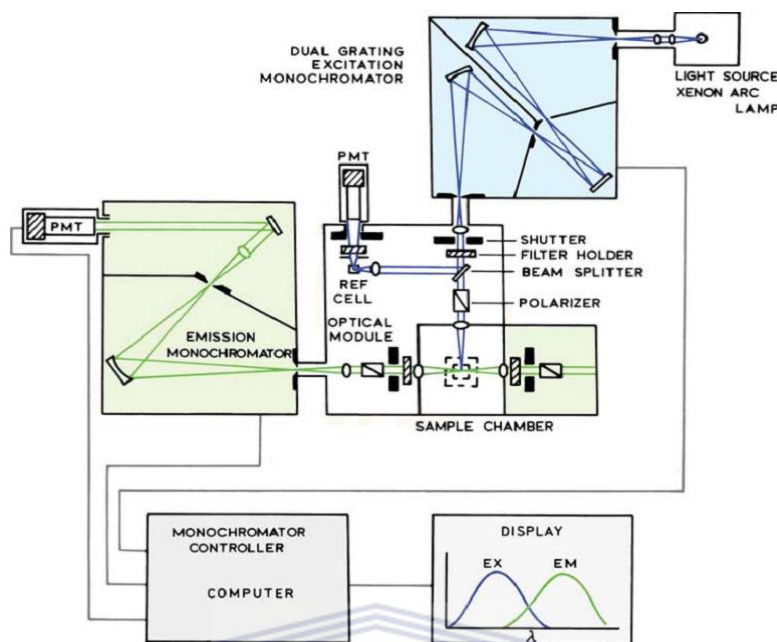


Figure 4.22: Schematic diagram of a spectrofluorometer. [209].

Applications: Fluorescence is several orders of conventional absorbance-based techniques that are more sensitive and more selective. The sensitivity increases while the emitted radiation is measured directly and can be increased simply by increasing the incident power. In the fluorescence-based technique, selectivity is much higher than in absorbance-based approaches. These two properties of the fluorescence-based techniques make fluorescence spectroscopy an ideal technique for various fields of application such as in bioanalytical studies, water quality and small or solid sample analysis. For bioanalytical study, fluorometric methods of analysis are probably most often performed in the clinical laboratory to determine the amount of a given species present in a biological sample (e.g., urine, liver tissue).

Chapter 4: Principle of secretive analytical techniques

4.2.5 Atomic force microscopy (AFM)

Atomic force microscopy (AFM) is an imaging technique used to determine topography and other properties of surfaces. AFM is the extended method of the scanning tunnelling microscopy (STM) technique which was developed to investigate the electrically non-conductive materials, like proteins and is a useful tool for nanoscience.

Principle: Images are taken by scanning the sample relative to the probing tip and digitising the deflection of the lever or the z-movement of the piezo as a function of the lateral position x , y . An AFM cantilever should have a high resonant frequency, the equation for the resonant frequency of a spring is:

$$\text{Resonant frequency} = \frac{1}{2\pi} \sqrt{\frac{\text{spring constant}}{\text{mass}}} \quad \text{Equation 4.26}$$

This equation shows that when the cantilever has a small mass, it can have both low spring constant and high resonant frequency. There are four principal kinds of operational modes according to the separation between the cantilever and the surface, the cantilever's oscillation amplitude and the normal or torsional bending of the cantilever. There are contact mode, noncontact mode, and intermittent contact mode and lateral force microscopy. When the microscope is operated in non-contact mode at tip-sample separations of 10 to 100 nm, forces such as Van Der Waals, electrostatic and magnetic or capillary forces can be sensed and they give information about surface topography, distributions of charges, magnetic domain wall structure or liquid film distribution. In this mode, ionic repulsion forces allow the surface topography to be traced with high resolution.

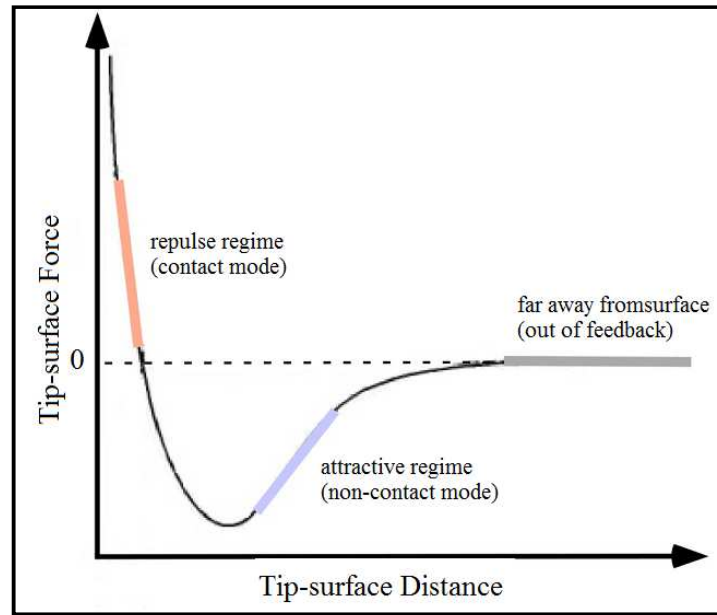


Figure 4.23: Typical force-separation curve.

Far from the sample, the cantilever is not affected by interatomic forces and is in its free equilibrium position. But when brought closer to the surface, attractive forces act upon the tip to bend the cantilever towards the sample. When the tip is in contact with the surface, repulsive forces dominate, deflecting the cantilever backwards. The thick lines indicate the normal ranges of operation for contact and noncontact modes and the long horizontal arrow represents the usual amplitude for intermittent contact.

Instrument: Figure 3.24 operates by measuring attractive or repulsive forces between a tip and the sample [210]. In its repulsive "contact" mode, the instrument lightly touches a tip at the end of a leaf spring or "cantilever" to the sample. Thus, in contact mode the AFM measures hard-sphere repulsion forces between the tip and sample. In noncontact mode, the AFM derives topographic images from measurements of attractive forces; the tip does not touch the sample [211-212].

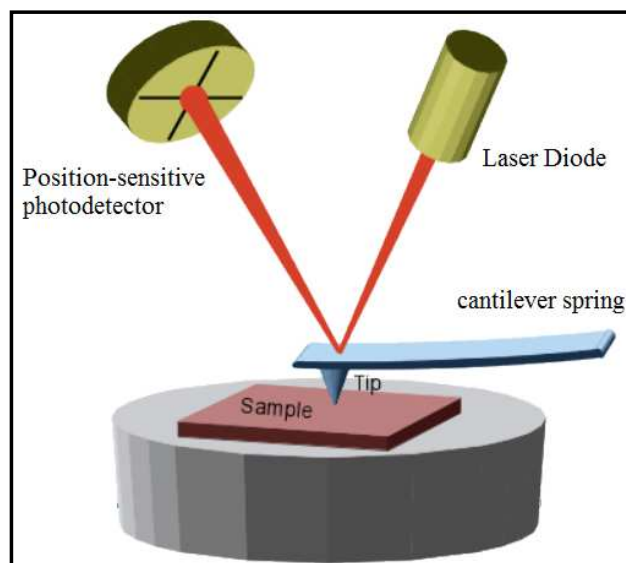


Figure 4.24: Concept of AFM and the optical lever.

Applications: AFM has many disadvantages such as limited vertical range, limited magnification range, the data are not independent of the tip, the tip or sample can be damaged, The advantages are easy sample preparation, accurate height information and work in a vacuum, air and liquids and living systems can be studied which make this technique applicable in different fields. AFM can be used for imaging to construct a picture of a CD stomper or human chromosomes; for measuring the thickness of an image as well as the resulting oscillation of the cantilever, the tip and the sample; for sensing to establish the composition of the sample; for manipulating by using 1024 cantilevers, the “Millipede” can write on a surface of polymer film. Each cantilever is individually controlled and can produce or erase a small pit that represents a bit of information. It is predicted that 100 GB of memory can be put on only one square inch using this technology.

Chapter 4: Principle of secretive analytical techniques

4.3 Conclusion

This chapter has bravely reviewed some of the analytical techniques which will be used for the purpose of this present work. The principle, instrumentation and some applications of each technique were described.



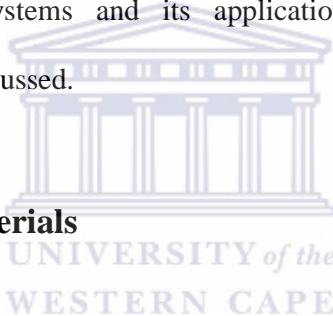
MATERIALS, REAGENTS AND EXPERIMENTAL METHODS

5.0 Introduction

This chapter present the reagents, materials and experimental procedures used to develop the electrochemical tetrodotoxin sensor. Furthermore, a detailed description and the application of polyaniline-modified electrode as tetrodotoxin sensor for neutral ionophores molecules are presented. Finally, the highlight of immobilisation procedures of biomolecular recognition systems and its applications as biosensors detector for tetrodotoxin analyte were discussed.

5.1 Reagents and materials

This section presents the list of chemical reagents and materials used in this study



Chapter 5: Materials, reagents and experimental methods

5.1.1 Reagents

Table 5.1a: List of chemical reagents used in this study

Name	Supply	% purity	Product number
Tetrodotoxin (TTX), citrate free	Latoxan	96%	Lot # L8503
Aniline	Sigma-Aldrich	99%,	Lot# 132934
Poly(4-styrenesulfonic acid) (PSSA)	sigma-Aldrich	18wt % in water	Lot# MKBF4647V
Perchloric acid	Sigma-Aldrich	70%,	lot # STBC0917V
Aptamer	Inqaba Biotec	/	/
Glutaraldehyde	Sigma-Aldrich	≥ 50 wt%	CAS: 340855
Acetonitrile anhydrous	Sigma-Aldrich	99.8%,	lot # STBC0960V
Phosphoric acid	SAFC	85 wt %	product # 31996DJ
Sodium acetate anhydrous	Sigma-Aldrich	> 99 %	Lot # W302406
Acetic acid, glacial	Sigma-Aldrich	≥ 99.7%	Lot # STBD7192V
Magnesium sulfate (MgSO ₄),	sigma-Aldrich	≥99.5%,	product # 7506- 500G
Lithium sulfate	sigma-Aldrich	≥ 98.0%,	product # 62613- 250G
Potassium sulfate	Kimix	99%,	/
Ammonium sulfate	Kimix	99%,	/
Sodium sulphate anhydrous	Kimix	99.5%	/
Tetradodecylammoniumtetrakis (4-chlorophenyl)borate (ETH500)	Sigma-Aldrich	99%,	lot # 1383901V

Chapter 5: Materials, reagents and experimental methods

Table 5.1: List of chemical reagents used in this study

Name	Supply	% purity	Product number
Benzo-18-crown-6 (B18C6)	Fluka	≥ 98.0%	EC No.2380413
4-tert-Butylcalix[4]arene-tetraacetic acid tetraethyl ester (Sodium ionophore X, NaX)	Fluka	/	Product # 71747
Ethanol	Kimix	99.9%	/
Tris-EDTA buffer solution pH 8.0 ± 0.1 (25°C)	Sigma-Aldrich	/	Lot # BCBM4893V
1,2-dichloroethane (1,2-DCE)	Sigma-Aldrich	99 %	Product # S11021-043
Chloroform	Sigma-Aldrich	99.9%	Product # S56297
Sodium Chloride	Sigma-Aldrich	≥ 99.5	product # BCBG7695V
Dimethyl sulfoxide	Sigma-Aldrich	≥ 99.7%,	lot # SZBD355SV
N,N-dimethylformamide anhydrous	Sigma-Aldrich	99.8%	lot # STBD14465V
Alumina slurries	Buehler 11b [0.45 kg]	1.0, 0.3 and 0.05 μm	

5.1.2 Materials

A conventional three-electrode in electrochemical cell was used during the experimental studies. Table 5.2 presents the list of working electrodes (WE) and their thickness (mm). The silver wire (pseudo-reference electrode) and Ag/AgCl were used as reference electrode and platinum wire as the auxiliary (counter) electrode.

Chapter 5: Materials, reagents and experimental methods

Table 5.2: Working electrodes used to carry out the experiment

WE	Diameter	Supply
Boron-doped diamond	3.5 mm	BAS
Glassy carbon	3.0 mm	Amel and BAS company
Platinum	1.0 mm	Amel and BAS
Platinum	1.6 mm	BAS
Gold	1.0 mm	Amel
Gold	1.6 mm	BAS
Nickel	4.0 mm	Amel
Prrolytic graphite	3.0 mm	BAS
Titanium	4.0 mm	Amel

5.1.3 Ion selective electrode

The plastic tip containing organic phase was used to cover the head of the silver wire electrode. Afterwards, the silver wire and platinum wire were inserted put in PTFE tubular-bolt (working electrode) containing 1ml of organic phase. At the bottom of the tubular-bolt, a dialysis membrane was used to separate the organic phase from the aqueous phase. This is to allow the ions to transfer from the aqueous phase to the organic phase.

5.2 General electronics instrumentation

The electrochemical experiments were carried out at 25°C using a MOD-7050 potentiostat (AMEL instrument) connected to a computer through a USB electrochemical interface.

Chapter 5: Materials, reagents and experimental methods

However, the electrochemical impedance spectroscopy (EIS) was performed on IM6ex ZAHNER elektrik with an impedance measurement unit.

The Ultraviolet-visible (UV-vis) spectroscopy was performed on the Thermo Electron Corporation Nicolet evolution 100 spectrometer and the fluorescence spectroscopy was carried out using the Nanolog Horiba Jobin Yvon spectrometer.

The photoluminescence analysis was performed using Horiba NanoLog™ 3-22-TRIAx (USA), with a double grating excitation and emission monochromators at a slit width of 5 nm.

FT-IR measurement was carried out by infrared spectrophotometer (Perkin Elmer model Spectrum 100 series).

The high resolution transmission electron microscopy (HRTEM) and energy-dispersive X-ray spectroscopy (EDS) analysis were done on a high resolution transmission electron microscope (Tecnai G2F20 X-Twin MAT (US)).

The Zeiss Auriga HRSEM scanning electron microscopy (SEM) machine was used while the AFM analysis was done on a VeecoNanoMan V model (Cambridge, USA).

5.3 Preparation of reagent solutions

5.3.1 Preparation of tetrodotoxin solution

1 mg, 319.28 g mol⁻¹ of TTX was directly weighed without any purification into 10 ml volumetric flasks containing 3 ml, 0.1 M OAc buffer. In order to have complete dissolution, the mixture was kept for 24 hours and then the solution was divided into six small vials of 0.5 ml, 1 mM TTX solution. Afterwards, one out of the six vials containing

Chapter 5: Materials, reagents and experimental methods

0.5 ml of TTX solution of 1mM, (0.1 M, 1000 μ l TTX solution) was diluted 100 times. From the TTX (0.1 mM, 1000 μ l) solution, 2 μ M, 250 μ l of TTX solution was further prepared by diluting 50 times and then used as a working solution.

5.3.2 Preparation of buffer solutions

The preparation of the buffer solutions used in this study is described below. Using the relationship between pH and pKa given by Henderson-Hasselbach the desired pH of the buffer solution was calculated using Equation 5.1.

$$pH = pK_a + \log\left(\frac{A^-}{AH}\right) \quad \text{Equation 5.1}$$

Where A is the base and AH is the acid

The pH of the solution was adjusted to 7 by adding drops of either acid or basic solution to prepare the PB solution pH 7.04

5.3.2.1 Acetate buffer (OAc) solution

0.1 M of acetic acid solution was prepared by diluting 291.036 μ l of glacial acetic acid in 100 mL of distilled water. Afterwards, 0.1 M of sodium acetate solution was prepared separately by dissolving 1.3608 g of sodium acetate powder in 100 ml of deionised water. Using the Henderson – Hasselbach relationship (Equation 5.1) 25 ml of acetic acid with pH 4.8 was added to 75 ml of sodium acetate solution to make the buffer solution.

Chapter 5: Materials, reagents and experimental methods

5.3.2.2 Sodium phosphate buffer (SPB) solution

0.1 M of sodium phosphate acid solution was prepared by weighing 1.7799 g of sodium phosphate dibasic dehydrate powder into 100 ml of distilled water. A basic solution of 0.1 M of sodium phosphate basic solution was prepared separately by dissolving 1.5601 g of sodium phosphate monobasic dehydrates powder in 100 ml of deionised water. Applying the Henderson – Hasselbach (see equation 5.1), 42.3 ml of sodium phosphate acid solution was added into 57.7 ml of sodium phosphate basic solution.

5.3.3 Preparation of liquid phase solution

K₂SO₄ solution

0.05M of K₂SO₄ solution was prepared by weighing 0.0436 g of K₂SO₄ powder into 5 ml of deionised water.

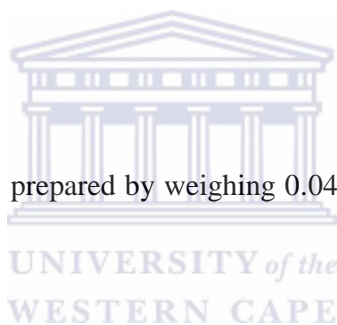
(NH₄)₂SO₄ solution

0.0661 g of (NH₄)₂SO₄ was weighed into volumetric flask containing 5 ml of deionised water. After complete dissolution of the powder, another 5 ml of deionised water was added to the solution in order to obtain 0.05M (NH₄)₂SO₄ solution.

Na₂SO₄ solution

0.05 M of Na₂SO₄ solution was prepared by accurately measuring 0.1611 g of Na₂SO₄ powder into 10 ml of deionised water. The solution was shaken until the complete dissolution of the Na₂SO₄ powder.

Li₂SO₄ solution



Chapter 5: Materials, reagents and experimental methods

The preparation of 0.05 M of Li_2SO_4 solution was made by dissolving 0.2748 g of Li_2SO_4 powder into 20 ml of deionised water. In order to achieve complete dissolution of the powder 30 ml of deionised water was further added into the solution.

MgSO₄ solution

0.05 M of MgSO_4 solution was prepared by dissolving 0.6018 g of MgSO_4 powder in 100 ml of deionised water.

5.3.4 Preparation of organic phase solution

Organic solutions presented in this section were prepared in three different concentrations of organic phase solution by varying salt amounts as showed in Table 5.3.

Table 5.3: Organic solutions used to carry out the ion transfer voltammetry experiment

Organic phase solution	Concentration of the solution [mol l^{-1}]	Amount of salt [g]	Dichloroethane [ml]
B18C6	0.5	0.0541	3
ETH500	0.5	0.1722	3
NaX	0.1	0.0099	1

5.3.5 Preparation of standard solution

In this section four different standard solutions of NaCl, KTN, H_3PO_4 and glutaraldehyde were prepared.

NaCl standard solution

Chapter 5: Materials, reagents and experimental methods

0.05844 g, of NaCl powder was weighed into 10ml volumetric flask containing 5 ml deionised water. After complete dissolution of the salt, more deionised water was added up to 10 ml of Joge mark to prepare 0.1 M of NaCl solution.

KTN standard solution

0.05 M standard solution of KTN solution was prepared by dissolving 0.0224 g of KTN powder in 3ml of deionised water.

H₃PO₄ standard solution

1 M of H₃PO₄ solution was prepared by diluting 11.53μl of 8.67 M H₃PO₄ solution in 100 ml of deionised water.

Glutaraldehyde standard solution

0.198M (2%) of glutaraldehyde solution was prepared by diluting 8 μl of 2.497 M (25% in H₂O) in deionised water.



5.3.6 Preparation of aptamer solution

100 μM of stock solution of oligos was prepared by dissolving 87.09 moles of NH₂-aptamer in 870.88 μl of Tri-EDTA (10 mM Tris-HCl, 1 mM disodium EDTA, pH 8.0). The stock solution was then divided into smaller aliquots for long-term storage to avoid frequent freeze-thaw cycles and to prevent accidental contamination. Afterwards, the stock solution was diluted to 50 μM. 50 μM of working solutions were prepared by diluting 500 μl of stock solution in 250 μl of OAc buffer solution at pH 4.8. A different 50 μM of working solutions was further prepared by diluting 50 μl of stock solution in 100 μl of OAc buffer solution at pH 7.04. All solutions were stored in the freeze at -20°C.

5.4 Electrodes preconditioned

Prior to use, the various electrodes were pre-treated as follows:

Reference electrode: The Ag/AgCl and Ag wire reference electrode were thoroughly rinsed in deionised water which was then stored in 3 M NaCl solution until when needed.

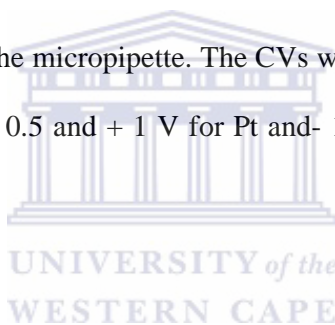
Counter electrode: The platinum wire counter electrode was acid treated by placing it directly in 2 M HCl or H₂SO₄ solution in order to remove/dissolve any soluble impurities. The counter electrode was then annealed on a flame. Annealing was important because it removes any trace impurities which might adsorb on the surface of the electrode.

Working electrode: The following steps were followed to ensure strict electrode hygiene.

- Alumina pads Buehler (Illinois, USA) was aligned on a glass substrate and alumina powder of 1 μM, 0.3 μM and 0.05 μM particle sizes was then spread on the surface of the pads.
- Sufficient amount of ultra-pure water was mixed with the alumina powder on the surface of the pads to form gel/slurries.
- Using circular motions, the surface of the working electrode was successively polished with formed alumina gel from the largest to the smallest alumina particle sizes. After the polishing step, each of the electrodes was rinsed by ultra-pure water.
- The cleaned electrode was then placed in an ultrasonic bath containing absolute ethanol followed by sonicating for 5 to 10 min.
- Finally the electrode was rinsed again in deionised water which was then followed by stream drying under argon gas.

5.5 Electro-inactivity of tetrodotoxin at solid electrodes

Different concentrations of TTX films were drop-coated consecutively on GC, Pt, Ti, Ni, PG, BDD, and Au electrodes and kept for 30 minutes to dry at room temperature. The potentiodynamic CVs of the modified TTX-electrode were scanned at 100 mV s^{-1} between - 5 and + 5 V, - 1.5 and + 2 V, - 1 and + 1 V, - 0.8 and + 1.1 V, - 0.8 and + 1.3 V, - 0.5 and + 1 V, - 1.8 and + 2.5 V using Au, BDD, GC, V, Ni, PG, Pt and Ti electrode respectively in 5 ml, 0.1 M OAc buffer pH 4.8 under argon gas. The CVs of unmodified-electrodes were firstly recorded in 5 ml, 0.1 M OAc after polishing. Afterwards, different concentrations of TTX were added into 1ml of 0.1 M OAc solution at different pH (4.10, 5.01, 6.03, 7.02, 8.03) using the micropipette. The CVs were recorded for this time only at the potential range between - 0.5 and + 1 V for Pt and- 1.7 and + 1 V for Ti electrode at 100 mV s^{-1} .



5.6 Electrokinetics of polymerisation of undoped and doped PANI films in perchloric acid/ acetonitrile

5.6.1 Electrosynthesis of undoped PANI films in perchloric acid/ acetonitrile

5.6.1.1 Electro-oxidation of aniline

In the electrochemical cell containing 0.1 M HClO_4 /5 mL acetonitrile, 0.05 M of aniline was added. The LSV technique was used to oxidize the aniline monomer between the potential range of - 0.2 and + 2 V for Pt, - 0.5 and + 2.5 V for PG, - 0.3 and + 2.5 V for Au

Chapter 5: Materials, reagents and experimental methods

and- 0.5 and + 1.8 V for GC electrode under argon gas. The purpose of this experiment was to determine the onset potential which was used to calculate the final potential using the equation: $E_2 = E_{\text{on-set}} + 0.4 \text{ V}$ to determine the electrochemical polymerisation.

5.6.1.2 Electrochemical polymerisation of aniline

Electrochemical polymerization of aniline on the bare GC, Pt, PG, Au electrodes was performed in the electrolyte solution of 0.1 M HClO₄/ACN containing 0.05 M of aniline. The electrolyte solution was degassed with argon gas for 10 min before the electropolymerisation process. The CV was then used at a cycling of 50 mV s⁻¹ between - 0.1 - 1.47 V for Au, 0.1 - 1.3 V for GC and PG, and 0.0 - 1.3V for Pt under the flow of argon gas. The CVs of electrodeposited PANI films was recorded over 15 cycles and the electrodes were then rinsed with ethanol to remove the excess of aniline monomer on the electrode surface. The modified PANI/Au, PANI/GC, PANI/Pt and PANI/PG electrode were prepared and ready for further characterization.

5.6.1.3 Stability of the modified-PANI electrode and reversibility of the system

The stability of the electrode vis-à-vis PANI film was studied by recording the cyclic voltammograms of PANI in an electrosynthesis potential range of each of the electrode at different scan rates in 0.1 M HClO₄/ACN mixture. The CVs were recorded for three multiple cycles under controlled potential in their respective electrosynthesis range of each electrode versus silver wire under argon gas. After the CVs were recorded, the modified-PANI electrode was placed into the same cell filled with 0.1M HClO₄ / ACN. The IES was

Chapter 5: Materials, reagents and experimental methods

measured immediately using different potential around the first anodic peak potential. The CV was then repeated at different scan rates of 15, 20, 50, 75, 100, 300, mV s^{-1} respectively.

5.6.2 Electrosynthesis of PSSA dopes PANI films in perchloric acid/ acetonitrile

Electrosynthesis of PSSA doped PANI on GC, Pt, PG and Au electrodes was performed in the electrolyte solution of 0.1 M HClO_4/ACN containing 0.05 M of aniline and 0.025 M of PSSA respectively. The electrolyte solution was degassed with argon gas for 10 min before electropolymerisation. Sequential polymerization was carried out by cyclic voltammetry between - 0.1 - 1.47 V for Au, 0.1 - 1.3 V for GC and PG, and 0.0 - 1.3V for Pt at 50 mV s^{-1} under argon gas. The CVs of electrodeposited of PANI films were recorded over 15 cycles and the electrodes was rinsed with ethanol to remove the excess aniline monomer on the electrode surface. The modified PSSA-PANI/Au, PSSA-PANI/GC, PSSA-PANI/Pt and PSSA-PANI/PG electrode was then ready for further characterization.

5.7 Indirect detection of TTX at modified-NaX/PANI-PSSA films electrodes

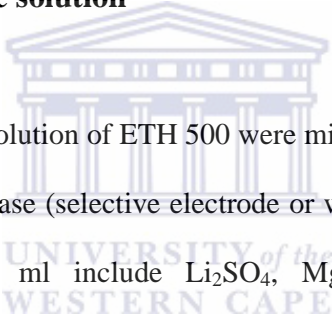
Different concentrations of NaX solution was drop-coated on PSSA-PANI/GC, PSSA-PANI/Pt, PSSA-PANI/ PG and PSSA-PANI/Au electrodes respectively and allowed to slowly dry for 2 hours at room temperature. Afterwards, the CV of the modified electrodes

Chapter 5: Materials, reagents and experimental methods

was carried out at 100 mV s^{-1} between -0.1 to 1.47 V for Au, 0.1 to 1.3 V for GC and PG, and 0.0 to 1.3 V for Pt at 50 mV s^{-1} in 5 ml , 0.1 M OAc buffer pH 4.8 under the flow of argon gas. The cyclic voltammograms at different concentration of Na^+ ion were recorded. Furthermore, different concentrations of TTX was added in the cell containing Na^+ and the CV was carried out to see the effect of TTX on Na^+ peak.

5.8 Investigation of ionophore complexation with TTX using ion transfer voltammetry

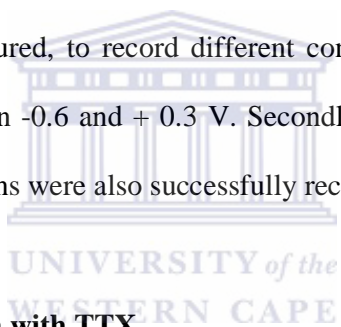
5.8.1 Choice of electrolyte solution

 50 mM of 0.5 ml NaX and a solution of ETH 500 were mixed and put into a PTFE tubular-bolt to prepare the organic phase (selective electrode or working electrode). The prepared organic phase each of 10 ml include Li_2SO_4 , MgSO_4 , $(\text{NH}_3)_2\text{SO}_4$, K_2SO_4 and Na_2SO_4 solution. This was then used in the aqueous phase as the electrolyte solution. The experiment was performed in the electrochemical cell containing two different phases (liquid and organic phase) with an assembling of selective electrodes as working electrode (organic phase). The working electrode include: platinum wire as counter electrode, and silver wire as the reference electrode (aqueous phase). Using the potentiodynamic method, the background CVs of each electrolyte solution was recorded between -0.6 and 0.3 V , -0.7 and 0.3 V , -0.7 and 0.3 V for MgSO_4 , Li_2SO_4 and Na_2SO_4 respectively at 10 mV s^{-1} . Thereafter, the suitable electrolyte solution was chosen from the background CVs of the electrolyte where cation did not form complex with the ionophore present in the organic phase (background CV without redox peak).

5.8.2 Ionophore complexation with TTX

5.8.2.1 NaX complexation with TTX

The mixture of 50 mM of 0.5 ml NaX and ETH 500 solutions were put into PTFE tubular-bolt to prepare 10 ml organic phase (selective electrode or working electrode) of MgSO₄ solution. This was used in aqueous phase as the electrolyte solution. The experiment was performed in the electrochemical cell containing two selective working electrode (of organic phase). The selective working electrode is of two different phases of platinum wire as the counter electrode and silver wire as reference electrode (aqueous phase). At 10 mV s⁻¹, the CV was firstly measured, to record different concentration of Na⁺ ion in 10 ml MgSO₄ at 10 mV s⁻¹ between -0.6 and + 0.3 V. Secondly, the cyclic voltammograms of TTX at different concentrations were also successfully recorded at 10 mV s⁻¹.



5.8.2.2 B18C6 complexation with TTX

The mixture of 50 mM of 0.5 ml B18C6 and ETH 500 solutions were put into PTFE tubular-bolt to prepare the organic phase (selective electrode or working electrode), an electrochemical cell containing 10 ml MgSO₄ solution was used as electrolyte solution (aqueous phase). The experiment was performed in the electrochemical cell containing both phases with an assembling of selective electrodes as working electrode (organic phase), platinum wire as counter electrode, and silver wire as reference electrode. The CV was used to record the different concentration of Na⁺ ion in 10 ml MgSO₄ at 10 mV s⁻¹

Chapter 5: Materials, reagents and experimental methods

between - 0.6 and + 0.3 V. Furthermore, the CVs of TTX at different concentrations were also recorded successively at 10 mV s^{-1} .

5.9 Investigation of ionophore complexation with TTX using ultraviolet/visible absorption

5.9.1 NaX complexation with TTX

Two different solutions of acetate buffer and deionised water were used as blanks for TTX and NaX respectively during UV-Vis measurements. The spectrum of each blank was recorded and thereafter 0.332 mM of TTX solution was diluted in the 3 ml cuvette containing water before measuring the spectrum of the TTX. Similarly, 1mM of NaX solutions was diluted with water in (4.5 cm, 3ml) cuvette then the spectrum of NaX was recorded. Afterward, the spectrum of both mixtures (0.332mM/1mM of TTX/NaX) was recorded between 200 and 800 nm.

5.9.2 B18C6 complexation with TTX

During the measurement of the UV-Vis, acetate buffer was used as the blank for TTX, B18C6 and a mixture of both TTX/B18C6. Distilled water was used as the blank for B18C6 in the UV-Vis absorbance measurements. The spectrum of each blank was first measured and recorded. Thereafter, the spectrum of the diluted TTX solution (by measuring 0.332 mM of TTX solution into cuvette containing water) was measured. In a

Chapter 5: Materials, reagents and experimental methods

similar way, 3.33 mM of B18C6 solutions was diluted with water in a cuvette and placed into the UV-Vis analyser and the spectrum of NaX was recorded. The spectrum of 0.332 mM/ 3.33 mM mixture of TTX and NaX was also recorded between 200 and 800 nm.

5.10 Electrochemical synthesis of neutral and p-doped PANI-PSSA in phosphoric acid

5.10.1 Electrochemical polymerisation procedure ion HClO_4/ACN and in H_3PO_4

Electrosynthesis of PSSA doped PANI on GC, Pt, PG, Au electrodes was performed in a 5 ml electrolyte solution of 1 M H_3PO_4 containing 0.05 M of aniline and 0.025 M of PSSA. The electrolyte solution was degassed with argon gas for 10 min before electrochemical polymerization. Subsequently, sequential polymerization was carried out on p-doped and neutral PANI-PSSA films using a CV. The p-doped films was scanned from + 1.1 to - 0.2 V for Au, GC and PG, and + 1.1 to 0.0 V for Pt at 50 mV s^{-1} while the neutral PANI-PSSA were scanned from - 0.2 to + 1.1 V for Au, GC and PG, and 0.0 to + 1.1 V for Pt at 50 mV s^{-1} under argon gas. The CVs of electrodeposited on the polymer films were recorded over 15 cycles and the reaction was stopped at the starting potential. The modified PSSA-PANI/Au, PSSA-PANI/GC, PSSA-PANI/Pt and PSSA-PANI/PG electrodes were rinsed with deionised water to remove excess of aniline monomer on the electrode surface. The scan rate voltammogram was then recorded by sweeping the potential of the working electrode under controlled potential at the electrochemical polymerization range of each respective electrode again silver wire under argon gas at sweep rates at 50 mV s^{-1} . The surface of the coated electrode with p-doped PANI-PSSA films and the neutral PANI-

Chapter 5: Materials, reagents and experimental methods

PSSA was blue and green respectively. This procedure was repeated for electrodeposited PSSA doped PANI composites in HClO_4/CAN and ready for characterization.

5.11 Characterisation of neutral and p-doped PANI-PSSA in buffer solutions

The characterization of the PSSA doped polyanilines was carried out by performing multi-scan rate cyclic voltammetry. The polymer films modified electrode was placed in degassed 0.1 M SPB solution with pH 7.04. The potential of the working electrode was then scanned between - 0.6 to + 0.6 V potential limits and multi-scan rate voltammograms was recorded at the scan rates of 10 to 100 mV s^{-1} . Also the polymer films modified electrode was placed in a degassed 0.1 M OAc buffer solution at pH 4.8. The potential of the working electrode was then scanned between -0.5 to + 0.6 V potential limits and multi-scan rate voltammograms was then recorded at scan rates of 10 to 75 mV s^{-1} . The CVs was measured for three multiple cycles in order to study the short time stability of the modified composite electrodes.

5.12 Electrochemical impedance measurement of neutral and p-doped PANI-PSSA

The three electrodes setup consists of a working electrode (modified neutral and p-doped PANI-PSSA electrode), counter electrode and reference electrode (Ag/AgCl). The impedance spectra were measured in 0.1 M SPB at the frequency between 100 Hz and 100 kHz with the formal potential of the PSSA-Emeraldine redox couple. On the other hand, the impedance spectra was recorded in 0.1 M OAc buffer at the frequency range of 1 Hz to

Chapter 5: Materials, reagents and experimental methods

100 kHz with a potential difference within - 0.5 and + 0.5V. The amplitude of the alternating voltage was 10 mV. Nyquist and Bode plots in which - Z'' vs Z' and $\log |Z|$ vs $\log (f)$ respectively, were chosen for the presentation of the data.

5.13 Solubility test

The solubility of the resultant polymers in two different laboratory reagents was tested. Exactly 1 mL of each of the following solvents was measured and placed in a 4 labelled stoppered vials. Two of the vials contained dimethyl sulfoxide (DMSO) and the other two dimethyl formamide (DMF). Two modified neutral PSSA-doped polyanilines electrodes were separately dipped into DMSO and DMF solvent which was then sonicated for 30 minutes. Similarly, two of the modified p-doped PSSA-doped polyanilines electrodes were also dipped into DMSO and DMF solvent and sonicated for 30 minutes. The neutral PSSA-PANI films were completely dispersed in DMSO while the p-doped PSSA-PANI films were dispersed in DMF but not in DMSO. The procedure was done for the polymers composites in order to evaluate the effect of the ending potential in the electrochemical polymerization process and the polarity of the solvent on the solubility of the resultant composites.

5.14 Determination of absorption bands of neutral and p-doped PANI-PSSA

In these set of experiments DMSO and DMF were used as the blank for neutral PSSA-PANI and p-doped PSSA-PANI films respectively. The spectrum of each blank was first recorded and 40 μ l of each of the resultant polymer composites solutions were diluted into

Chapter 5: Materials, reagents and experimental methods

the 4 cm cuvette containing DMSO or DMF depending on the polymer composite to measure. The UV-Vis was then measured between 200-800 nm and recorded.

5.15 Emission wavelength of neutral and p-doped PANI-PSSA

The same neutral and p-doped PSSA-PANI composite solutions were used to measure the absorption spectra. The wavelength absorption obtained was used to measure the emission spectra of monochromators at a slit width of 5 nm. The fluorescence emission was measured at 285 and 350 nm for the neutral PSSA-PANI composite and at 350 and 621 nm for the p-doped PSSA-PANI composite in DMF solution. Whilst, in DMSO solvent the emission spectra were recorded at 342, 448, and 602 nm for neutral PSSA-PANI and at 296 and 418 nm for the p-doped PSSA-PANI composite. The above wavelengths used were obtained from the absorption spectra of the neutral and p-doped PSSA-PANI composite in DMSO and DMF respectively.

5.16 FTIR measurement of neutral and p-doped PANI-PSSA composites

The spectrum of each composite was measured using FTIR (Perkin Elmer model Spectrum 100 series was recorded between 4000-400 cm^{-1}). Before the analysis the neutral and p-doped PSSA-PANI samples dispersed in DMSO and DMF respectively were prepared by dropping their suspension directly into the crystal (window) of the device.

5.17 Characterisation of neutral and p-doped PANI-PSSA using SEM analysis

Scanning electron microscopy was used to characterize the modified surface morphology of the neutral and p-doped PSSA-PANI/GC and to determine elemental composition and/or atomic percentage of the samples. The images were observed using the secondary electron (SE) mode with interchangeable accelerating voltages of 200 kV and a maximum resolution of 1 μm . The SEM samples for quantum dots were prepared by placing the solid nanomaterial onto a carbon adhesive mounted on aluminium stubs. The samples for neutral and p-doped PSSA-PANI were prepared by electrodeposition onto screen printed electrodes (glassy carbon).



5.18 Characterisation of neutral and p-doped PANI-PSSA using TEM analysis

The morphology and size distribution of the quantum dots or nanocrystals materials were performed using a high resolution transmission electron microscope (HRTEM) operating at 25 kV (field emission). Specimens for the high resolution transmission electron microscopy (HRTEM) were prepared by putting drops of the dispersed material on a carbon-coated copper grid. This was then allowed to dry by evaporation under an infra-red lamp before loading onto the grid (sample holder) and driven into the microscope unit for the analysis. HRTEM was also used to determine elemental composition and/or atomic percentage of each sample.

5.19 Application of p-doped PANI-PSSA films in the construction of electrochemical tetrodotoxin biosensors

5.19.1 The attachment of glutaraldehyde on the modified p-doped PSSA-PANI/GC

The modified p-doped PSSA-PANI/GC electrode was immersed into a 5 % solution of glutaraldehyde for four hours at room temperature. The modified Glu/PANI-PSSA/GC electrode was prepared and rinsed with buffer solution to remove the unbounded glutaraldehyde. The prepared Glu/PANI-PSSA/GC platform was further electrochemically characterized using CV and IES.

5.19.2 The immobilisation of aptamer on GLu/PANI-PSSA/GC electrode

Amino-aptamer was immobilised onto the modified Glu/PANI-PSSA/GC electrode through the linkage between amino groups and the active carbonyl groups of glutaraldehyde. The modified Glu/PANI-PSSA/GC electrode was deep-coated into 130 μ l of OAc buffer or SPB solution through NH_2 -aptamer solution at different concentration. The electrode was then incubated in the refrigerator at +4 $^\circ\text{C}$ for four hours. After the incubation process, NH_2 -Apt/Glu/PANI-PSSA/GC electrodes were rinsed with SPB solution to remove physically absorbed aptamer. The prepared NH_2 -Apt/Glu/PANI-PSSA/GC platform was further electrochemically characterised using CV and IES. Thereafter, the suitable concentration of aptamer was determined.

5.20 The detection of TTX using the biosensor NH₂-Aptamer/Glu/PANI-PSSA/GC

The NH₂-Apt/Glu/PANI-PSSA/GC biosensor was deep-coated into 130 µl of OAc buffer solution at different concentrations of TTX. The biosensor was incubated for 30 minutes in the refrigerator at +4°C. After the incubation, NH₂-Apt/Glu/PANI-PSSA/GC biosensor was then rinsed with OAc solution to remove physically absorbed TTX. The prepared TTX/NH₂-Apt/Glu/PANI-PSSA/GC tetrodotoxin biosensor was further electrochemically characterized using CV and IES and the suitable concentration TTX was determined.



**INVESTIGATION OF ELECTROINACTIVITY OF
TETRODOTOXIN AND ITS COMPLEXATION TO
IONOPHORES**

6.0 Introduction

Tetrodotoxin is a neurotoxin with 60% of death and various applications. The determination and detection of this neurotoxin has been investigated by many researchers. Sequel to the previous works reported in chapter two, it was found that no electrochemical technique had been used to determine tetrodotoxin. This chapter thus, will firstly present the electrochemical technique employed in this research study to investigate the electroactivity of tetrodotoxin on bare electrodes. Then the results obtained on the detection of TTX based on the modified ionophore/PANI/electrode via the undoped and doped PANI will be presented. Thereafter, the ionophores complexation of TTX using ion-transfer voltammetry and UV/Vis absorption studies will be presented.

6.1 Electro-inactivity of TTX

Determining the electro-inactivity of TTX was the first objective of this study. The electroactivity property of TTX is the ability to be oxidised (lose electron), reduced (gain electrons) or oxidised and reduced at the same time.

Chapter 6: Investigation of electroactivity of tetrodotoxin and its complexation to ionophores

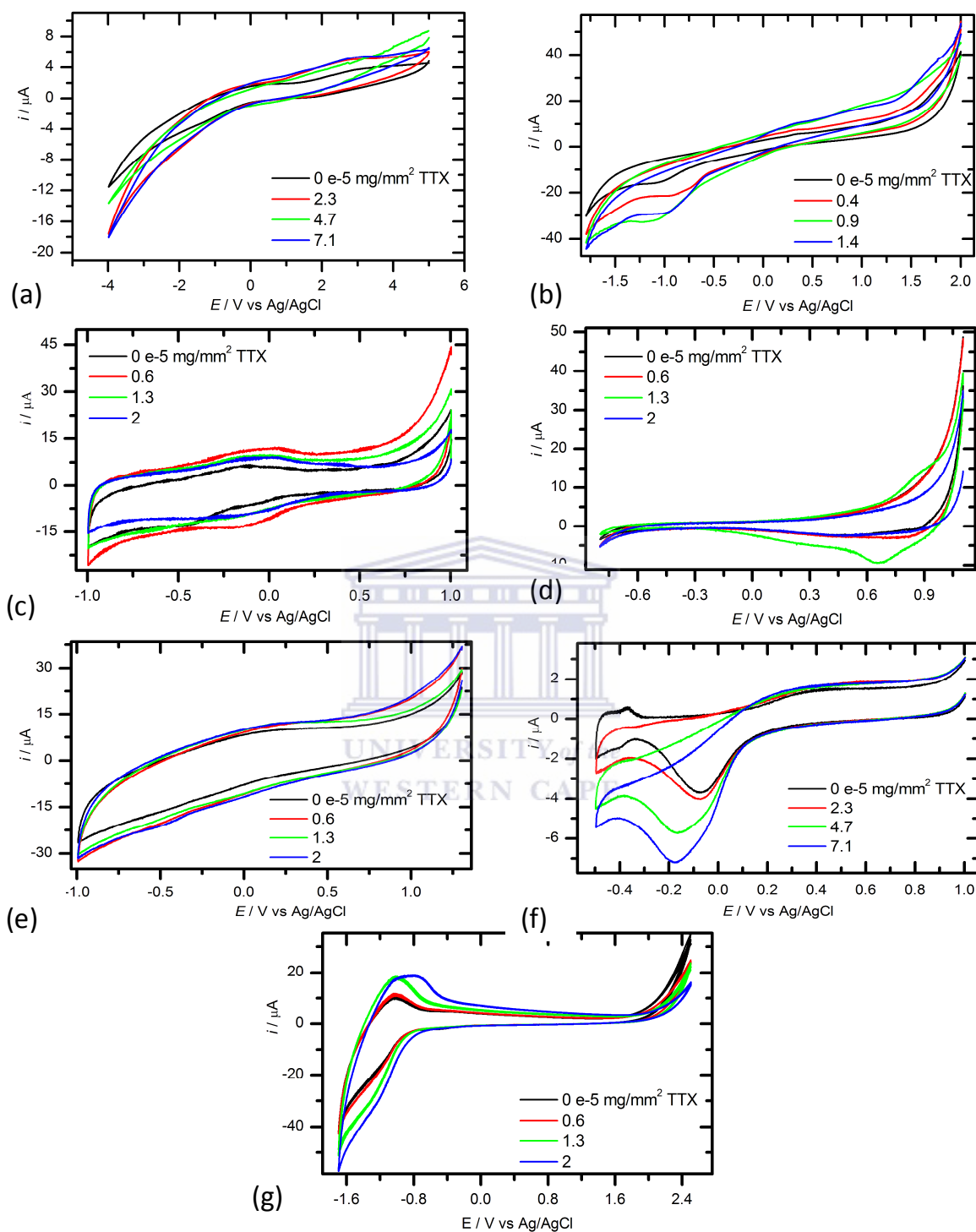


Figure 6.1: Cyclic voltammograms (CVs) of drop-coated TTX films on bare (a) Au, (b) GC, (c) BDD, (d) Ni, (e) PG, (f) Pt and (g) Ti electrodes in 10 ml acetate buffer, pH 4.8 at different concentrations at 100 mV s^{-1} .

Chapter 6: Investigation of electroinactivity of tetrodotoxin and its complexation to ionophores

This property was studied using cyclic voltammetric (CV) analysis in acetate buffer in a pH 4 to 5 with seven precious electrodes: gold (Au), boron-doped diamond (BDD), glassy carbon (GC), nickel (Ni), pyrolytic graphite (PG), platinum (Pt), and titanium (Ti) electrodes. For pH 4.8, electrochemistry response was not observed for all electrodes (Fig.6.1). Thus, the hypothesis of TTX dissolving in acetate buffer solution at pH 4.8 or of its electro-inactivity been given. On the titanium and platinum electrodes, the CVs of TTX show an increase of peak current when the concentration of TTX in increased. The same experiment was repeated on platinum (results not showed) and on titanium electrode where the SWVs were also recorded. The SWV is the best electroanalytical technique for the determination of electroactive organic and inorganic molecules that are adsorbed on the electrode surface [25].



Chapter 6: Investigation of electroactivity of tetrodotoxin and its complexation to ionophores

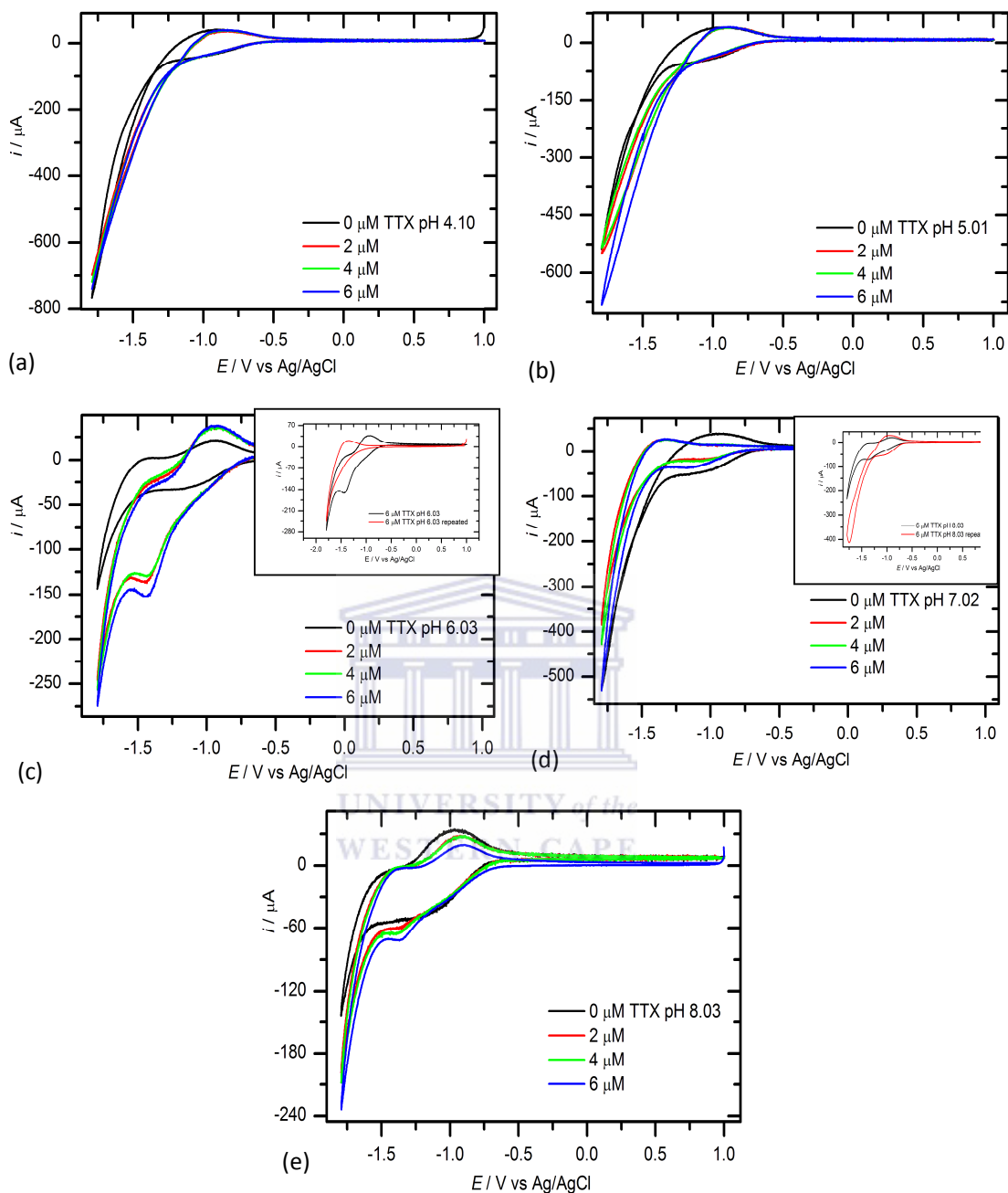


Figure 6.2: CVs of drop-coated TTX films on bare electrodes in 1mL acetate buffer, (a) pH 4.10, (b) pH 5.01, (c) pH 6.03, (d) pH 7.02, (e) pH 8.03 at different concentrations.

Figures 6.2 and 6.3 show the CVs and SWVs respectively of TTX on titanium at different pH (4, 5, 6, 7 and 8) and different concentrations in 1 ml of 0.1 M acetate buffer. CVs (Fig

Chapter 6: Investigation of electroactivity of tetrodotoxin and its complexation to ionophores

6.2) show that TTX is not electroactive as it was showing in figure 6.1. It is seeing that when the experiment is repeated at the same condition, the reduction shown at -1.4 V (Fig. 6.2c, d, e) disappeared. The SWVs (Fig. 6.3) were recorded at the same condition to confirm the result obtained using the CV analysis.

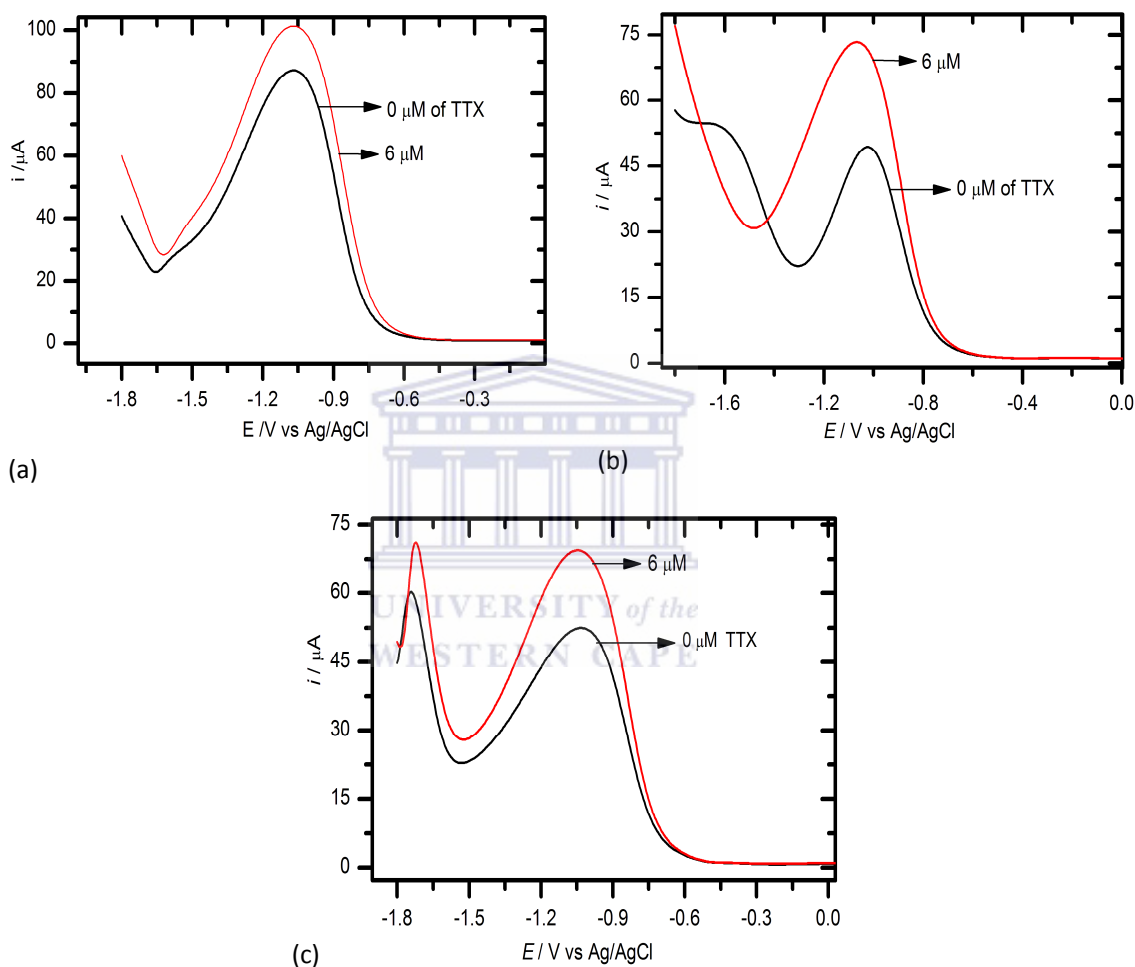


Figure 6.3: SWVs of drop-coated TTX films on bare electrodes in 1 ml acetate buffer (a) pH 6.03, (b) pH 7.05, and (c) pH 8.03 at 100 mV s^{-1} .

The voltammogram recorded in a blank buffer solution (black line) is characterised by the presence of one large peak around -1.05 V, corresponding to the oxidation of Ti. With the addition of TTX in the electrolyte solution (red line) the peak current increases. This is

Chapter 6: Investigation of electroinactivity of tetrodotoxin and its complexation to ionophores

indicating that the electron exchange process was not inhibited [213] but, TTX was adsorbed on electrode surface. The increase peak current on platinum electrode between 0 to -0.18 V corresponds to the reduction of oxygen in an electrolyte solution because after 10 to 20 minutes push with argon, this peak disappeared. Thus, according to the CVs and SWVs, TTX is electro-inactive as it cannot be detected on bare electrodes only. This conclusion leads us to make a specific transducer to develop the electrochemical tetrodotoxin biosensors.

6.2 The electrokinetics of the electropolymerisation of undoped and doped PANI films in HClO_4/ACN

6.2.1 The electro-oxidation of aniline

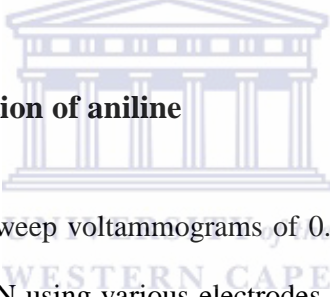


Figure 6.4 shows the linear sweep voltammograms of 0.05 M aniline in organic solution containing 0.1 M HClO_4/ACN using various electrodes. Two oxidation peaks, P_1 and P_2 , are apparent around + 0.8 and + 1.6 V for curves (a), (c), (d) respectively, P_1 and P_2 are apparent between + 1.07 and + 1.6 V for curves (b). The first peak (P_1) has been related to the oxidation of aniline [214] The second peak (P_2) has been related either to the oxidation of p-aminodiphenylamine to form the benzidine [214] species diffusing close to the electrode, or to the overoxidation of aniline film an enough amount of polymer was deposited on the electrode. The onset potential (E_{onset}) which is the potential corresponding to the oxidation of aniline was determined graphically from LSVs (Tab. 6.1). To compare the different scans obtained with the different electrode systems, the current related to each electrode and onset potential was determined. The characteristic peak of aniline for each

Chapter 6: Investigation of electroinactivity of tetrodotoxin and its complexation to ionophores

electrode is clearly seen in all cases. From the E_{onset} , final potential (E_2) used for the electropolymerisation was calculated by

$$E_2 = E_{onset} + 0.4 V \quad \text{Equation 6.1}$$

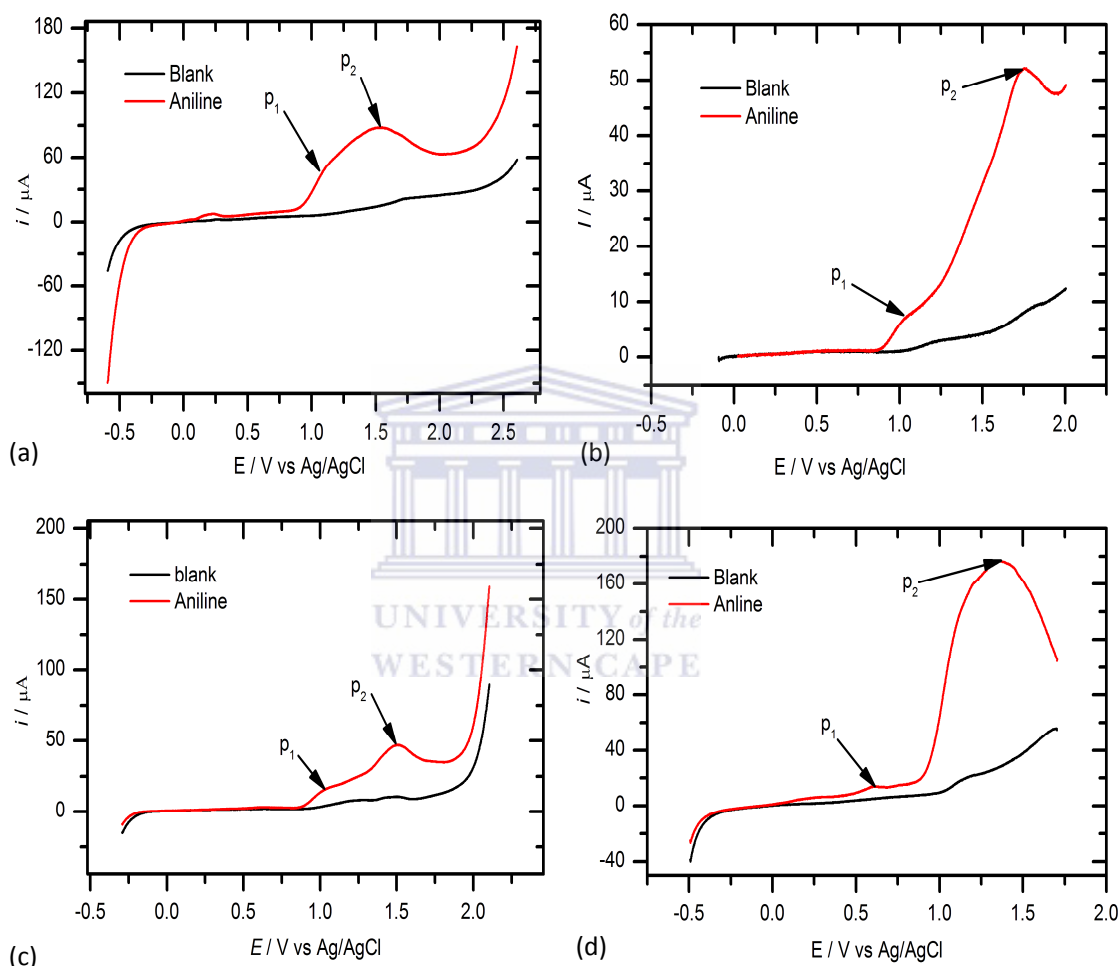


Figure 6.4: Linear scan voltammograms of 50 mM aniline in 0.1 M $HClO_4/ACN$ using (a) Pt, (b) PG, (c) Au, (d) GC electrode and silver wire reference electrode at $50 mV s^{-1}$.

The kinetics of the oxidation of aniline was studied by measuring the open circuit voltage (E_{ocv}) of aniline at different concentration. The rate of the oxidation ($k_{a-onset}$) and the extension coefficient (α) can be determined using the equation

Chapter 6: Investigation of electroinactivity of tetrodotoxin and its complexation to ionophores

$$i_c = i_o e^{\frac{(1-\alpha)nF(E-E_{OCV})}{RT}} \quad \text{Equation 6.2}$$

Where

$$i_o = nFA C_R^{bulk(1-\alpha)} C_O^{bulk \alpha} K^o \quad \text{Equation 6.3}$$

The opened circuit voltage (E_{OCV}) of aniline at different concentrations and different scan rates was determined and it was found that E_{OCV} depends on the concentration of aniline (Fig. 6.5).

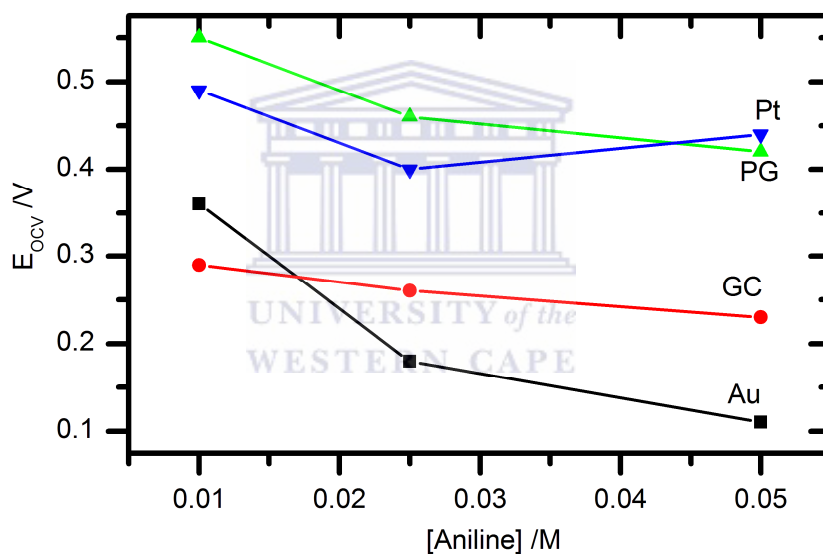


Figure 6.5: Dependence of open circuit voltage on the concentration of aniline in 0.1 M $HClO_4/ACN$.

Using the Butler-Volmer equation (Equation.6.4), the electrochemical oxidation kinetic can be exploited through Tafel slopes [5] as show in Figure 6.6 .

$$\log|i_{net}| = \log\left(nFAK^o C_o^{bulk(1-\alpha)} C_R^{bulk \alpha}\right) - \frac{(1-\alpha)nF}{2.3RT}(E - E_{OCV}) \quad \text{Equation 6.4}$$

Chapter 6: Investigation of electroinactivity of tetrodotoxin and its complexation to ionophores

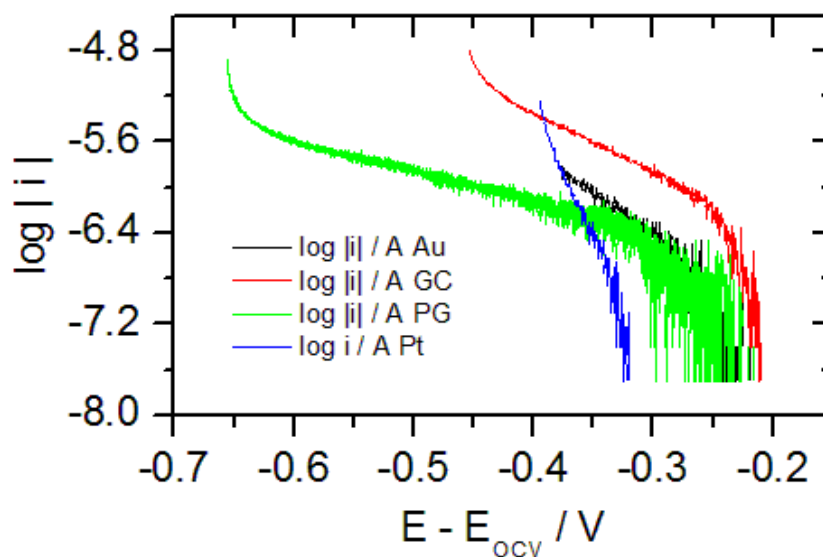


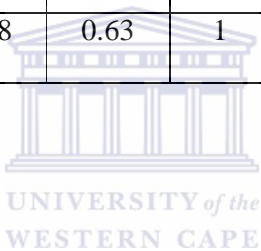
Figure 6.6: Anodic Tafel plot.

Using the equation $R_{ct} = dE/di \leftrightarrow dE = R_{ct}di \rightarrow di/dE = 1/R_{ct}$, the charge transfer resistance (R_{ct}), exchange current (i_0) were determined. The transfer coefficient (α) was determined from the slope, $slope = (1 - \alpha)nF/2.3RT$ and the kinetic parameters of aniline (Tab.6.1) was also determined from the value of α [5].

Chapter 6: Investigation of electroinactivity of tetrodotoxin and its complexation to ionophores

Table 6.1: Kinetics parameters evaluated from the plot $\log i$ vs. E of linear sweep voltammogram data near to the E_{onset}

WE	Range [V]	Intercept	Slope [V ⁻¹]	R^2	$\alpha_a n_a$	n_a	α_a	$k_{\text{et(onset)}} 10^{-8}$ [cm s ⁻¹]	$i_{\text{net (onset)}}$ [$\mu\text{A mm}^2$]	E_{onset} [V]
GC	0.88–0.96	-24.5± 0.1	14.7± 0.1	0.999	0.37	1	0.39	6.75	3.26	0.94
AU	0.88–0.94	-31.6± 0.1	20.7± 0.1	0.996	0.53	1	0.55	2.1	2.05	0.89
PG	0.96–1.04	-17.6 0.0	19.7± 0.0	0.998	0.50	1	0.53	0.6	2.06	0.93
Pt	0.87–0.94	-36.1± 0.3	24.6± 0.3	0.988	0.63	1	0.66	6.94	0.33	0.89



Chapter 6: Investigation of electroinactivity of tetrodotoxin and its complexation to ionophores

6.2.2 Cyclic voltammograms of PANI in HClO₄/ACN

Cyclic voltammetry was used to investigate the electrochemical polymerisation of aniline in 0.1 M HClO₄/ACN at various potentials with different electrodes at 50 mV s⁻¹ over 15 cycles. The best criterion for PANI films formed on the electrode surface for wide applicability and, usually good performance of electrode is a method of synthesis and the medium for the synthesis. The polymerisation was carried out by potentiodynamic scan in HClO₄/ACN after polishing the electrode with different diameters of alumina powder. Figure 6.7 shows the CVs recorded during the continuous scan over 15 cycles at 50 mV s⁻¹ scan rates in different potential ranges and on the various electrodes in 0.1 M HClO₄/ACN containing 0.05 M aniline. For the first potential sweep, aniline is oxidised, resulting in an irreversible anodic current peak. Part of the product yielded from aniline oxidation is deposited on the electrode surface, which corresponds to the growth process taking place with cathodic current peak (C') appearing. The intensity of first peak current decreases and finally disappears when the number of cycles increases. The CVs show that the current increases in each successive cycle which confirms the electropolymerization of PANI films. The redox peak at about 0.40 to 0.50 V (AA') corresponds to the transformation of the reduced leucoemeraldine state to the partly oxidised emeraldine state. The redox peak around 0.70 and 1 V (CC') is attributed to the transition leucoemeraldine reduction state to pernigraniline full oxidation state. Intermediate reactions such as *p*-benzoquinone, *p*-aminophenol and some dimers reductions occur during the polymerisation and these molecules are known to be trapped in the polymer [124]. The intermediate peaks (BB') is generally attributed to the redox reaction of *p*-benzoquinone [103, 215-216]. During the

Chapter 6: Investigation of electroinactivity of tetrodotoxin and its complexation to ionophores

anodic scan, the first oxidation peaks are obtained in the initial cycle and the peak potential maintained almost the same.

Generally in electropolymerisation processes, the increase of the voltammetric peak current density and the scan number are an indication of the growth rate of polymer. The polymerisation rate (V) for the cathodic peak related to the quantity of polymer is measured and plotted against scan number in Figure. 6.8. Using the equation $V = -k_{app} [\text{monomer}]$ (cathodic peak), where k_{app} is a set of apparent-first-order reaction rate constant, V is the rate of polymerisation which corresponds to the slope of the curve [5], the quantity of polymer formed on the electrode surface was determined. As shown in Figure 6.8, the amount of PANI deposited on PG is almost double the amount formed on GC, Pt, and Au electrodes. The apparent rate constant (k_p^{app}) for the polymerisation step per cycle was estimated from the plot $i_{pc-growth}$ vs. cycle number. This parameter determines the kinetic of the electropolymerisation.

Chapter 6: Investigation of electroinactivity of tetrodotoxin and its complexation to ionophores

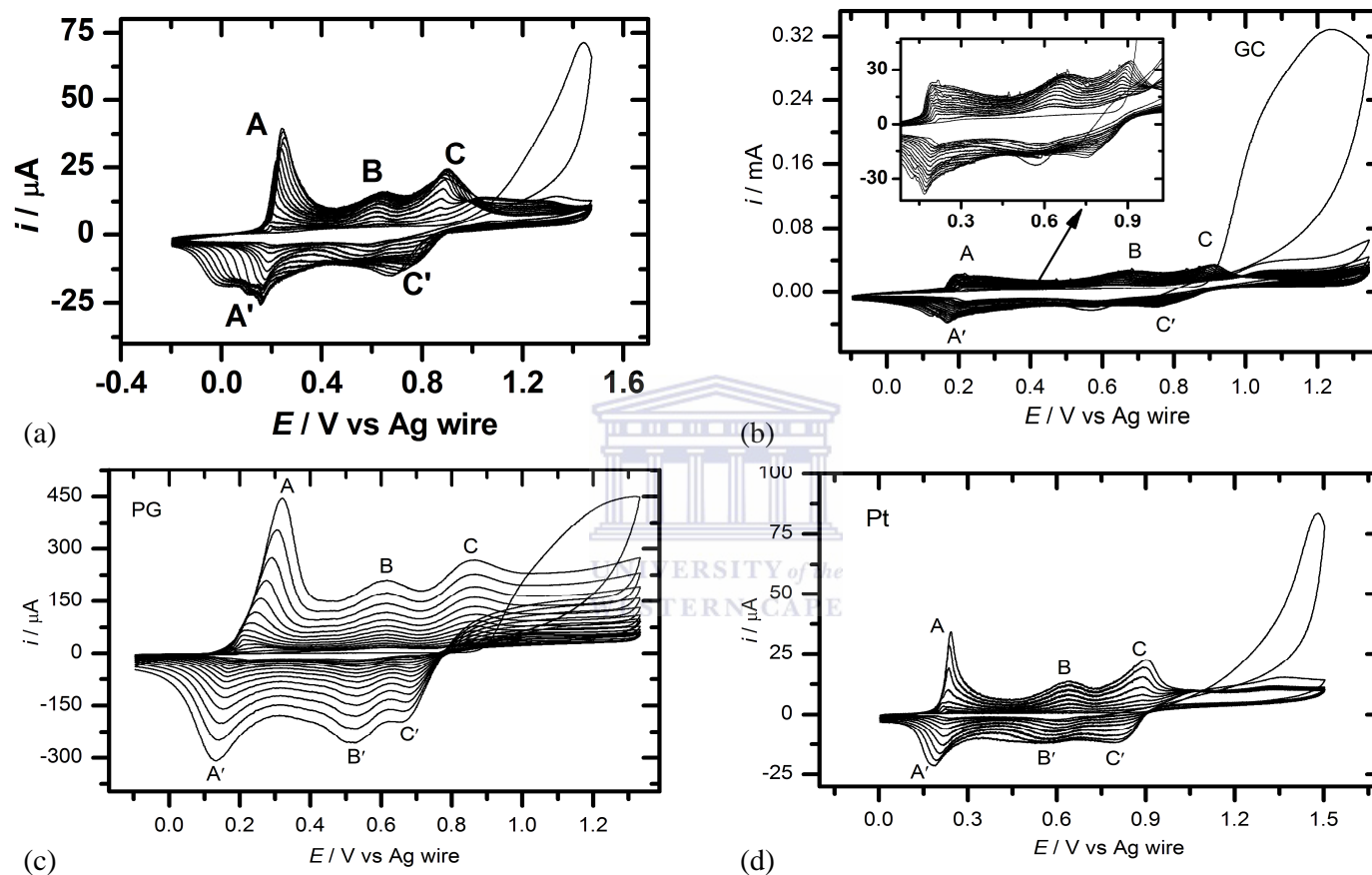


Figure 6.7: Cyclic voltammograms (15 cycles) recorded during potentiodynamic growth of PANI films on (a) Au, (b) GC, (c) PG, and (d) Pt in 0.1 M $HClO_4/ACN$ containing 0.05 M aniline at 50 mV s^{-1} scan rates.

Chapter 6: Investigation of electroinactivity of tetrodotoxin and its complexation to ionophores

During the potentiodynamic growth of individual PANI films, the anodic current measured during each potential scan cycle was integrated to generate the anodic charge transfer density Q_a . The following values were obtained for each electrode: $Q_a(\text{Pt}) < Q_a(\text{GC}) < Q_a(\text{Au}) < Q_a(\text{PG})$. This electropolymerisation charge transferred at the interface between the electrode surface and the solution is proportional to the quantity of polymer formed on the electrode surface. Thus, the previous values of Q_a obtained, show that more PANI is formed on the PG electrode surface. The study of rates of electron transfer reactions at the interface electrode surface|electrolyte solution is a fundamental issue in electrochemistry.

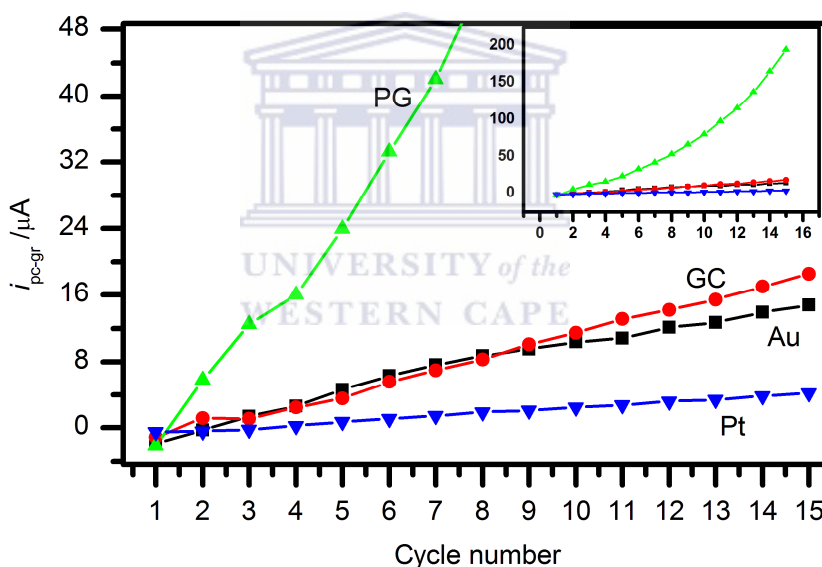


Figure 6.8: The cathodic growth peak of PANI vs cycle number.

The kinetics of the reaction rate at the surface of the electrode is of great importance for a basic understanding of the kinetics of heterogeneous electron transfer reactions because electrode processes are considered to commonly occur via a reaction pathway involving specifically adsorbed intermediates [217]. For the experimental determination of rate

Chapter 6: Investigation of electroinactivity of tetrodotoxin and its complexation to ionophores

constants for reversible or quasi-reversible reactions at the electrode surface, the slope of the graph i_{pc-gr} vs. N_{cycle} (Fig.6.8) was calculated. The first cathodic peak current which is the growth-peak (i_{pc-gr}) of polymer in the redox process of PANI was taken into account and used for calculations of charge transfer and polymerisation rate. That slope calculated per area of each surface of electrode was directly proportional to the apparent heterogeneous rate constant k_{app} of polymerisation per cycle and it was observed that $k_{app-polym}$ (Pt) < $k_{app-polym}$ (GC) < $k_{app-polym}$ (Au) < $k_{app-polym}$ (PG) (Tab. 6.2). The above values of k_{app} are related to the values of Q_a which explain the amounts of PANI formed on the electrode surface during the electropolymerisation process.

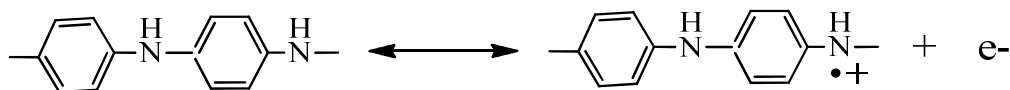
Table 6.2: Kinetic parameters of PANI from potentiodynamic process on various electrodes in 0.1 M HClO₄/ ACN

WE	A [cm ²]	Q _a [C cm ⁻²]	i _{pc-gr} [A]	n [mmole]	i _{pc-gr} [μA cm ⁻²] vs. N _{cycle}			
					Range	R ²	a [μA cm ⁻²]	b(k _{app,polym}) [Acm ⁻² s ⁻¹]
Au	0.0201	13.65	0.20	0.14	1 - 9	0.998	-66.7±0.1	77.11±0.03
GC	0.0707	9.6	0.19	0.09	6 - 15	0.999	-42.6± 0.1	20.22±0.01
PG	0.0707	35.9	0.59	0.37	4 - 8	0.997	-21.1±0.1	133.5±0.04
Pt	0.0201	5.15	0.09	0.05	1 - 15	0.998	-51.7± 0.1	17.41±0.14

Chapter 6: Investigation of electroinactivity of tetrodotoxin and its complexation to ionophores

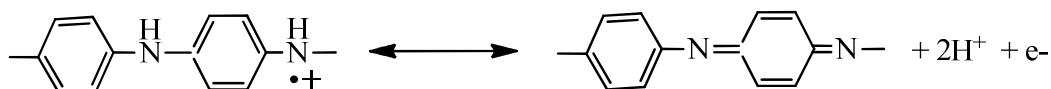
6.2.3 Stability of the modified-PANI electrodes and reversibility of the system

The electrochemical stability of conducting polymers is of primary interest, particularly in different fields of technology such as batteries, electrochromic devices and sensors, supercapacitors. Their stability depends on the type of acids, which constitutes the salt with PANI [218]. Among all the conducting polymers, it is known that polyaniline and polypyrrole have good electrochemical stability [218]. The cyclic voltammetry and the electrochemical impedance spectroscopy (EIS) were used to study the stability of the electrode surface vis-à-vis PANI. The stability of the modified electrode over three repetitive scans within the potential window of each electrode in 0.1 M HClO₄/ ACN solution should be emphasized. Figure 6.9 shows cyclic voltammograms of electropolymerised PANI films on each electrode in the same conditions. CVs of PANI deposited on each electrode surface are characterised by three main pairs of redox peaks. The redox peaks have been assigned using Pekmez formalism [219]: The first redox peak appearing between 0.36 and 0.45 V is the oxidation leucoemeraldine to leucoemeraldine radical cation interpreted by the following reaction:



The second is the emeraldine radical cation to emeraldine and the third redox peak between 0.8 and 1 V is the transformation of the pernigraniline radical cation to pernigraniline as shown in the following reaction

Chapter 6: Investigation of electroinactivity of tetrodotoxin and its complexation to ionophores



While the middle peaks correspond to the intermediate reaction taking place. The overview of three cycles of CVs PANI show that the peak current and peak potential are constant which explains the excellent short time stability of the electrode vis-à-vis PANI. Table 6.4 presents the potential and current values respectively of the redox peaks obtained from CVs of PANI. The table 6.4 shows that $\Delta E_{p1}(\text{Au}) < \Delta E_{p1}(\text{Pt}) < \Delta E_{p1}(\text{GC}) < \Delta E_{p1}(\text{PG})$; $\Delta E_{p3}(\text{PG}) < \Delta E_{p3}(\text{GC}) < \Delta E_{p3}(\text{Pt}) < \Delta E_{p3}(\text{Au})$; $E_{o'1}(\text{Pt}) < E_{o'1}(\text{GC}) < E_{o'1}(\text{Au}) < E_{o'1}(\text{PG})$; $E_{o'3}(\text{Au}) < E_{o'3}(\text{PG}) < E_{o'3}(\text{GC}) < E_{o'3}(\text{Pt})$;



Chapter 6: Investigation of electroactivity of tetrodotoxin and its complexation to ionophores

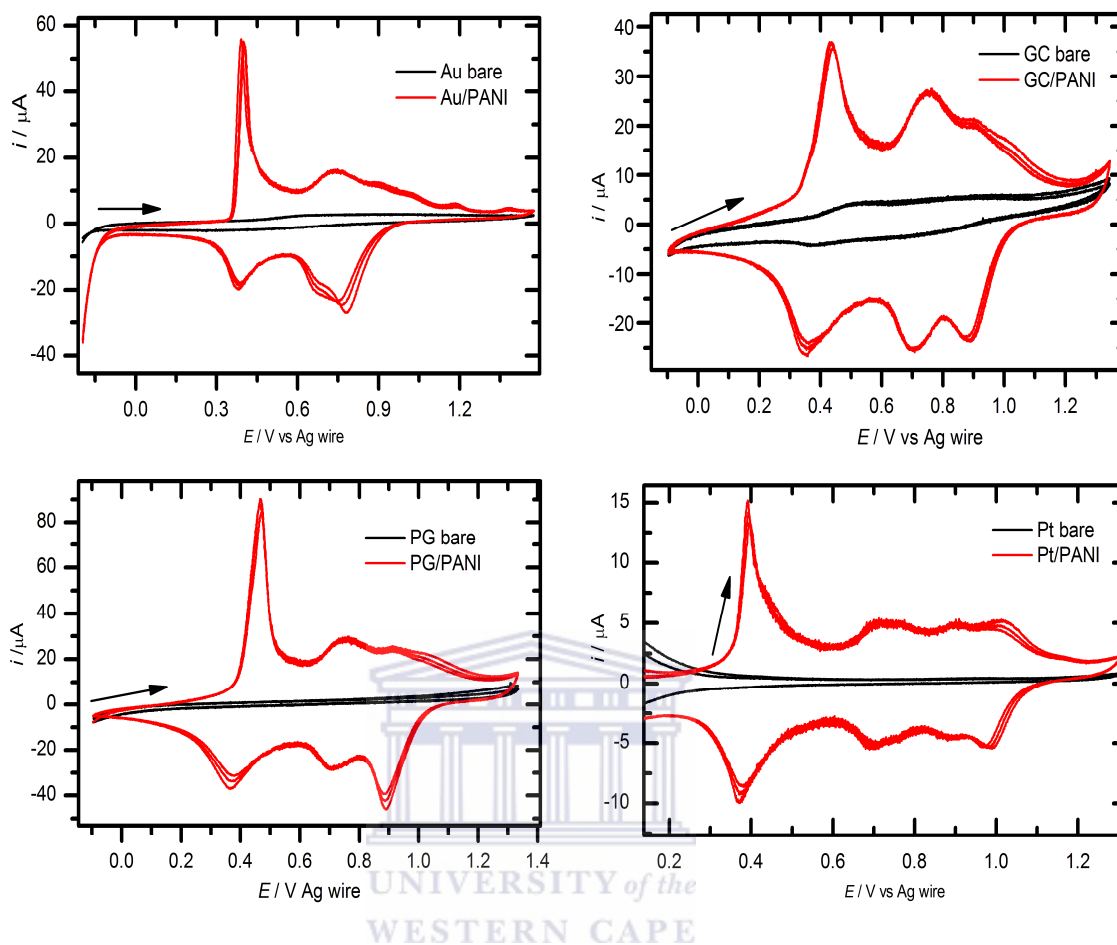


Figure 6.9: Overview of 3 cycles CVs of PANI films on Au, GC, PG and Pt electrode in 0.1 M HClO_4/ACN at a scan rate 50 mV s^{-1} .

Thus, PG, Au and Pt electrodes have good characteristic vis-à-vis PANI; this can be accounted to their small values of ΔE_p and the Formal potential $E^{\circ'}$. The formal potential was taken as the average of the anodic and cathodic peak potential, $E^{\circ'} = (E_{pa} + E_{pc})/2$, the peak separation $\Delta E_p = E_{pa} - E_{pc}$.

Chapter 6: Investigation of electroinactivity of tetrodotoxin and its complexation to ionophores

Table 6.3: Parameters evaluated from CVs of PANI vs Ag wire electrode in HClO₄/ ACN

Electrode	Au	GC	PG	Pt
E_{pa1} [V]	0.40	0.43	0.47	0.39
E_{pa2} [V]	0.73	0.76	0.73	0.72
E_{pa3} [V]	0.90	0.91	0.91	1.03
E_{pc1} [V]	0.38	0.35	0.37	0.37
E_{pc2} [V]	0.68	0.69	0.71	0.69
E_{pc3} [V]	0.78	0.89	0.89	0.98
ΔE_{p2} [V]	0.02	0.08	0.1	0.02
ΔE_{p1} [V]	0.05	0.07	0.02	0.02
ΔE_{p3} [V]	0.12	0.02	0.02	0.05
E°_1 [V]	0.39	0.39	0.42	0.38
E°_2 [V]	0.71	0.73	0.72	0.71
E°_3 [V]	0.84	0.9	0.9	1.01
i_{pa1} [μ A]	54.5	36.5	88.4	14.8
i_{pa2} [μ A]	16.3	26.5	27.9	4.9
i_{pa3} [μ A]	11.9	20.5	24.5	4.6
i_{pc1} [μ A]	- 18.8	- 24.6	- 33.1	- 9.0
i_{pc2} [μ A]	- 20.0	-24.9	- 27.3	- 4.8
i_{pc3} [μ A]	- 23.8	- 22.9	- 42.4	- 4.8
i_{pa1}/i_{pc1}	- 3.0	- 1.5	- 2.7	- 1.6
i_{pa2}/i_{pc2}	- 0.9	- 1.1	- 1.0	- 1.0
i_{pa3}/i_{pc3}	- 0.5	- 0.9	- 0.6	- 0.5

Table 6.3 shows that the ratio of the growth peak current (i_{pa3}/i_{pc3}) is approximately equal to - 1 which characterises an irreversible system. The range of the first oxidation peak was used for EIS to investigate the stability of the PANI deposited on the surface of each electrode.

6.2.4 Electrochemical impedance spectroscopy (EIS) of PANI

Chapter 6: Investigation of electroinactivity of tetrodotoxin and its complexation to ionophores

The EIS measurements of the PANI films were performed at various electrode potentials corresponding to the stability and the conductivity studies. As said above, the first redox couple which appears around 0.3 and 0.45 V is associated with the conversion of the fully reduced leucoemeraldine base to the partially oxidized emeraldine form, and the third redox current peaks occurring between 0.8 and 1 V pertains to the conversion of emeraldine to the fully oxidized pernigraniline form. This indicates that electrons are involved in the redox reaction associated with the first peaks while the redox reaction related to the third anodic peak require protons as part of the reaction. However, the EIS measurement allows not only to study the stability of the modified electrode, but also to investigate on the charge transfer electron (R_{ct}) which is inversely proportional to the conductivity of the material on the surface of the electrode. Thus, the first anodic peak obtained in the redox process of PANI was taken into account for electrochemical impedance spectroscopy analysis at different potentials around this peak. The impedance spectra were recorded at different potential values in different ranges depending on the electrode: between 0.076 and 0.576 V for Au; 0.063 and 0.563 V for GC; 0.129 and 0.529 V for PG; and 0.167 and 0.567 V for Pt. Figure 6.10 shows the Nyquist plots of the PANI-modified electrodes in the solution of 0.1 M HClO₄/ ACN, recorded at different potential values. Three regions could be distinguished for the fully oxidised conducting form of PANI at some potentials: i) a semicircle is observed at high frequencies, describing the double layer capacitor related to the charge transfer resistance (R_{ct}) at the electrode|solution interface; ii) a transition zone at intermediary frequencies; iii) a Warburg line at low frequencies describing the diffusion process. For the other potentials, we observed only one region which corresponds to the Warburg line at low frequencies. The

Chapter 6: Investigation of electroinactivity of tetrodotoxin and its complexation to ionophores

charge transfer resistance, R_{ct} could be determined and the corresponding value is the diameter of the semicircle attributed to the faraday reaction taking place.



Chapter 6: Investigation of electroinactivity of tetrodotoxin and its complexation to ionophores

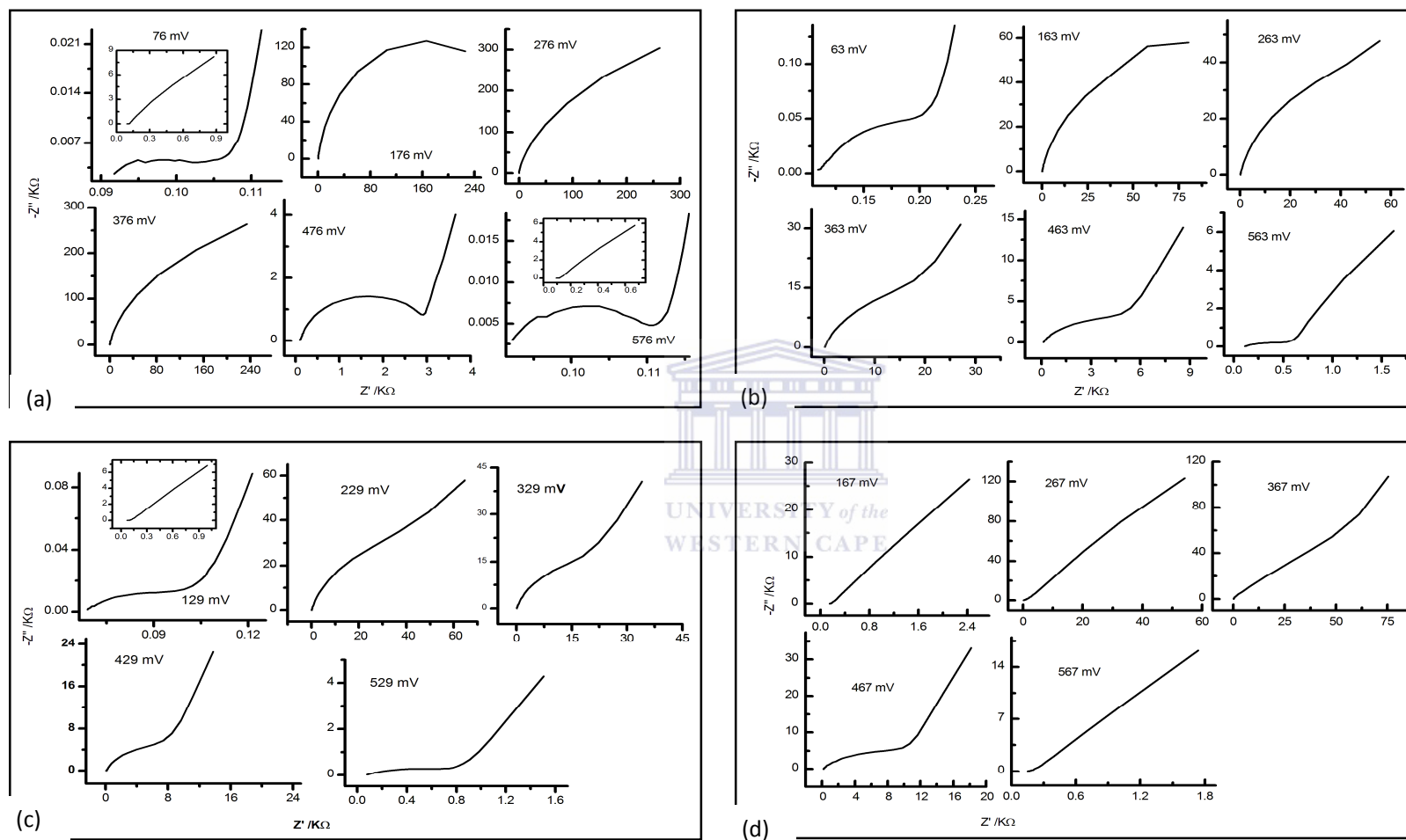


Figure 6.10: Nyquist plots of PANI films prepared in 0.1M HClO₄/ACN on (a) Au, (b) GC, (c) PG, (d) Pt electrodes at different potential.

Chapter 6: Investigation of electroactivity of tetrodotoxin and its complexation to ionophores

Figure 6.11 is the bode plot of PANI prepared in HClO_4/ACN recorded at different potential which shows that PANI is very conducting at the frequency less than 2 kHz. At frequency greater than 2 kHz, the PANI on electrode surface is a good resistor with the phase angle equal to zero.

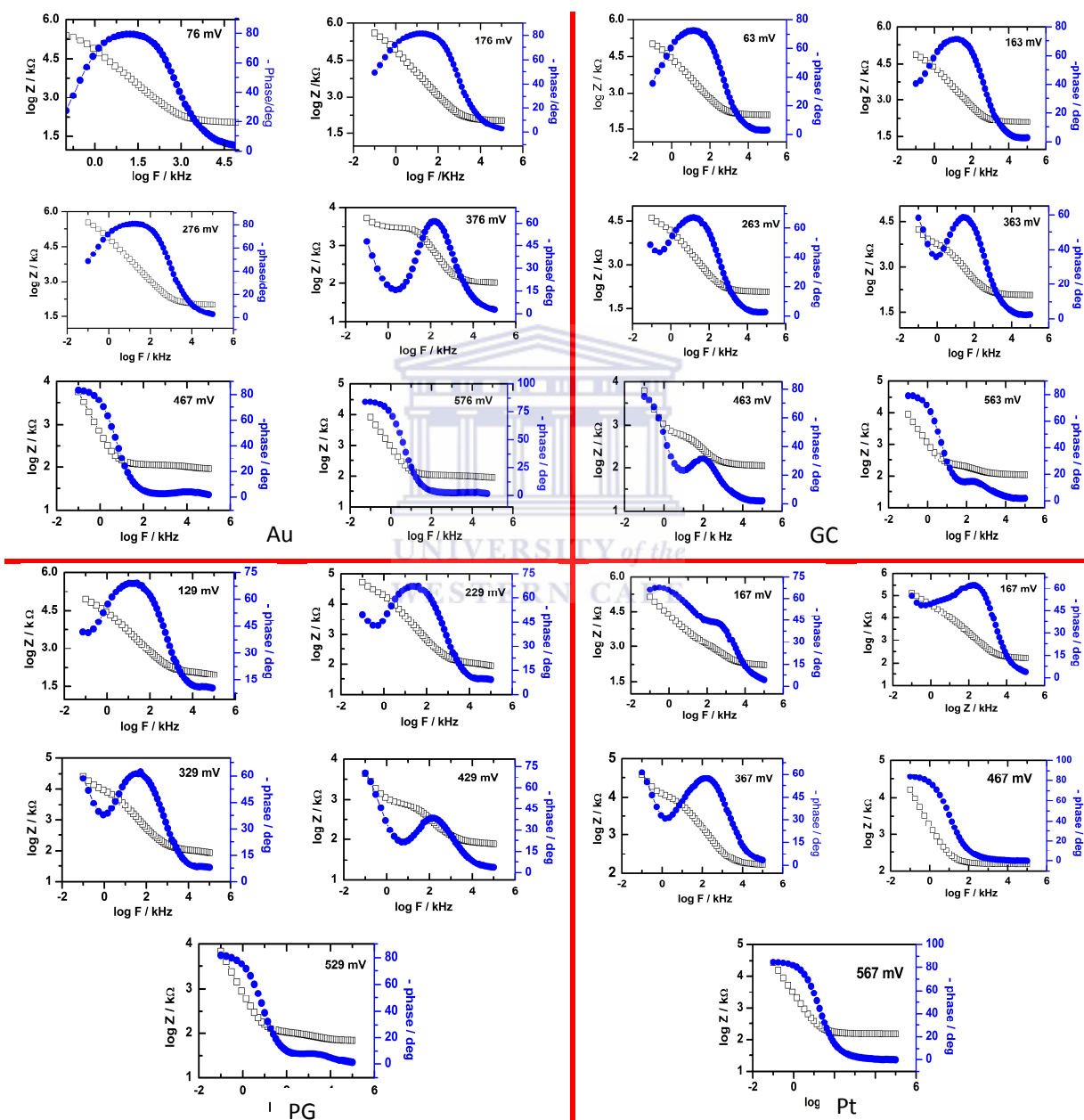


Figure 6.11: Bode plots of PANI films prepared in $0.1 \text{ M HClO}_4/\text{ACN}$ on various electrodes at different potential.

Chapter 6: Investigation of electroinactivity of tetrodotoxin and its complexation to ionophores

Table 6.4: Comparison of impedimetric parameters of PANI modified-electrodes [220-221]

WE	Potential [mV]	R_{ct} [k Ω]	Phase angle [$^{\circ}$ C]	$\log F$ [kHz]	F [kHz]	Comments
Au	76	0.10	79.73	1.21	16.22	Conductor
	176	169.63	82.61	1.19	15.49	Conductor
	276	/	81.57	1.13	13.49	Conductor
	376	/	61.90	2.16	144.51	Conductor
	476	2.10	0	> 2	0.1	Resistor
	576	0.02	0	> 2	0.09	Resistor
GC	63	0.12	73.69	1.01	12.59	Conductor
	163	59.14	72.20	1.15	14.13	Conductor
	263	39.12	67.71	1.21	16.22	Conductor
	363	16.64	59.42	1.44	27.54	Conductor
	463	5	79	1.97	93.33	Conductor
	563	0.44	14.87	2.42	263.03	Conductor
PG	129	0.09	69.88	1.30	19.95	Conductor
	229	26.17	67.93	1.38	23.98	Conductor
	329	14.38	62.19	1.54	34.67	Conductor
	429	6.267	69.06	2.16	144.54	Conductor
	529	0.839	10	-0.99	0.10	Conductor
Pt	167	/	65.90	2.46	288.40	Conductor
	267	/	63.45	2.23	169.82	Conductor
	367	/	57.96	2.17	147.9	Conductor
	467	8.7	0	> 2	> 0.30	Resistor
	567	/	0	>2	>0.30	Resistor

Chapter 6: Investigation of electroactivity of tetrodotoxin and its complexation to ionophores

6.2.5 Study of PANI films

The cyclic voltammogram diagnostics for an electrode reaction at the planar macroelectrode involves chemically stable and soluble redox couple: $O + ne^- \rightleftharpoons R$. The above system can be reversible, quasi-reversible or irreversible. Figure 6.12 shows a series of voltammograms of PANI recorded on various electrodes at different scan rates in 0.1 M $HClO_4/ACN$ were used to study the reversibility of the system. It was found that the peak current increase along with the rising of scan rate, while the ΔE_p expands slowly.

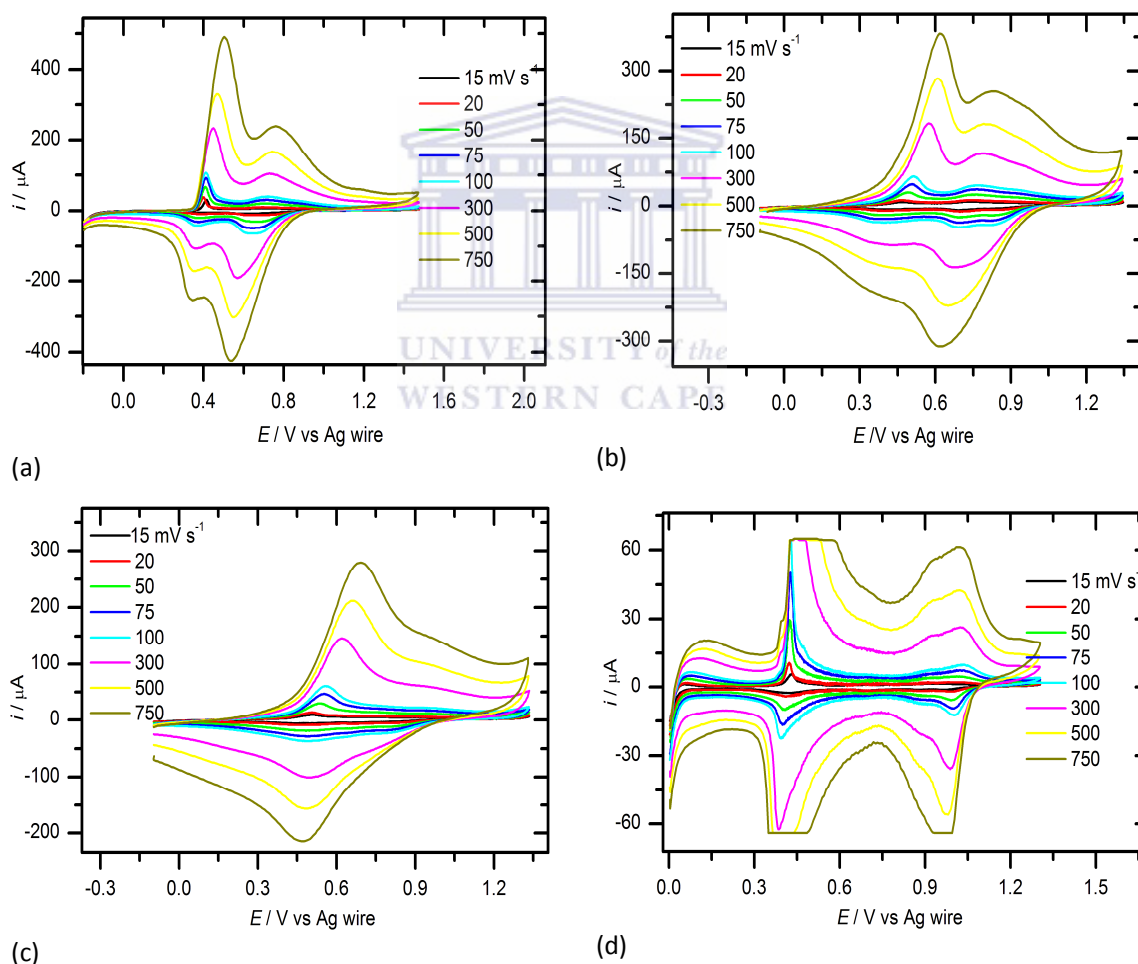


Figure 6.12: Cyclic voltammograms of the PANI electrodeposited on (a) Au, (b) GC, (c) PG, and (d) Pt electrodes in 0.1 M $HClO_4/ACN$ at different potential scan rates.

Chapter 6: Investigation of electroinactivity of tetrodotoxin and its complexation to ionophores

In order to calculate the kinetic parameters of PANI redox on electrode surface, the scan rate was increased. For the redox monolayer modified electrode, the peak potential can be given as follows [222]:

$$E_{pa} = E'^0 - \frac{2.3RT}{(1-\alpha)nF} \log(1-\alpha) + \frac{2.3RT}{(1-\alpha)nF} \log\left(\frac{RT}{nF} k_s\right) + \frac{2.3RT}{(1-\alpha)nF} \log v \quad \text{Equation 6.5}$$

$$E_{pc} = E'^0 - \frac{2.3RT}{\alpha nF} \log \alpha + \frac{2.3RT}{\alpha nF} \log\left(\frac{RT}{nF} k_s\right) - \frac{2.3RT}{\alpha nF} \log v \quad \text{Equation 6.6}$$

The transfer coefficient α was calculated according to the slope of cathodic process (Fig.6.13), and the result is given in Table 6.6.

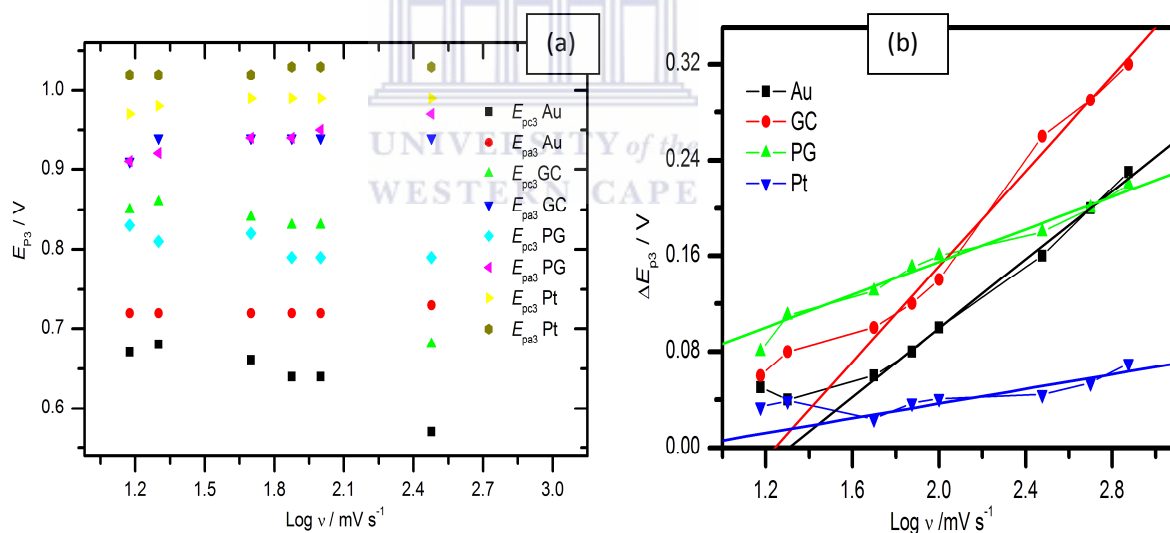


Figure 6.13: (a) A plot of E_{p3} vs. $\log v$ and (b) plot of ΔE_{p3} vs. $\log v$ for the voltammograms of PANI films deposited on different electrode surface in 0.1 M HClO_4/ACN .

Chapter 6: Investigation of electroinactivity of tetrodotoxin and its complexation to ionophores

Table 6.5: Kinetic parameters of PANI films on various electrodes obtained from the plot E_{pc} -growing versus logarithm of scan rate

WE	A [cm ²]	Plot E_{pc3} vs. $\log v$					
		Range	R^2	a [V]	b [s ⁻¹]	b [s ⁻¹ cm ⁻²]	α_A
Au	0.0201	1.297 – 2.482	-0.965	0.81 ± 0.03	-0.09±0.01	-4.48±0.01	0.01
GC	0.0707	1.17- 2.48	-0.982	1.2 ± 0.1	-0.2 ± 0.0	-2.83± 0.0	0.02
PG	0.0707	1.17 – 2.48	-0.792	0.8 ± 0.0	-0.1 ± 0.0	-1.41± 0.0	0.04
Pt	0.0201	1.17 – 2.48	0.806	0.96±0.01	0.01± 0.01	0.50± 0.01	0.12

According to the above equation (6.5 and 6.6), ΔE_p can be obtained:

$$\Delta E_p = \frac{2.3RT}{(1-\alpha)} \left[\alpha \log(1-\alpha) + (1-\alpha) \log \alpha - \log \left(\frac{RT}{nF} \right) - \log k_s \right] + \frac{2.3RT}{(1-\alpha)\alpha nF} \log v$$

Equation 6.7

According to the plot ΔE_{pc3} versus $\log v$ (Fig.6.13b), the electrode reaction constant k of PANI film is calculated (Tab.6.6). The value of k_s obtained on gold and platinum electrodes were very high compared to the result obtained in PANI prepared in 0.5 M H₂SO₄ on anodic aluminum oxide membrane as a template by Ziyi Wang *et al.* (5.8 s⁻¹) [223].

Chapter 6: Investigation of electroinactivity of tetrodotoxin and its complexation to ionophores

Table 6.6: Data obtained from the plot ΔE_{pc3} vs. $\log v$

WE	Plot ΔE_{pc3} vs $\log v$					
	Range [mV s ⁻¹]	R ²	<i>a</i> [V]	<i>b</i> [s ⁻¹]	<i>k_s</i> [s ⁻¹]	<i>k</i> [s ⁻¹ cm ⁻²]
Au	1.69 – 2.89	0.998	-0.19 ± 0.01	0.14 ± 0.01	1.75 ± 0.01	87.06 ± 0.01
GC	1.69 – 2.89	0.995	-0.25 ± 0.02	0.19 ± 0.01	0.02 ± 0.02	0.28 ± 0.02
PG	1.69 – 2.89	0.986	0.02 ± 0.01	0.07 ± 0.01	1.41 × 10 ⁻⁷ ± 0.01	1.99 × 10 ⁻⁶ ± 0.01
Pt	1.69 – 2.89	0.933	-0.02 ± 0.01	0.03 ± 0.01	5.87 ± 0.01	292.04 ± 0.01

For the application of PANI film, the study of the thickness of PANI film (thin or thick film) is reported. After electrochemical synthesis of the PANI films on the electrode surface, the voltammogram obtained was used to determine the peak potential and the peak current for each redox process taking place during the potentiodynamic growth of PANI films.

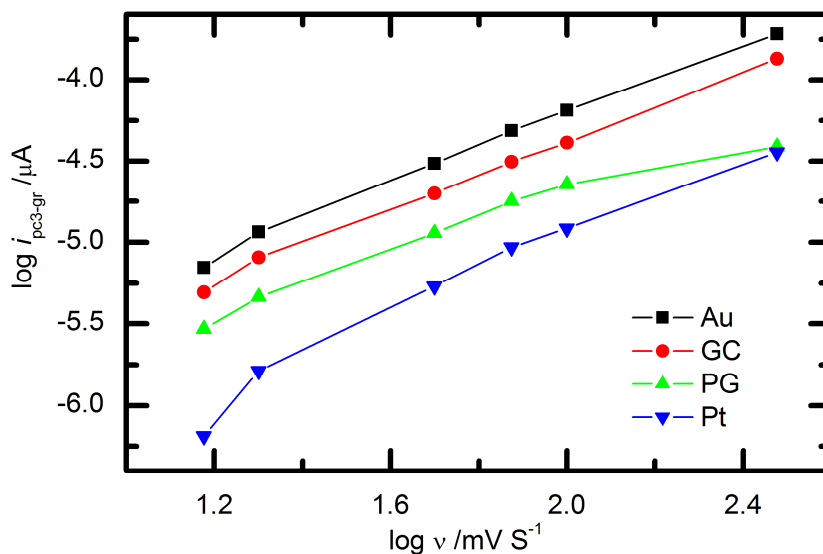


Figure 6.14: The plot of logarithm of the growing PANI peak (i_{pc3}) vs. $\log v$.

Chapter 6: Investigation of electroinactivity of tetrodotoxin and its complexation to ionophores

The first cathodic peak which is implied on the study of the stability of the electrode vis-à-vis PANI was also used to determine the thickness of polymer film. Figure 6.14 shows the plot of the logarithm of PANI growth peak against logarithm of scan rates.

Table 6.7: Study of PANI films base on the slope (b) of the plot $\log i_{pc-gr}$ vs. $\log v$

WE	A [cm ²]	log i_{pc-gr} vs. log v				
		Range [mV s ⁻¹]	R^2	a [μ A]	b [μ A mV ⁻¹ s ⁻¹]	b [μ A mV ⁻¹ s ⁻¹ cm ⁻²]
Au	0.0201	1.17 – 2.48	0.998	-6.38 ± 0.06	1.08 ± 00.4	53.73 ± 0.04
GC	0.0707	1.17 – 2.48	0.999	-6.54 ± 0.05	1.08 ± 0.03	15.27 ± 0.03
PG	0.0707	1.17 – 2.48	0.981	-6.47 ± 0.15	0.87 ± 0.09	12.31 ± 0.04
Pt	0.0201	1.17 – 2.48	0.985	-7.54 ± 0.21	1.29 ± 0.11	64.18 ± 0.08

As can be seen on the Table 6.7, the slope of the plot $\log i_{pc-gr}$ vs. $\log v$ is approximately equal to 1, characteristic of PANI thin film. The calculated values of the polymerisation rate (k_p^{app}) and the charge transfer (Q_a) within the electrode interface|solution related to the quantity of the PANI formed on the electrode surface demonstrated that more polymers have formed on PG and GC than on Au and Pt electrodes. The EIS results pointed out an enhancement in the stability and conductivity of PANI. The conductivity properties were studied using Nyquist plot, thanks to the presence of R_{ct} in small value at some potential, therefore, characteristic of the Faradaic reaction taking place. The conductivity was also studied using the Bode plot, considering the phase angle (high value). CVs of PANI also showed regular peak potential and peak current during the voltammetric scan (3 cycles) which confirmed the good stability of the electrodes vis-à-vis PANI as

Chapter 6: Investigation of electroinactivity of tetrodotoxin and its complexation to ionophores

demonstrated on EIS analysis. From the results, PG and Pt have been chosen to be more suitable for electrodeposition of polyaniline in HClO_4/ACN at room temperature.

6.2.6 Characterisation of electropolymerised PANI on PG and Pt electrode in acetate buffer pH 4.8

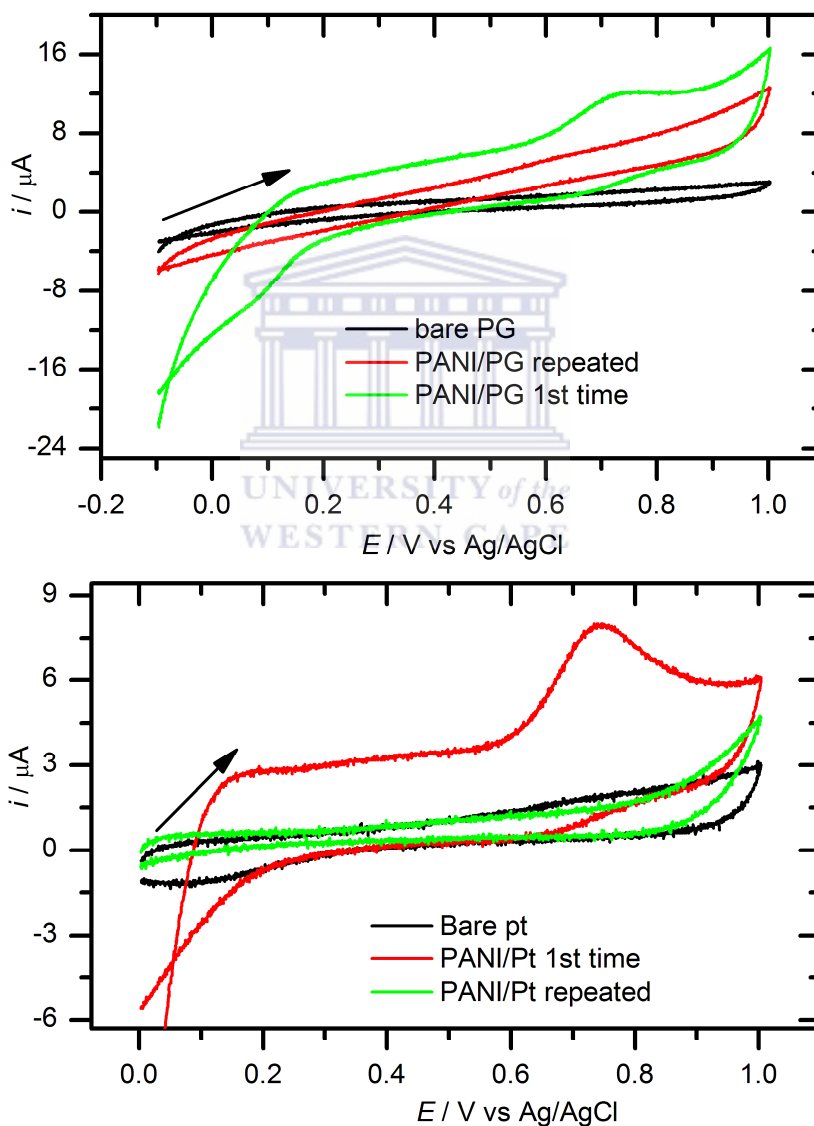


Figure 6.15: CVs of PANI in OAc buffer on Pt and PG electrode at 50 mV s^{-1} .

Chapter 6: Investigation of electroinactivity of tetrodotoxin and its complexation to ionophores

For the application of PANI modified-electrode in electrochemical TTX sensor, the CVs of PANI/PG and PANI/Pt was recorded in OAc buffer pH 4.8. The specific buffer solution was used as an electrolyte because of the active medium of TTX. One oxidation peak was observed at 0.74 V on PANI/Pt and PANI/PG for the first cycle when scanning forward (Fig. 6.15). When the modified-PANI/electrode was scanned again, that peak disappeared so the current produced was due to the modification of electrode surface with PANI. Thus, PANI is not electroactive in OAc buffer pH 4.8.

Since the polyaniline layer does not produce current in such a device, its conductivity is irrelevant. The conductivity is one of the most important properties investigated in electrochemical sensors or biosensors. However, PANI needs to be doped when it is used as a conductor of electronic current and this type of doping leads to important conductivity changes. For this concept of doping, it was reported that, PSSA is the only one doping that can effectively maintain the inherent electroactivity of PANI in the neutral and alkaline media [103, 224-228] amongst other doping materials. Therefore, PANI was doped with PSSA to enhance the conductivity, electroactivity and stability of the PANI to be applied on electrochemical TTX sensor.

6.3 Indirect detection of TTX on modified-ionophore/PANI

6.3.1 Electrochemical synthesis of PSSA doped PANI in HClO₄/ACN

The PANI–PSSA was prepared in a solution of 0.05 M aniline and 0.1 M HClO₄/ ACN by potential cycling between - 0.1 to 1.3 V on PG versus a Ag wire electrode at a scan rate of

Chapter 6: Investigation of electroinactivity of tetrodotoxin and its complexation to ionophores

50 mV s^{-1} in the presence 0.025 M of PSSA. Cyclic voltammogram of the electropolymerisation of PANI-PSSA is plotted on Figure 6.16. The same redox peaks gotten on the electropolymerisation of aniline (Fig.6.7) are found when aniline is doped with PSSA (Fig. 6.16). But these redox peaks appeared at small stable potential (peak potential are not shifted as it was with aniline only) comparing to the potential obtained in (Fig.6.7). High peak currents are obtained when aniline monomer is doped with PSSA than when aniline is electropolymerised alone. The difference observed with the regulation and small peak potential shows on one hand explained the PANI stability and rapid protonation of PANI when it is doped with PSSA [229] and on the other hand, the high peak current obtained explained the increase of the electrical conductivity [228] of PANI doped PSSA and the quantity of films formed on the electrodes surface.

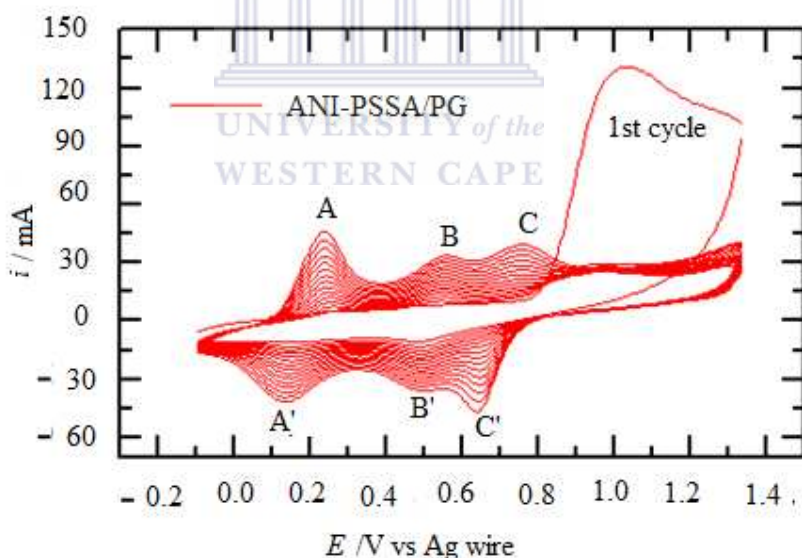


Figure 6.16: CVs of polymerization of 25 mM PSSA doped 0.05 M aniline in 0.1 M HClO_4 /ACN at 50 mV s^{-1} , 15 cycles on PG electrode.

Chapter 6: Investigation of electroinactivity of tetrodotoxin and its complexation to ionophores

Cyclic voltammograms taken showed that the PANI–PSSA film displayed all the four redox couples expected for doped PANI highlighting the superior PSSA stabilising effect as said before. Cyclic voltammograms of the PANI and PANI–PSSA films at 50 mV s^{-1} recorded on PG in the potential region -0.1 to $+1.3 \text{ V}$ in $0.1 \text{ M HClO}_4/\text{ACN}$ are shown on Figure 6.16. The resultant PANI–PSSA modified electrodes were conductive in OAc buffer solution pH 4.8 (result not showed) showing well-formed redox peaks between -0.25 and 0.3 V .

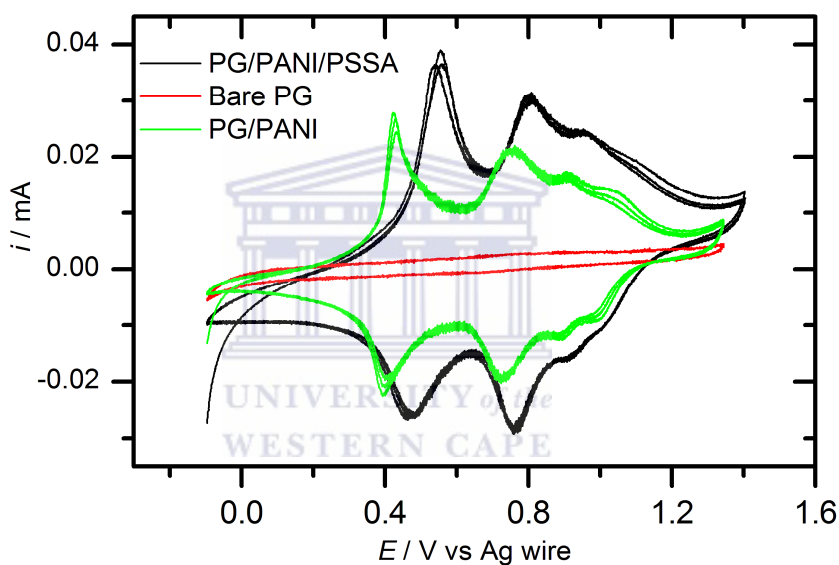


Figure 6.17: Overview of 3 cycles CVs PANI-PSSA in $0.1 \text{ M HClO}_4/\text{ACN}$ at 50 mV s^{-1} on PG electrode.

6.3.2 Sodium ion sensor based on NaX/PANI-PSSA/PG

The ultimate goal of the synthesis of PANI–PSSA was to access their possible applications in electrochemical TTX sensor construction as effective electron transfer mediators. For this purpose, the neutral compound, sodium ionophore X was used to study the indirect detection of TTX. As TTX blocks the sodium channel, the sodium sensor was investigated

Chapter 6: Investigation of electroinactivity of tetrodotoxin and its complexation to ionophores

and this sodium sensor was used for the detection of TTX. After CV of PANI-PSSA was recorded, the CV of the sodium ionophore X (NaX) drop-coated on the PANI-PSSA modified electrode was also recorded in OAc buffer electrolyte pH 4.8 at 50 mV s^{-1} . As shown in Figure 6.18, the redox peak of NaX/PANI-PSSA/PG is between -0.48 and 0.4 V with the formal potential of $E^{\circ} = -0.04 \text{ V}$ and the peak potential separation $\Delta E_p = 0.88 \text{ V}$ while the formal potential of PANI-PSSA was $E^{\circ} = -0.025 \text{ V}$ with $\Delta E_p = 0.55 \text{ V}$. The increase of ΔE_p when NaX is drop-coated is due to the slow electron transfer reaction at the electrodes. The peak current reduced when NaX is drop-coated on PANI-PSSA/PG is due to the lower electrical resistivity of electrode which may yield a high faradic current. After adding different concentrations of NaCl solution into the electrolyte solution, the peak potential gradually shifted and the peak current decreased with increasing concentration of NaCl. Figure 6.18 shows that NaX detects Na^+ present in electrolyte, however the challenge is that NaX is Cl^- selective. A change in concentration recorded can be attributed to Cl^- from NaCl solution added into the OAc buffer solution.

Chapter 6: Investigation of electroinactivity of tetrodotoxin and its complexation to ionophores

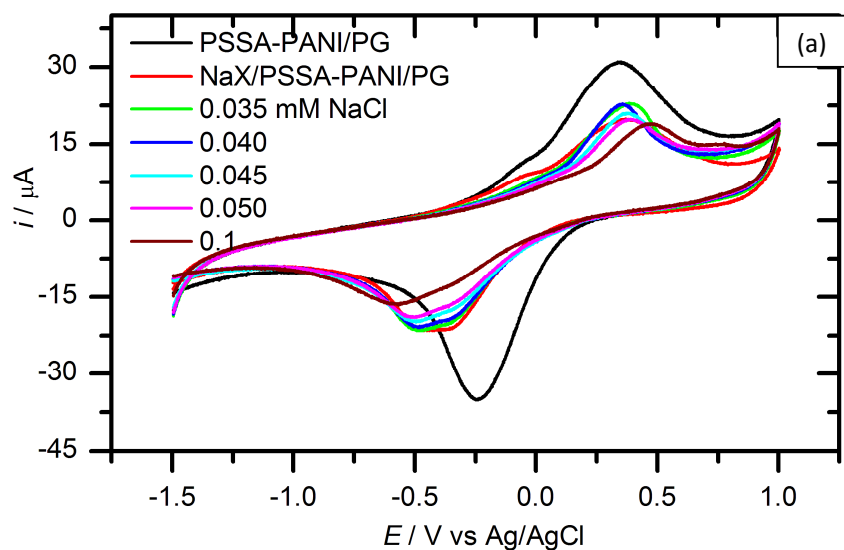


Figure 6.18: CVs of different concentration of NaCl solution on NaX/PANI-PSSA/PG in 0.1 M OAc buffer pH 4.8 at 50 mV s^{-1} .

To prove that NaX/PANI-PSSA sensor functions well for Na^+ , the same experiment was repeated with NaOAc so that the OAc ion will neutralise the OAc ion in the buffer and only Na^+ will be in electrolyte. Figure 6.19 shows that the peak current significantly decreased after the NaX is attached but it becomes constant with increase in the concentration of NaOAc solution into the electrolyte solution. From these results (Fig.6.19) the sodium sensor based on NaX/PANI-PSSA cannot be developed on metal electrode. The purpose of this experiment was to develop the sodium sensors and apply on tetrodotoxin sensor since both Na^+ and TTX^+ have the same site of action in the body. Thus, the change of redox peak with an increase in concentration observed was due to the Cl^- ion not Na^+ ion. This indication gave rise to the novel idea of developing sodium sensors using ion-transfer voltammetry technique.

Chapter 6: Investigation of electroinactivity of tetrodotoxin and its complexation to ionophores

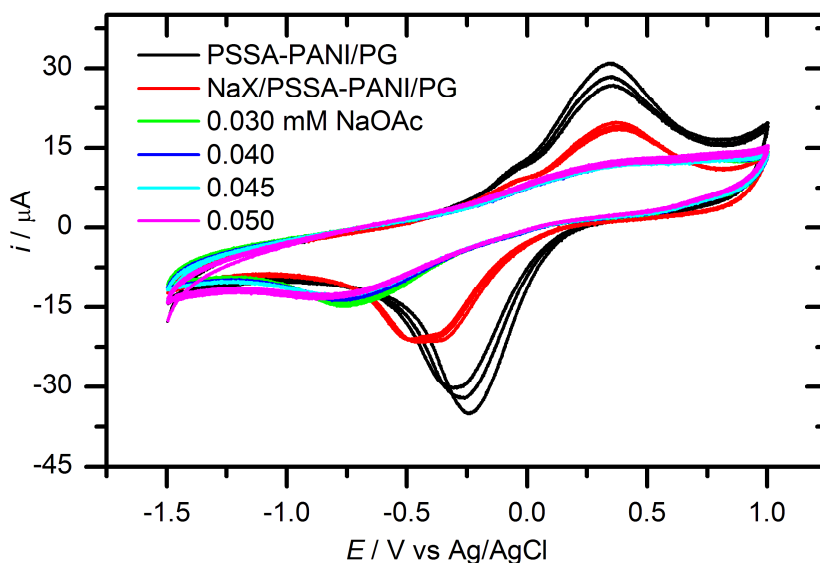


Figure 6.19: Overview of 3 cycles CVs of different concentration of NaOAc in 0.1 M OAc buffer pH 4.8 at 50 mV s^{-1} on PG electrode.

6.4 Electrochemical tetrodotoxin sensor based on neutral selective NaX and B18C6 ionophores

Tetrodotoxin is a puffer fish toxin which is 10,000 times deadlier than cyanide in rats, and 10 to 100 times as lethal as the black widow spider venom [230]. The incidences of tetrodotoxin poisoning may seem infrequent, but the development of simple, portable, and specific detection methods for this super neurotoxin would be invaluable in light of the reported 60% human fatality rate recorded as well as for quality control, quarantine, and forensic purposes. In this study, a simple sensor for TTX based on a principle mimicking the very mechanism the poison relies on for binding itself to Na-selective channels is proposed. “TTX mimics the hydrated sodium cation, goes through the mouth of the sodium- channel, with the peptide complex binding to a peptide glutamate side group, among others, and then further tightens its hold when the peptide changes. Following

Chapter 6: Investigation of electroinactivity of tetrodotoxin and its complexation to ionophores

complex conformational changes, TTX is further electrostatically attached to the Na⁺ gate channel opening” [231]. In the approach proposed in this study, sodium-selective ionophore will be impregnated into a carboxylic acid functionalised conducting polymer via in-situ co-deposition on order to develop a TTX-specific recognition surface. The resulting surface will be interrogated with cyclic voltammetry in situ in a solution of TTX.

6.4.1 Investigation of ionophore complexation of TTX using ion transfer voltammetry

In the electrochemical system employed in this study, concentration of the redox couple in the aqueous phase (electrolyte solution) was in excess compared to the concentration of the ion which is studied previously [232]. The excess of concentration of the redox couple in the aqueous phase is to make the platinum in water interface unpolarisable and it can act as a reference/counter electrode for the aqueous phase. Ionophores that are used in potentiometric ion-selective electrodes were chosen to ensure selective transfer of the Na⁺ or TTX⁺ ions from the aqueous solution into the membrane. The supporting electrolyte in organic phase (50 mM ETH500 in 1,2-DCE) is to increase the membrane conductivity therefore should have very low solubility in water [233].

6.4.1.1 Choice of electrolyte solution

The conventional electrochemical cell used for recording the anodic final rise voltammograms of the transfer of alkaline metal ion across O|W (organic|water) interface is represented as follows:

Chapter 6: Investigation of electroinactivity of tetrodotoxin and its complexation to ionophores

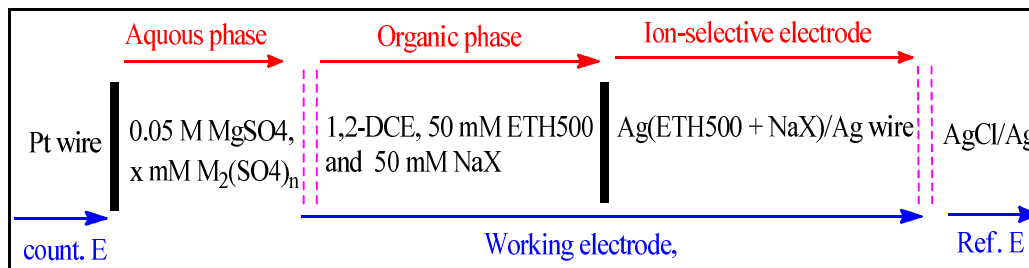


Figure 6.20: Conventional scheme of electrochemical cell (I) used for the purpose of this study in ion transfer voltammetry.

The reaction under this study was:



Where $M^{n+} = K^+, NH_4^+, Li^+, Mg^{2+}$

The background CV of three different electrolyte solutions, K_2SO_4 , $(NH_4)_2SO_4$, Li_2SO_4 , and $MgSO_4$ were investigated in the purpose to find which ion will not interfere with Na^+ or TTX^+ ion. Figure 6.20 illustrates the measurements of transfer potentials of various background electrolytes using cyclic voltammetry with the conventional cell presented above. The anodic peaks ($E_{pa} = 0.0$ V, $i_{pa} = 3.2$ μ A), ($E_{pa} = - 5.5$ V, $i_{pa} = - 3.8$ μ A) and ($E_{pa} = - 0.4$ V, $i_{pa} = 2$ μ A) correspond to the transfer of K^+ , NH_4^+ , and Li^+ ions respectively from the aqueous solution to the organic, while the cathodic ($E_{pc} = - 0.58$ V, $i_{pc} = - 5.8$ μ A) and ($E_{pc} = -0.31$ V, $i_{pc} = 2$ μ A) peaks correspond to the transfer back of K^+ and NH_4^+ respectively into the aqueous solution. No peak was observed related to Mg^{2+} transfer across the water|1,2-DCE interface for the high concentration of the $MgSO_4$ solution.

Chapter 6: Investigation of electroinactivity of tetrodotoxin and its complexation to ionophores

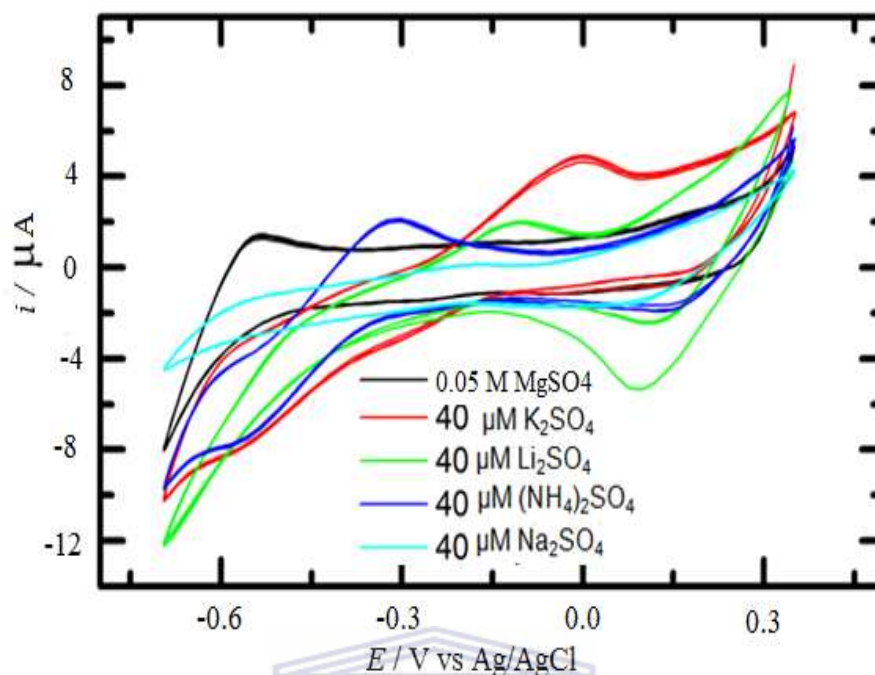


Figure 6.21: Overview 3 cycles background CVs of different electrolyte solutions obtained with NaX at the W|1,2-DCE interface, scan rate 0.01 V s^{-1} .

The diffusion coefficients D of each ion in the aqueous solution was calculated from the limiting diffusion anodic currents given in Table 6.8 using the Cottrell equation. The complex formation constant $k_{M^{n+}NaX}^0 = 200 \text{ M}^{-1}$ was calculated as well from the reaction in solution (Equation. 6.9)

$$|i_p| = (2.29 \times 10^5) n^{3/2} A D^{1/2} C v^{1/2} \quad \text{Equation 6.9}$$

Where i_p is the peak current (i_{pa} anodic and i_{pc} cathodic), n is the electron stoichiometry, A is the electrode area (cm^2), D is the diffusion coefficient, C is the concentration (mol cm^{-3}), v is the scan rate (mV s^{-1})

Chapter 6: Investigation of electroinactivity of tetrodotoxin and its complexation to ionophores

$$k_{M^{n+}NaX}^0 = \frac{[M^{n+}NaX]}{[NaX][M^{n+}]} \quad \text{Equation 6.10}$$

Table 6.8: Kinetic parameters of the interfacial transfer reaction obtained from background CVs of different electrolytes solution

Electrolyte	E_{pa} [V]	E_{pc} [V]	ΔE_p [V]	$E^{o'}$ [V]	i_{pa} [μ A]	i_{pc} [μ A]	i_{pa}/i_{pc}	$D \times 10^{-7}$ [A cm s ^{1/4} mol ^{-1/2} V ^{-1/4}]	$k_{M^{n+}NaX}^0$ [M ⁻¹]
K ₂ SO ₄	0.0	-0.58	0.58	0.29	3.2	-5.8	-0.55	1.2	200
(NH ₄) ₂ SO ₄	-5.5	-0.31	5.19	2.91	-3.8	2	-1.9	1.4	200
Li ₂ SO ₄	-0.4	/	/	/	2	/	/	0.99	200

6.4.1.2 TTX⁺ ion sensor based on NaX in MgSO₄ solution

As mentioned before, the sodium sensor was developed using ion transfer voltammetry based on sodium ionophore X (NaX) on ETH500 solution in 0.05 M MgSO₄ electrolyte solution.

Typical cyclic voltammogram for Na⁺ transfer when the ligand, NaX is in access is shown in Figure. 6. 21. This figure shows a cyclic voltammogram of different concentrations of Na⁺ ion in the aqueous solution with a dialysis membrane gel electrode in Cell (I) (Fig.6.19). No Na⁺ ion diffusion was observed means that no complex was formed between Na⁺ ion and NaX ionophore.

Chapter 6: Investigation of electroinactivity of tetrodotoxin and its complexation to ionophores

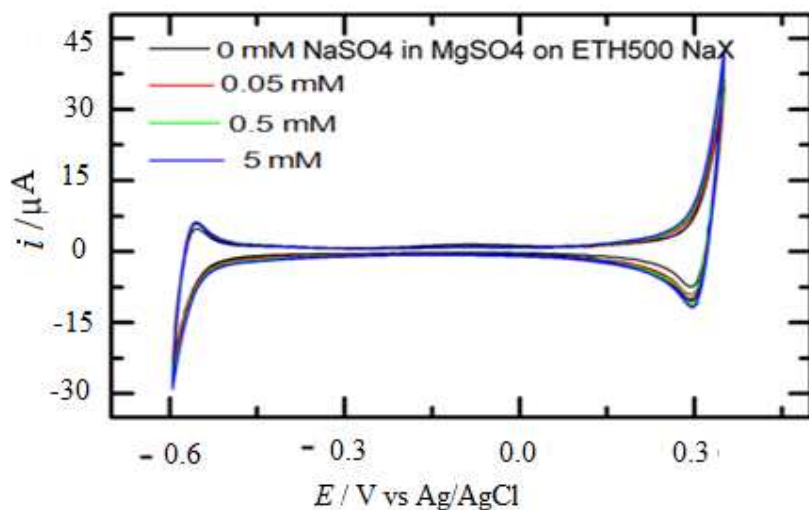


Figure 6.22: Overview of 3 cycles of Cyclic voltammograms obtained for different concentrations of Na^+ ion transfer across the $0.05 \text{ M MgSO}_4 | 1,2\text{-DCE}/50 \text{ mM ETH 500}$ interface, using 10 mM NaX at 0.01 V s^{-1} .

Figure 6.22 presents the CV recorded during the potentiodynamic TTX^+ ions exchange. The ion-transfer voltammetry based on NaX shows that no TTX^+ ion was transferred from the aqueous to organic phase even when the concentration of TTX was increased. While, TTX^+ ion does not diffuse to organic phase with NaX ionophore, the affinity of NaX to form the complex with TTX is virtually impossible. This can be due to the size of NaX different from the diameter of the active site (guanidinium group) of TTX (Tab.6.9) or it can be explained by the steric hindrance as well as the overall of the two compounds (Tab.6.10).

Chapter 6: Investigation of electroinactivity of tetrodotoxin and its complexation to ionophores

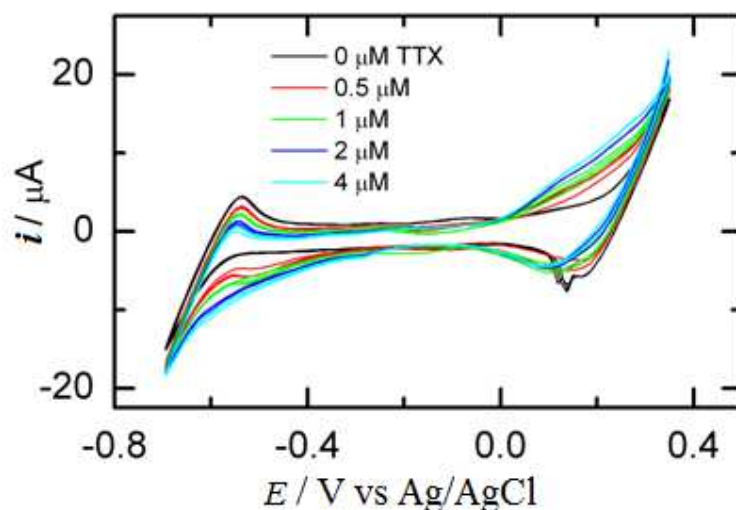


Figure 6.23: Overview of 3 cycles of CVs obtained for different concentrations of TTX^+ ion transfer across the $0.05 \text{ M MgSO}_4 | 1,2\text{-DCE}/50 \text{ mM ETH 500}$ interface, using 50 mM NaX at 0.01 V s^{-1} .

Figure 6.23 shows the influence of K^+ ion peak on the CVs of different concentrations of TTX^+ and Na^+ ions transfer across the 0.05 M MgSO_4 was added in electrolyte, then the TTX solution as well as potassium which showed more diffusion. No transfer ion across the O|W interface was observed when Na^+ and TTX^+ ions were added. But when the K^+ ion was dropped into the electrolyte solution, a redox peak that corresponds to the diffusion of K^+ into organic phase (anodic peak) was observed).

Chapter 6: Investigation of electroinactivity of tetrodotoxin and its complexation to ionophores

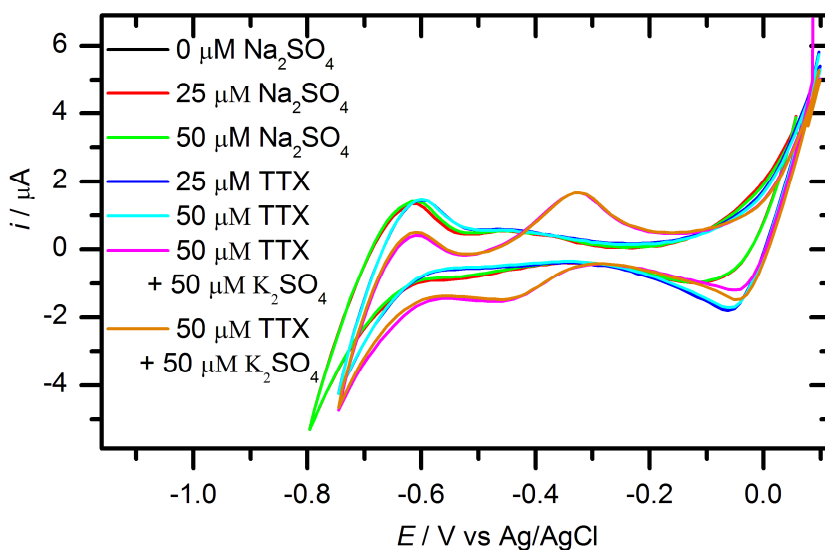


Figure 6.24: Influence of K^+ ion peak on the CVs of different concentrations of TTX^+ and Na^+ ions transfer across the $0.05\text{ M MgSO}_4/1,2\text{-DCE}/50\text{ mM ETH 500}$ interface, using 50 mM NaX at 0.01 V s^{-1} .

In Figures 6.19, 20, 21 and 22 show that NaX does not form a complex with Na^+ and TTX^+ ions across O|W interface electrode. According to literature [234-236], dibenzo-18-crown-6 sodium-selective ionophore is used to investigate the Na^+ sensor based on the B18C6 ionophore.

6.4.1.3 TTX^+ sensor based on B18C6 in $MgSO_4$ solution

To avoid any flow of Na^+ ion from the Ag/AgCl reference electrode into the water electrolyte solution, the Ag/Ag₂SO₄ was made and used as reference electrode in aqueous phase solution.

Chapter 6: Investigation of electroinactivity of tetrodotoxin and its complexation to ionophores

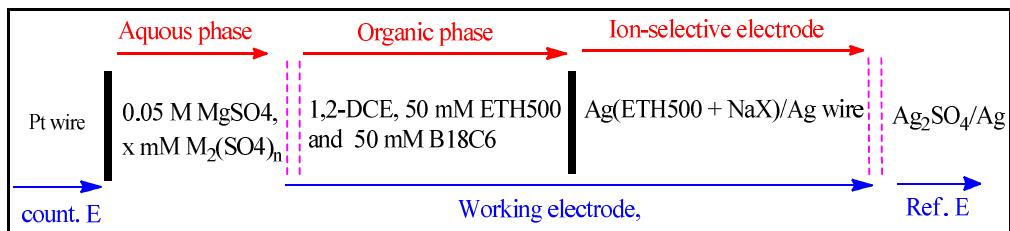
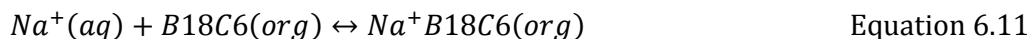


Figure 6.25: Conventional scheme of electrochemical cell (II) used for the purpose of this study in ion transfer voltammetry.

Firstly, voltammetric Na^+ sensor in contact with 0.05 M MgSO_4 aqueous electrolyte solution was made based on B18C6 ionophore. The selectivity of this voltammetric Na^+ sensor using different concentration of Na_2SO_4 solution was investigated. One anodic peak $E_{\text{pa}} = -0.08$ V, $i_{\text{pa}} = 3$ μA was obtained which corresponds to the transfer of Na^+ into organic phase and one cathodic peak $E_{\text{pc}} = -0.28$ V, $i_{\text{pc}} = 1.9$ μA . This explains the reversal of to the aqueous electrolyte solution as explained previously. The concentration of Na^+ ion in an aqueous electrolyte solution increases the peak current. The value of the diffusion coefficient $D = 5.105 \times 10^{-7}$ $\text{A cm s}^{1/4} \text{ mol}^{-1/2} \text{ V}^{-1/4}$ and the complex formation constant $k_{\text{Na}^+\text{B18C6}}^0 = 200 \text{ M}^{-1}$ were calculated using the Equation 6.8 and 6.9, respectively. The reaction follows the protocol in Equation 6.11



Chapter 6: Investigation of electroactivity of tetrodotoxin and its complexation to ionophores

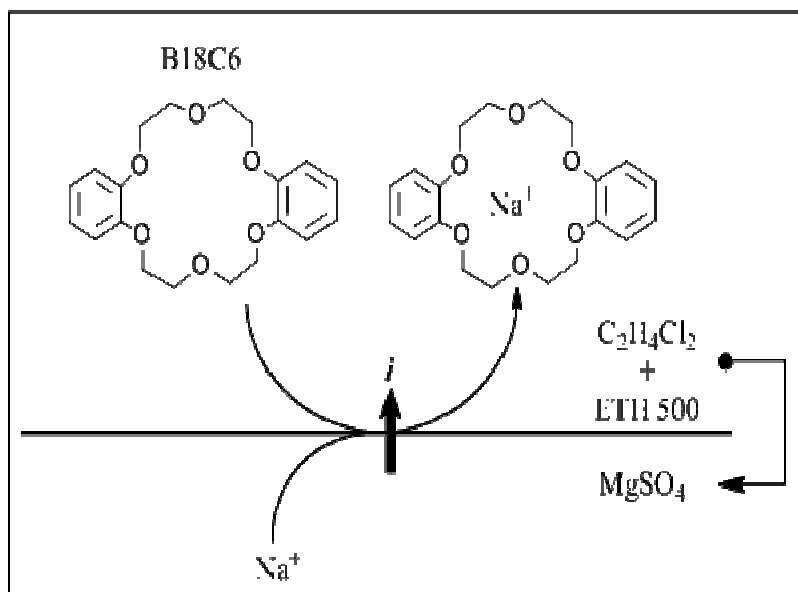


Figure 6.26: Principle of the voltammetry Na^+ ion-selective electrode based on the facilitated transfer of Na^+ at the 1,2-DCE/ETH 500/organic phase interface by B18C6.

From Figure 6.27, it was proved that sodium sensor could be successfully developed using ion transfer voltammetry based on B18C6 selective ionophore. The hypothesis that sodium and TTX may have the same chemical properties has proven to be accurate due to the fact that TTX blocks the sodium channel in human body, in this study, the sodium sensor was simulated to detect TTX.

Chapter 6: Investigation of electroinactivity of tetrodotoxin and its complexation to ionophores

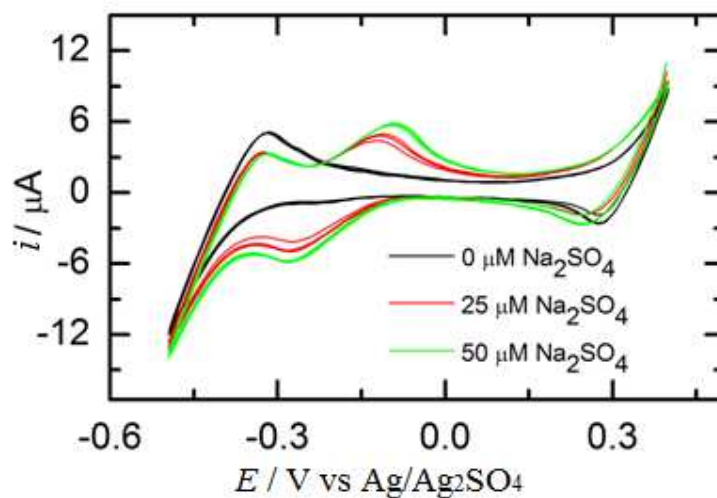


Figure 6.27: Overview of 3 cycles CVs of different concentrations of Na^+ ion transfer across the 50 mM MgSO_4 |1,2-DCE/ 50 mM ETH 500 interface, using 50 mM B18C6 at 0.01 V s^{-1} .

Figure 6.28 shows the typical cyclic voltammograms of different concentration of TTX^+ ions transfer across the water|DCE interface facilitated by the ligand (B18C6) with the Cell (II) present on Figure 6.25. The CV of TTX^+ ion transfer was firstly carried out across the 50 mM MgSO_4 |1,2-DCE/ 50 mM ETH 500 interface with 50 mM B18C6 at 0.01 V s^{-1} in MgSO_4 . Figure 6.28a shows on CV of TTX^+ ion recorded for an organic electrolyte solution (ETH500) without the ligand (L) versus Ag_2SO_4 reference electrode. Results show that no diffusion or complex formation was occurred. The CVs of TTX^+ ions at different concentration were recorded three consecutive times for the organic phase ligand. As shown in Figure 6.28b, c, and d, no electrochemical reaction took place into the cell (II). It is thus deduced that the neutral B18C6 is Na^+ ion selective but not selective to TTX^+ ion.

Chapter 6: Investigation of electroinactivity of tetrodotoxin and its complexation to ionophores

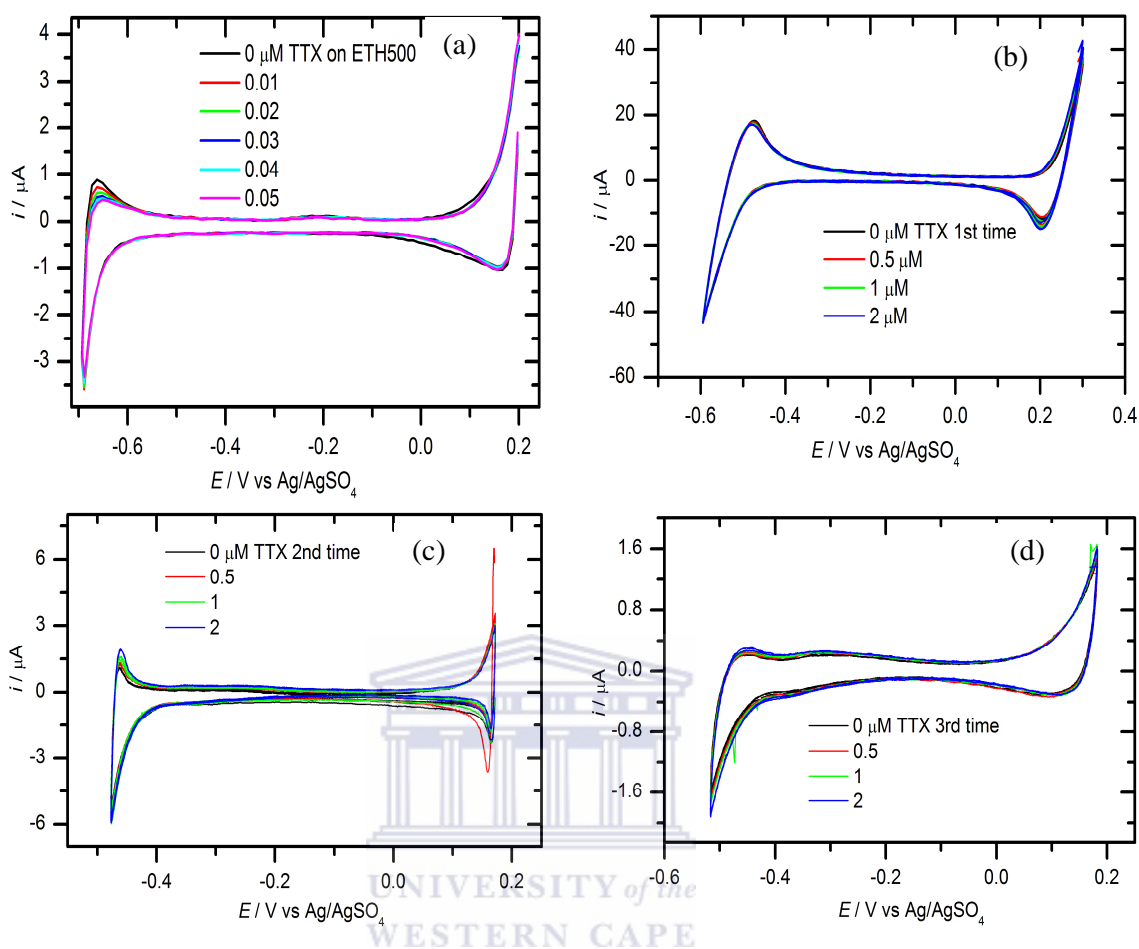


Figure 6.28: a) CV of different $[\text{TTX}^+]$ transferred across the $0.05 \text{ M MgSO}_4 | 1,2\text{-DCE} / 50 \text{ mM ETH } 500$ without B18C6 , (b), (c) and (d) CV repetition at different $[\text{TTX}^+]$ ion transfer across the $0.05 \text{ M MgSO}_4 | 50 \text{ mM B18C6}$ interface at 0.01 V s^{-1} .

6.4.2 Investigation of ionophore complexation of TTX using UV-Vis absorption

When an appropriate wavelength of light is absorbed by a molecule (i.e. excitation), the electronic state of the molecule changes from the ground state to one of many vibrational levels in the excited electronic states [237]. In UV-Vis spectroscopy, a compound is generally analysed and determined by irradiating a crude compound with UV light.

Chapter 6: Investigation of electroinactivity of tetrodotoxin and its complexation to ionophores

6.4.2.1 UV-Vis spectroscopy analysis of TTX, NaX and TTX/NaX

UV-Vis absorption spectra of the analysis of TTX registered in acetate buffer pH 4.8 is presented in Figure 6.29. Thorough interpretations of UV/Vis spectroscopy schematics are shown in Figures 6.29 and 6.30. For this analysis, 1.16 μM of TTX is dissolved in 3 ml of 0.1 M acetate buffer pH 4.8. The absorption spectrum of TTX shows two absorption peaks. The first absorption at 232.9 nm with high absorbance, corresponds to multiple chromophores $-\text{C}-\text{O}-\text{H}$ and $=\text{C}-\text{N}-\text{H}$, there involve $n \rightarrow \sigma^*$ electronic transitions (Fig. 6.29) and the second absorption appeared at 280.2 nm with low absorbance is related to the chromophore $\text{N}=\text{C}-\text{N}$ from guanidinium group which involves $n \rightarrow \pi^*$ electronic transition (Fig. 6.30). This result was closely related to Saito *et al.* experiments where an analysis of TTX and its derivatives in toxic and nontoxic pufferfish were done [238].

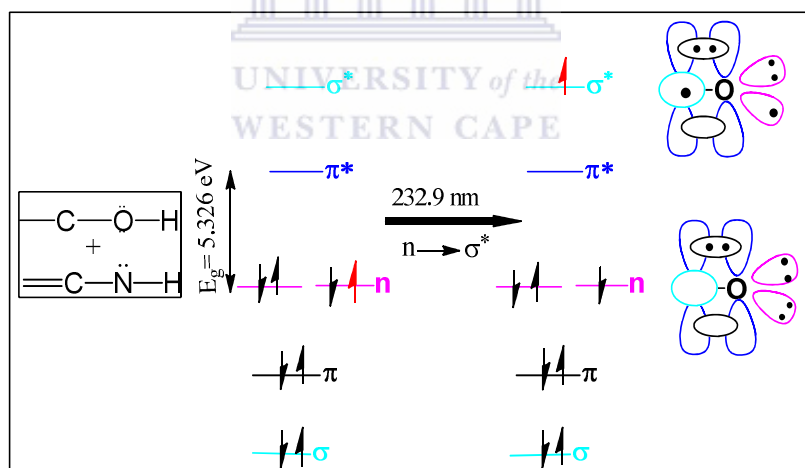


Figure 6.29: $n \rightarrow \sigma^*$ electronic transition and band gap energy during the absorption of $-\text{C}-\text{O}-\text{H}$ and $=\text{C}-\text{N}-\text{H}$ chromophores in TTX molecule.

Chapter 6: Investigation of electroinactivity of tetrodotoxin and its complexation to ionophores

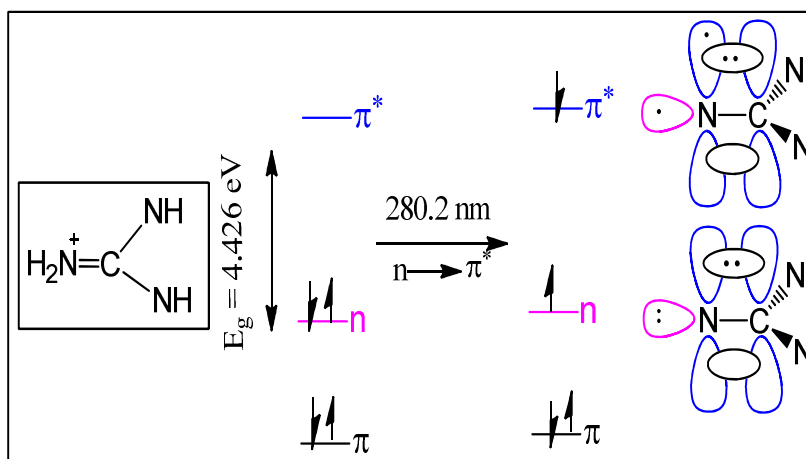


Figure 6.30: $n \rightarrow \pi^*$ electronic transition and band gap energy during the absorption of $-N=C-N-$ chromophores in TTX molecule.

The UV-Vis absorption spectrum of NaX is given in Figure 6.31. The first absorption band at 250.4 nm, corresponds to chromophores $-C=C-$ of benzene group $\pi \rightarrow \pi^*$ electronic transition (Fig. 6.31). The chromophore $C=C$ normally absorbed around 165 nm thus, the increasing of wavelength to 250.4 nm can be explained by the presence of carbonate group ($-OCOO-$, very strong attractive group by mesomeric) attached to the aromatic ring. The second absorption band appeared at 278.5 nm which is related to the chromophore $=C-O-$ bonded directly to the aromatic ring which involves $n \rightarrow \pi^*$ electronic transition (Fig. 6.32). The high absorbance and wavelength observed on this second absorption is due to the presence of the strong attractive group (carboxylic group $-COO-$) attached to this chromophore. The third absorption band appeared at 370.6 nm corresponding to a chromophore $-C=O$ of carbonate group, $n \rightarrow \pi^*$ electronic transition (Fig.6.33). Indeed, all inductive donor groups bound to a chromophore reduces its absorption and all attractive groups bound to a chromophore increases its absorption by inductive effect [239-240].

Chapter 6: Investigation of electroinactivity of tetrodotoxin and its complexation to ionophores

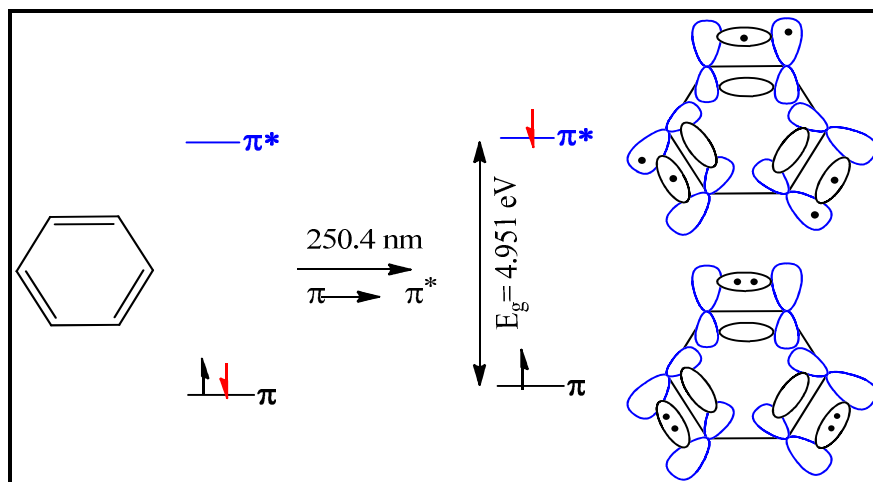


Figure 6.31: $\pi \rightarrow \pi^*$ electronic transition and band gap energy during the absorption of $=C=C-$ chromophores in NaX molecule.

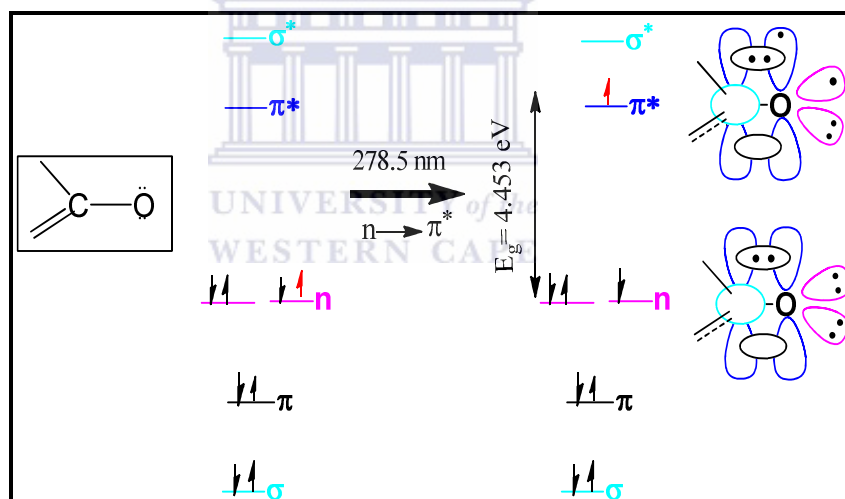


Figure 6.32: $n \rightarrow \pi^*$ electronic transition and band gap energy during the absorption of $=C=O-$ chromophores in NaX molecule.

Chapter 6: Investigation of electroinactivity of tetrodotoxin and its complexation to ionophores

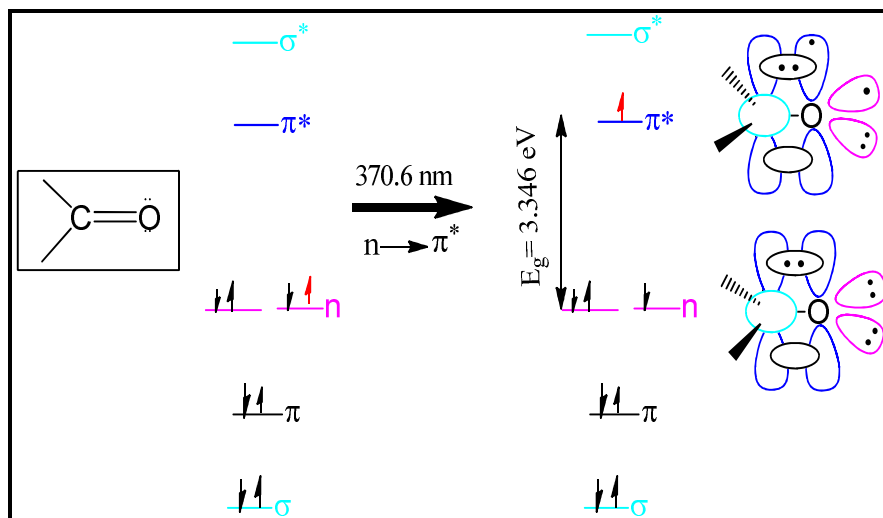


Figure 6.33: $n \rightarrow \pi^*$ electronic transition and band gap energy during the absorption of $\text{C}=\text{O}$ chromophores in NaX molecule.

Figure 6.34 shows the UV-Vis absorption spectra of the mixture of TTX /NaX in green line with three absorption peaks. The same interpretation for NaX spectra is given to the spectra of the mixture of TTX /NaX for the absorption peaks at 250.4, 278.5 and 370.6 nm (Fig. 6.32, 6.32 and 6.33 respectively). This result demonstrates that no bond has been formed between TTX and NaX and none has disappeared from the chemical structure of our ionophore (NaX) when TTX and NaX are mixed in solution. But the change observed at 250.4, 278.5 and 370,6 nm can be explained by the perturbation of the system after mixture or the perturbation of the shape of the compound due to the second excited state. Thus, this result is in confirmation with respect to ion transfer voltammetry (Fig. 6.22 and 6.23) proving that chemical reaction occurred between NaX and TTX.

Chapter 6: Investigation of electroinactivity of tetrodotoxin and its complexation to ionophores

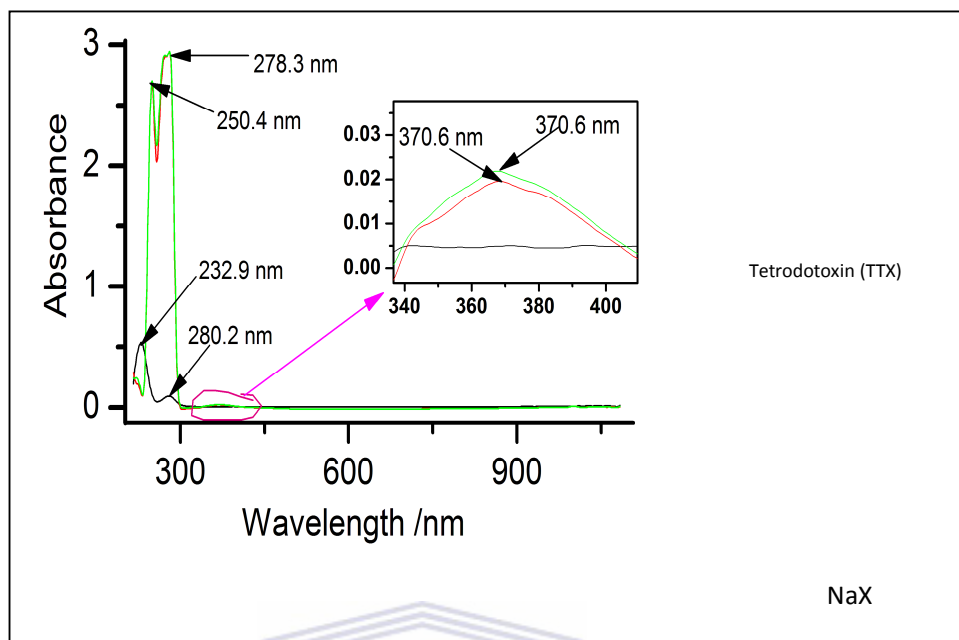


Figure 6.34: UV-Vis absorption spectrum of 3.33 μM TTX (back line), 1000 μM NaX (red line) and TTX/ NaX (green line) in water.

6.4.2.2 UV-Vis absorption of TTX, B18C6 and TTX/B18C6

Figure 6.35 presents the UV-Vis absorption spectrum of TTX, B18C6 and TTX/B18C6 in water. The spectra of B18C6 (red line) shows two absorptions peaks at 222.03 nm and 274.10 nm. According to the chemical structure of B18C6, two absorption bands were expected to correspond to the chromophores $-\text{C}=\text{C}-$ and $\text{C}-\text{O}-\text{C}$. The first absorption band at 222.03 nm corresponds to the chromophore $\text{C}-\text{O}-\text{C}$, $n \rightarrow \sigma^*$ electronic transition. The second absorption band appearing at 274.10 nm is for $-\text{C}=\text{C}-$ chromophore, $\pi \rightarrow \pi^*$ electronic transaction. The representation of these electronic transitions follow the rule as shown in Figure 6.30 and 6.29 for $\text{C}-\text{O}-\text{C}$ and $-\text{C}=\text{C}-$ respectively. Table 6.9 gives a preview of the band gap energy data. The green curve which is the mixture of TTX/B18C6

Chapter 6: Investigation of electroinactivity of tetrodotoxin and its complexation to ionophores

presents two absorption bands at 222.03 nm and 274.10 nm which correlate with B18C6. The increasing of absorbance observed with the solution mixture (TTX/B18C6) can be attributed to the increase of the concentration of respective chromophores (C–O–C and C=C from B18C6 and TTX, C=N from TTX) and the extra-molecular interaction between TTX and B18C6. No chemical reaction occurs however between TTX and B18C6.

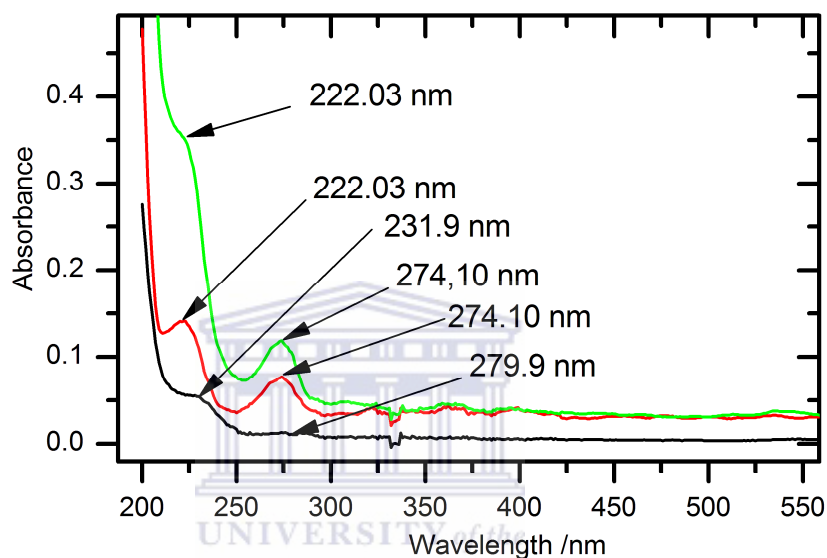


Figure 6.35: UV-Vis absorption spectrum of 9.33 μM TTX (back line), 3330 μM B18C6 (red line) and TTX/B18C6 (green line) in water.

The band gap energy was calculated using the Tauc *et al.* (1966) equation [241]. The Beer-Lambert equation (Equation 6.11) was used here to determine the UV-Vis data of TTX, B18C6, NaX, and TTX/B18C6 (tab. 6.9)

$$A = \epsilon Cl \quad \text{Equation 6.11}$$

$$(AE)^{1/2} = B(E - E_g) \quad \text{Equation 6.12}$$

$$E = h\nu \quad \text{Equation 6.13}$$

Chapter 6: Investigation of electroinactivity of tetrodotoxin and its complexation to ionophores

where A is absorbance, ε = extension coefficient, C = concentration of the analyte, l = length of the cuvette, $B = 3.6 \times 10^5 \text{ cm}^{-1/2} \text{ eV}^{1/2}$, E_g is band gap energy, h is the Planck's constant, ν is the wavelength.

Table 6.9: UV-Vis absorption data of TTX, NaX, B18C6 and TTX/B18C6

	Peak	Absorbance	λ_{max} (nm)	$\varepsilon/\text{L mol}^{-1}$ cm^{-1}	$\Delta E_{n \rightarrow \sigma^*}$ (eV)	$\Delta E_{n \rightarrow \pi^*}$ (eV)	$\Delta E_{\pi \rightarrow \pi^*}$ (eV)
TTX	1	0.51	232.9	3413.65	5.325		
	2	0.08	280.2	535.48		5.326	
NaX	1	2.68	250	595.56			4.953
	2	2.91	275.3	646.67		4.51	
	3	0.02	370.6	4.44		3.35	
B18C6	1	0.14	221.6	9.34	5.595		
	2	0.074	274.8	4.67			4.512

Table 6.10 gives distances between some atoms of active site of each compound (TTX, NaX, and B18C6) responsible for possible complex formations. Indeed, the diameter of that active site can be assumed from the distance between opposite atoms which form the diagonal of the active site. As shown in Table 6.10, the diameter of guanidinium group of TTX is given by the diagonals $d_{\text{H}23\text{-H}25} = 3.66 \text{ \AA}$ and $d_{\text{H}24\text{-H}26} = 3.663 \text{ \AA}$. The diameter of 18-crown-6 which is the active site of B18C6 is given by the distances $d_{\text{O}11\text{-O}25} = 6.12 \text{ \AA}$ and $d_{\text{O}7\text{-O}14} = 6.166 \text{ \AA}$.

Chapter 6: Investigation of electroinactivity of tetrodotoxin and its complexation to ionophores

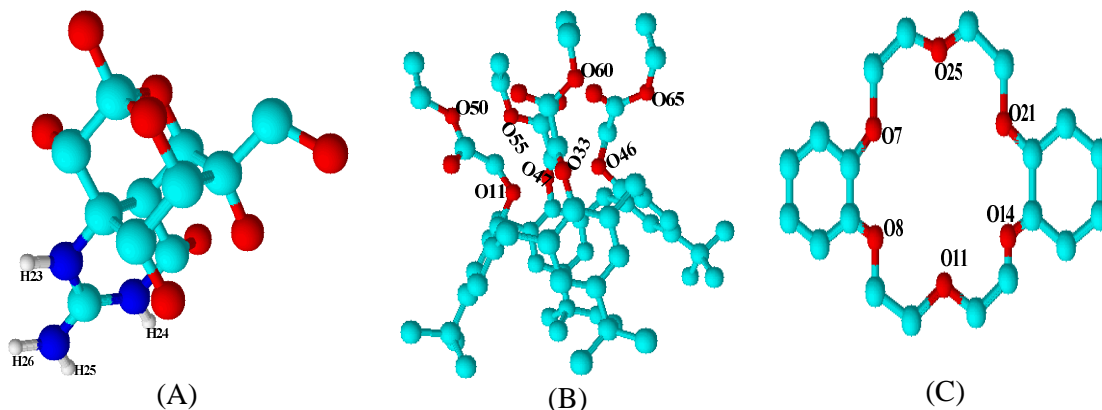


Figure 6.36: Chemical structure of (A) tetrodotoxin (TTX), (B) sodium ionophore X (NaX) and (C) Dibenzo-18-crown-6 (B18C6). Atoms: Hydrogen (white color), (carbon (cyan color), oxygen (red color), and nitrogen (blue color).

For NaX, the active site is formed by four carbonate groups but because of the donor and attractive effect, the reaction may be oriented to the oxygen atoms close to the aromatic group. The diameter of NaX is given by the distance between oxygen atoms directly bonded to the benzyl ring which is responsible for the complexation because of their electron doublet due to the strong donor group (benzyl ring) attached to them. The diagonals of the NaX active site are $d_{O55-O60} = 4.827\text{\AA}$ and $d_{O50-O65} = 8.117\text{\AA}$. Comparing these diameters, it is observed that guanidinium group of TTX cannot penetrate the NaX and B18C6 active site because of small diameter size ($d_{\text{Ligand}} < 2d_{\text{TTX}^+}$). The different values calculated from Chemdraw software and presented in Table 6.10 also explain the results obtained both in ion transfer voltammetry and UV-Vis absorption spectroscopy.

Chapter 6: Investigation of electroinactivity of tetrodotoxin and its complexation to ionophores

Table 6.10: Active site and distances between atoms responsible for complex formation

Compound	Active site	Distance between atoms (Å) implied on active site
Tetrodotoxin	Guanidinium group	$d_{H23-H26} = 2.449$ $d_{H24-H25} = 2.453$ $d_{H24-H26} = 3.663$ $d_{H23-H25} = 3.66$ $d_{H23-H24} = 4.23$ $d_{H25-H26} = 1.75$
Sodium ionophore X	Four Carbonate groups	$d_{O33-O47} = 5.368$ $d_{O11-O46} = 3.924$ $d_{O55-O60} = 4.827$ $d_{O50-O65} = 8.117$
Dibenzo-18-crown-6	18-crown-6	$d_{O11-O25} = 6.12$ $d_{O8-O21} = 6.001$ $d_{O7-O14} = 6.166$

UNIVERSITY of the
WESTERN CAPE

6.5 Conclusion

The electrochemical tetrodotoxin sensor developed on neutral selective ionophores based on ion-transfer voltammetry and UV-Vis absorption analysis was investigated. Selective ionophore immobilised on solid modified PANI-PSSA/electrode platform or applied in ion transfer electrode, indicated that NaX and B18C6 ionophores as specific agents cannot detect TTX when used to develop a sensor. Using the ion-selective electrode and UV-Vis absorption spectroscopy, it was found that the electrochemical TTX sensor cannot be developed based on neutral NaX and B18C6 selective ionophore. It is important to note that this was the first investigation of selective NaX and B18C6 ionophore complexation

Chapter 6: Investigation of electroinactivity of tetrodotoxin and its complexation to ionophores

of TTX using ion transfer voltammetry and Uv-vis absorption spectroscopy techniques. Another specific agent more selective, sensitive, stable and with low cost is therefore proposed. No enzyme for TTX has yet been discovered and antibody anti-tetrodotoxin is very expensive. The only option in this instance is to immobilise the aptamer-tetrodotoxin (discovered in 2013 by Xing *et al.*) [242] on modified-PANI-PSSA/electrode which is electrochemically polymerised in aqueous medium. The previous electrosynthesis of PANI-PSSA films was done in an organic medium because the ionophore was used was not soluble in aqueous medium as the case of electro-co-polymerisation of aniline doped PSSA with ionophore.



**APPLICATION OF ELECTROCHEMICALLY
SYNTHESISED NEUTRAL AND P-DOPED PANI-PSSA FOR
THE DETERMINATION OF TETRODOTOXIN**

7.0 Introduction

The purpose of this chapter is to construct a mediator (platform) based on doped polyaniline which would be used for detection of tetrodotoxin. Gospodinova *et al.* demonstrated that synthesis of conducting PANI is acid dependent, whereas the linear chain growth of PANI occurred solely in a strongly acidic medium [243]. In this case, besides doped synthesized PANI, sufficient PSSA is essential to increase the inherent electroactivity [103] and conductivity [244] of PANI prior to be used in buffer electrolyte and afford a strongly acidic medium for linear chain growth of PANI. PSSA has been found to be an effective doping that could be used to prepare the PANI–PSSA films on solid electrode using cyclic voltammetry [103, 245]. When aniline is polymerised with PSSA, after apply a certain potential to the system and cycling for some time, the blue or green PANI–PSSA can be obtained depending on the final (stopping) potential or the scanning direction reaction. Indeed, if the scan stops at anodic potential (cathodically scanned), the polymer films formed is the blue-bernalanine which is called in this study p-doped PANI-PSSA. When the scan is stop at cathodic potential (anodically scanned) the polymer formed is green-emeraldine called in this study neutral PANI–PSSA. This chapter presents the electrochemical polymerisation of PSSA doped aniline in phosphoric acid on

Chapter 7: Application of electrochemically synthesised neutral and P-doped PANI–PSSA for the determination of tetrodotoxin

various bare electrodes. The modified-PANI–PSSA electrode is applied on electrochemical tetrodotoxin biosensor and the PANI is used as a surface probe to generate the electron into the system.

7.1 Electrosynthesis of neutral and p-doped PANI–PSSA films

The CV curves recorded during the electrosynthesis of neutral and p-doped PANI–PSSA films on four various electrodes in 1 M H₃PO₄ are shown in Figure 6.28. CVs of the polymerisation of neutral PANI–PSSA films exhibit three redox peak pairs between 0.02 and 0.20 V (AA'), 0.4 and 0.53 V (BB'), 0.57 and 0.7 V (CC'). Comparing to the CVs obtained during the cyclic voltammetry of PANI, it is found that the doping has reduced the potential peak of PANI films formed on the electrode surface with the standard deviation ≤ 0.3 . The discussions given to Figure 6.6 are attributed to Figure 7.1. These peaks are due to doping and undoping of protons and anions ion the PANI film. The redox peak between 0.1 and 0.3 V is attributed to leucoemeraldine/emeraldine transformation of PANI–PSSA while the redox peak between 0.4 and 0.5V is due to emeraldine/ pernigraniline transformation [124].

Chapter 7: Application of electrochemically synthesised neutral and P-doped PANI-PSSA for the determination of tetrodotoxin

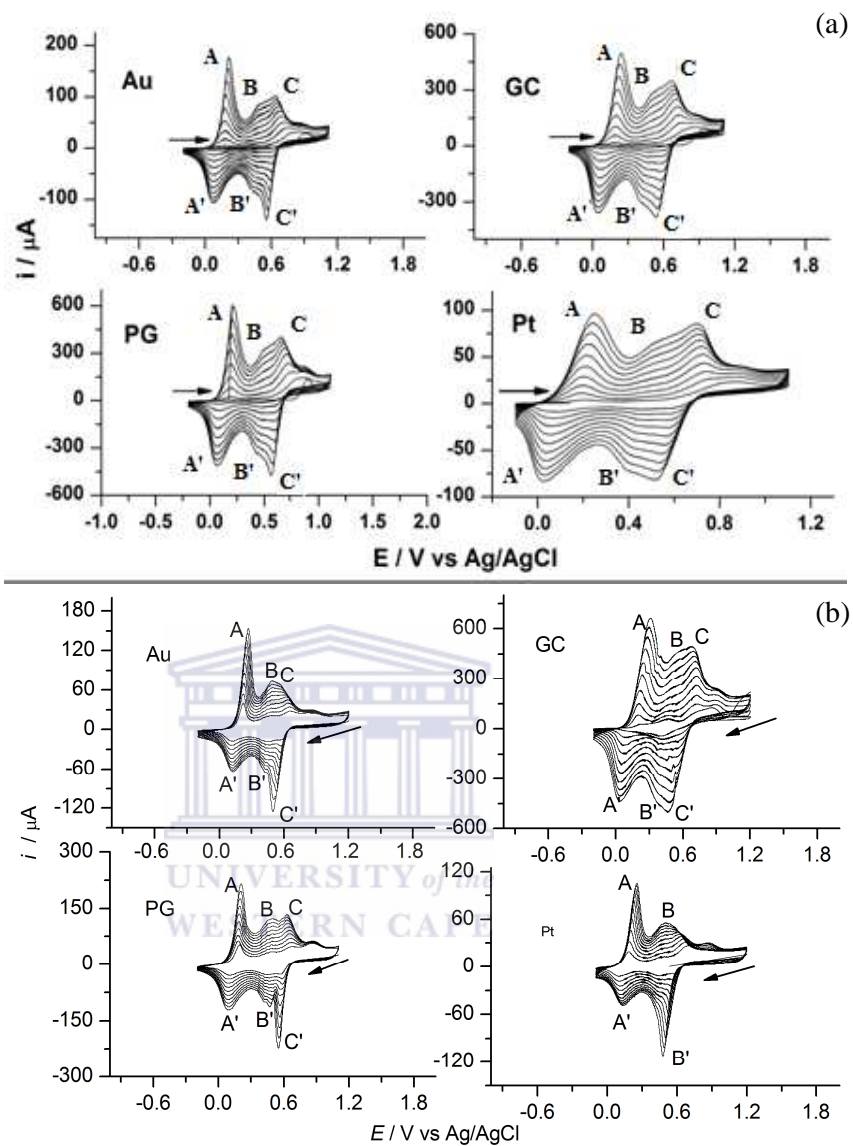


Figure 7.1: Cyclic voltammograms (15 cycles) recorded during potentiodynamic growth of PANI-PSSA films on Au, GC, PG, and Pt in 1 M H_3PO_4 containing 0.05 M aniline / 0.025 M PSSA at 0.050 V s^{-1} scan rates.

Chapter 7: Application of electrochemically synthesised neutral and P-doped PANI–PSSA for the determination of tetrodotoxin

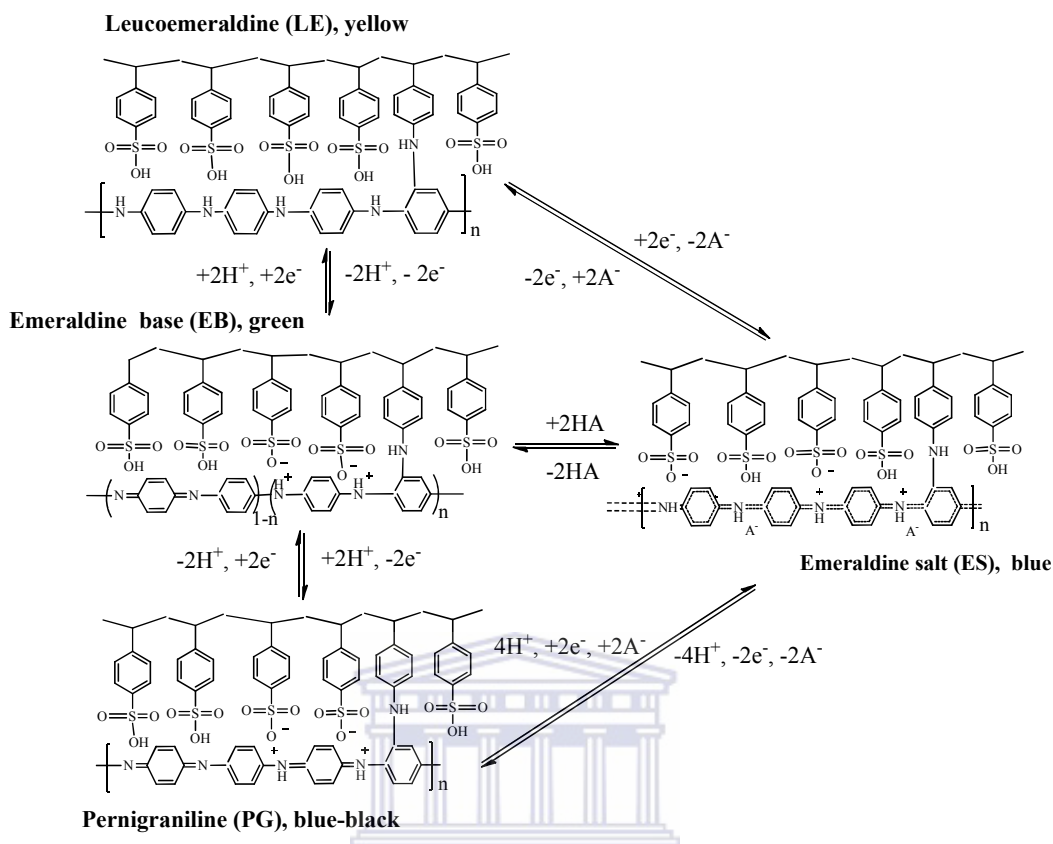


Figure 7.2: Electrochemical transitions between PANI–PSSA's base forms are shown vertically as a series of successive reduction reactions from LB to EB, and to PB. Transitions to the ES form of PANI are shown via diagonal and horizontal reactions.

7.2 Electrochemical active zone of neutral and p-doped PANI–PSSA in H_3PO_4

Cyclic voltammetry behaviour of the neutral and p-doped PANI–PSSA deposited on the bare Au, GC, PG, and Pt electrodes is characterized by two pairs of redox peak in 1 M H_3PO_4 electrolyte solution (Fig. 7.3). The CVs recorded over three repetitive cycles show excellent stability of the PANI–PSSA due to the PSSA doping.

Chapter 7: Application of electrochemically synthesised neutral and P-doped PANI–PSSA for the determination of tetrodotoxin

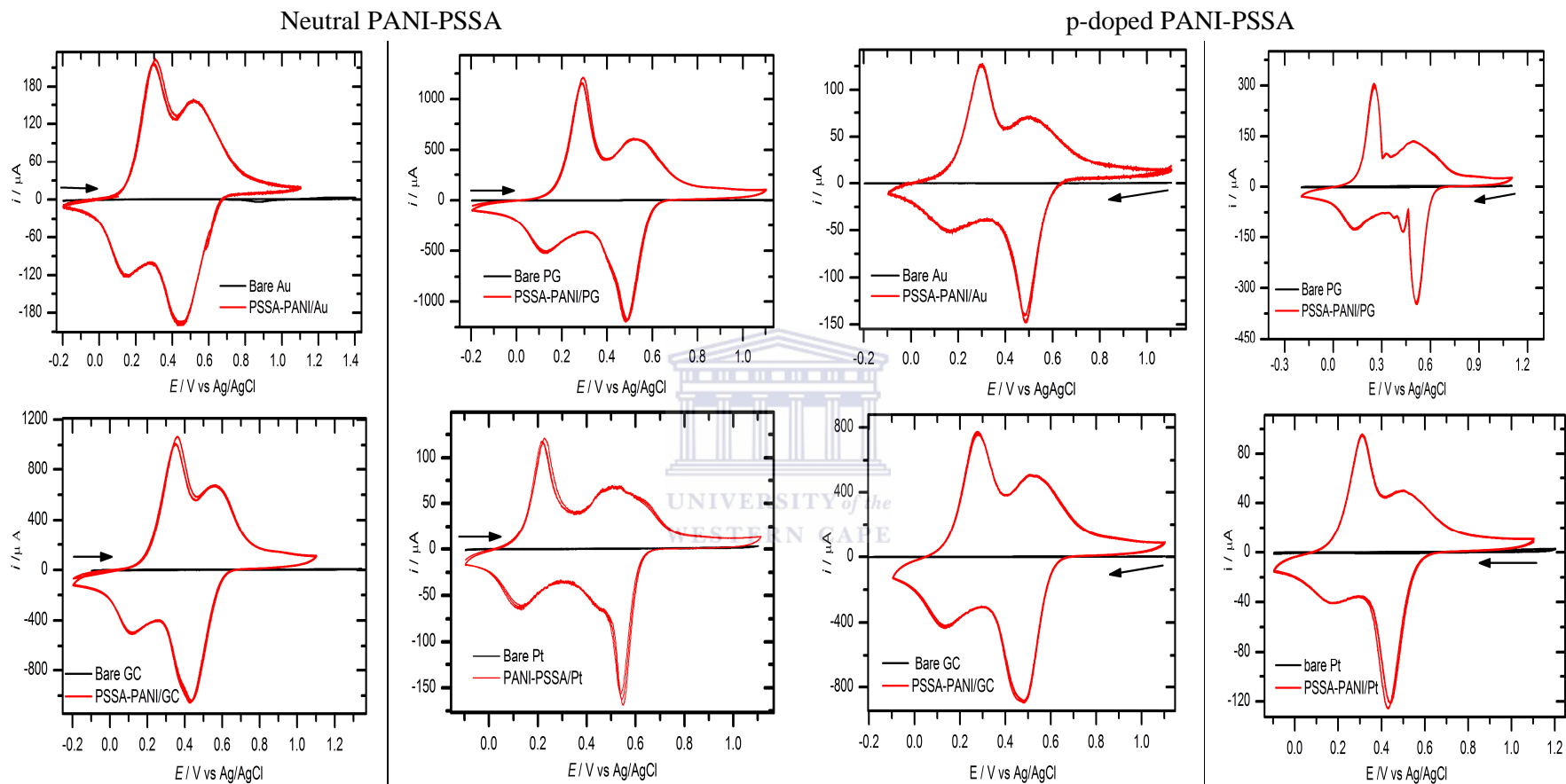


Figure 7.3: Overview of 3 cycles CVs of neutral and p-doped PSSA–PANI in 1 M H_3PO_4 on Au, GC, PG and Pt electrodes. Scan rates $0.050 V s^{-1}$.

Chapter 7: Application of electrochemically synthesised neutral and P-doped PANI–PSSA for the determination of tetrodotoxin

Using Figure 7.3, the value of characteristic peaks of PANI–PSSA films synthesised in two different directions are given in Table 7.1. Since the polymer obtained using two different of polymerisation methods exhibited different colours (blue and green), the difference in experimental values was expected. The neutral PANI–PSSA films with green colour depict the reduced base form of PANI while the p-doped PANI–PSSA films obtained with blue colour depict the full oxidation state of PANI. The peak separation potential, ΔE_p , for the redox reactions, which is the potential difference between anodic and cathodic peak potentials, decreases in p-doped PANI–PSSA as compared to ΔE_p of the neutral PANI–PSSA. The small ΔE_p on p-doped suggests that the rates of the leucoemeraldine/emeraldine and emeraldine/ pernigraniline electron transfer increases significantly. This gives an indication that the leucoemeraldine/emeraldine and emeraldine/ pernigraniline redox reaction are electrochemically favoured, resulting in faster redox kinetics. The small ΔE_p of p-doped in comparison with ΔE_p of neutral PANI–PSSA indicates that the redox overpotential of p-doped PANI–PSSA is significantly lowered at the bare electrodes, and the electrochemical redox activity of p-doped PSSA–PANI is highly improved [246]. The proportion between the first oxidation peak current and the reduction peak current (i_{pa1}/i_{pc1}) is about - 1.5 for neutral and - 2.5 for p-doped, indicating an irreversible electrochemical process. Furthermore, i_{pa2}/i_{pc2} is closed to - 1 indicates a reversible process.

Chapter 7: Application of electrochemically synthesised neutral and P-doped PANI–PSSA for the determination of tetrodotoxin

Table 7.1: Values of peak characteristics of electrodeposited PANI–PSSA films in 1 M H₃PO₄ at three sweep cycles

WE	Neutral PSSA-PANI				P-doped PSSA-PANI			
	Au	GC	PG	Pt	Au	GC	PG	Pt
E_{pa1} [V]	0.295	0.347	0.287	0.312	0.298	0.279	0.249	0.311
E_{pa2} [V]	0.515	0.563	0.528	0.570	0.499	0.520	0.499	0.498
E_{pc1} [V]	0.147	0.113	0.121	0.115	0.163	0.139	0.127	0.174
E_{pc2} [V]	0.447	0.435	0.486	0.457	0.486	0.481	0.512	0.439
ΔE_{p1} [V]	0.148	0.234	0.166	0.197	0.135	0.14	0.122	0.137
ΔE_{p2} [V]	0.068	0.128	0.042	0.113	0.013	0.039	-0.013	0.059
E^0_1 [V]	0.221	0.240	0.204	0.218	0.231	0.209	0.188	0.243
E^0_2 [V]	0.481	0.499	0.507	0.514	0.493	0.501	0.506	0.469
i_{pa1} [μ A]	219.5	1060.6	1204.6	105.8	127.3	770.28	307.07	95.13
i_{pa2} [μ A]	158.6	671.1	603.7	80.8	71.01	499.5	134.8	49.24
i_{pc1} [μ A]	-120.4	-497.1	-510.2	-70.86	-50.92	-425.6	-124.7	-41.21
i_{pc2} [μ A]	-197.1	-1052.0	-1184.4	-127.8	-145.12	-884.4	-344.6	-121.4
i_{pa1}/i_{pc1}	-1.82	-2.13	-2.36	-1.49	-2.5	-1.81	-2.46	-2.31
i_{pa2}/i_{pc2}	-0.80	-0.64	-0.51	-0.63	-0.46	-0.56	-0.39	-0.41

The PSSA–PANI films obtained after 15 cycles was studied in phosphate buffer using the cyclic voltammetry. The cyclic voltammograms obtained (results not shown) shown that polymer films were not stable on the electrode surface. After the first cycle in PB, the peak current significantly decreases with increasing sweep number.

Chapter 7: Application of electrochemically synthesised neutral and P-doped PANI–PSSA for the determination of tetrodotoxin

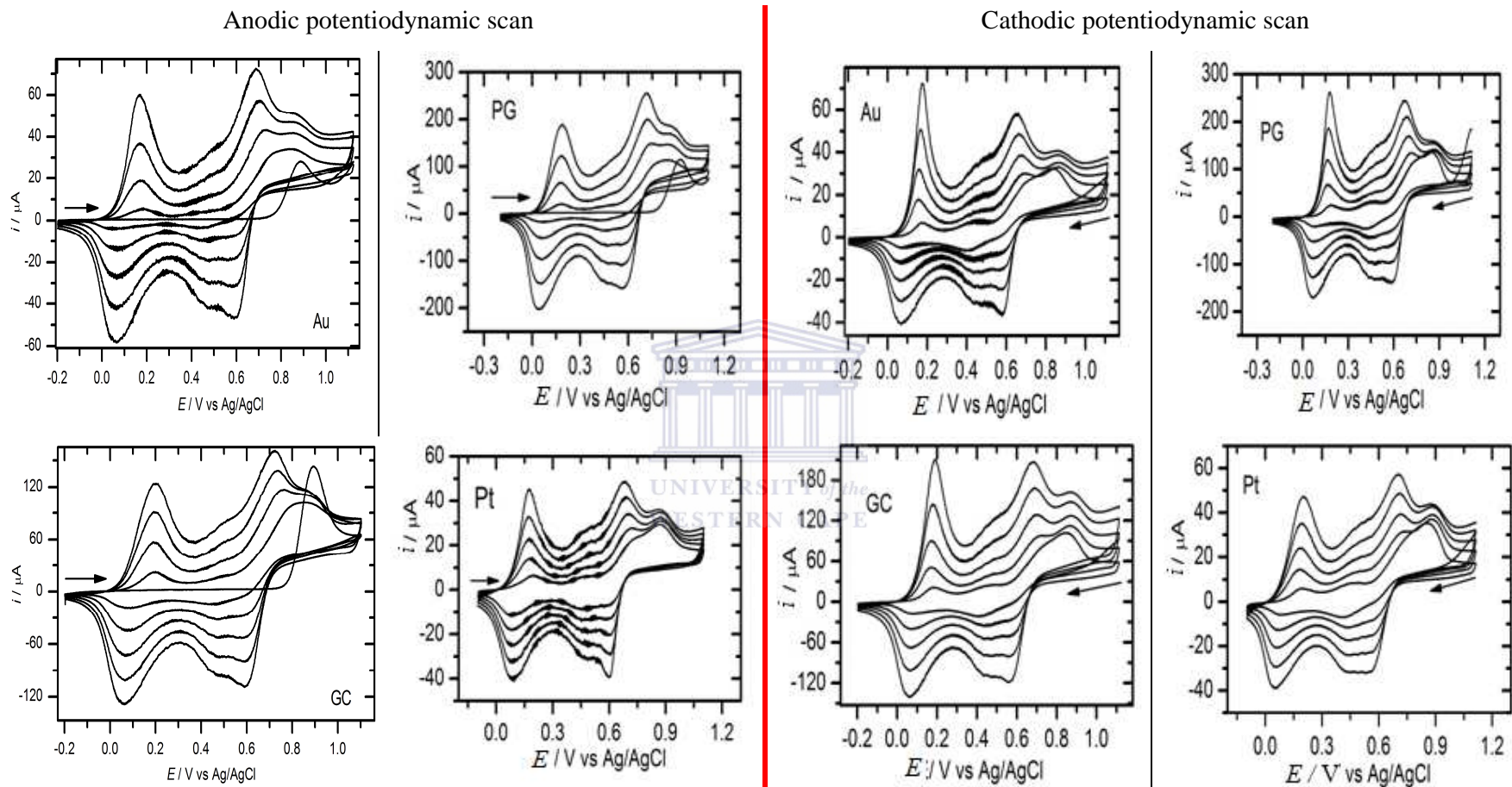
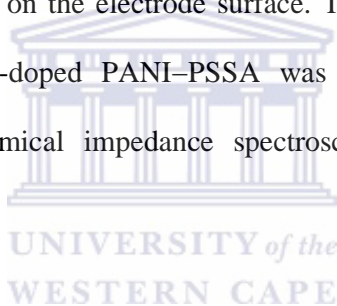


Figure 7.4: CVs of 5 cycles recorded during potentiodynamic growth of PANI–PSSA films on Au, GC, PG, and Pt in 1 M H_3PO_4 containing 0.05 M aniline / 0.025 M PSSA at 50 mV s^{-1} scan rates.

Chapter 7: Application of electrochemically synthesised neutral and P-doped PANI–PSSA for the determination of tetrodotoxin

The polymer films disintegrate into the electrolyte solution when the modified-PSSA–PANI electrode is kept in solution for between 30 mins to an hour. Because of this fact, the number of cycle was reduced to 10 cycles, the same challenge was facing and then the number of cycle was reduced to 5 cycles to pursue the aim of this study. Figure 7.4 presents the cyclic voltammograms recorded during the anodic and cathodic potentiodynamic scan of PSSA doped aniline monomer in H_3PO_4 at 50 mV s^{-1} over 5 cycles. The anodic peak (at 0.18V) revealing a characteristic peak of polymerisation; showed that the current produced with p-doped is higher than that produced with neutral PANI-PSSA. This increase of current indicates that the rate of deposition of the p-doped is quicker than neutral polymer on the electrode surface. The electrochemical behaviour of the resulting neutral and p-doped PANI–PSSA was thereafter examined by cyclic voltammetry and electrochemical impedance spectroscopy in SPB and OAc buffer solutions.

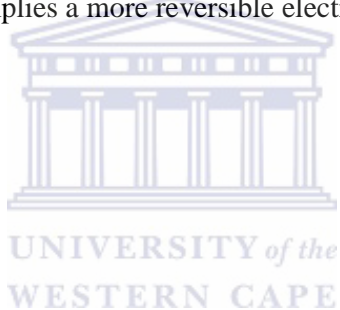


7.3 Electrochemical activity of neutral and p-doped PANI–PSSA SPB

The electroactivity and the stability of the two forms of polymer films synthesised above is studied in phosphate buffer solutions for further application in an electrochemical biosensor for the determination of TTX based on an aptamer. The polymer films formed after five repetitive sweeps on bare electrodes were directly characterised in 0.1 M PB pH 7.04 at various scan rates over the potential window from - 0.6 to 0.6 V. From 5 to 100 mV s^{-1} , the oxidation and reduction peak currents of PSSA–PANI films increase in 0.1 M PBS. The oxidation peak potential positively shifts while the reduction peak potential negatively

Chapter 7: Application of electrochemically synthesised neutral and P-doped PANI–PSSA for the determination of tetrodotoxin

shifts with an increase in scan rate. The oxidation peak currents exhibit a linear relationship with the scan rates (Fig.7.5), suggesting that the electrode processes are limited by adsorption [247]. Three repetitive cycles are recorded on modified neutral and p-doped PANI–PSSA/electrode. It is shown that in SPB, the p-doped is more stable than neutral PANI–PSSA on gold, glassy carbon, platinum, pyrolytic graphite electrodes. Table 7.2 shows high value of redox peak separation potentials $\Delta E_p > 200/n$ mV ($n = 2$) calculated in for both polymer films indicating that the electrode reaction taking place is an irreversible process. ΔE_p of neutral PANI–PSSA is higher than the one calculated on p-doped PANI–PSSA in a phosphate buffer. The ratio of redox peak current (i_{pa}/i_{pc}) was calculated to be ≈ 1 , which implies a more reversible electrode reaction.



Chapter 7: Application of electrochemically synthesised neutral and P-doped PANI-PSSA for the determination of tetrodotoxin

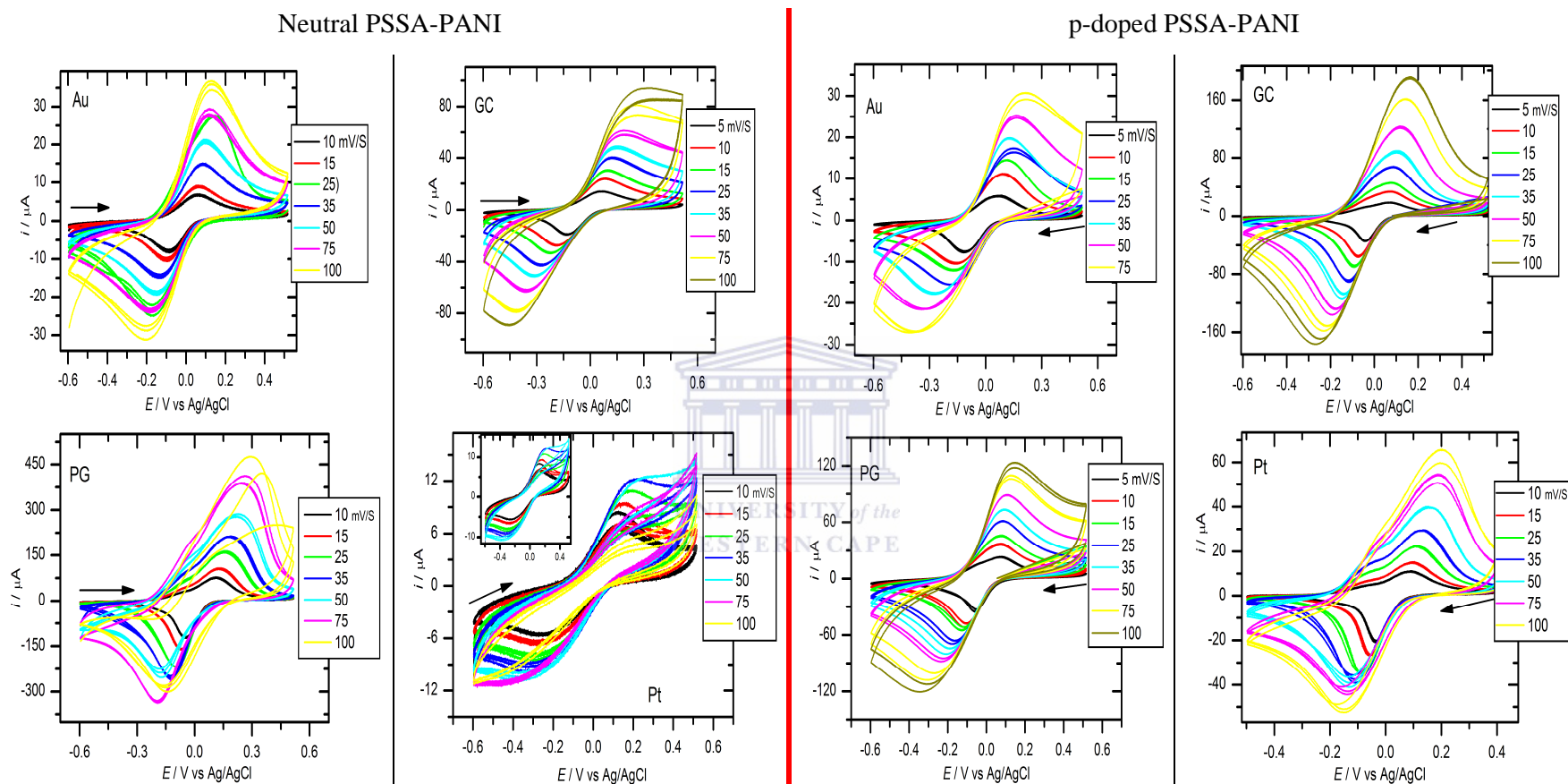


Figure 7.5: Cyclic voltammograms of the PANI-PSSA electrodeposited on Au, GC, PG, and Pt electrodes in 0.1 M PB pH 7.04 at different potential scan rates.

Chapter 7: Application of electrochemically synthesised neutral and P-doped PANI-PSSA for the determination of tetrodotoxin

The chemical reaction involved during the anodic and cathodic sweep of both neutral and p-doped PANI-PSSA in phosphate buffer is described in Figures 7.6 and 7.7.

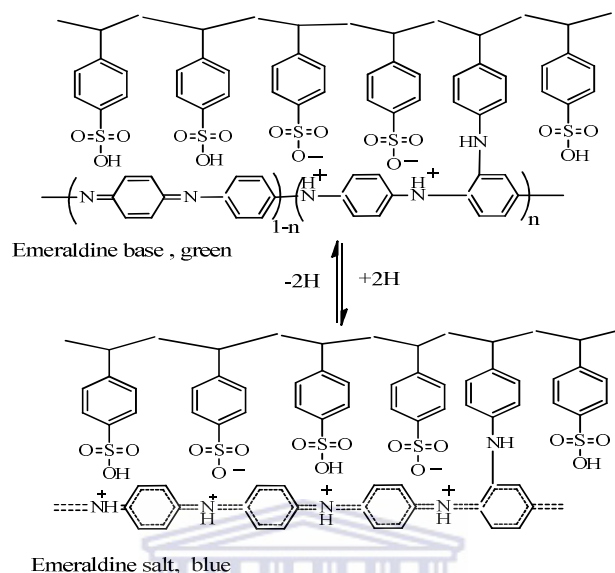


Figure 7.6: Electrode surface reactions during the cyclic voltammetry of neutral PANI-PSSA.

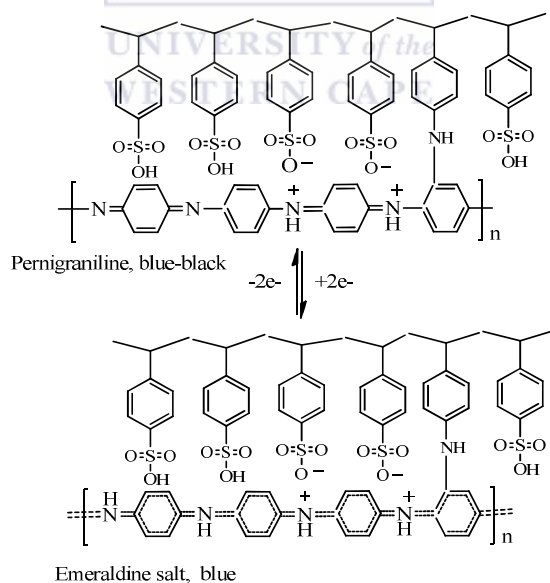


Figure 7.7: Electrode surface reactions during the cyclic voltammetry of p-doped PANI-PSSA.

Chapter 7: Application of electrochemically synthesised neutral and P-doped PANI–PSSA for the determination of tetrodotoxin

Table 7.2: Values of peak characteristics of electrodeposited neutral PANI–PSSA films on various electrodes in 0.1 M PB pH 7.04 over three sweep cycles at different scan rates

WE	ν [mV s ⁻¹]	E_{pa} [V]	E_{pc} [V]	ΔE_p [V]	E^{*0} [V]	i_{pa} [μ A]	i_{pc} [μ A]	i_{pa}/i_{pc}
Au	10	0.062	-0.090	0.152	-0.014	6.88	-7.70	-0.89
	15	0.067	-0.098	0.165	-0.016	8.93	-9.98	-0.89
	25	0.091	-0.169	0.260	-0.079	14.65	-14.36	-1.02
	35	0.096	-0.138	0.234	-0.021	20.01	-18.46	-1.08
	50	0.099	-0.152	0.251	-0.027	20.74	-23.51	-0.88
	75	0.121	-0.178	0.299	-0.029	27.75	-24.67	-1.12
	100	0.130	-0.199	0.329	-0.035	36.44	-28.61	-1.27
GC	5	0.069	-0.129	0.198	-0.030	14.09	-18.57	-0.76
	10	0.080	-0.184	0.264	-0.052	24.09	-27.04	-0.89
	15	0.104	-0.226	0.330	-0.061	30.20	-33.15	-0.91
	25	0.128	-0.274	0.402	-0.073	40.67	-42.13	-0.96
	35	0.138	-0.319	0.457	-0.091	48.96	-51.11	-0.96
	50	0.176	-0.354	0.530	-0.089	57.18	-62.38	-0.92
	75	0.234	-0.419	0.653	-0.093	71.99	-77.48	-0.93
PG	10	0.118	-0.047	0.165	0.036	78.44	-119.41	-0.66
	15	0.135	-0.067	0.202	0.034	106.55	-155.95	-0.68
	25	0.176	-0.092	0.168	0.042	162.76	-216.32	-0.75
	35	0.189	-0.125	0.314	0.032	210.20	-254.14	-0.83
	50	0.218	-0.170	0.378	0.024	285.72	-242.34	-1.17
	75	0.250	-0.196	0.446	0.027	385.49	-328.72	-1.17
	100	0.281	-0.142	0.423	0.0695	478.71	-290.33	-1.45
pt	10	0.126	-0.241	0.367	-0.058	6.84	-5.52	-1.24
	15	0.141	-0.283	0.424	-0.071	7.13	-6.54	-1.09
	25	0.220	-0.295	0.515	-0.038	7.91	-7.89	-1.00
	35	0.170	-0.314	0.484	-0.072	7.64	-9.33	-0.82
	50	0.218	-0.333	0.551	-0.057	8.30	-10.67	-0.78
	75	0.175	-0.432	0.607	-0.129	7.49	-11.09	-0.68
	100	0.166	-0.421	0.587	-0.128	4.51	-9.33	-0.48

Chapter 7: Application of electrochemically synthesised neutral and P-doped PANI–PSSA for the determination of tetrodotoxin

Table 7.3: Values of peak characteristics of electrodeposited p-doped PANI–PSSA films on various electrodes in 0.1 M PB pH 7.04 over three sweep cycles at different scan rates

WE	ν [mV s ⁻¹]	E_{pa} [V]	E_{pc} [V]	ΔE_p [V]	E^{0} [V]	i_{pa} [μ A]	i_{pc} [μ A]	i_{pa}/i_{pc}
Au	5	0.071	-0.113	0.184	-0.021	5.89	-7.49	-0.79
	10	0.093	-0.160	0.253	-0.034	10.91	-10.33	-1.06
	15	0.116	-0.163	0.279	-0.024	14.59	-11.99	-1.22
	25	0.122	-0.207	0.329	-0.043	16.44	-15.30	-1.07
	35	0.132	-0.286	0.418	-0.077	19.74	-17.63	-1.12
	50	0.164	-0.321	0.485	-0.079	25.37	-21.25	-1.19
	75	0.209	-0.376	0.585	-0.084	30.99	-27.06	-1.15
GC	5	0.069	-0.042	0.111	-0.014	18.58	-33.28	-0.56
	10	0.073	-0.073	0.146	0.000	33.51	-55.28	-0.61
	15	0.077	-0.092	0.169	-0.008	44.78	-68.48	-0.65
	25	0.089	-0.117	0.206	-0.014	67.31	-88.69	-0.76
	35	0.099	-0.139	0.238	-0.02	88.83	-106.42	-0.83
	50	0.123	-0.177	0.3	-0.027	121.61	-127.46	-0.95
	75	0.149	-0.214	0.363	-0.033	161.12	-152.21	-1.06
100	0.163	-0.246	0.409	-0.042	190.10	-168.02	-1.13	
PG	5	0.071	-0.054	0.125	0.009	22.50	-34.99	-0.64
	10	0.076	-0.108	0.184	-0.032	35.74	-47.18	-0.76
	15	0.080	-0.127	0.207	-0.024	45.91	-54.95	-0.84
	25	0.084	-0.168	0.252	-0.042	60.99	-65.49	-0.93
	35	0.093	-0.197	0.29	-0.052	73.26	-74.31	-0.99
	50	0.105	-0.221	0.326	-0.058	88.35	-84.33	-1.05
	75	0.130	-0.271	0.401	-0.071	108.16	-100.91	-1.07
100	0.142	-0.303	0.445	-0.081	122.69	-112.49	-1.09	
Pt	10	0.088	-0.034	0.122	0.027	11.12	-20.42	-0.54
	15	0.100	-0.053	0.153	0.024	14.83	-26.46	-0.56
	25	0.113	-0.086	0.199	0.014	22.27	-34.39	-0.65
	35	0.136	-0.104	0.24	0.016	29.36	-37.27	-0.79
	50	0.155	-0.134	0.289	0.011	39.88	-39.12	-1.02
	75	0.183	-0.137	0.32	0.046	54.41	-43.60	-1.25
	100	0.202	-0.141	0.343	0.031	65.85	-52.25	-1.26

Additionally, the peak potential (E_p) increases with increased scan rates (ν), and a linear relationship can be obtained between E_p and $\log(\nu)$, as shown in Figure 7.8. This indicates

Chapter 7: Application of electrochemically synthesised neutral and P-doped PANI–PSSA for the determination of tetrodotoxin

that the oxidation of both neutral and p-doped PANI–PSSA is an irreversible electrode process. For an irreversible charge-transfer electrode process, the plot of E_p and $\log v$ is a straight line with a slope = $-RT/\alpha nF$ for E_{pc} and slope = $RT/(1-\alpha)nF$ for E_{pa} (where α stands for the electron transfer coefficient).

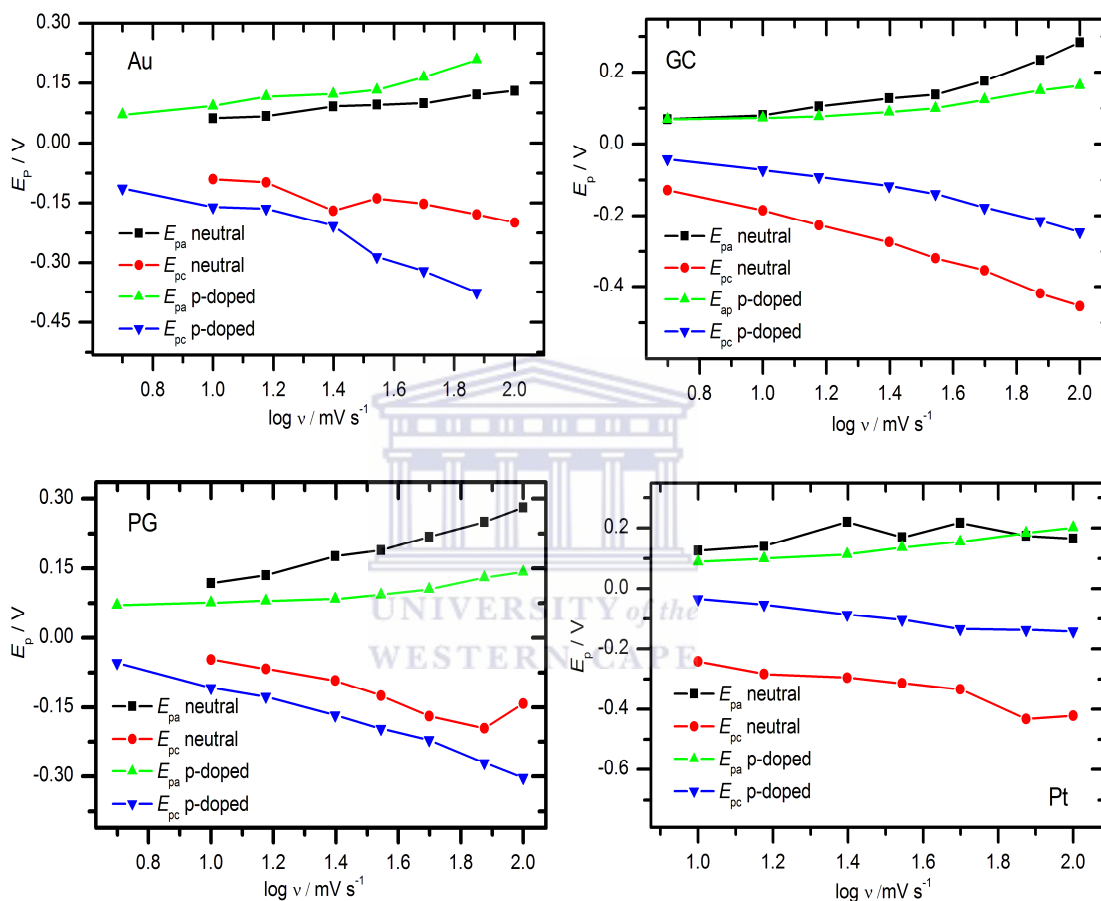


Figure 7.8: A plot of E_p vs. $\log v$ for the voltammograms of neutral and p-doped PANI–PSSA films deposited on bare of different electrodes in 0.1 M sodium phosphate buffer pH 7.04.

The kinetic investigation of electrochemical reaction electrode processes was studied by determining the transfer coefficient α , electrode reaction constant k_s of neutral and p-doped PANI–PSSA, and the diffusion coefficient D_0 . The transfer coefficient α is calculated

Chapter 7: Application of electrochemically synthesised neutral and P-doped PANI–PSSA for the determination of tetrodotoxin

according to the slope of anodic and cathodic process (Fig. 7.8). The transfer coefficient α is applied only to an electrode reaction that consists of a single elementary step involving the simultaneous uptake of n electrons from the electrode in the case of α_c , or the release of the electrode in the case of α_a .

Table 7.4: Anodic and cathodic transfer coefficient of neutral and p-doped PANI–PSSA films on various electrodes obtained from the plot $E_{pa,c}$ versus logarithm of scan rate

			Au	GC	PG	Pt
Neutral PANI–PSS A	E_{pa} vs. $\log v$	Range	0.99 – 1.87	0.99 – 1.99	0.994 – 1.87	0.99 – 1.70
		R^2	0.977	0.958	0.995	0.812
		a	-0.01 ± 0.01	-0.13 ± 0.04	-0.04 ± 0.01	-0.00 ± 0.07
		b	0.01 ± 0.01	0.19 ± 0.03	0.15 ± 0.01	0.13 ± 0.05
		α_a	0.4	0.93	0.91	0.89
	E_{pc} vs. $\log v$	R^2	-0.864	-0.996	-0.985	-0.976
		a	0.003 ± 0.04	0.09 ± 0.02	0.14 ± 0.02	-0.12 ± 0.01
		b	-0.09 ± 0.03	-0.27 ± 0.01	-0.18 ± 0.02	-0.13 ± 0.02
		α_c	0.16	0.05	0.08	0.11
		p-doped PANI–PSS A	E_{pa} vs. $\log v$	R^2	0.939	0.969
a	-0.03 ± 0.03			-0.03 ± 0.02	-0.01 ± 0.02	-0.01 ± 0.02
b	0.12 ± 0.02			0.09 ± 0.01	0.06 ± 0.01	0.09 ± 0.01
α_a	0.9			0.84	0.77	0.84
E_{pc} vs. $\log v$	R^2		-0.972	-0.985	-0.992	-0.995
	a		0.13 ± 0.05	0.11 ± 0.02	0.09 ± 0.02	0.11 ± 0.01
	b		-0.27 ± 0.03	-0.17 ± 0.01	-0.18 ± 0.1	-0.14 ± 0.01
	α_c	0.05	0.08	0.08	0.1	

The transfer coefficient α_a and α_c are immediately obtained from the slope of the plot of E_p against $\log v$ (Eq. 7.1 and 7.2). For each electrode, the same linear range is used for both neutral and p-doped PANI–PSSA.

Chapter 7: Application of electrochemically synthesised neutral and P-doped PANI–PSSA for the determination of tetrodotoxin

$$E_{pc} = E^{o'} - \frac{RT}{2nF} \left(0.780 + \frac{2.3}{2} \log \left(\frac{2nFD_o}{RT(k^o)^2} \right) \right) - \frac{2.3RT}{2anF} \log v \quad \text{Equation 7.1}$$

$$b = -\frac{2.3RT}{2anF} \rightarrow \alpha_c = -\frac{2.3RT}{2nFb} \quad \text{Equation 7.2}$$

From Table 7.3, the values of α_a and α_c are compared and according to Equation 7.2, it is shown that when α is high, the peak potential separation ΔE_p is low while the reaction electrode process is becomes faster. In the both cases neutral and p-doped PANI–PSSA, α_a is higher than α_c . The Equations 7.1 and 6.2 for electrochemical polymerisation kinetics is then established and used to evaluate α .

The electrochemical rate constant k_s is calculated from the intercept of the plot ΔE_p verses $\log v$ using the Equation 7.1. The peak potential separation (ΔE_p) increases with an increase in scan rate and the linear relation is established. The reaction was carried out at room temperature for all the four electrodes and the electrochemical rate constant, k_s , was found to be dependent polymer type formed on the electrode surface. For GC, PG and Pt electrodes, the value of k_s is higher for p-doped PANI–PSSA than when the neutral PANI–PSSA films are formed while for Au electrode, k_s is high during the synthesis of neutral PANI–PSSA as compared to k_s obtained when the p-doped PANI–PSSA films are formed. This indicates that the reaction is fast on PG, GC, and Pt electrodes during the synthesis of p-doped PANI–PSSA and on Au electrode, the reaction proceeds fast during the deposition of neutral PANI–PSSA.

Chapter 7: Application of electrochemically synthesised neutral and P-doped PANI–PSSA for the determination of tetrodotoxin

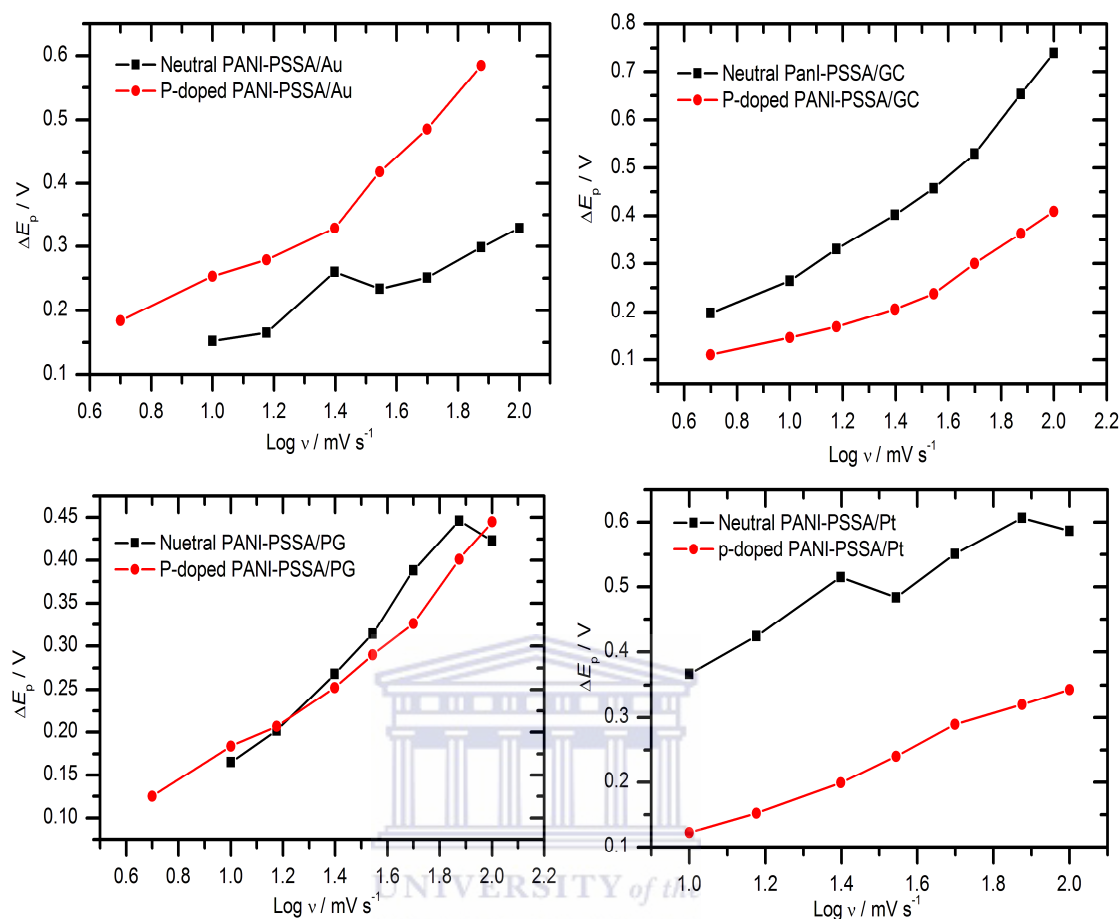


Figure 7.9: A plot of ΔE_p vs. $\log v$ for the voltammograms of neutral and p-doped PANI–PSSA films deposited on bare of different electrodes in 0.1 M sodium phosphate buffer pH 7.04.

The relation between the peak current (i_p) obtained from the CV scan and $\text{sqrt}(v)$ of CV is shown in Figure 7.10 and a linear relationship is also observed. From this observation, it can be said that the oxidation of aniline may be controlled by a diffusion process. Using the slope of the curve i_{pa} vs. $\text{sqrt}(v)$, the diffusion coefficient D_0 of neutral and p-doped PANI–PSSA could be calculated using the following Randle Sevcik equation:

$$D_0^{1/2} = \frac{\text{slope} \times (RT)^{1/2}}{0.4463(nF)^{3/2} AC_0} \quad \text{Equation 7.3}$$

Chapter 7: Application of electrochemically synthesised neutral and P-doped PANI-PSSA for the determination of tetrodotoxin

where slope is determined from the curve (i_{pa} vs. $\text{sqrt } v$), A is the area of electrode surface, C_0 is the concentration of PANI-PSSA formed on the electrode surface and this value is calculated using the limiting reagent (PSSA) from the chemical reaction:

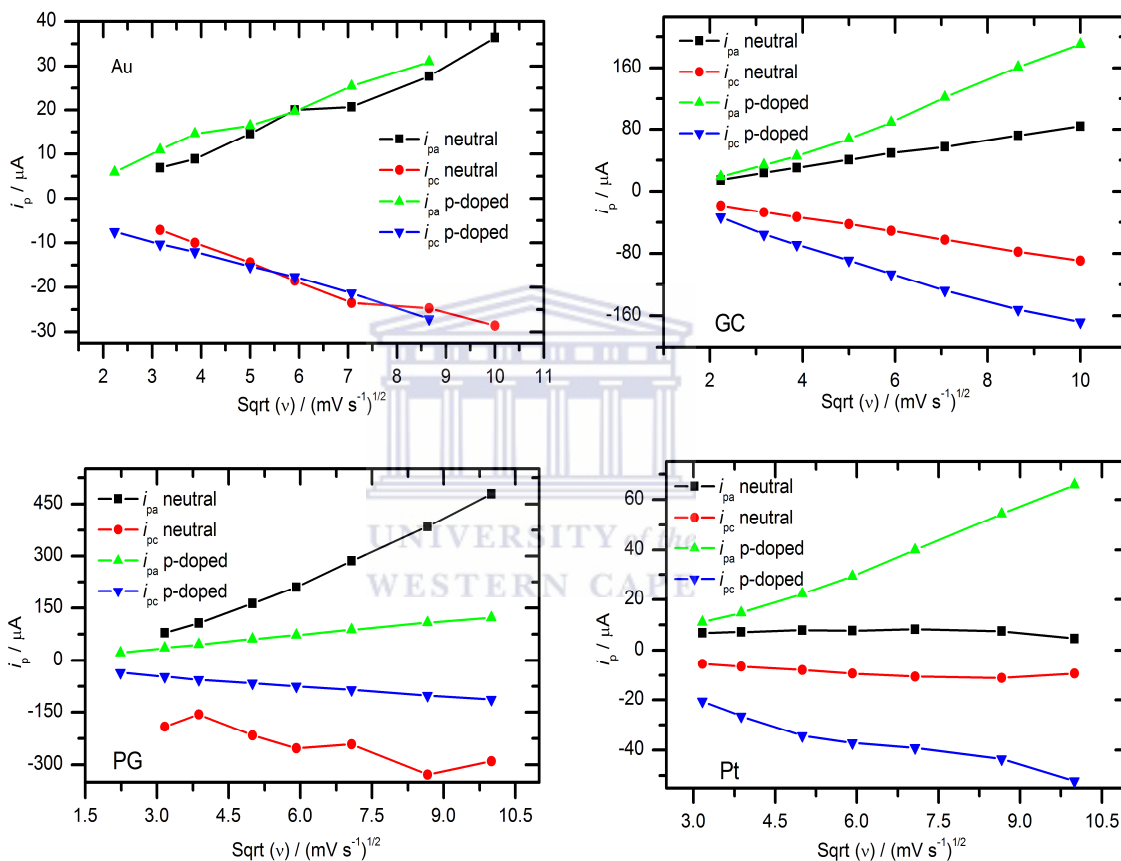
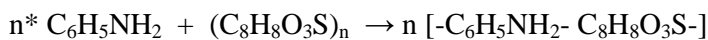


Figure 7.10: A typical Randles-Sevcik plot showing the peak current and square root of voltammograms scan rates for the neutral and p-doped PANI-PSSA films deposited on of different bare electrodes in 0.1 M PB pH 7.04.

Chapter 7: Application of electrochemically synthesised neutral and P-doped PANI–PSSA for the determination of tetrodotoxin

Table 7.5: Electrode reaction rate constant of neutral and p-doped PANI–PSSA films on various electrodes obtained from the plot ΔE_p versus logarithm of scan rate

		Au	GC	PG	Pt
Neutral	Range [mV s ⁻¹]	1.543–2.000	0.697–1.397	1.175–1.698	1.000–2.000
PANI–PSSA	R^2	0.987	0.993	0.993	0.958
	a	-0.11 ± 0.04	0.11 ± 0.02	-0.21 ± 0.04	0.15 ± 0.05
	b	0.22 ± 0.03	0.37 ± 0.01	0.35 ± 0.03	0.23 ± 0.03
	k_s [s ⁻¹]	18.28 ± 0.03	3.25 ± 0.01	4.31 ± 0.03	5.38 ± 0.03
P-doped	Range [mV s ⁻¹]	1.543–2.000	0.697–1.397	1.175–1.698	1.000–2.000
PANI–PSSA	R^2	0.998	0.996	0.999	0.997
	a	-0.40 ± 0.04	0.01 ± 0.01	-0.06 ± 0.01	-0.12 ± 0.01
	b	0.53 ± 0.02	0.13 ± 0.01	0.23 ± 0.01	0.23 ± 0.01
	k_s [s ⁻¹]	4.84 ± 0.02	8.07 ± 0.01	11.83 ± 0.01	8.07 ± 0.01

Chapter 7: Application of electrochemically synthesised neutral and P-doped PANI–PSSA for the determination of tetrodotoxin

As shown in Equation 7.3, D_0 increases along with its slope. Table 7.5 gives the value of D_0 calculated and it can be seen that the neutral PANI–PSSA diffuses faster than p-doped PANI–PSSA on Au and PG electrodes. Unlike on GC and Pt electrode, the p-doped PANI–PSSA diffuses faster than the neutral PANI–PSSA on Au and PG electrodes. According to Bard and Faulkner equation (Eq.7.4), the oxidation peak current was plotted against scan rate (i_{pa} vs. v , figure not shown). The slope of this curve was used to calculate the surface concentration Γ^* given in Table 7.5. The films thickness (L) in cm was also calculated from the slope of the curve i_{pc} vs. \sqrt{v} using the Equation 7.5.



Chapter 7: Application of electrochemically synthesised neutral and P-doped PANI–PSSA for the determination of tetrodotoxin

Table 7.6: Diffusion coefficient of neutral and p-doped PANI–PSSA films on various electrodes obtained from the plot i_p versus square root of scan rate

		Au	GC	PG	Pt
Neutral	Range [V s ⁻¹]	2.228-7.085	3.169-8.667	3.169-8.667	3.169-8.667
PANI–PSSA	R^2	0.985	0.999	0.997	0.593
	a	-3.11±1.81	-4.42±0.97	-110.9 ±13.1	6.69±0.61
	b	4.32±0.38	8.86±0.18	56.26±1.22	0.15±0.10
	$D_0 \times 10^{-5}$ [cm ² s ⁻¹]	3.21	1.87	11.87	0.11
	$\Gamma^* \times 10^{-3}$ [mol cm ⁻²]	5.45 ±0.34	2.62±0.06	16.74±0.15	0.27±0.01
	L [nm]	0.629	0.302	1.00	3.077
P-doped	R^2	0.988	0.995	0.999	0.996
PANI–PSSA	a	-1.47±1.39	-38.69±5.69	-5.20±0.81	-15.92±2.19
	b	3.73 ± 0.29	22.46±1.03	13.17±0.14	7.94±0.37
	$D_0 \times 10^{-5}$ [cm ² s ⁻¹]	2.77	4.74	2.78	5.89
	$\Gamma^* \times 10^{-3}$ [mol cm ⁻²]	4.43±0.03	6.88±0.09	3.57±0.08	8.15±0.02
	L [nm]	5.00	7.00	4.00	9.00

Chapter 7: Application of electrochemically synthesised neutral and P-doped PANI–PSSA for the determination of tetrodotoxin

$$\frac{i_{pa}}{\nu} = \frac{n^2 F^2 A \Gamma^*}{4RT} \quad \text{Equation 7.4}$$

$$\frac{i_{pc}}{\nu^{1/2}} = \frac{0.4463(nF)^{3/2} A D_0 \Gamma^*}{L(RT)^{1/2}} \quad \text{Equation 7.5}$$

The kinetic parameters (α , k , D_0 , L , Γ^*) of both polymer films calculated after their characterisation in phosphate buffer show that: the transfer coefficient of neutral PANI–PSSA is higher than the α of p-doped for all the electrodes; the electrode reaction rate constant of p-doped is higher for GC, Pt, PG electrodes than the k of neutral PANI–PSSA; the diffusion coefficient of neutral is higher on Au and PG electrode while the D_0 of p-doped is higher on GC and Pt electrode. This suggests that, the Au electrode is well indicated for the neutral PANI–PSSA electrosynthesis when studied in phosphate buffer solution. On the other hand, it is revealed that GC, PG, Pt electrodes are more inclined to be used in electrochemical synthesis of p-doped PANI–PSSA and characterised in phosphate buffer.

7.4 Characterisation of neutral and p-doped PANI–PSSA in SPB using EIS

The better understanding of the electron transfer and the diffusion process discussed previously in cyclic voltammetry process can also be studied using electrochemical impedance spectroscopy technique. Using this technique, it is possible to separate different processes occurring in the electrode such as diffusion, polymer|solution interface kinetic, and electronic conductivity in the polymer. Figure 7.11 presents the Nyquist diagrams

Chapter 7: Application of electrochemically synthesised neutral and P-doped PANI–PSSA for the determination of tetrodotoxin

obtained for PANI–PSSA films on Au, GC, PG, and Pt electrodes. Analysing these diagrams, only diffusion process on bare electrode was observed while with modified-PANI–PSSA electrodes, a well-defined semicircle as well as the Warburg were obtained. The semicircle which measures the charge transfer (R_{ct}) across the interface between electrode surface and electrolyte solution is used to study the kinetics of the electrode reaction while the Warburg measures the impedance (Z_W) when the polymer is diffused into electrolyte solution. The diffusion process observed on bare electrodes produces the capacitive current that blocks the flow of the faradic current [248]. Thus, the interface between the bare electrode surface and the electrolyte solution works like a capacitor.

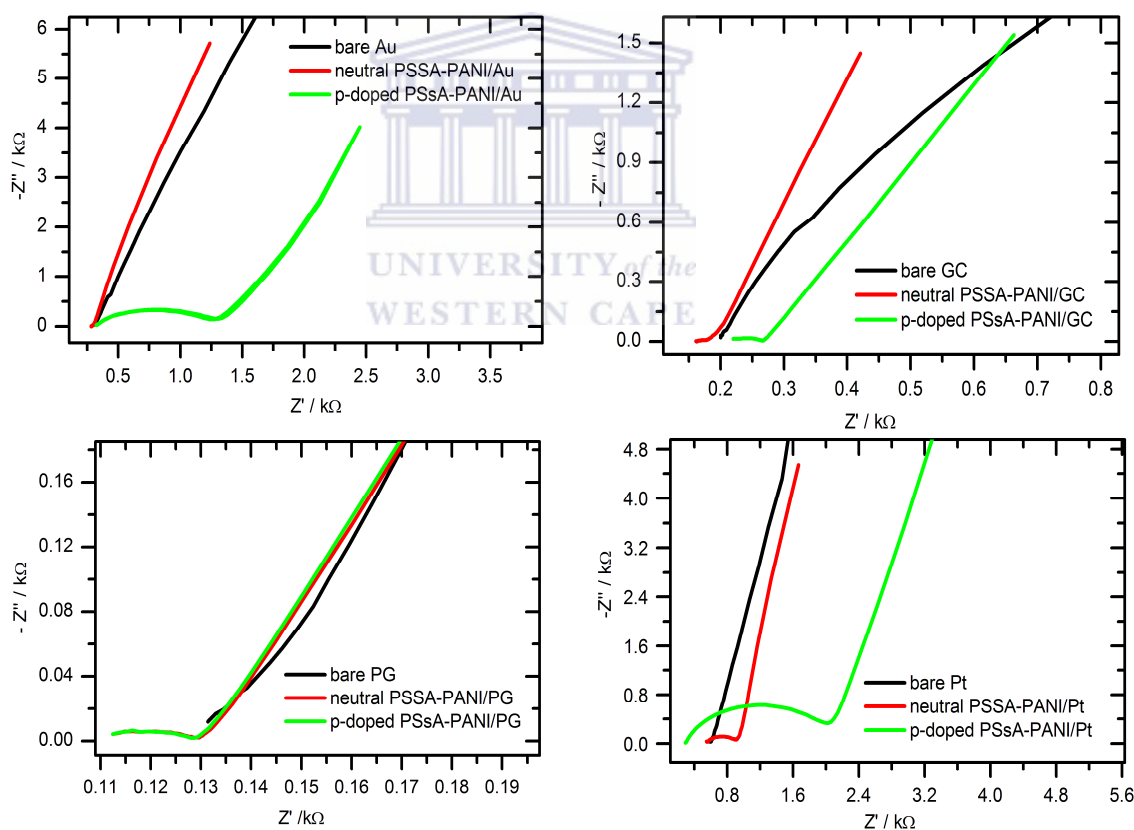


Figure 7.11: Nyquist plot of neutral and p-doped modified-PANI–PSSA electrodes in 0.1 M sodium phosphate buffer pH 7.04 at a frequency range 100 mHz to 100 kHz.

Chapter 7: Application of electrochemically synthesised neutral and P-doped PANI–PSSA for the determination of tetrodotoxin

The semicircle obtained with neutral PANI–PSSA modified electrodes is smaller than the semicircle obtained with p-doped PANI–PSSA modified electrodes. The faradic and capacitive current flowing when the electrode is modified is due to the electrochemical reaction taking place (oxidation and reduction). This makes the p-doped PANI–PSSA more suitable to be applied on the development of electrochemical sensors and biosensors. Unlike on Au electrode, the diffusion part which is represented by the Warburg impedance (Z_W) shows that on GC, PG, Pt electrodes, the diffusion of the H^+ ions through the neutral polymer material occurs faster than through the p-doped polymer.

The charge transfer resistance (R_{ct}) due to the faradic reaction taking place in the PANI–PSSA/electrode|electrolyte interface is presented in Table 7.7. From this charge transfer resistance, the exchange current density and the interfacial heterogeneous electron transfer rates are calculated using the Equation 7.6 [249]:

$$R_{ct} = \frac{RT}{nFi_0} \leftrightarrow i_0 = \frac{RT}{nFR_{ct}} \quad \text{Equation 7.6}$$

$$i_0 = nFAk^0C^* \leftrightarrow k^0 = \frac{i_0}{nFAC^*} \quad \text{Equation 7.7}$$

where n is the number of electrons transferred, F is the Faraday constant ($96485.34 \text{ C mol}^{-1}$), R is the gas constant ($8.314 \text{ J mol}^{-1}\text{K}^{-1}$), T is the reaction temperature ($298 \text{ }^\circ\text{K}$), i_0 is the standard exchange current (A), A is the geometric area of the electrode (cm^2), k^0 is the heterogeneous standard rate transfer constant (cm s^{-1}), and C^* is the concentration of electrolyte solution.

Chapter 7: Application of electrochemically synthesised neutral and P-doped PANI–PSSA for the determination of tetrodotoxin

The R_{ct} values of neutral PANI–PSSA is smaller than R_{ct} of p-doped polymers films. These results indicate that the faradic reaction on the neutral PANI–PSSA/electrode|electrolyte interface takes place faster while with a p-doped polymer, the reaction is slow. The exchange current density which is the rate of oxidation and reduction of polymer at an equilibrium electrode is calculated. Equation 7.7 shows that i_0 is inversely related to R_{ct} so; i_0 of neutral polymer films is higher than the i_0 of p-doped polymer on GC, PG, Pt electrodes. The standard heterogeneous rate constant is higher for neutral PANI–PSSA as compared to the p-doped PANI-PSSA as seen in Table 7.7. Klink *et al.* reported in Mathebe *et al.* a small value for k^0 for electroactive polymers of PANI and PANI–ASA in 1 M HCl [250]. This value was compared values obtained for k^0 for both neutral and p-doped PANI–PSSA in sodium phosphate buffer in this study. Since the purpose of this electrodeposition of PANI–PSSA films is used a platform for the detection of tetrodotoxin, both neutral and p-doped polymer films are further studied in the tetrodotoxin medium (acetate buffer).

Table 7.7: Diagnostic parameters for neutral and p-doped-modified electrodes

Electrode	Neutral PANI-PSSA			p-doped PANI-PSSA		
	R_{ct} [Ω]	$i_0 \times 10^{-4}$ [A]	$k^0 \times 10^{-4}$ [cm s ⁻¹]	R_{ct}	$i_0 \times 10^{-4}$ [A]	$k^0 \times 10^{-4}$ [cm s ⁻¹]
Au	0	–	–	1014 ± 7	0.26	1.34
GC	28.04 ± 1	9.16	13.41	55.13 ± 1	4.66	6.82
PG	20.93 ± 1	12.4	18.16	20.94 ± 1	12.27	17.96
Pt	419 ± 3	0.61	3.14	1840 ± 12	0.21	3.08

Chapter 7: Application of electrochemically synthesised neutral and P-doped PANI-PSSA for the determination of tetrodotoxin

7.5 The study of the electroactivity of neutral and p-doped PANI-PSSA films in acetate buffer pH 4.8

Figure 7.11 presents the cyclic voltammograms obtained by cycling over the potential window of - 0.5 to 0.6 V. The voltammograms are recorded after three repetitive cycles to study both the electroactivity of polymers and the stability of the modified electrodes.



Chapter 7: Application of electrochemically synthesised neutral and P-doped PANI-PSSA for the determination of tetrodotoxin

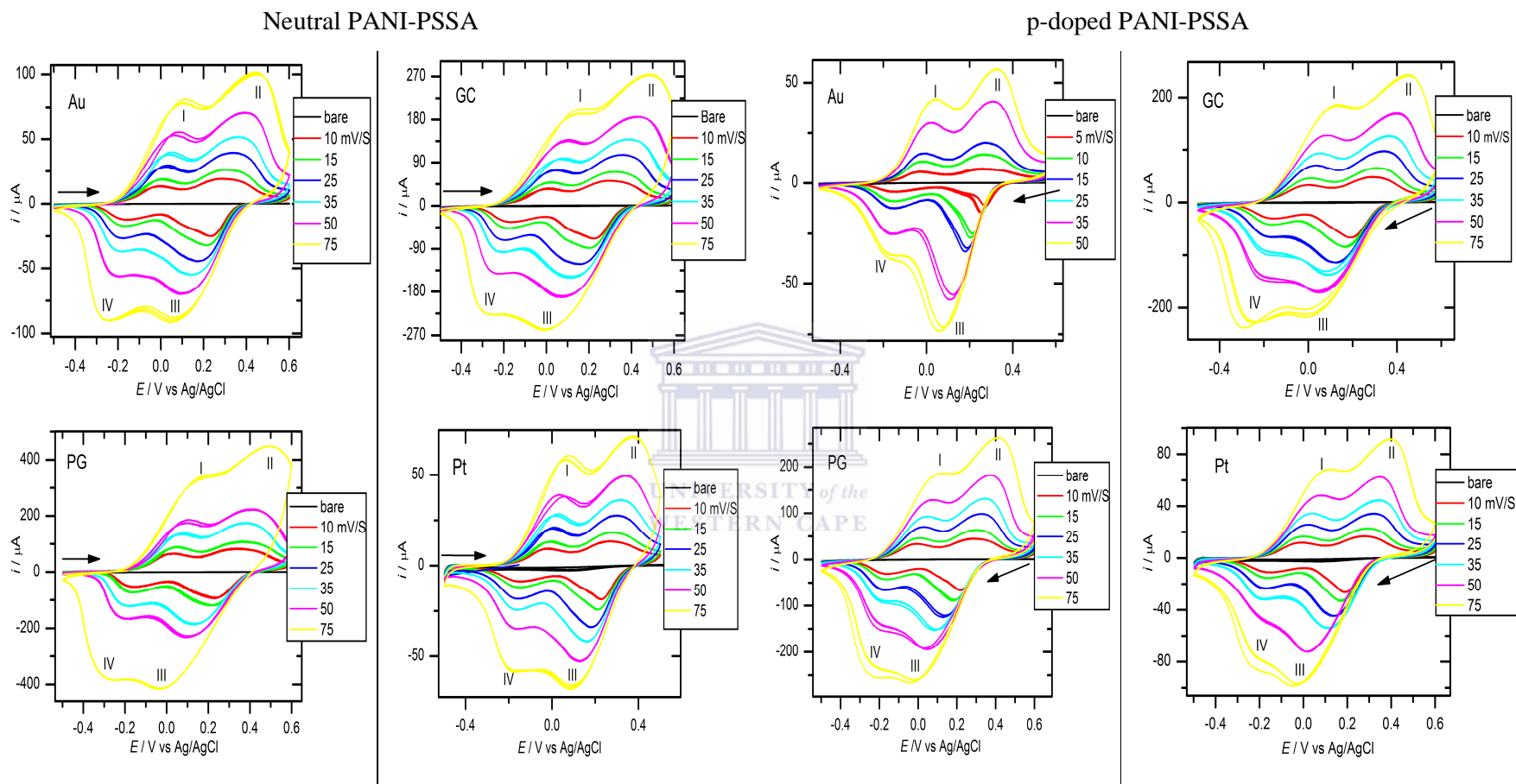


Figure 7.12: Cyclic voltammograms of the PANI-PSSA electrodeposited on Au, GC, PG, and Pt electrodes in 0.1 acetate buffer pH 4.8 at different potential scan rates.

Chapter 7: Application of electrochemically synthesised neutral and P-doped PANI–PSSA for the determination of tetrodotoxin

The cyclic voltammograms for the polymer in acid media on Pt electrode are similar to literature reported [219]. For both neutral and p-doped polymer, the first oxidation peak (I) corresponds to the polyleucoemeraldine radical cation which is further oxidized at 0.1 V to blue polyemeraldine (II) at higher potential of 0.4 V. On the reverse scan, the blue polyemeraldine is reduced first to the partly reduced polyemeraldine radical cation (III) at 0.1 V and then to fully reduced polyleucoemeraldine (IV) [250-251] at - 0.2 V. The anodic peak potentials, E_{pa} and the cathodic peak potentials, E_{pc} , as well as the corresponding peak currents (i_{pa} and i_{pc} , respectively) vary with the values of the scan rates. This shows linear relation between the peak potential and the scan rate explaining the electroactivity of the polymer. On the other hand, the linear relation between peak current shows the diffusion of electrons of conjugated benzene ring units along the polymer chain. Figure 7.12 also shows that the scan rate increases with an increase in peak potential E_p . When the scan rate is lower than 25 mV s^{-1} , the change of cathodic and anodic peak potential, E_{pc} and E_{pa} is not significant with the increase of the scan rate, but E_{pc} shifted negatively while E_{pa} shift positively as the scan rate increased. E_{pa} (I) and E_{pc} (III) peaks tend towards the same value, 0.1 V. The ratio i_{pa} (I)/ i_{pc} (III) is |0.9| at the fast scan rate of 75 mVs^{-1} for both neutral and p-doped polymer films. This indicates that a neutral and p-doped PANI-PSSA film grown above 50 mV s^{-1} exhibits irreversible electrochemistry. The separation peak potential, ΔE_p , the formal potentials, E^0 and the ratio i_{pa}/i_{pc} for each neutral and p-doped PANI–PSSA modified electrodes are hereby calculated (Tab. 7.9)

Chapter 7: Application of electrochemically synthesised neutral and P-doped PANI–PSSA for the determination of tetrodotoxin

Table 7.8: Electrochemical potential parameters of neutral PANI–PSSA films

WE	ν [mV s ⁻¹]	$E_{pa(I)}$ [V]	$E_{pa(II)}$ [V]	$E_{pc(IV)}$ [V]	$E_{pc(III)}$ [V]	ΔE_{p1} [V]	ΔE_{p2} [V]	E^{θ}_1 [V]	E^{θ}_2 [V]
Au	10	-0.008	0.280	-0.155	0.236	0.147	0.044	-0.082	0.258
	15	0.003	0.308	-0.165	0.220	0.168	0.088	-0.081	0.264
	25	0.015	0.350	-0.178	0.17	0.193	0.180	-0.082	0.26
	35	0.043	0.376	-0.203	0.136	0.246	0.240	-0.08	0.256
	50	0.065	0.409	-0.206	0.108	0.271	0.301	-0.071	0.258
	75	0.105	0.447	-0.252	0.062	0.357	0.385	-0.074	0.2545
GC	10	0.007	0.316	-0.159	0.230	0.166	0.086	-0.076	0.273
	15	0.017	0.327	-0.178	0.209	0.195	0.118	0.081	0.268
	25	0.026	0.363	-0.203	0.152	0.229	0.211	-0.088	0.257
	35	0.057	0.389	-0.222	0.118	0.279	0.271	-0.083	0.2535
	50	0.072	0.443	-0.244	0.075	0.316	0.368	-0.086	0.259
	75	0.149	0.496	-0.286	-0.007	0.435	0.503	-0.069	0.244
PG	10	0.023	0.339	-0.156	0.234	0.179	0.105	-0.067	0.2865
	15	0.046	0.355	-0.164	0.217	0.210	0.138	-0.059	0.286
	35	0.073	0.383	-0.182	0.125	0.255	0.258	-0.055	0.254
	50	0.087	0.432	-0.199	0.097	0.286	0.335	-0.056	0.264
	75	0.178	0.492	-0.277	-0.036	0.455	0.528	-0.049	0.228
Pt	10	-0.019	0.263	-0.147	0.228	0.128	0.035	0.083	0.245
	15	-0.017	0.287	-0.157	0.214	0.140	0.073	-0.087	0.250
	25	-1E-3	0.3	-0.164	0.181	0.163	0.119	-0.083	0.240
	35	0.013	0.325	-0.169	0.163	0.182	0.162	-0.078	0.244
	50	0.034	0.339	-0.174	0.123	0.208	0.216	-0.07	0.231
	75	0.064	0.374	-0.187	0.096	0.251	0.278	-0.062	0.235

Chapter 7: Application of electrochemically synthesised neutral and P-doped PANI–PSSA for the determination of tetrodotoxin

Table 7.9: Electrochemical current parameters of neutral PANI–PSSA films

WE	ν [mV s ⁻¹]	$i_{pa(I)}$ [μ A]	$i_{pa(II)}$ [μ A]	$i_{pc(IV)}$ [μ A]	$i_{pc(III)}$ [μ A]	$i_{pa(I)}/i_{pc(IV)}$	$i_{pa(II)}/i_{pc(III)}$
Au	10	13.63	19.25	-11.78	-24.44	-1.2	-0.8
	15	18.83	25.87	-16.98	-31.57	-1.1	-0.8
	25	29.14	39.03	-26.37	-44.23	-1.1	-0.9
	35	38.69	52.39	-35.57	-54.28	-1.1	-0.9
	50	54.07	70.35	-55.19	-68.74	-0.9	-1.0
	75	80.55	100.18	-89.29	-89.29	-0.9	-1.1
GC	10	35.66	52.78	-34.02	-66.86	-1.1	-0.8
	15	49.03	71.32	-44.57	-86.57	-1.1	-0.8
	25	73.89	106.74	-70.85	-119.41	-1.0	-0.9
	35	98.04	139.63	-95.91	-146.55	-1.0	-0.9
	50	135.09	188.22	-139.96	-188.14	-0.9	-1.0
	75	199.75	275.92	-222.73	-257.73	-0.9	-1.1
PG	10	64.32	82.57	-51.03	-90.76	-1.3	-0.9
	15	89.04	107.29	-72.52	-117.24	-1.2	-0.9
	25	142.7	178.91	-117.74	-182.87	-1.2	-1.0
	35	142.7	178.91	-117.74	-182.87	-1.2	-1.0
	50	186	222.11	-164.82	-226.08	-1.1	-0.9
	75	338.19	450.4	-318.49	-417.61	-1.1	1.1
Pt	10	9.55	13.33	-8.63	-18.44	-1.1	-0.7
	15	13.33	18.14	-11.87	-24.02	-1.1	-0.8
	25	20.66	27.46	-18.22	-33.83	-1.1	-0.8
	35	28.45	36.74	-24.09	-40.79	-1.2	-0.9
	50	38.55	49.82	-34.19	-52.17	-1.1	-0.9
	75	58.86	70.77	-58.12	67.06	-1.0	-1.1

Chapter 7: Application of electrochemically synthesised neutral and P-doped PANI–PSSA for the determination of tetrodotoxin

Table 7.10: Electrochemical potential parameters of p-doped PANI–PSSA films

WE	ν [mV s ⁻¹]	$E_{pa(I)}$ [V]	$E_{pa(II)}$ [V]	$E_{pc(IV)}$ [V]	$E_{pc(III)}$ [V]	ΔE_{p1} [V]	ΔE_{p2} [V]	E^{0_1} [V]	E^{0_2} [V]
Au	10	-0.028	0.263	-0.149	0.21	0.121	0.053	-0.090	0.240
	15	-0.021	0.267	-0.159	0.186	0.138	0.081	-0.090	0.230
	25	-0.016	0.272	-0.016	0.188	0	0.140	-0.020	0.230
	35	0.021	0.312	-0.159	0.111	0.180	0.201	-0.070	0.210
	50	0.047	0.331	-0.182	0.079	0.229	0.252	-0.07	0.210
GC	10	0.003	0.289	-0.156	0.195	0.159	0.094	-0.077	0.242
	15	0.013	0.315	-0.166	0.166	0.179	0.149	-0.077	0.241
	25	0.034	0.344	-0.178	0.125	0.212	0.219	-0.072	0.235
	35	0.058	0.374	-0.185	0.088	0.243	0.286	-0.064	0.231
	50	0.078	0.398	-0.194	0.048	0.272	0.350	-0.058	0.223
	75	0.145	0.455	-0.259	-0.006	0.404	0.461	-0.057	0.225
PG	10	-0.007	0.287	-0.157	0.222	0.150	0.065	-0.082	0.255
	15	0.009	0.307	-0.166	0.179	0.175	0.128	-0.079	0.243
	25	0.027	0.321	-0.182	0.13	0.209	0.191	-0.078	0.226
	35	0.041	0.357	-0.182	0.095	0.223	0.262	-0.071	0.226
	50	0.080	0.375	-0.189	0.041	0.269	0.334	-0.055	0.208
	75	0.116	0.417	-0.211	-0.016	0.327	0.433	-0.048	0.201
Pt	10	-0.029	0.259	-0.146	0.226	0.117	0.033	-0.088	0.243
	15	-0.019	0.274	-0.153	0.211	0.134	0.063	-0.086	0.243
	25	0.002	0.302	-0.159	0.181	0.161	0.121	-0.079	0.242
	35	0.012	0.318	-0.166	0.168	0.178	0.150	-0.077	0.243
	50	0.031	0.339	-0.169	0.127	0.200	0.212	-0.069	0.233
	75	0.063	0.381	-0.182	0.089	0.245	0.292	-0.059	0.235

Chapter 7: Application of electrochemically synthesised neutral and P-doped PANI–PSSA for the determination of tetrodotoxin

Table 7.11: Electrochemical current parameters of p-doped PANI–PSSA films

WE	v [mV s ⁻¹]	$i_{pa(I)}$ [μA]	$i_{pa(II)}$ [μA]	$i_{pc(IV)}$ [μA]	$i_{pc(III)}$ [μA]	$i_{pa(I)}/i_{pc(IV)}$	$i_{pa(II)}/i_{pc(III)}$
Au	10	10.59	14.24	-8.83	-24.84	-1.2	-0.6
	15	14.51	20.04	-12.25	-31.95	-1.2	-0.6
	25	14.75	20.27	-24.84	-32.19	-0.6	-0.6
	35	29.87	40.89	-25.19	56.59	-1.2	-0.7
	50	41.93	56.6	-35.66	-71.83	-1.2	-0.8
GC	10	32.96	48.13	-28.79	-66.35	-1.1	-0.7
	15	46.14	65.29	-41.07	-83.51	-1.1	-0.8
	25	70.69	96.74	-63.46	-113.41	-1.1	-0.9
	35	92.81	126.71	-93.44	-135.54	-0.9	-0.9
	50	128.85	168.81	-145.53	-167.65	-0.9	-1.0
	75	184.87	244.81	-225.45	-211.53	-0.8	-1.2
PG	10	33.68	44.17	-29.88	-64.07	-1.1	-0.7
	15	45.43	64.3	-41.62	-87.56	-1.1	-0.7
	25	72.52	98.7	-63.47	-120.53	-1.1	-0.8
	35	94.4	131.53	-89.66	-149.06	-1.1	-0.9
	50	129.18	181.94	-142.41	-192.83	-0.9	-0.9
	75	186.24	263.23	-232.29	-260.83	-0.8	-1.0
Pt	10	9.29	13.21	-8.78	18.45	-1.1	0.7
	15	12.98	18.21	-23.96	-23.96	-0.5	-0.8
	25	20.69	27.97	-17.89	-32.94	-1.2	-0.8
	35	27.97	36.35	-24.07	-41.42	-1.2	-0.9
	50	38.54	49.21	-34.64	-51.98	-1.1	-0.9
	75	58.18	71.04	-57.57	-66.54	-1.0	-1.1

The linear relation between the peak potential and the scan rate explained above can be observed graphically (Fig. 7.13). The reversibility of the system is studied by plotting the graph E_p versus logarithm of scan rate. For each anodic and cathodic peaks obtained on

Chapter 7: Application of electrochemically synthesised neutral and P-doped PANI-PSSA for the determination of tetrodotoxin

Figure 7.12, there is an uptake or release electrons which results in electron transfer coefficient α_c . The transfer coefficient α applies only to an electrode reaction that consists of a single elementary step involving the simultaneous uptake of n electrons from the electrode as the case of α_c , or to the electrode as the case of α_a .

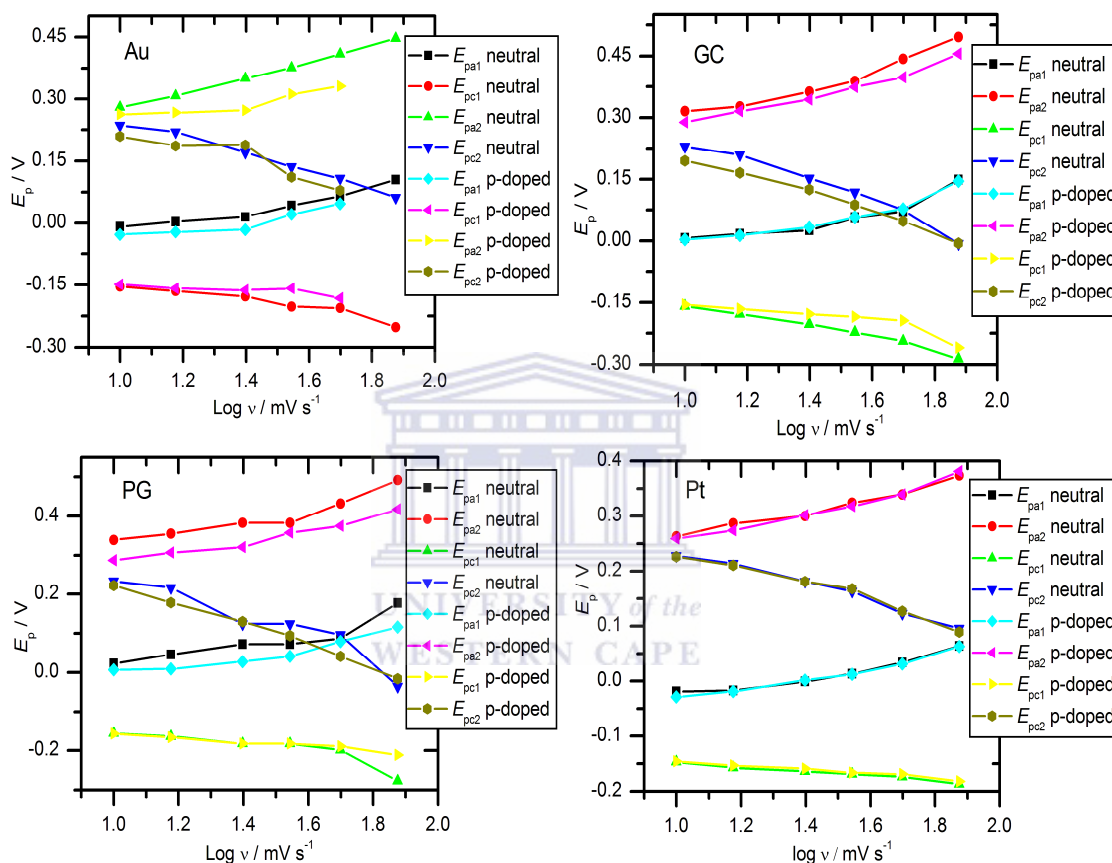


Figure 7.13: A plot of E_p vs. $\log v$ for the voltammograms of neutral and p-doped PANI-PSSA films deposited on different bare electrodes in 0.1 M acetate buffer pH 4.8.

Figure 7.13 shows that E_{pc} decreases while E_{pa} increases as the scan rate increases. Tables 7.12 and 7.13 present the value of α_a and α_c calculated from the slope of the graphs E_{pa} and E_{pc} vs. $\log v$ using the Equation 6.5 and 6.6 for α_a and α_c respectively. The reaction occurs on peak (IV) and peak (II) faster than the reaction takes place on peak (I) and (III) for

Chapter 7: Application of electrochemically synthesised neutral and P-doped PANI-PSSA for the determination of tetrodotoxin

neutral and p-doped polymer. This is explained with the values of α_{c1} and α_{a2} calculated (Tab7.9) which shows that for the deposition of p-doped polymer, the reaction is faster compared to the deposition of neutral polymer on the electrode surface.



Chapter 7: Application of electrochemically synthesised neutral and P-doped PANI–PSSA for the determination of tetrodotoxin

Table 7.12: Anodic and cathodic transfer coefficient of neutral PANI–PSSA films

		Au	GC	PG	Pt
E_{pa1} vs. $\log v$	Range [mV s ⁻¹]	0.999-1.697	1.00-1.696	1.00-1.696	1.00-1.696
	R^2	0.967	0.959	0.972	0.961
	a	-0.12 ± 0.02	-0.09 ± 0.02	-0.06 ± 0.01	-0.10 ± 0.02
	b	0.10 ± 0.02	0.09 ± 0.02	0.09 ± 0.01	0.08 ± 0.01
	α_{a1}	0.41	0.34	0.34	0.26
E_{pa2} vs. $\log v$	R^2	0.999	0.966	0.950	0.990
	a	0.09 ± 0.01	0.13 ± 0.04	0.21 ± 0.03	0.16 ± 0.01
	b	0.18 ± 0.00	0.18 ± 0.03	0.12 ± 0.02	0.11 ± 0.01
	α_{a2}	0.67	0.67	0.51	0.46
	E_{pc1} vs. $\log v$	R^2	-0.975	-0.998	-0.978
a		-0.07 ± 0.01	-0.04 ± 0.01	-0.09 ± 0.01	-0.11 ± 0.00
b		-0.08 ± 0.01	-0.12 ± 0.00	-0.06 ± 0.01	-0.04 ± 0.00
α_{c1}		0.74	0.49	0.99	1.47
E_{pc2} vs. $\log v$		R^2	-0.992	-0.993	-0.961
	a	0.44 ± 0.01	0.47 ± 0.02	0.45 ± 0.05	0.38 ± 0.02
	b	-0.19 ± 0.01	-0.23 ± 0.02	-0.21 ± 0.03	-0.15 ± 0.02
	α_{c2}	0.31	0.26	0.28	0.39

Chapter 7: Application of electrochemically synthesised neutral and P-doped PANI–PSSA for the determination of tetrodotoxin

Table 7.13: Anodic and cathodic transfer coefficient of p-doped PANI–PSSA films

		Au	GC	PG	Pt
E_{pa1} vs. $\log v$	Range [mV s^{-1}]	1.00-1.696	1.00-1.696	1.00-1.696	1.00-1.696
	R^2	0.920	0.986	0.926	0.994
	a	-0.14 ± 0.04	-0.11 ± 0.02	-0.10 ± 0.03	-0.12 ± 0.01
	b	0.11 ± 0.02	0.11 ± 0.01	0.09 ± 0.02	0.08 ± 0.01
	α_{a1}	0.46	0.46	0.34	0.26
E_{pa2} vs. $\log v$	R^2	0.911	0.998	0.979	0.998
	a	0.15 ± 0.04	0.13 ± 0.01	0.16 ± 0.02	0.14 ± 0.01
	b	0.09 ± 0.03	0.16 ± 0.01	0.13 ± 0.01	0.12 ± 0.00
	α_{a2}	0.34	0.63	0.55	0.51
	E_{pc1} vs. $\log v$	R^2	-0.847	-0.999	-0.975
a		-0.11 ± 0.02	-0.10 ± 0.00	-0.11 ± 0.01	-0.11 ± 0.00
b		-0.04 ± 0.01	-0.05 ± 0.00	-0.05 ± 0.01	-0.03 ± 0.00
α_{c1}		1.48	1.18	1.18	1.97
E_{pc2} vs. $\log v$		R^2	-0.918	-0.995	-0.996
	a	0.41 ± 0.06	0.41 ± 0.02	0.48 ± 0.02	0.38 ± 0.02
	b	-0.19 ± 0.05	-0.21 ± 0.01	-0.25 ± 0.01	-0.14 ± 0.02
	α_{c2}	0.31	0.28	0.24	0.42

Chapter 7: Application of electrochemically synthesised neutral and P-doped PANI–PSSA for the determination of tetrodotoxin

The separation of peak potentials ($E_{pa} - E_{pc}$) increased with an increasing scan rate. When the scan rate was above 25 mV s^{-1} , the wave shape distorted severely. This indicates that the electrode reaction becomes electrochemically irreversible at higher scan rates. There is an overlap of curves ΔE_{p1} and ΔE_{p2} vs. $\log v$ (Fig.7.14) at 25 and 50 mV s^{-1} for p-doped and neutral polymer respectively, which explains the fact that E_{pa} (I) is equal to E_{pc} (III) at these scan rates.

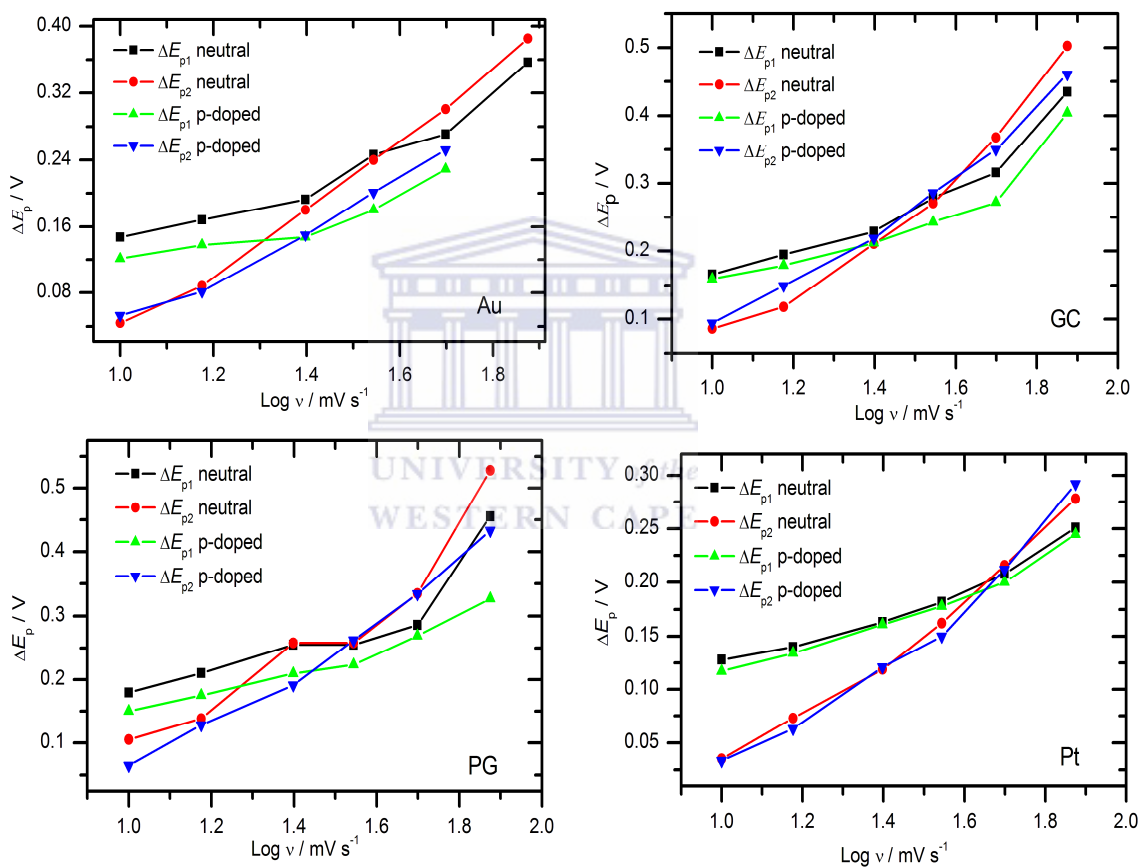


Figure 7.14: A plot of ΔE_p vs. $\log v$ for the voltammograms of neutral and p-doped PANI–PSSA films deposited different bare electrodes in 0.1 M acetate buffer pH 4.8.

For the irreversible electrode reaction, the relationship between peak potential and the scan rate follows Laviron's equation (Eqs.6.5 and 6.6) [252]. ΔE_p is calculated for neutral and p-doped PANI–PSSA films grown at different scan rates and the results show that the

Chapter 7: Application of electrochemically synthesised neutral and P-doped PANI-PSSA for the determination of tetrodotoxin

undoped PANI electrosynthesised at 50 mV s^{-1} exhibit $\Delta E_p > 100/n$. This value of ΔE_p is characteristic of an irreversible system. Using the Equation 6.7, the electrode rate constant k_s is calculated and given in Table.7.14



Chapter 7: Application of electrochemically synthesised neutral and P-doped PANI–PSSA for the determination of tetrodotoxin

Table 7.14: Electrode reaction rate constant of neutral and p-doped PANI–PSSA film study in acetate buffer

			Au	GC	PG	Pt
Neutral PANI–PSSA	ΔE_{p1} vs. $\log v$	Range	1.00-1.696	1.00-1.696	1.00-1.696	1.00-1.696
		R^2	0.977	0.988	0.982	0.988
		a	-0.04 ± 0.03	-0.07 ± 0.03	0.04 ± 0.02	0.01 ± 0.01
		b	0.18 ± 0.02	0.22 ± 0.02	0.15 ± 0.02	0.11 ± 0.01
		k_{s1} [s^{-1}]	13.13±0.03	19.22±0.03	2.48±0.02	38.46±0.01
	ΔE_{p2} vs. $\log v$	R^2	0.997	0.985	0.977	0.993
		a	-0.34 ± 0.02	-0.34 ± 0.06	-0.23 ± 0.06	-0.22 ± 0.02
		b	0.38 ± 0.02	0.40 ± 0.04	0.33 ± 0.04	0.25 ± 0.01
		k_{s2} [s^{-1}]	16.03±0.02	16.03±0.06	19.23±0.06	19.01±0.02
		P-doped PANI–PSSA	ΔE_{p1} vs. $\log v$	R^2	0.933	0.994
a	-0.03 ± 0.04			-0.01 ± 0.01	-0.01 ± 0.02	-0.00 ± 0.01
b	0.14 ± 0.03			0.16 ± 0.01	0.16 ± 0.02	0.12 ± 0.00
k_{s1} [s^{-1}]	38.46±0.04			38.46±0.01	38.46±0.02	38.46±0.01
ΔE_{p2} vs. $\log v$	R^2			0.993	0.997	0.994
	a		-0.25 ± 0.03	-0.28 ± 0.02	-0.32 ± 0.03	-0.23 ± 0.03
	b		0.29 ± 0.02	0.37 ± 0.02	0.38 ± 0.02	0.25 ± 0.02
	k_{s2} [s^{-1}]		16.37±0.03	16.67±0.02	18.92±0.03	19.23±0.03

Chapter 7: Application of electrochemically synthesised neutral and P-doped PANI–PSSA for the determination of tetrodotoxin

The results shown that the k_s of p-doped PANI–PSSA is higher than k_s of neutral PANI–PSSA for all modified electrodes. This indicates that the rate of reaction on p-doped modified electrodes is faster than on neutral PANI–PSSA modified electrodes.

Figure 7.15 has shown that the potential scan rate has an influence on the cyclic voltammetry behaviour of the neutral and p-doped PANI–PSSA films. A higher scan rate resulted in a higher current flow, as expected for a surface wave [252]. The oxidation and reduction peak current i_{pa} and i_{pc} respectively are proportional to the scan rate over the range 3.171-7.060 mV s⁻¹.



Chapter 7: Application of electrochemically synthesised neutral and P-doped PANI-PSSA for the determination of tetrodotoxin

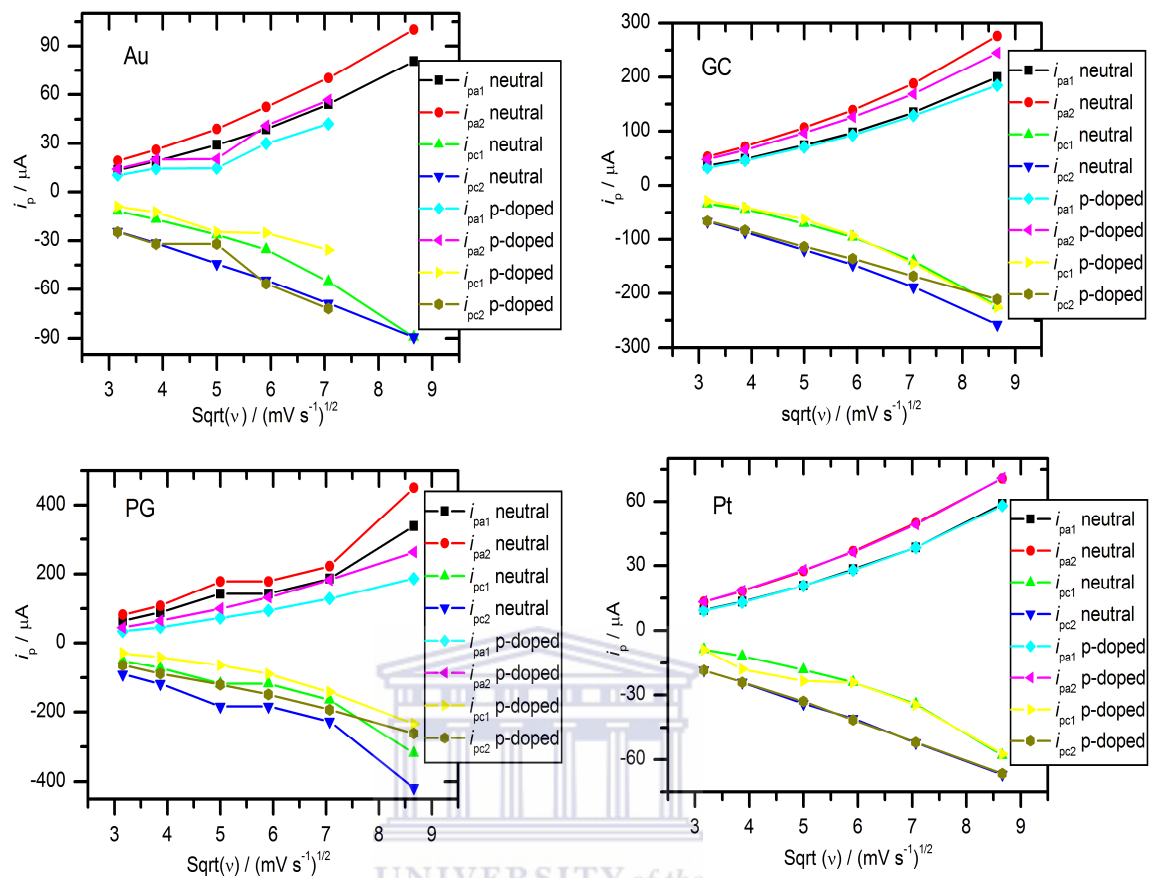


Figure 7.15: A plot of i_p vs. square root v for the voltammograms of neutral and p-doped PANI-PSSA films deposited on different bare electrodes in 0.1 M acetate buffer pH 4.8.

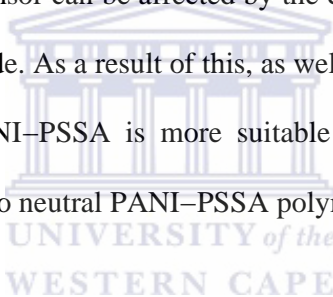
Chapter 7: Application of electrochemically synthesised neutral and P-doped PANI–PSSA for the determination of tetrodotoxin

Table 7.15: Electron transport diffusion coefficient of neutral and p-doped PANI–PSSA film study in acetate buffer

			Au	GC	PG	Pt
Neutral PANI–PSSA	i_{pa1} vs. $v^{1/2}$	Range	3.171-7.060	3.171-7.060	3.171-7.060	3.171-7.060
		R^2	0.994	0.995	0.976	0.996
		a	-20.6 ± 3.3	-48.1 ± 7.8	-25.9 ± 20.3	-15.2 ± 2.1
		b	10.3 ± 0.6	25.3 ± 1.5	30.1 ± 3.9	7.5 ± 0.0
		$D_0 \times 10^{-5}$ [cm ² s ⁻¹]	7.63	5.33	6.35	5.53
	i_{pa2} vs. $v^{1/2}$	$F^* \times 10^{-3}$ [mol cm ⁻²]	1.36 ± 0.01	0.94 ± 0.05	2.49 ± 0.74	0.99 ± 0.01
		L [nm]	1.565	1.08	3.39	1.134
		R^2	0.996	0.996	0.969	0.996
		a	-24.3 ± 3.6	-61.2 ± 8.9	-24.1 ± 26.9	-17.6 ± 2.6
		b	13.1 ± 0.7	34.6 ± 1.7	35.6 ± 5.2	9.3 ± 0.5
P-doped PANI–PSSA	i_{pa1} vs. $v^{1/2}$	$D_0 \times 10^{-5}$ [cm ² s ⁻¹]	9.7	7.29	7.5	6.93
		$F^* \times 10^{-3}$ [mol cm ⁻²]	1.65 ± 0.02	1.28 ± 0.03	3.32 ± 1.34	1.17 ± 0.01
		L [nm]	1.896	1.474	3.823	1.36
		R^2	0.943	0.995	0.996	0.996
		a	-17.4 ± 8.4	-47.4 ± 7.2	-47.4 ± 6.4	15.6 ± 2.1
	i_{pa2} vs. $v^{1/2}$	b	7.9 ± 8.4	24.3 ± 1.4	24.5 ± 1.2	7.5 ± 0.4
		$D_0 \times 10^{-5}$ [cm ² s ⁻¹]	1.46	5.13	5.16	5.56
		$F^* \times 10^{-3}$ [mol cm ⁻²]	1.05 ± 0.12	0.88 ± 0.02	0.86 ± 0.03	0.99 ± 0.01
		L [nm]	0.301	1.015	0.989	1.140
		R^2	0.945	0.997	0.996	0.997
i_{pa2} vs. $v^{1/2}$	a	-23.5 ± 11.1	-53.2 ± 7.2	-70.6 ± 9.5	-16.9 ± 2.1	
	b	10.8 ± 2.1	30.8 ± 1.4	34.9 ± 1.8	9.1 ± 0.4	
	$D_0 \times 10^{-5}$ [cm ² s ⁻¹]	8.00	6.5	7.36	6.82	
	$F^* \times 10^{-3}$ [mol cm ⁻²]	1.42 ± 0.16	1.13 ± 0.03	1.26 ± 0.04	1.17 ± 0.01	
	L [nm]	1.634	1.303	1.452	1.363	

Chapter 7: Application of electrochemically synthesised neutral and P-doped PANI–PSSA for the determination of tetrodotoxin

The electron transport diffusion coefficient, D_0 , through the polymer chain, may be evaluated by the Randle Sevcik analysis of hydrodynamic voltammetry data [250]. Using i_{pa1} (peak I) or i_{pa2} (peak II), the value of D_0 of neutral PANI–PSSA is greater than the D_0 of p-doped PANI–PSSA. This indicates that the neutral polymer diffuses faster than p-doped polymer in acetate buffer. These values of D_0 are higher compared to what has been reported in the literature for electroactive polyanilines of similar film characterises in 1 M HCl medium [219] and to what has been reported on PANI–ASA in 1 M HCl [102, 250]. This diffusion process corresponds to the higher current produced on the neutral PANI–PSSA modified electrodes than the on p-doped PANI–PSSA. In electrochemical sensor, the response of the sensor can be affected by the currents produced by the material used in modifying the electrode. As a result of this, as well as the influence of the diffusion coefficient, the p-doped PANI–PSSA is more suitable to develop the electrochemical sensor for TTX as compared to neutral PANI–PSSA polymer film.



7.6 The study of R_{ct} for neutral and p-doped PANI-PSSA in acetate buffer pH 4.8

7.6.1 Charge transfer resistance (R_{ct}) of different bare electrode potentials

Before modifying the electrode surface with the PANI–PSSA, the bare electrode was first studied. The bare of GC, Au, Pt, and PG electrodes are analyzed using the electrochemical impedance spectroscopy. In 0.1 M acetate buffer pH 4.8, the impedance spectra of bare electrodes are recorded at different potentials at the frequency of 100 mHz to 100 kHz with amplitude of 10 m. Figure 7.16 shown that at - 0.5 V, small impedance is obtained as

Chapter 7: Application of electrochemically synthesised neutral and P-doped PANI-PSSA for the determination of tetrodotoxin

compared to the other potentials. So the impedance spectrum of bare Au, GC, PG, and Pt electrodes can be recorded at - 0.5 V in OAc buffer pH 4.8

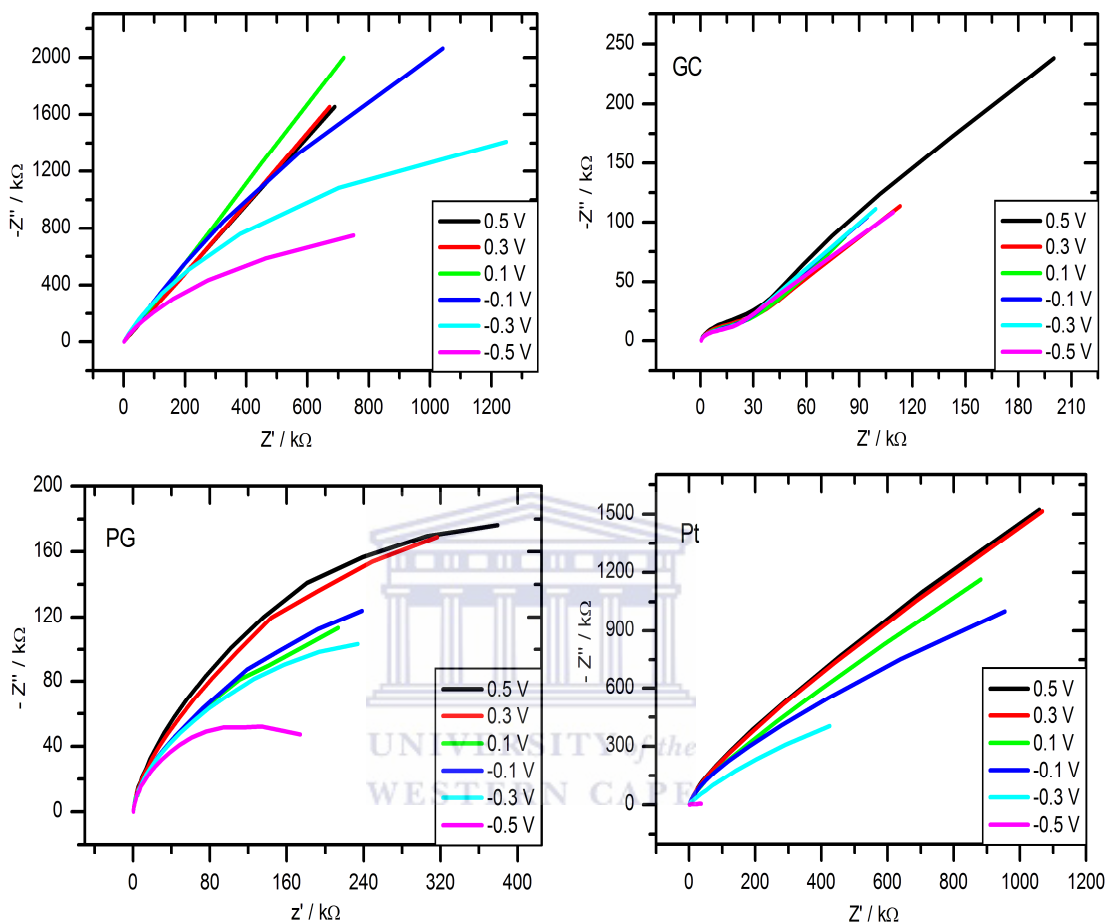


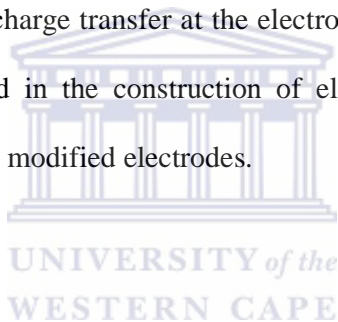
Figure 7.16: Nyquist plot for bare Au, GC, PG, and Pt electrodes in 0.1 M acetate buffer pH 4.8.

7.6.2 The determination of R_{ct} for the modified neutral and p-doped PANI-PSSA/GC

The impedance spectra of neutral and p-doped PANI-PSSA modified electrodes were recorded at different potential values at the range of the potential window used to record the cyclic voltammograms. Before the EIS measurement, both polymer films were cycled

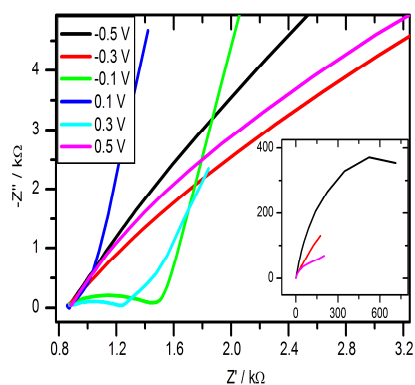
Chapter 7: Application of electrochemically synthesised neutral and P-doped PANI–PSSA for the determination of tetrodotoxin

three times around the polymer films redox system until a stable voltammogram was obtained in order to check the stability of the polymer films. Figure 7.17 represents a series of Nyquist diagrams for neutral and p-doped PANI–PSSA measured in OAc between the potential ranges of - 0.5 to 0.5 V which corresponds to a working potential range. At the potential values of 0.3, 0.1 and - 0.1 V a faradic and capacitive reaction was observed while the potential values of -0.5, - 0.3, and 0.5 V for the capacitive reaction was observed (see discussion given on paragraph 7.4). At 0.5, - 0.3 and - 0.5 V this results were expected as shown via the cyclic voltammogram where a lower current is produced at this potential value. The most important result is the behaviour of the polymer film in the potential range from - 0.1 to 0.3 V with the charge transfer at the electrode|solution interface; this kinetic parameter could be exploited in the construction of electrochemical sensors based on PANI–PSSA redox mediators modified electrodes.

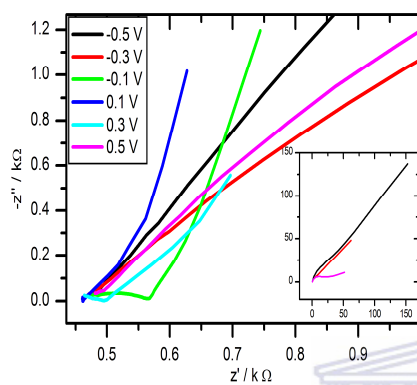


Chapter 7: Application of electrochemically synthesised neutral and P-doped PANI-PSSA for the determination of tetrodotoxin

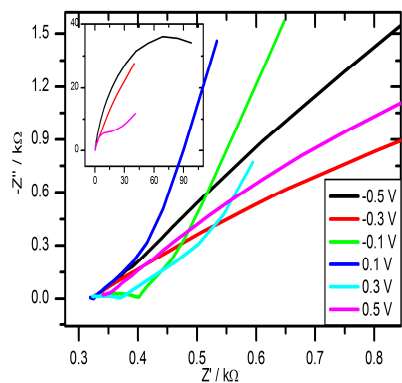
Neutral PANI-PSSA



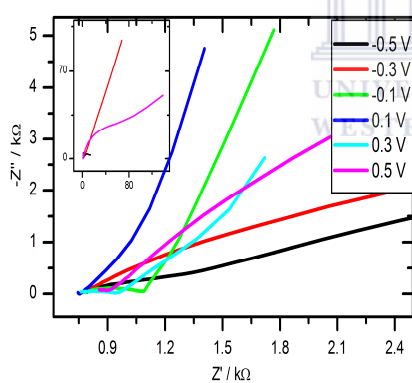
(a)



(b)

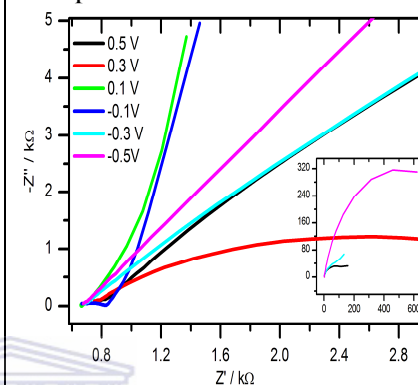


(c)

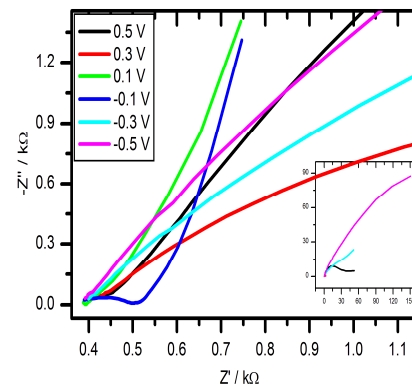


(d)

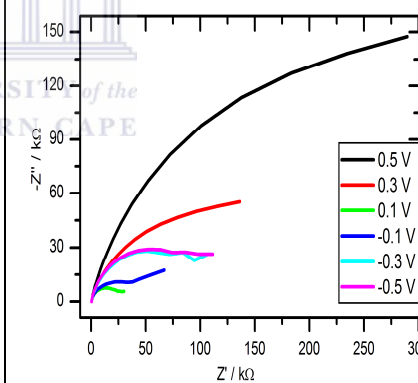
P-doped PANI-PSSA



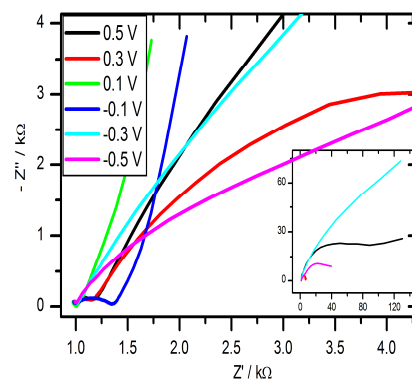
(a')



(b')



(c')



(d')

Figure 7.17: Nyquist plot for neutral and p-doped PANI-PSSA in 0.1 M acetate buffer pH 4.8 on (a) and (a') Au, (b) and (b') GC, (c) and (c') PG, (d) and (d') Pt electrodes.

Chapter 7: Application of electrochemically synthesised neutral and P-doped PANI–PSSA for the determination of tetrodotoxin

The equivalent circuit in accordance with the Nyquist plot as presented in Figure 7.18. In this model, the double-layer capacity and the Warburg impedance for semi-infinite linear diffusion are replaced by two constant-phase elements CPE1 and CPE2 which correspond, respectively, to a capacity at an inhomogeneous electrode surface and to the diffusion of ions in the electrode. Thus, the double-layer capacity and Warburg impedance of the Randles circuit are replaced by the constant-phase elements. The purpose of this study brings the focus of analysis on the charge transfer resistance (R_{ct}) and the double-layer capacity (C_{dl}). The proposed equivalent circuit for the modified PSSA-doped PANI electrode is represented and can be compared with the PTS-doped PANI electrode [253]. Fitting of the equivalent circuit was carried out using the ac impedance simulator of the Zview2 software and the resistances of the equivalent circuit are reported in Table 7.12.



Figure 7.18: Equivalent circuit for neutral and p-doped PANI-PSSA electrode. R_s is the solution resistance, R_1 is the charge transfer resistance (R_{ct}), $CPE1$ denote constant-phase element.

Chapter 7: Application of electrochemically synthesised neutral and P-doped PANI–PSSA for the determination of tetrodotoxin

Table 7.16: Equivalent circuit resistance deduced by fitting Nyquist plots to circuit of neutral and p-doped PANI–PSSA

WE	Potential [V]	R_{ct} [Ω]		R_s [Ω]	
		Neutral PANI–PSSA	p-doped PANI–PSSA	Neutral PANI–PSSA	p-doped PANI–PSSA
Au	-0.5	894980 \pm 28890	848430 \pm 20100	838.4 \pm 5.90	676.8 \pm 3.12
	-0.3	62762 \pm 22310.3	90051 \pm 2440	825.3 \pm 6.98	670.7 \pm 3.89
	-0.1	620.6 \pm 3.89	168.9 \pm 1.73	843.5 \pm 1.62	645.6 \pm 1.24
	0.1	0.0	0.0	868.3 \pm 0.52	684.9 \pm 3.1
	0.3	386.1 \pm 1.57	3457 \pm 99.5	856.4 \pm 0.79	721.5 \pm 21.33
	0.5	71240 \pm 2617.6	88187 \pm 2512.8	832.9 \pm 11.22	774.5 \pm 18.05
GC	-0.5	52343 \pm 1289.2	41511 \pm 2019	477.4 \pm 2.77	370 \pm 5
	-0.3	17368 \pm 475.83	16092 \pm 642	459.1 \pm 2.58	364.7 \pm 6.46
	-0.1	108.2 \pm 1.512	110.3 \pm 1.18	459.7 \pm 1.12	384.3 \pm 0.83
	0.1	0.0	0.0	460.1 \pm 0.122	392.4 \pm 0.19
	0.3	37.07 \pm 3	3349 \pm 49.85	497.4 \pm 0.5	413.3 \pm 4.7
	0.5	14799 \pm 283.19	25198 \pm 363.8	482.9 \pm 3.5	454.2 \pm 5.44
PG	-0.5	64936 \pm 1913	58065 \pm 1479.1	327.7 \pm 2.70	305.9 \pm 3.78
	-0.3	13836 \pm 525.13	55573 \pm 1580.3	314.7 \pm 1.98	300.4 \pm 4.2
	-0.1	83.09 \pm 0.95	20896 \pm 473	319.6 \pm 0.609	289 \pm 5
	0.1	0.0	21019 \pm 397	324 \pm 0.19	303 \pm 4
	0.3	48.92 \pm 0.49	67301 \pm 2308	320.5 \pm 0.360	311 \pm 3
	0.5	13372 \pm 274.91	94793 \pm 391	343.5 \pm 2.14	326 \pm 2
Pt	-0.5	13295 \pm 490	38546 \pm 1600	1225 \pm 34	2657 \pm 160
	-0.3	11521 \pm 419	41072 \pm 1282	755 \pm 3	2635 \pm 171
	-0.1	338.8 \pm 2.86	374.1 \pm 2.9	761 \pm 1.33	975.71.48
	0.1	0.0	0.0	754.7 \pm 0.33	1007 \pm 0.38
	0.3	204.4 \pm 2.14	8037 \pm 194.21	744 \pm 1.37	1156 \pm 16.125
	0.5	54800 \pm 1186.9	55335 \pm 1368.9	895.3 \pm 5.00	1201 \pm 15.33

Chapter 7: Application of electrochemically synthesised neutral and P-doped PANI-PSSA for the determination of tetrodotoxin

Figure 7.19 shows the dependence of R_{ct} on the electrode potential. R_{ct} decreased monotonously from -0.5 to -0.1 V and increased again from -0.1 to 0.5 V. This increasing effect of R_{ct} when electrode potential shifts in the anodic direction (-0.1 to 0.5 V) was reported by Umeda *et al.*[254]. These authors have shown that R_{ct} certainly reflects the surface charge transfer when the R_{ct} decreases and the electrode potential shifts to the cathodic direction. The reference [198] has shown that the charge transfer and double layer charging across the interface film|solution must be considered [255].

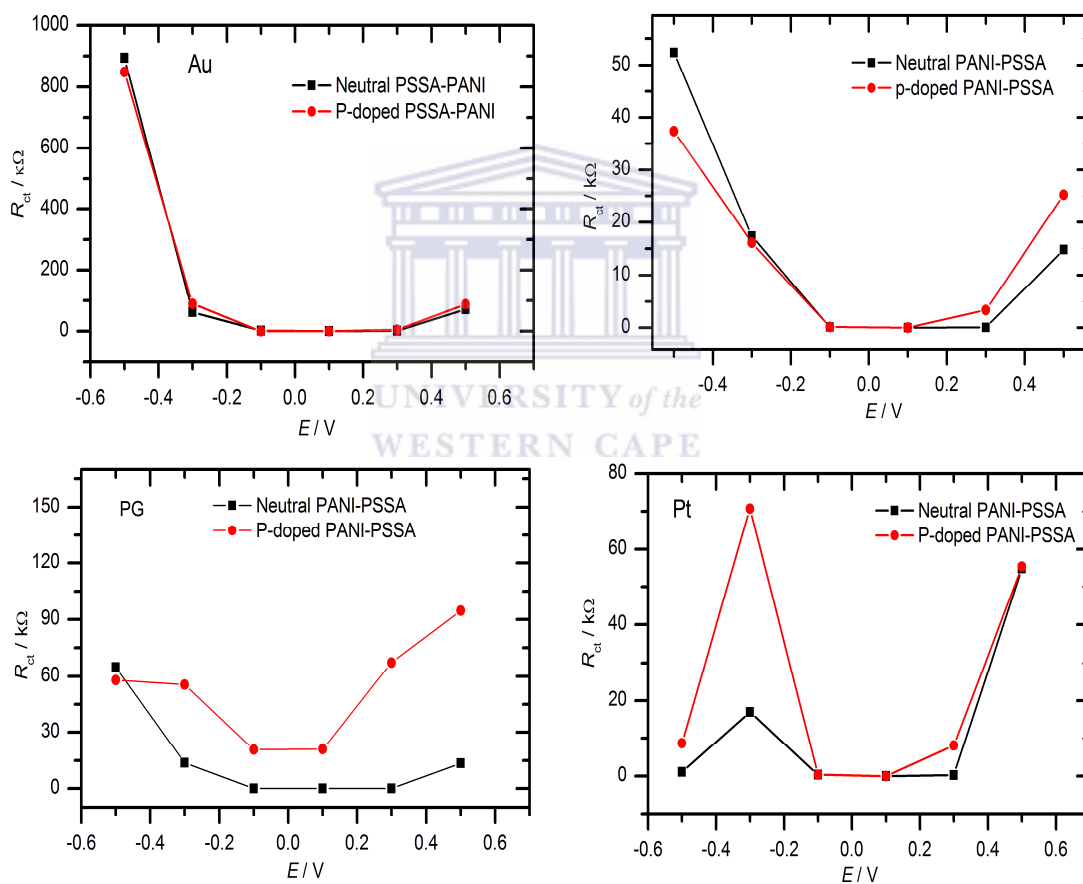


Figure 7.19: Plot of charge transfer resistance (R_{ct}) versus potential.

The shape of the curve is parabola with a minimum at 0.1 V where $R_{ct} = 0 k\Omega$. For the electrochemical biosensor view, the best potential for further experiment is the potential

Chapter 7: Application of electrochemically synthesised neutral and P-doped PANI–PSSA for the determination of tetrodotoxin

with the R_{ct} value different to zero but close to zero. As can be seen from Figure 7.19, the potential with R_{ct} close to zero is -0.1 V. Thus, the impedance analysis of neutral and p-doped PANI–PSSA modified electrodes should be measured at - 0.1 V for further application. This conclusion is taken based on some research reports [254, 256-257].

Table 7.17: Electrochemical kinetic parameters of neutral and p-doped PANI–PSSA study in acetate buffer pH 4.8

WE	Neutral PANI-PSSA			p-doped PANI-PSSA		
	R_{ct} [Ω]	$i_0 \times 10^{-5}$ [A]	$k^0 \times 10^{-5}$ [cm s ⁻¹]	R_{ct} [Ω]	$i_0 \times 10^{-5}$ [A]	$k^0 \times 10^{-5}$ [cm s ⁻¹]
Au	621 ± 4	4.14	21.33	169 ± 2	15.21	78.34
GC	108 ± 2	23.79	34.84	110 ± 1	23.36	34.21
PG	83 ± 1	30.96	45.34	20896 ± 473	0.123	0.18
Pt	339 ± 3	7.58	39.05	374 ± 3	6.87	35.38

Unlike on gold electrode, the R_{ct} value for neutral PANI–PSSA is smaller than R_{ct} of p-doped polymers films on other electrodes. These results indicate that the faradic reaction on the neutral PANI–PSSA modified electrode|electrolyte interface is faster and with the p-doped polymer, the reaction is slow. The exchange current density (i_0) which is the rate of the oxidation and reduction reaction at an equilibrium electrode is calculated. Equation 7.5 shows that i_0 is inversely related to R_{ct} thus, i_0 of neutral polymer films is higher on GC, PG, and Pt electrodes than the i_0 of p-doped polymer. The standard heterogeneous rate constant (k^0) is higher for neutral PANI–PSSA as compared to the p-doped PANI–PSSA (Tab. 6.17). A similar work was done, small value of k^0 for electroactive polymers of

Chapter 7: Application of electrochemically synthesised neutral and P-doped PANI–PSSA for the determination of tetrodotoxin

PANI and PANI–ASA in 1 M HCl [102, 250] was compared to this value obtained of k^0 for both neutral and p-doped PAN–PSSA in sodium phosphate buffer.

The electrochemical synthesis and characterisation of neutral and p-doped PANI–PSSA on Au, GC, PG, and Pt electrodes in sodium phosphate buffer pH 7.04 and acetate buffer pH 4.8 using cyclic voltammetry and electrochemical impedance spectroscopy is done. The electrosynthesis of neutral PANI–PSSA on GC electrode in KCl characterised in 0.2 M Na_2HPO_4 and 0.1 M citric acid buffer pH 7.0 has been reported [103]; results show similarity to the observation recorded in this work on GC electrode in sodium phosphate buffer pH 7.04. Qakala on the other hand reported similar results for neutral PANI–PSSA films prepared in H_3PO_4 and the CV was measured on GC electrode in McIIB buffer [258]. The kinetic parameters of neutral and p-doped PANI–PSSA calculated in both media phosphate and acetate buffer on different electrode shows that: (i) p-doped polymer is more stable than neutral in phosphate buffer as well as in acetate buffer; (ii) both modified-polymer/electrodes are irreversible in phosphate as well as in acetate buffer; (iii) acetate buffer is more appropriate for polymer films application as electrochemical sensors and biosensor than sodium phosphate buffer; (iv) Au and PG electrodes are more specified for the electrochemical synthesis of neutral PANI–PSSA than GC and Pt electrodes which are more directed to the polymerisation of p-doped PANI–PSSA; (v) the cyclic voltammograms of neutral and p-doped polymer films in acetate buffer is reported for the first time on Au, GC, PG, and Pt electrodes in this study.

Chapter 7: Application of electrochemically synthesised neutral and P-doped PANI–PSSA for the determination of tetrodotoxin

7.7 Effect of polarity of solvent on the solubility of neutral and p-doped PANI–PSSA

The electroactivity studied of neutral and p-doped PANI–PSSA polymer films dispersed in two different solvents was further investigated. A major handicap towards large scale PANI applicability is related to its insolubility and intractability. The solubility of the PANI has been targeted for the incorporation of sulphonated heteronuclear aromatic hydrocarbons into the PANI backbone. In view of this, the solubility of both forms of PANI–PSSA is tested out in two different solvents. Results showed that the neutral and p-doped PANI–PSSA exhibited considerable improved solubility in polar organic solvents such as DMF and DMSO. However, it was found that the neutral PANI–PSSA was very soluble in DMSO while the p-doped PANI–PSSA was more soluble in DMF. Similar reports were obtained for substituted doped PANI in other reports [102, 259-260]. The total solubility was characterised by the colour obtained; the neutral PANI–PSSA films formed on the electrode surface gave a green colour as observed in DMSO but not in DMF. The p-doped PANI–PSSA films formed on the electrode surface was blue and this colour was observed in DMF but not in DMSO (Fig. 7.20). The difference of solubility obtained can be explained with the polarity of the solvents. Indeed, according to the classification solvent in terms of polarity, DMSO and DMF are dipolar aprotic solvents but DMSO is more polar than DMF. As shown in Figures 7.6 and 7.7 the base emeraldine green has more ions than in salt emeraldine blue. It is known that the more polar the solvent the more it dissolves anionic compounds. Thus, base emeraldine green was more dispersed in DMSO than in DMF and the salt emeraldine blue with fewer ions dissolved more in DMF.

Chapter 7: Application of electrochemically synthesised neutral and P-doped PANI–PSSA for the determination of tetrodotoxin



Figure 7.20: Neutral and p-doped PANI–PSSA dispersed in DMF and DMSO.

7.8 The characterisation of neutral and p-doped PANI–PSSA using UV-Vis absorption analysis

The ultimate aim of this chapter was to apply the prepared polymer composites for the fabrication of biosensors. With biosensors, conducting polymer composites are expected to provide a suitable micro-environment for biomolecule immobilisation as well as to electromediate between the aptamer redox centre and the electrode. For the composites to occupy the above posts, it is demanded that they must be both stable and electroactive. In this respect, spectroscopy techniques come in handy

The neutral and p-doped polymers were dispersed in DMF and DMSO and the electronic absorption spectra of both polymers composites are given in Figure 7.20. Three major absorption peaks were observed at 277, 350 and 630 nm showing characteristic band at 350.6 nm similar to the one of undoped PANI. The peak is due to the electronic transition $\pi \rightarrow \pi^*$ related to the C=C of the extent of conjugation between the adjacent phenylene or

Chapter 7: Application of electrochemically synthesised neutral and P-doped PANI–PSSA for the determination of tetrodotoxin

(benzoid) rings in the polymeric chain [102, 251]. The band around 277 and 290 nm corresponds to the chromophores C–N of DMF and PANI–PSSA, $n \rightarrow \sigma^*$ transition. The broad peak shown at 630 nm is attributed to the shifting of electron from benzenoid ring to quinonoid ring [261].

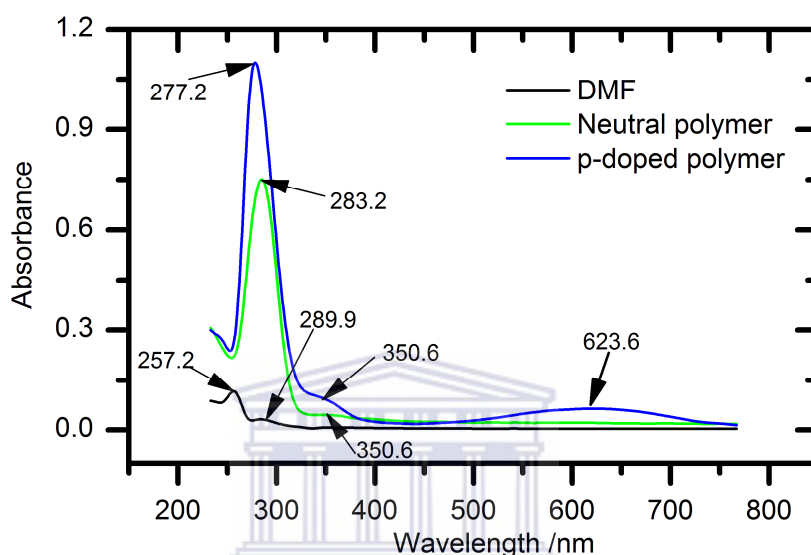


Figure 7.21: UV-vis spectra of neutral PANI–PSSA and p-doped PANI–PSSA composites in DMF as solvent.

Figure 7.22 is the absorption spectra of both composites dispersed in DMSO. The spectrum of p-doped polymer (blue line) and neutral polymer (green line) reveals four and five characteristics peaks respectively. The first peak observed at 243 nm involves the transition $n \rightarrow \sigma^*$ due to the chromophores C–S of DMSO. The peak in wavelength range 293.9 and 300.6 is due to the $\pi \rightarrow \pi^*$ transition of benzenoid ring of aniline (C=C), the absorption band at 344.6 nm is due to the $\pi \rightarrow \pi^*$ transition of benzenoid ring of PSSA. This higher wavelength shift is due to the presence of a strong donor group, $-\text{SO}_3\text{H}$, attached to the benzenoid ring of PSSA. The absorption in wavelength range 421.3 to 450.6

Chapter 7: Application of electrochemically synthesised neutral and P-doped PANI–PSSA for the determination of tetrodotoxin

nm are due to polaron $\rightarrow \pi^*$ transition [261]. A broad peak at 605.6 is observed on neutral polymer curve (green line) corresponds to the shifting of electron from benzenoid ring to quinonoid ring while the absorption in the p-doped and neutral polymer composites, in DMF and DMSO respectively is explained by the polarity of the solvent. The shifting of electron from benzenoid to quinonoid ring is dependent on the solvent dissolved the polymer composites.

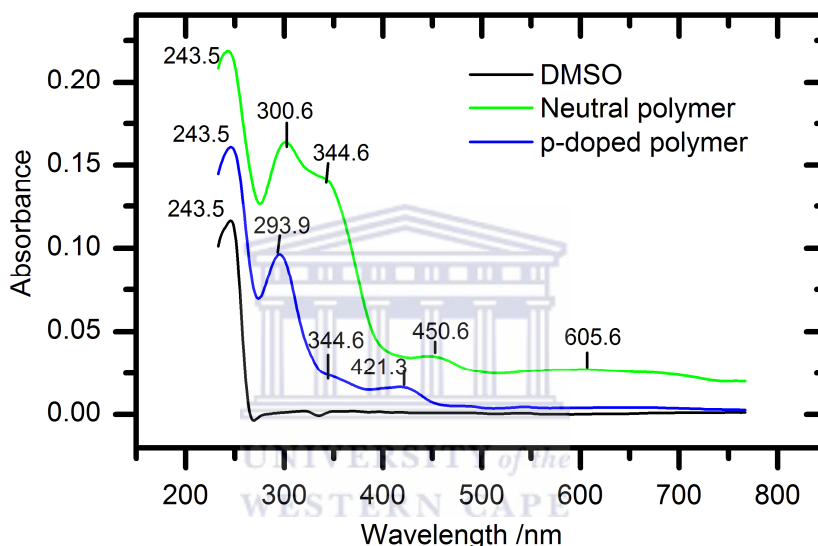


Figure 7.22: UV-vis spectra of neutral PANI-PSSA and p-doped PANI–PSSA composites in DMSO as solvent.

7.9 Emission wavelengths of neutral and p-doped PANI–PSSA

The absorption wavelengths obtained using UV-Vis analysis was used to measure the intensity of the photons emitted from the polymers after absorbing photons. The emission wavelengths of both neutral and p-doped polymers were measured using fluorescence emission spectroscopy. Figure 7.23 illustrates the fluorescence emission spectra of neutral and p-doped PANI–PSSA dispersed into the DMF and DMSO at different excitation

Chapter 7: Application of electrochemically synthesised neutral and P-doped PANI–PSSA for the determination of tetrodotoxin

wavelengths. It is clearly seen that the fluorescence spectrum of neutral PANI–PSSA exhibits strong fluorescence emission than that of p-doped composites at 350 nm in DMF. However, the fluorescence spectrum of p-doped PANI–PSSA at 296 nm exhibits strong fluorescence emission than the spectrum of neutral PANI–PSSA at 342 nm in DMSO. The difference of the fluorescence emission observed with the two polymer composites is due to the polarity of the solvent. When the polymer is excited with the corresponding excitation wavelength, the emission band is observed at the emission wavelength higher than the excitation wavelength. It is observed that when the excitation wavelength is less than 350 or greater than 350 in DMF and less than 342 nm in DMSO, the emission intensity is not significant. The best excitation band for both neutral and p-doped in DMF is 350 nm while in DMSO the best excitation wavelength is 342 nm and 296 nm for neutral polymer and p-doped polymer respectively. The emission band in DMSO is monochromatic, showing the defined molecular structure and weak interchain interaction or electron photon-coupling effect at the excited state of composite [262]. In DMF, the emission is polychromatic indicating the strong interaction effect at the excited state of the PANI–PSSA composites.

Chapter 7: Application of electrochemically synthesised neutral and P-doped PANI-PSSA for the determination of tetrodotoxin

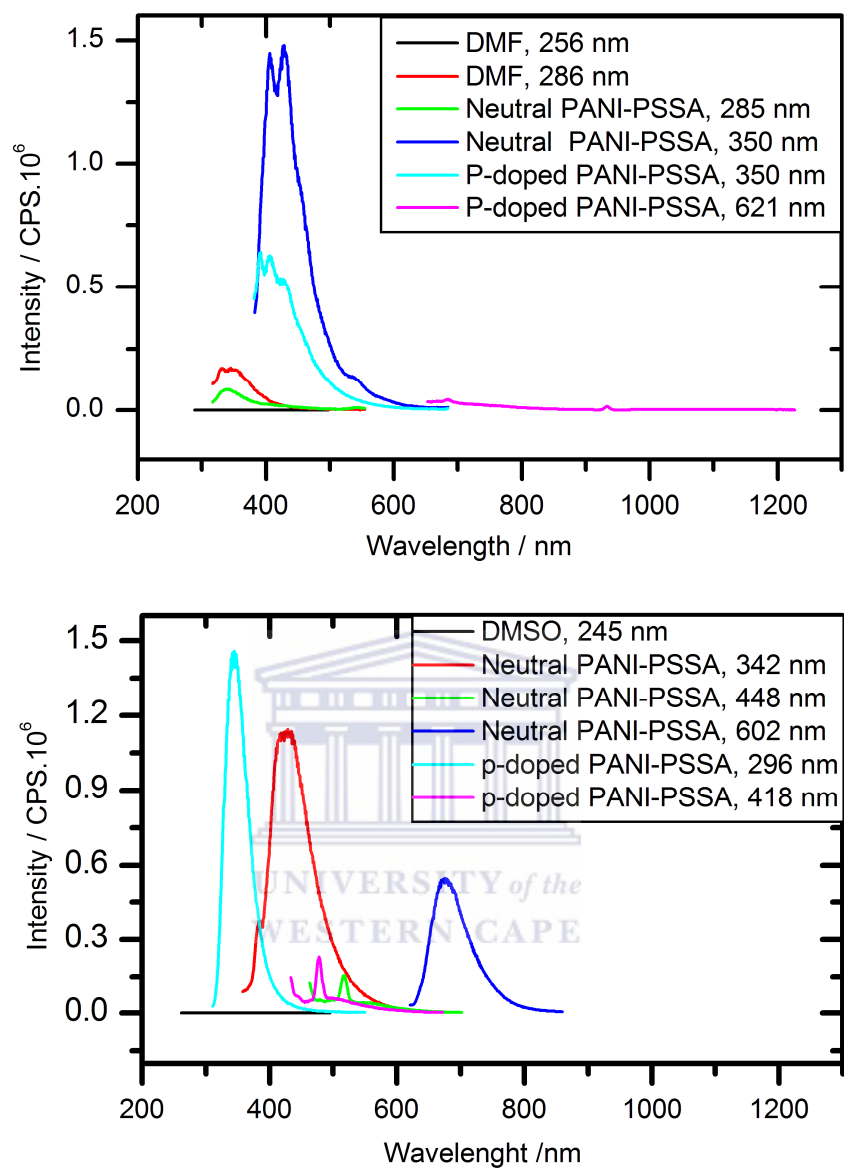


Figure 7.23: Emission spectra of neutral and p-doped obtained in DMF and DMSO solvent.

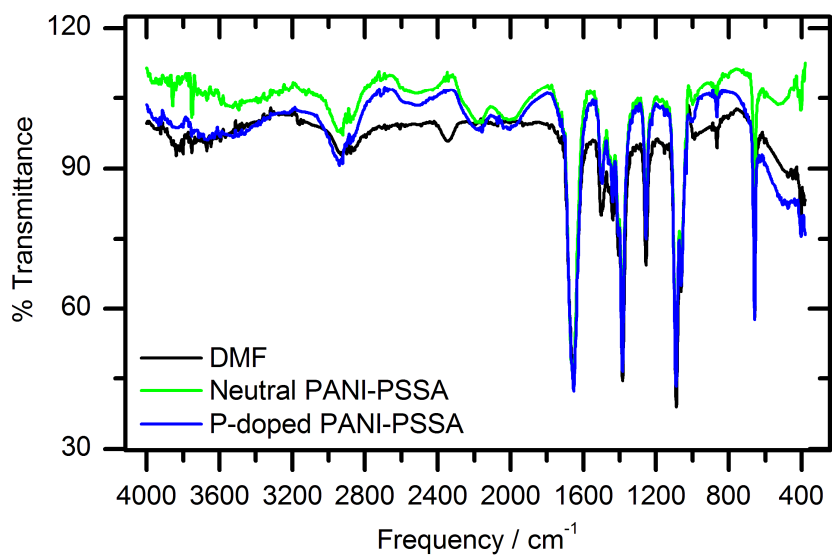
Chapter 7: Application of electrochemically synthesised neutral and P-doped PANI–PSSA for the determination of tetrodotoxin

7.10 Characterisation of neutral and p-doped PANI–PSSA using FTIR analysis

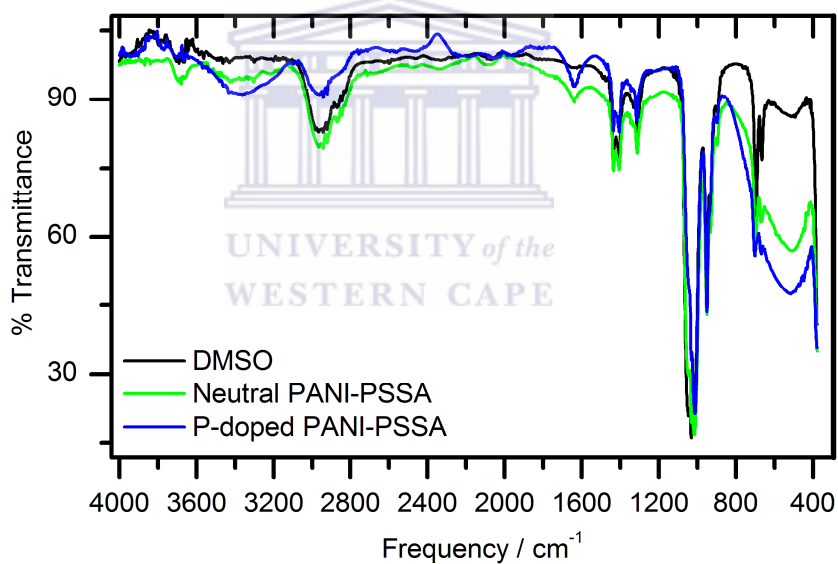
The neutral and p-doped polymer films were prepared on bare electrodes surface and dissolved in DMF and DMSO for spectroscopic analysis. The FTIR spectra of neutral and p-doped PANI–PSSA solutions were then recorded. In DMF, the spectrum shows main characteristic vibrations around 3671, 2942, 2515, 2178 and 2000, 1662, 1093 cm^{-1} . The peak at 3671 cm^{-1} is attributed to –OH and –NH stretching in PSSA while peak around 2942 cm^{-1} represents the –CH– stretching in PSSA chain. In the range of 1662 to 1093 cm^{-1} , neutral and p-doped observed is due to the –C=C– vibration of benzenoid ring, –NH– deformation, due to the –C–N– stretching and C–N benzenoid ring stretching in the polymer chain [263]. The bands at 12178 cm^{-1} and 2000 cm^{-1} are the characteristic bands of N–quinoid and benzenoid rings and their presence enhance the conducting state of the polymer. The FTIR studies reveal the formation of composite materials and help to obtain their compositions qualitatively. In case of composites, the out of plane H deformation, i.e. para coupling was observed at $\sim 655 \text{ cm}^{-1}$. The peak at 1082–1284 cm^{-1} corresponds to –SO₃H stretching in all these compositions. The similar vibrations were also reported by Lin der-shyu who studied the electrochemical response time and the electron paramagnetic resonance of the substituted polyaniline (PANI) complexes poly(o-phenetidine)–poly(styrene sulfonic acid) and poly(2-ethylaniline) [264].

In DMSO (Fig.7.24b), characteristic vibrations are observed around 3386, 2960, 1635, 1436 to 1319, and 1311 to 1019 cm^{-1} . The same interpretations given to the spectrum recorded in DMF are applied on the spectrum obtained in DMSO.

Chapter 7: Application of electrochemically synthesised neutral and P-doped PANI-PSSA for the determination of tetrodotoxin



(a)



(b)

Figure 7.24: FT-IR spectra of neutral and p-doped PANI-PSSA composites in (a) DMF and (b) DMSO.

The difference between the two polymers observed in DMF is that the intensity of this band increases in p-doped polymer than neutral polymer composites. On the other hand, in DMSO, the vibrations are more intense on neutral PANI-PSSA polymer than on p-doped

Chapter 7: Application of electrochemically synthesised neutral and P-doped PANI–PSSA for the determination of tetrodotoxin

PANI–PSSA polymer composites. The characteristic bands of both PSSA and PANI reported literature review (Chapter 3, section 3.1.4) confirms the presence of both phases in composite materials. These results when compared to the PANI and PSSA alone, shows all the bands possessing a systematic shifting that indicates the existence of significant interaction between PANI and PSSA in the composite material.

7.11 Characterisation of neutral and p-doped PANI–PSSA using SEM analysis

After the FTIR analysis of both polymer composites, the SEM analysis was done further. Figure 7.25 is showing the SEM micrographs of both polymers electrodeposited on bare screen printed GC electrodes. The images were taken at the same conditions. The micrograph of bare screen-printed carbon electrode shows a smooth surface. The effect of the different ways of electrochemical polymerisation done under the same conditions was clearly observed in the SEM images. Both neutral and p-doped PANI–PSSA particles possess almost uniform distribution of size with spherical shapes. Diameter of the particles observed from SEM images changes approximately from 70 to 100 nm for both neutral PANI–PSSA and a small diameter of about 40 nm for PANI–PSSA synthesised chemically in H₂O/HCl was reported by Cho *et al.* [245]. The image (Fig. 26) shows that the spherical balls of neutral polymers are dispersed on the electrode surface while the balls of p-doped polymers are closely packed. The spherical balls close packing of the polymer is expected to increase the conductivity of the p-doped polymer (Fig.27). This indicates that the movement of electrons in neutral PANI–PSSA is slower compared to p-doped PANI-PSSA polymer composites chain.

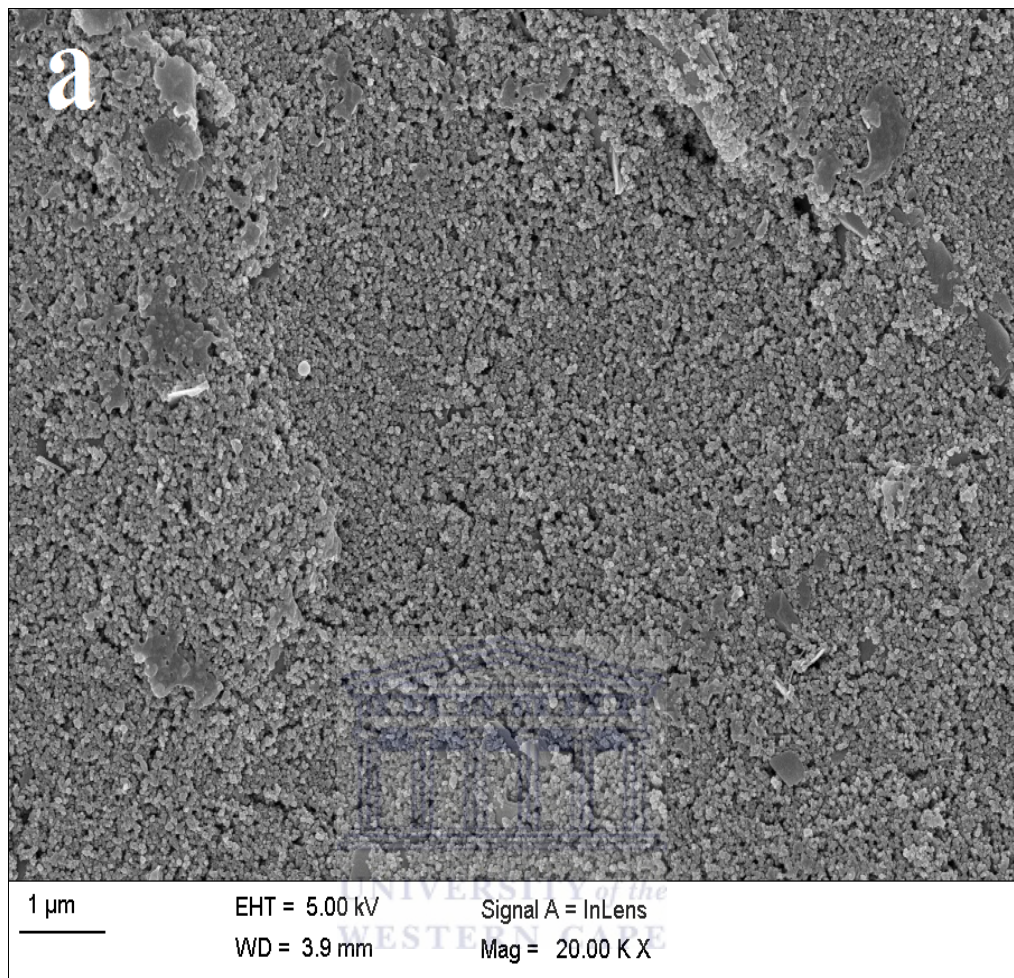


Figure 7.25: SEM images of bare screen-printed carbon electrode.

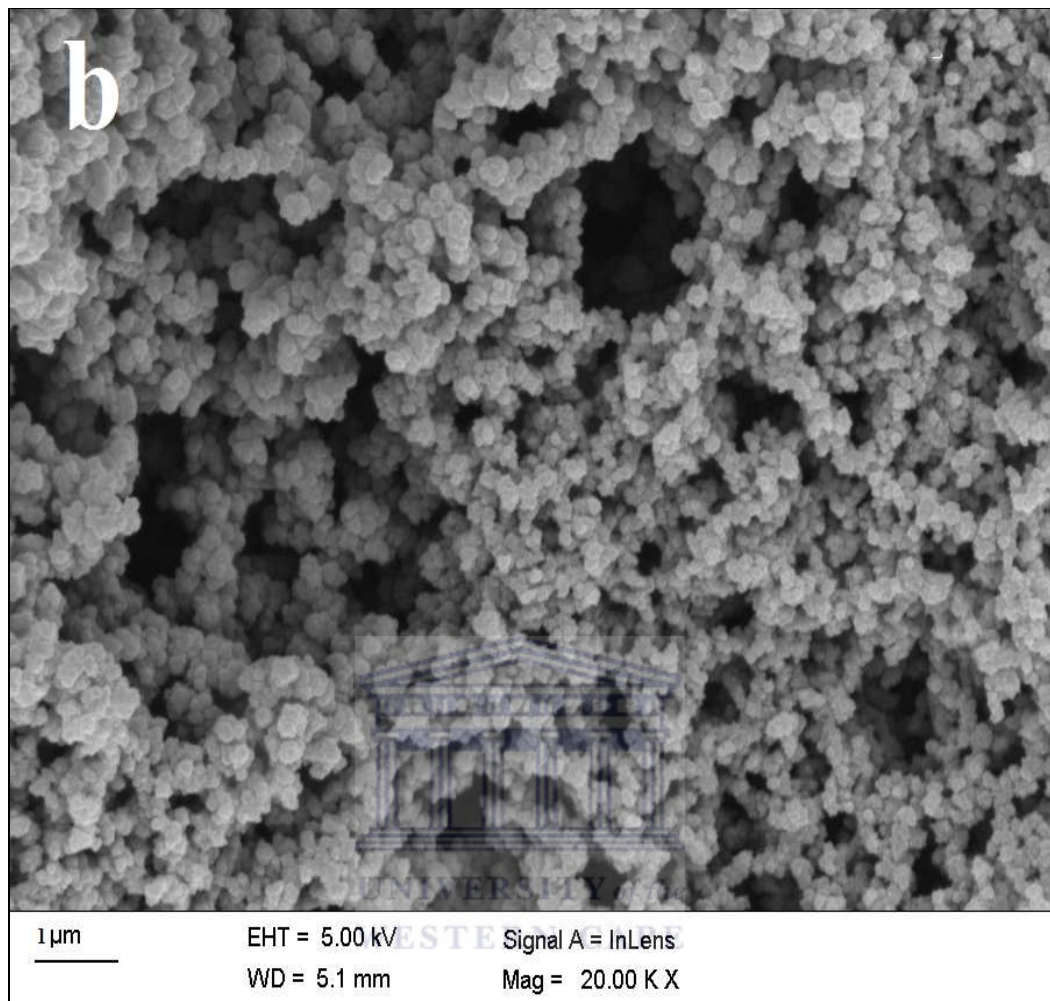


Figure 7.26: SEM images of neutral PANI-PSSA composites.

Chapter 7: Application of electrochemically synthesised neutral and P-doped PANI-PSSA for the determination of tetrodotoxin

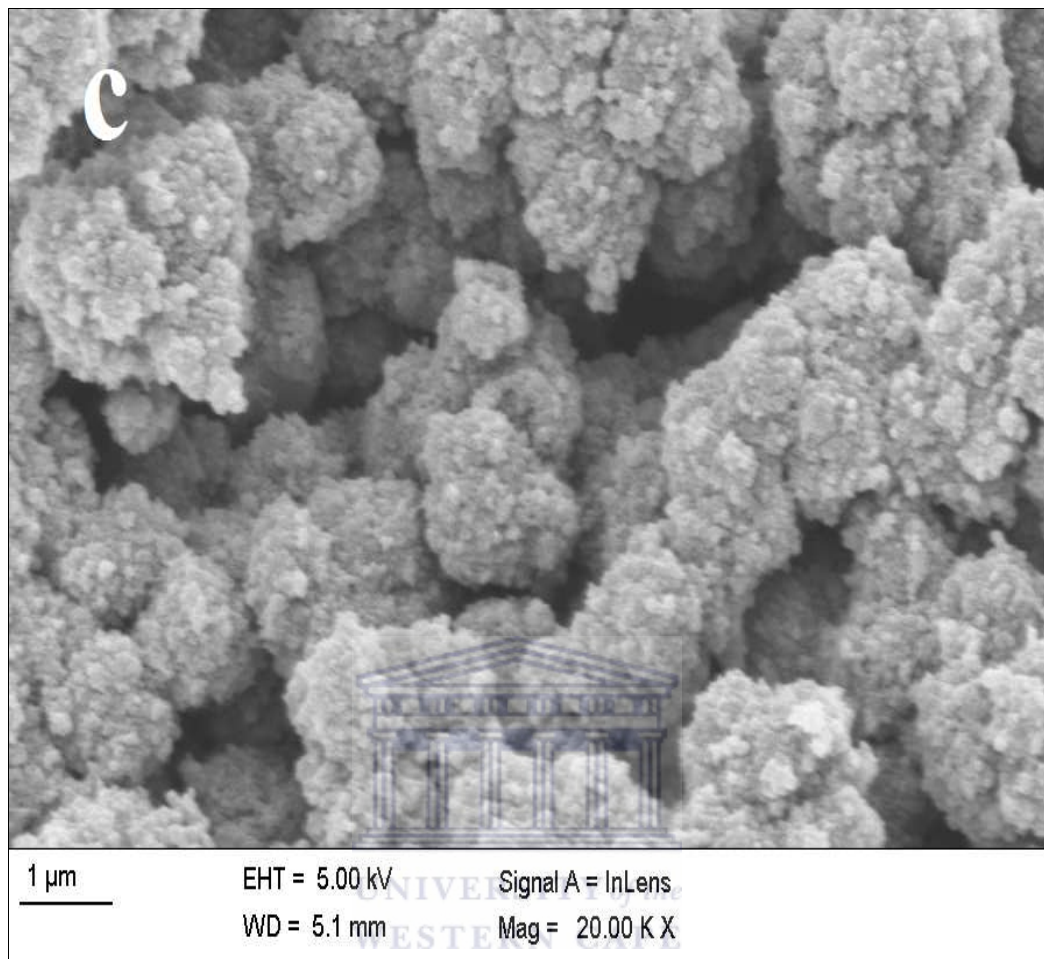


Figure 7.27: SEM images of p-doped PANI-PSSA composites.

Chapter 7: Application of electrochemically synthesised neutral and P-doped PANI–PSSA for the determination of tetrodotoxin

7.12 Characterisation of neutral and p-doped PANI-PSSA using TEM analysis

TEM micrographs (Fig. 7.26) were further obtained to examine the shape and size distribution of the neutral and p-doped PANI–PSSA composites. The TEM images confirm the difference of morphology found with SEM images between neutral and p-doped PANI–PSSA. Image (b) shows that the p-doped composites have porous and smooth chain structure which may cause considerable increase of the conductive path way resulting in high conductivity. This agrees with results obtained by Mavundla *et al.* [265].



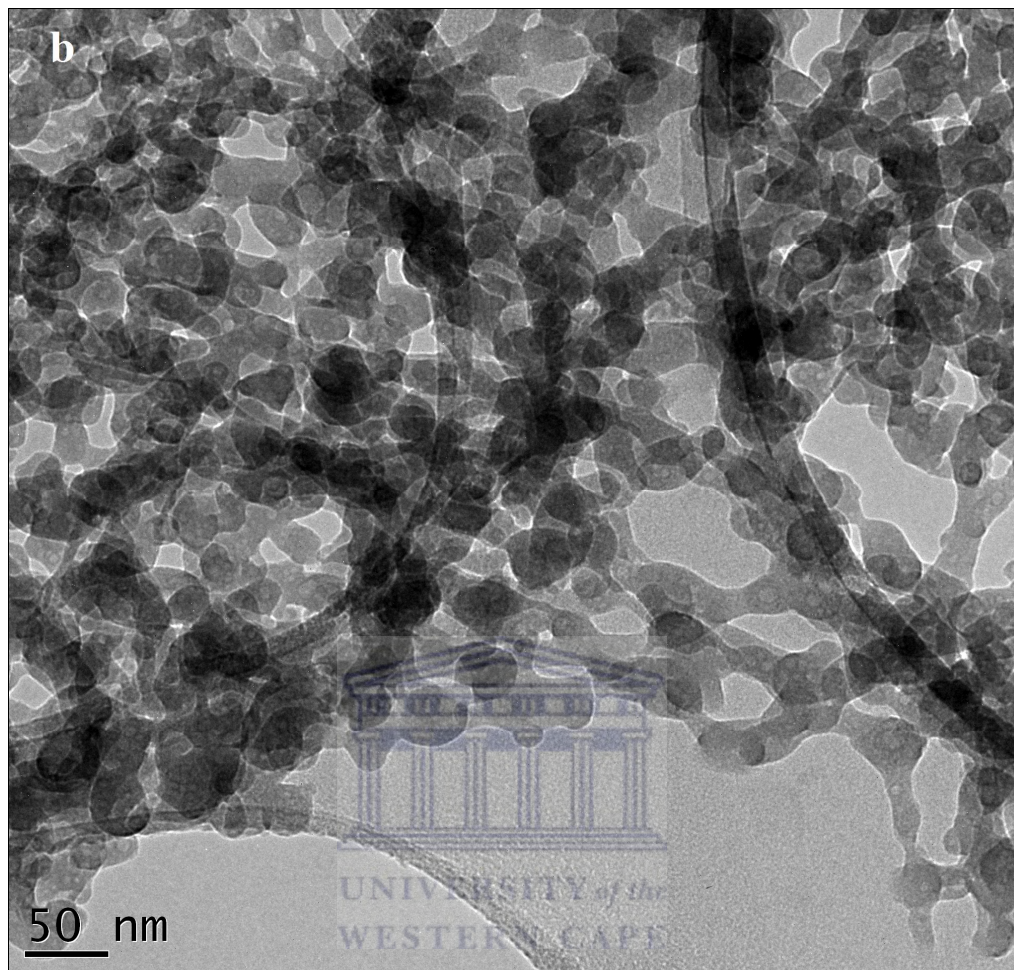


Figure 7.28: TEM images of neutral PANI-PSSA composites.

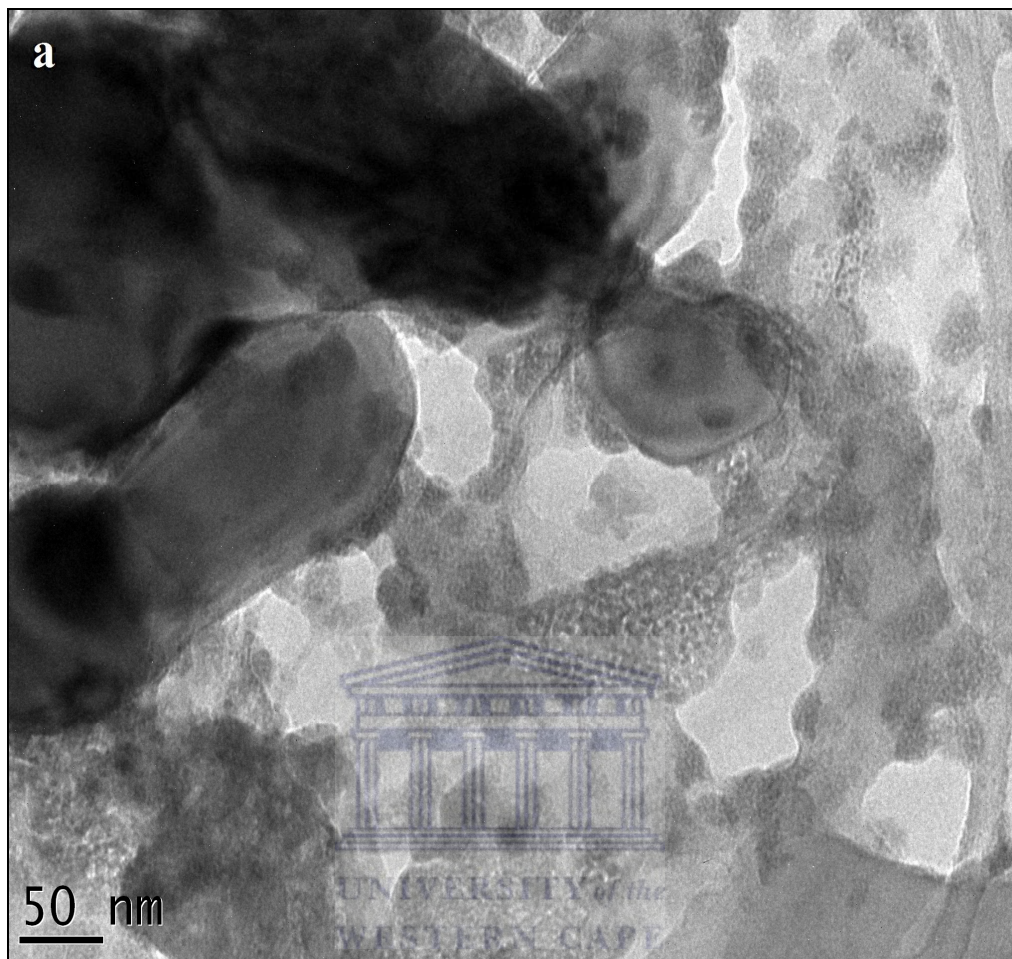


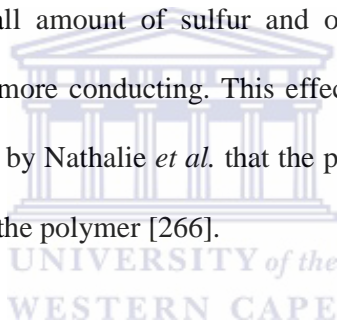
Figure 7.29: TEM images of (b) p-doped PANI-PSSA composites.

The Energy Dispersive X-ray Spectroscopy (EDS) coupled with TEM analysis of both polymers was carried out to give elemental composition of individual points and/or to map out the lateral distribution of elements from the imaged area. The spark creates an emission of radiation from the excited sample surface with wavelengths characteristic of the elemental composition. The spectrum of radiation is separated into the distinct element lines and the intensity of each line is measured. These were then precisely converted into concentration values for each element present. EDS analysis results (Fig. 7.28 and 7.29)

Chapter 7: Application of electrochemically synthesised neutral and P-doped PANI–PSSA for the determination of tetrodotoxin

showed the presence of carbon, oxygen, sodium and phosphorus on the surface of the neutral and p-doped PANI–PSSA composites. The sodium and phosphorus atoms shown on the spectra arise from the sodium phosphate buffer as a result of dispersion in DMF or DMSO solvent. Figure 7.28 shows the intensity of the O, N, S, and C atoms is smaller as compared to the intensity obtained in Figure 7.29.

Unlike the p-doped polymer, the neutral polymer possesses a high conductivity compared to the p-doped PANI–PSSA. This can be explained with the fact the p-doped contained high quantity of sulfur and oxygen while the neutral contains very small quantity of sulfur and oxygen atoms. The small amount of sulfur and oxygen atoms present in neutral PANI–PSSA make the later more conducting. This effect of oxygen and sulfur atom on the conductivity was reported by Nathalie *et al.* that the presence of sulfur, nitrogen atoms decreases the conductivity of the polymer [266].



Chapter 7: Application of electrochemically synthesised neutral and P-doped PANI-PSSA for the determination of tetrodotoxin

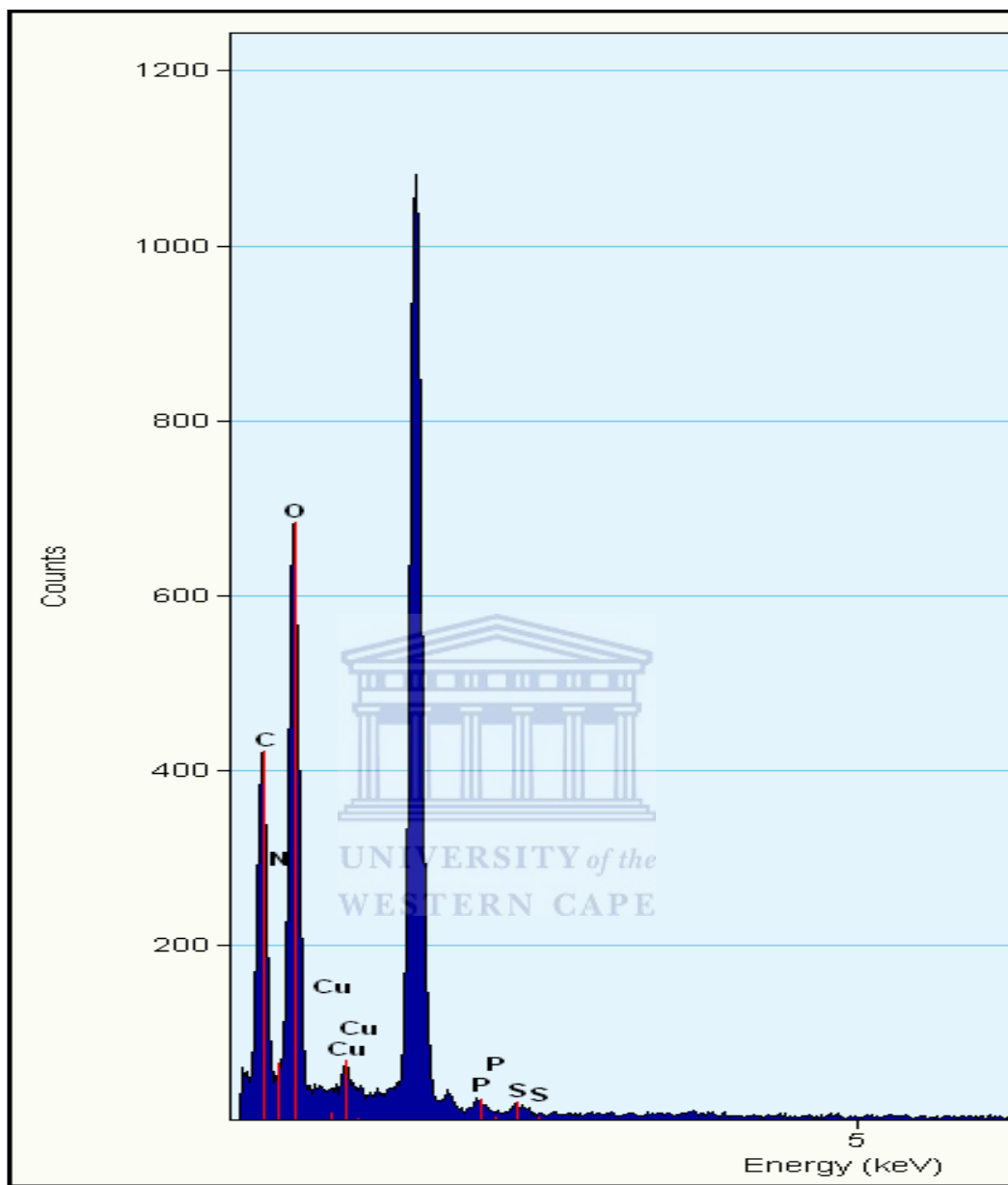


Figure 7.30: Energy-dispersive X-ray spectrum (EDX) of neutral PANI-PSSA PANI-PSSA films in DMF.

Chapter 7: Application of electrochemically synthesised neutral and P-doped PANI-PSSA for the determination of tetrodotoxin

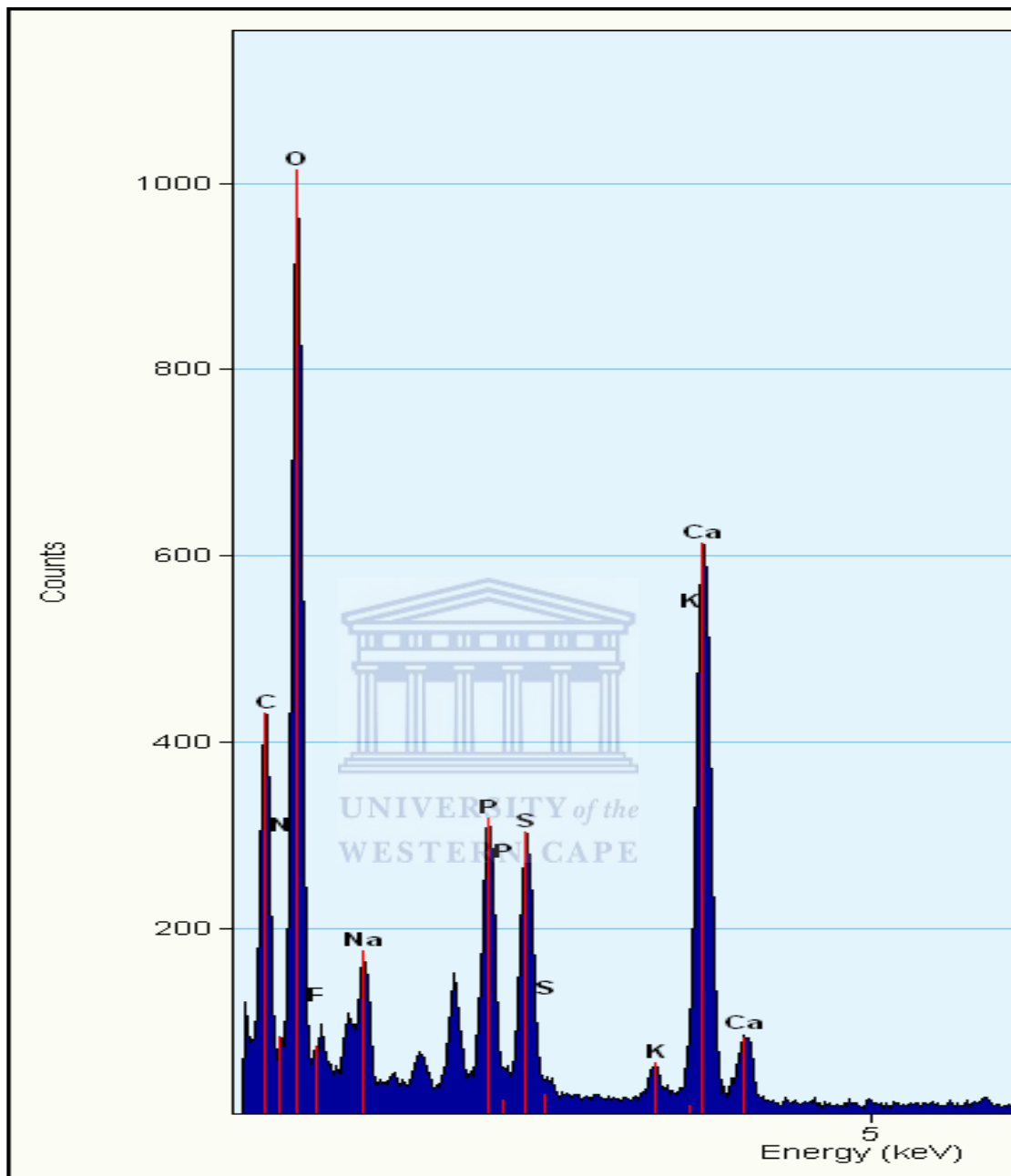


Figure 7.31: Energy-dispersive X-ray spectrum (EDX) p-doped PANI-PSSA films in DMF.

Chapter 7: Application of electrochemically synthesised neutral and P-doped PANI–PSSA for the determination of tetrodotoxin

7.13 Application of p-doped PANI–PSSA films on the construction of biosensor for the detection of tetrodotoxin

After analysis and interpretations of the electrosynthesised neutral and p-doped PANI–PSSA in sodium phosphate and acetate buffer solutions, p-doped and acetate buffer were chosen for further experiments. The detection of TTX is carried on with aminylated aptamer based on p-doped PANI–PSSA modified electrode where the glutaraldehyde is attached. The glutaraldehyde being a cross-linker agent and a dialdehyde engages its aldehyde group to form the covalent bond with amine group of other molecules. For this detection specifically, –CHO, of glutaraldehyde reacts with amine group of PANI chains in the PANI–PSSA film at one end and amine group, –NH–, of NH₂–aptamer at the other end which results the formation of stable covalent bond.

7.14 Detection of TTX based on PANI–PSSA, GLu/PANI–PSSA and NH₂–Atp/Glu/PANI–PSSA /Au sensors

The detection of TTX was firstly done on three different electrodes. All three electrodes were modified with p-doped PANI–PSSA. The first modified electrode was directly dipped into 5 μM of TTX solution for four hours and the cyclic voltammograms and EIS spectra were recorded (Figs.7.28a and b). On the second and third modified electrodes, the glutaraldehyde was attached by deeping the modified electrode into the glutaraldehyde (Glu) solution for four hours. The second modified-Glu/PANI–PSSA/electrode was incubated for four hours into TTX solution and the CV and EIS spectra were recorded (Fig.7.28c and d). Afterwards, the third modified-Glu/PANI–PSSA electrode,

Chapter 7: Application of electrochemically synthesised neutral and P-doped PANI–PSSA for the determination of tetrodotoxin

NH₂–aptamer (Apt) was immobilised by dipping into 2 μM of aptamer for four hours. The modified-Apt/Glu/PANI–PSSA/electrode was also dipped into TTX solution for 4 hours and the CV and impedance spectra were measured (Fig. 7.32e and f). Figure 7.32 is showing that, the detection using PANI–PSSA/Au is not relevant, but the glutaraldehyde is added (Glu/PANI–PSSA/Au), the detection is improved for 53% and when the aptamer is immobilized (Apt/Glu/PANI–PSSA/Au), the biosensor the response is more pronounced. Therefore, aptamer enhance the charge transfer resistance which subsequently improves the sensor creating great importance and necessary for its use as a specific agent for the detection of TTX.



Chapter 7: Application of electrochemically synthesised neutral and P-doped PANI-PSSA for the determination of tetrodotoxin

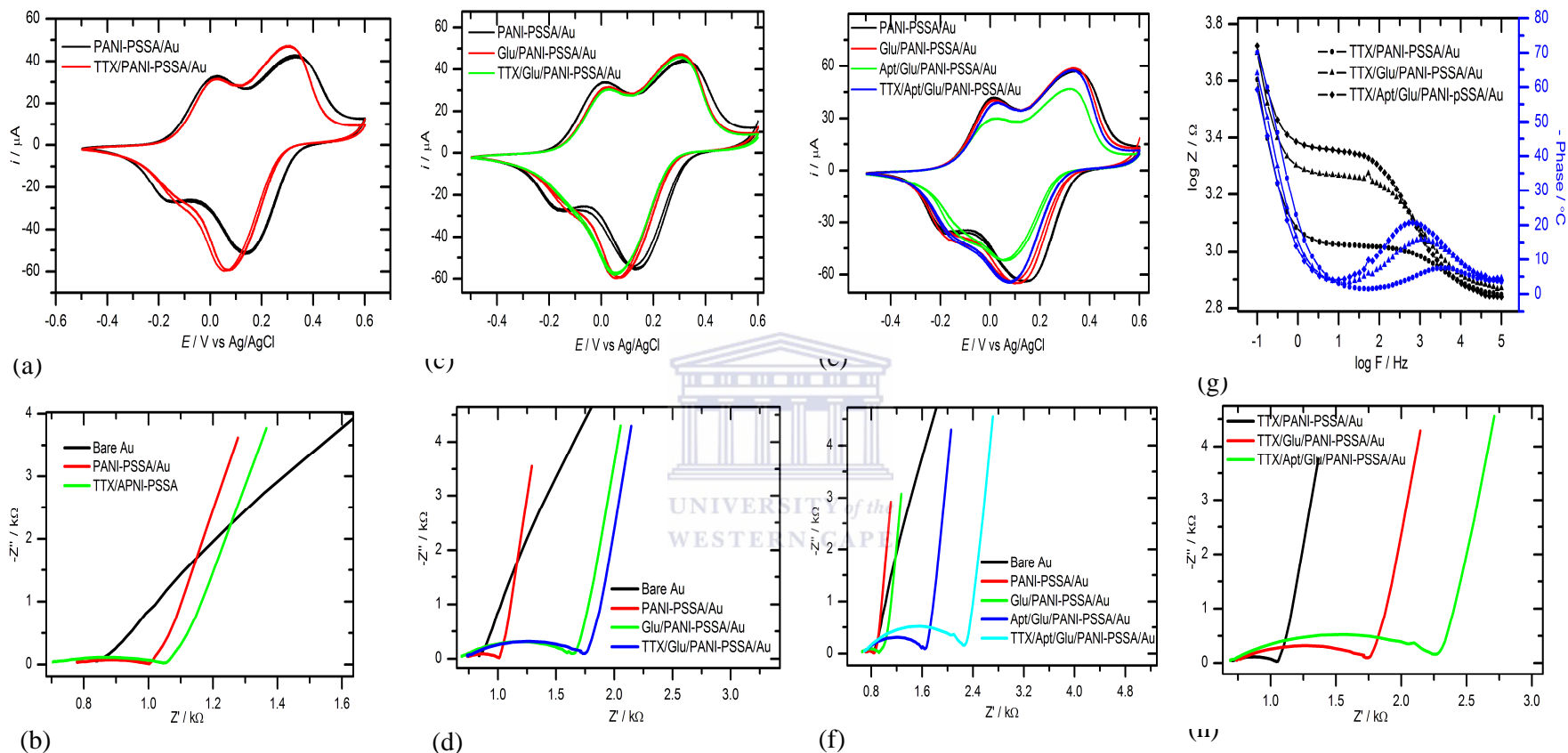


Figure 7.32: Cyclic voltammograms for the detection of TTX based on (a) *p*-PANI-PSSA, (c) Glu/PANI-PSSA, (e) Apt/Glu/PANI-PSSA and EIS measurements for the detection based on (b) *P*-PANI-PSSA, (d) Glu/PANI-PSSA, (f) Apt/Glu/PANI-PSSA. (g) The bode plot of (h) which present together the three separated detections.

Chapter 7: Application of electrochemically synthesised neutral and P-doped PANI–PSSA for the determination of tetrodotoxin

Table 7.18: Nyquist plot parameters analysis for the detection of TTX

Sensors	$CPEI-T_x$ 10^{-6} [C]	$CPEI-P$ [C]	R_s [Ω]	R_{ct} [Ω]	$Wo-p$ [Ω]	Chi-squared
PANI–PSSA/GC	8.62±0.00	0.59±0.22	664±3	411±113	0.47±0.00	0.0005
Glu/PANI–PSSA/GC	4.66±1.06	0.65±0.10	715±2	1128±136	0.48±0.00	0.0010
Apt/Glu/PANI–PSSA/GC	4±3	0.68±0.07	679±2	1723±146	0.48±0.00	0.0008

7.15 Detection of TTX based on NH₂–Apt/Glu/PANI–PSSA/GC

After proving that the aptamer increases Apt/Glu/ PANI–PSSA/GC sensor response, the experiment was repeated for four hours incubation. As described in paragraph (7.14), the cyclic voltammogram of each step of biosensor was recorded. All these CVs were obtained in 0.1 M acetate buffer pH 4.8. Figure 7.33 shows the CVs of successively modified-PANI–PSSA/GC, Glu/ PANI–PSSA /GC and Apt/Glu/ PANI–PSSA /GC electrode recorded in 0.1M OAc buffer, pH 4.8, over three repetitive scans between the potential of -0.5 to 0.6 V at 25 mV s⁻¹. It was observed that the peak current decreases when the glutaraldehyde is attached to the PANI–PSSA, it also decreases when the aptamer is immobilised on the Glu/PANI–PSSA, and continue to decrease when the TTX is trapped by the Apt/Glu/PANI–PSSA. Similarly, the peak potential shifts to a lower potential as the electrode is modified successively. After the TTX is trapped by the aptamer, there is an enhancement of the cathodic peak (c1) at around - 0.1 V while the cathodic peak (c2) at 0.01V shifted.

Chapter 7: Application of electrochemically synthesised neutral and P-doped PANI–PSSA for the determination of tetrodotoxin

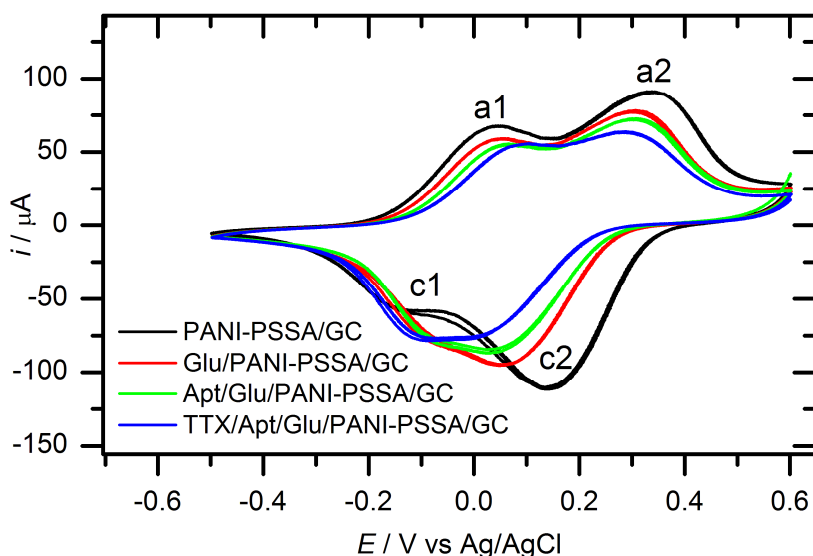


Figure 7.33: Overview of three cycles of cyclic voltammograms responses obtained after each in 0.1 M OAc buffer pH 4.8 with 0.02 mM glutaraldehyde (4 h incubation), 2 μ M aptamer (4 h incubation), and 5 μ M TTX (30 mins incubation).

The increase of the peak current at - 0.1 V demonstrates an effective modification of electrode with glutaraldehyde or aptamer. The reverse cathodic peaks is decreased which indicates that an electron transfer reaction is as a result of binding process. The Glu/PANI–PSSA composites are functioning as electron-transfer mediators between the glassy carbon electrode and the aptamer biomolecule. It was also assumed that the Apt/Glu/ PANI–PSSA sensors were thin homogeneous films in which the TTX reduction charge is propagated along the polymer chain by fast electron reactions involving the reduced and oxidized forms of the polymers [102]. The peak separation, ΔE_p , is greater than $200/n$ mV and ratio i_{pa}/i_{pc} for the oxidation wave was approaching unity in each step. These values indicate that the system is irreversible.

Chapter 7: Application of electrochemically synthesised neutral and P-doped PANI–PSSA for the determination of tetrodotoxin

Table 7.19: Characteristic peaks obtained from the CVs of each step of TTX biosensor

Modified /GC	E_{pa1} [V]	E_{pa2} [V]	E_{pc1} [V]	E_{pc2} [V]	ΔE_{p1} [V]	ΔE_{p2} [V]	E^{θ}_1 [V]	E^{θ}_2 [V]	i_{pa1} [μ A]	i_{pa2} [μ A]	i_{pc1} [μ A]	i_{pc2} [μ A]	$i_{pa1}/$ i_{pc1}	$i_{pa2}/$ i_{pc2}
PANI–PSSA	0.04	0.34	-0.15	0.14	0.19	0.2	-0.05	0.24	67.6	90.9	-55.6	-111	-1.2	-0.8
Glu/PANI–PSSA	0.05	0.31	-0.11	0.05	0.16	0.26	-0.03	0.18	59.5	77.3	-67.2	-95.7	-0.9	-0.8
Apt/Glu/PANI–PSSA	0.06	0.29	-0.10	0.04	0.16	0.25	-0.02	0.16	55.0	73.1	-73.6	-86.3	-0.7	-0.8
TTX/Apt/Glu/ PANI–PSSA	0.09	0.29	-0.09	0.01	0.18	0.28	0	0.15	55.4	63.0	-76.4	-75.0	-0.7	-0.8



Chapter 7: Application of electrochemically synthesised neutral and P-doped PANI–PSSA for the determination of tetrodotoxin

The surface modification of the electrodes for the preparation of aptasensor at each step has been monitored using EIS. The Nyquist plot was used to study the Glu/PANI–PSSA/GC/ response to DNA aptamer probe immobilisation and TTX detection response. Figure 7.32a shows the Nyquist plots of PANI-PSSA/GC, Glu/PANI–PSSA/GC and Apt-DNA /PANI–PSSA/GC aptaelectrode.

The R_{ct} of the PANI–PSSA/GC electrode increases after immobilisation of glutaraldehyde which is due to the non-conducting behaviour of glutaraldehyde [267-268]. The further increase in R_{ct} values after Apt-DNA is immobilised on the modified glutaraldehyde/PANI–PSSA/GC electrode can be attributed to the presence of negatively charged backbone of DNA. This negative charge on the electrode causes repulsion between the similarly charged redox couple of the system increasing the charge transfer resistance [267]. This is also due to the formation of protein insulating layer that reduces the electron transfer from the redox mediator solution to the electrode surface which is presented on bode plot (Fig. 7.34) with the reduction of phase angle.

Chapter 7: Application of electrochemically synthesised neutral and P-doped PANI-PSSA for the determination of tetrodotoxin

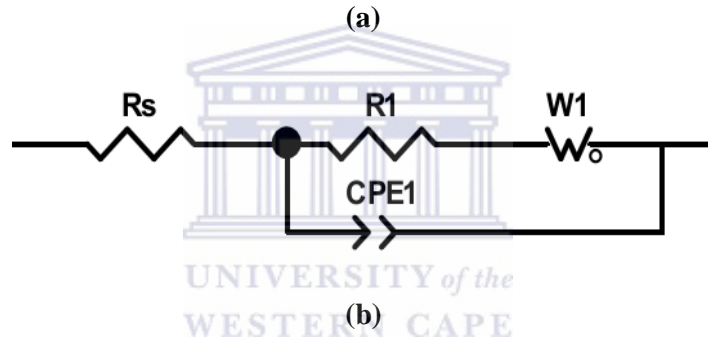
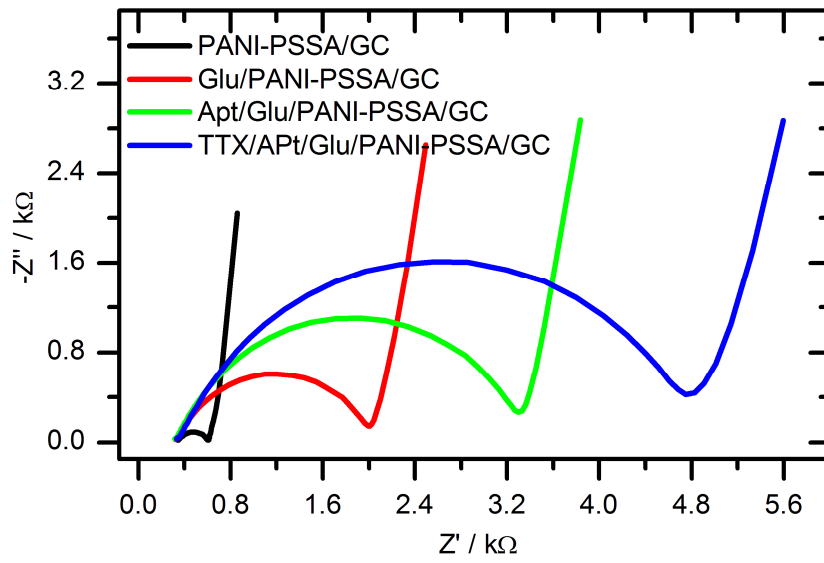


Figure 7.34: (a) Nyquist plot recorded after each step of TTX biosensor in 0.1 M acetate buffer pH 4.8 at formal potential. (b) An equivalent circuit model used in this biosensor analysis.

Similar results have been obtained with cyclic voltammetry measurements with the decrease of peak current after each modification (Fig. 7.31) as it is well known that the current is inversely proportional to R_{ct} . To obtain the electrical parameters, the impedance data was fitted using the circuit model (Fig. 7.34b) consisting of solution resistance R_s , Warburg impedance Z_w (W_0), charge transfer resistance R_{ct} and constant phase element CPE. The straight line (angle $\approx 45^\circ$) observed at the low frequency region of the Nyquist plot (Fig. 7.34a) explains the diffusion controlled nature of the system [269] and the Warburg element Z_w

Chapter 7: Application of electrochemically synthesised neutral and P-doped PANI–PSSA for the determination of tetrodotoxin

is determined. Table 7.20 shows the values of the fitting results of equivalent circuit. Capacitance (CPE) also increased because a new layer of charge has been concentrated on the PANI–PSSA surface causing an increase in double layer thickness

Table 7.20: Values of the equivalent circuit parameters of the fitting curves

Electrode	<i>CPE</i> [nF]	<i>R_s</i> [Ω]	<i>R_{ct}</i> [Ω]	<i>W_o</i> [kΩ/s ^{1/2}]	Chi-squared
PANI–PSSA	0.66 ± 0.19	333 ± 2	309 ± 59	0.46 ± 0.0	0.003
Glu/PANI–PSSA	0.75 ± 0.32	316 ± 1	1809 ± 81	0.46 ± 0.0	0.001
Apt/Glu/PANI–PSSA	0.77 ± 0.02	318 ± 1	3157 ± 91	0.47 ± 0.01	0.001
TTX/Apt/Glu/ PANI–PSSA	0.76 ± 0.01	338 ± 2	4743 ± 99	0.45 ± 0.01	0.002

Figure 7.35 is the Bode plot characteristic change of phase angle (Φ) and the total impedance against the logarithms of frequency response of the system. It is shown that the phase angle and logarithms impedance increase at a higher frequency after each step of modification of PANI–PSSA/GC with glutaraldehyde, aptamer and after the TTX is bound to the aptamer. All the phase angle values are below 50 °C which indicates that the PANI–PSSA, Glu/PANI–PSSA and the Apt/Glu/PANI–PSSA platforms are insulators at high frequency of 10³ Hz. At low frequency, the conductivity decreases when the platform is modified further. The PANI–PSSA is very conducting (Φ around 70°C), when the glutaraldehyde is attached, the surface of the electrode becomes a semiconductor (Φ around 50°C) and when the aptamer is binding and when TTX is bound, the modified surface electrode becomes an insulator (Φ less than 40°C). The diminution of the conductivity after each modification step is observed on Nyquist plot by the increase of charge transfer

Chapter 7: Application of electrochemically synthesised neutral and P-doped PANI-PSSA for the determination of tetrodotoxin

resistance. This can also be explained by the progressive reduction of the current observed on the CVs (Fig.7.33a) which means the inhibition of the moving of electrons by the glutaraldehyde and aptamer.

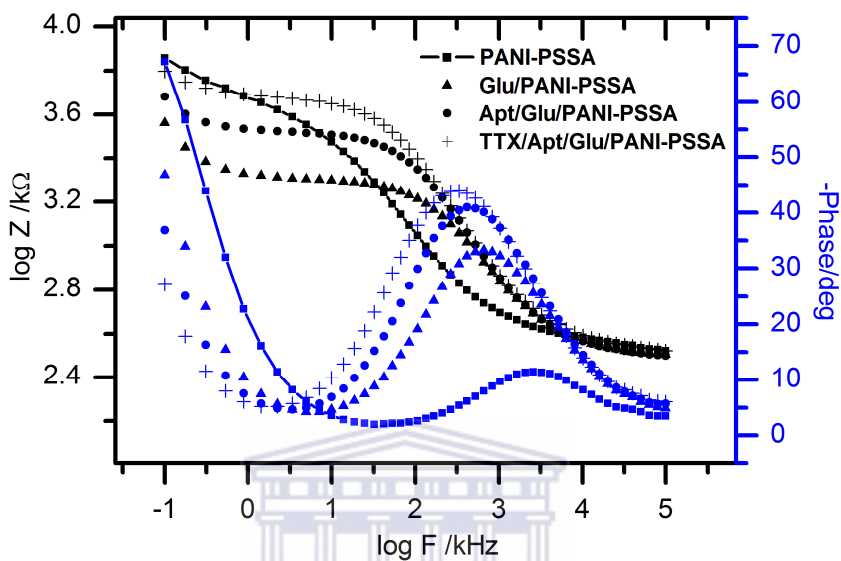
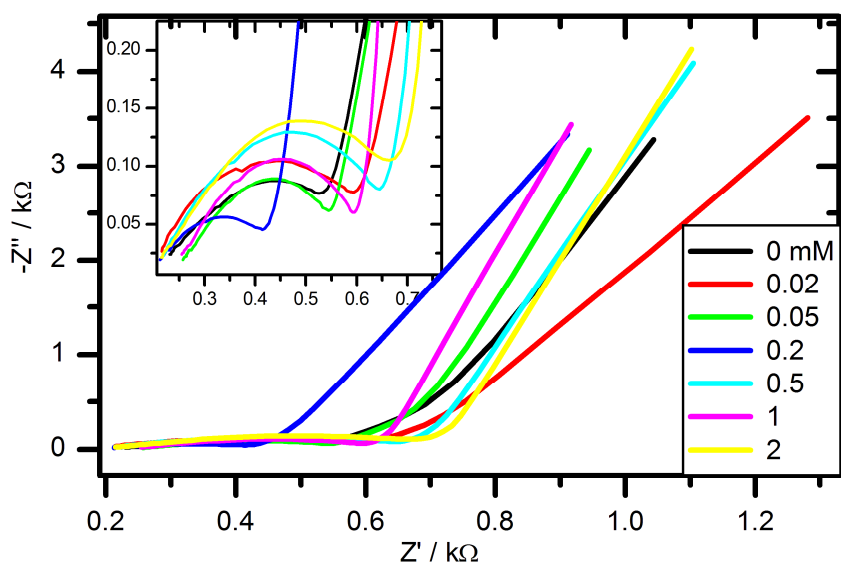


Figure 7.35: Bode plot of the overlay of each step of immobilization of glutaraldehyde, aptamer and TTX in 0.1 M acetate buffer pH 4.8 at formal potential.

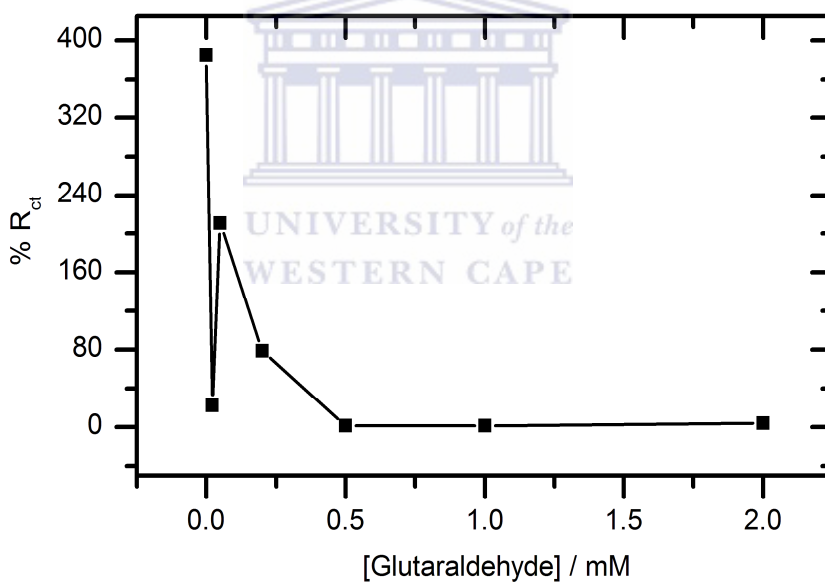
7.16 Optimisation of glutaraldehyde concentration

Different concentrations of glutaraldehyde were used to study the effect of concentration of glutaraldehyde on the biosensor response. Figure 7.36a gives the Nyquist plot of the biosensor response at different concentration of glutaraldehyde on seven different glassy carbon electrodes. Seven different electrodes were used for this purpose in order to investigate on the reproductivity of the biosensors. The seven bare electrodes was first study (see Annex) and it was found that all their surface are different each other.

Chapter 7: Application of electrochemically synthesised neutral and P-doped PANI-PSSA for the determination of tetrodotoxin



(a)



(b)

Figure 7.36: (a) Nyquist plot of TTX aptasensor developed on seven different GC electrodes at different concentration of aldehyde and fixed concentration of aptamer, 2 μM , and 5 μM TTX. (b) Absolute value of the relative variation (%) of the charge transfer resistance as a function of concentration of glutaraldehyde.

Chapter 7: Application of electrochemically synthesised neutral and P-doped PANI–PSSA for the determination of tetrodotoxin

It was shown that the biosensor can be reproduced on any glassy carbon electrode but with a difference in term of the experimental value calculated. The R_{ct} value for each biosensor was fitted using the equivalent circuit schematised in Figure 7.34b.

Because of the difference active surface of electrode, to evaluate the critical concentration of the glutaraldehyde, the relative change of percentage of R_{ct} (% R_{ct}) was plotted again concentration of glutaraldehyde. The % R_{ct} decreases with the increasing of the concentration of glutaraldehyde from 0 to 0.5 mM and slightly increases from 0.5 to 2 mM. The concentration of 0.5 mM was fixed to be sufficient for glutaraldehyde-aptamer binding. Table 7.21 presents the values of R_{ct} evaluating after immobilisation of glutaraldehyde on the PANI–PSSA films and after binding the TTX on the Apt/Glu/PANI–PSSA biosensor. The difference between the R_{ct} after immobilising the Glu ($R_{ct(Glu)}$) and the R_{ct} after attaching the TTX ($R_{ct(TTX)}$), $\Delta R_{ct} = |R_{ct(TTX)} - R_{ct(Glu)}|$, was calculated. Using the Equation 7.8, the relative variation of charge transfer resistance was calculated as well.

$$\%R_{ct} = \frac{\Delta R_{ct}}{R_{ct}(Glutaraldehyde)} \times 100 \quad \text{Equation 7.8}$$

Chapter 7: Application of electrochemically synthesised neutral and P-doped PANI–PSSA for the determination of tetrodotoxin

Table 7.21: EIS parameters determined from the equivalent circuit of the fitting curves

[Glutaraldehyde] / mM	$R_{ct}(\text{Glu})$		$R_{ct}(\text{TTX})$		ΔR_{ct} [Ω]	% R_{ct}
	E^{θ}_1	R_{ct}	E^{θ}_2	R_{ct}		
	[V]	[Ω]	[V]	[Ω]		
0	0.226	105 ± 19	0.237	509 ± 13	404 ± 6	385
0.02	0.254	680 ± 10	0.221	531 ± 8	149 ± 2	22
0.05	0.265	122 ± 4	0.226	380 ± 6	258 ± 2	211
0.2	0.259	172 ± 7	0.243	307 ± 5	135 ± 2	79
0.5	0.265	480 ± 6	0.226	539 ± 6	59 ± 0	1.2
1	0.265	423 ± 5	0.226	418 ± 4	5 ± 1	1.2
2	0.265	572 ± 9	0.232	597 ± 9	25 ± 0	4

7.17 Optimisation of aptamer concentration

The effect of concentration of aptamer of detection has been investigated using CV and EIS for fixed TTX concentration. This was investigated in the same way as the optimisation of the concentration of glutaraldehyde was done. The EIS measurements were carried out on two respective formal potentials obtained from the cyclic Voltammograms. Figure 7.37a and b is showing the biosensor response using different concentration of aptamer at first and second formal potential. The first formal potential $E^{\theta}_1 = (E_{pa1+} - E_{pc1})/2$ and the second one is $E^{\theta}_2 = (E_{pa2} - E_{pc2})/2$. As explained earlier, the same principle used to evaluate the fixed concentration of glutaraldehyde was used to evaluate the fixed concentration of aptamer. Figure 7.37c is the plot of % R_{ct} evaluated from Figure 7.37a and b using the same equivalent circuit of Figure 7.37b versus concentration of aptamer at E^{θ}_1 and E^{θ}_2 . The % R_{ct} increases with increasing of the concentration of aptamer from 0 to 0.05 μM and

Chapter 7: Application of electrochemically synthesised neutral and P-doped PANI–PSSA for the determination of tetrodotoxin

decreases from 0.05 to 10 μM . Following the above observations therefore, 0.05 μM is sufficient to form the aptamer-TTX binding to get a significant biosensor response.

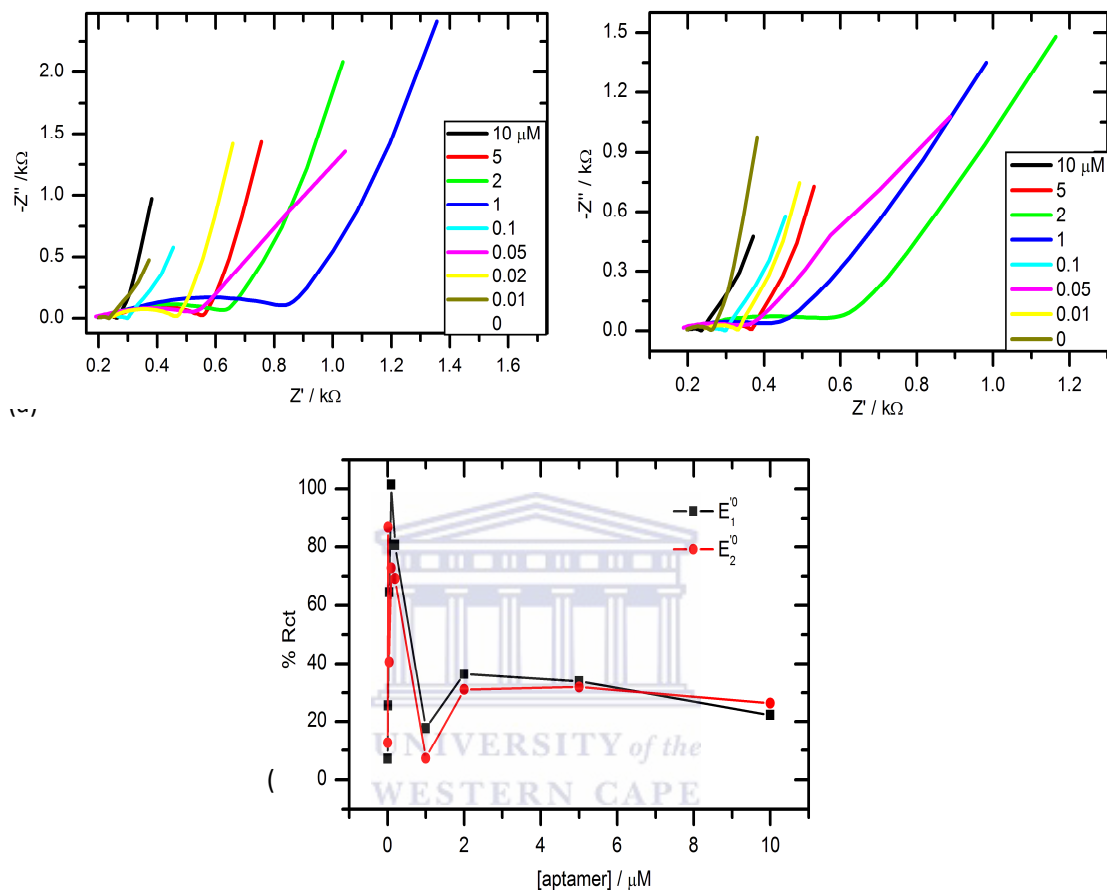


Figure 7.37: EIS response of TTX biosensor (TTX/Apt/Glu/PANI–PSSA) at different concentration of aptamer in OAc buffer pH 4.8. Calibration curve for the TTX/Apt/Glu/PANI–PSSA biosensor response to different concentrations of aptamer.

The difference between the R_{ct} after immobilising the aptamer ($R_{ct(\text{Apt})}$) and the R_{ct} after attaching the TTX ($R_{ct(\text{TTX})}$), $\Delta R_{ct} = |R_{ct(\text{TTX})} - R_{ct(\text{Apt})}|$, was calculated. The relative change of percentage of R_{ct} was calculated as follows:

$$\%R_{ct} = \frac{\Delta R_{ct}}{R_{ct}(\text{Aptamer})} \times 100 \quad \text{Equation 7.9}$$

Chapter 7: Application of electrochemically synthesised neutral and P-doped PANI–PSSA for the determination of tetrodotoxin

Table 7.22: Concentration of aptamer and charge transfer resistance recorded at two different formal potential

[Aptamer] / μ M	$R_{ct(Apt)}$		$R_{ct(TTX)}$		ΔR_{ct}		% R_{ct}	
	[Ω]		[Ω]		[Ω]			
	E'^0_1	E'^0_2	E'^0_1	E'^0_2	E'^0_1	E'^0_2	E'^0_1	E'^0_2
0	72.8 \pm 0.4	63 \pm 1	78 \pm 1	71 \pm 1	5.2 \pm 1	8 \pm 0	7 \pm 3	13 \pm 1
0.01	82 \pm 1	60 \pm 1	102.8 \pm 0.4	112 \pm 1	21 \pm 0	52 \pm 0	26 \pm 0	87 \pm 0
0.05	240 \pm 2	157 \pm 4	395 \pm 5	221 \pm 5	155 \pm 3	64 \pm 1	65 \pm 2	40.8 \pm 0.3
0.1	404 \pm 6	257 \pm 6	420 \pm 1	420 \pm 1	16 \pm 5	163 \pm 5	4 \pm 1	63 \pm 1
0.5	984 \pm 12	1029 \pm 12	1195 \pm 15	1195 \pm 15	211 \pm 3	166 \pm 3	21.4 \pm 0.3	16.1 \pm 0.3
1	621 \pm 6	373 \pm 5	731 \pm 11	400 \pm 7	110 \pm 5	27 \pm 0	178 \pm 1	7 \pm 0
2	364 \pm 4	203 \pm 3	497 \pm 7	266 \pm 5	133 \pm 4	63 \pm 2	37 \pm 1	31 \pm 1
5	222 \pm 1	91.7 \pm 0.4	297 \pm 2	120.8 \pm 1	75 \pm 1	29 \pm 1	33.8 \pm 1	31.7 \pm 3
10	52.5 \pm 0.3	28.1 \pm 0.4	64.2 \pm 0.4	35.5 \pm 0.3	11.7 \pm 0.1	7.4 \pm 0.1	22.3 \pm 0.3	26.3 \pm 0.3

Chapter 7: Application of electrochemically synthesised neutral and P-doped PANI-PSSA for the determination of tetrodotoxin

The arms of this structure (Fig.7.38) are duplex DNA and each component single strand is involved in forming two arms. This gives rise to a junction point where the single strands cross each other, and which formed a recognition site for interactions with analyte [270]. For this aptamer, the six bases crossed each other from A₁₁ to T₁₇ single strands is the active site of this tetrodotoxin-aptamer.

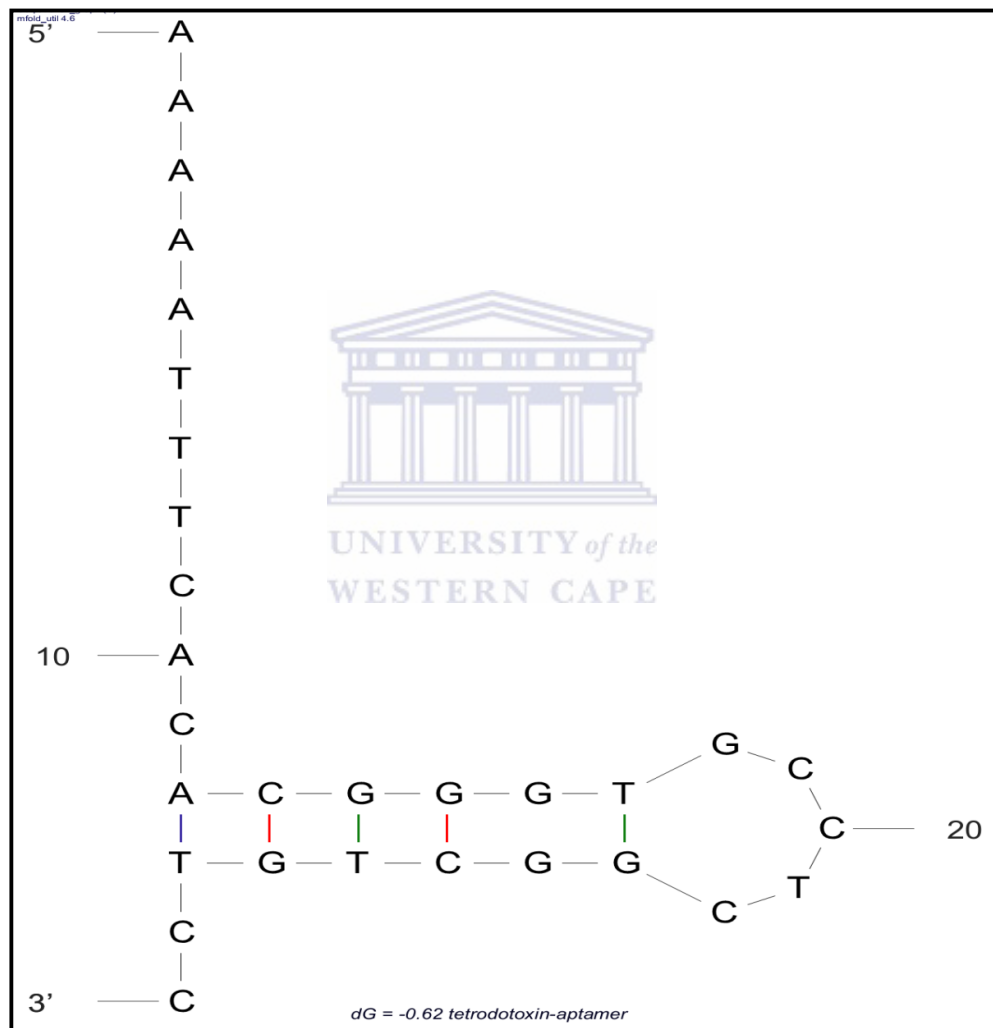


Figure 7.38: Linear structure of the most stable NH₂-aptamer for TTX obtained from RNA Institution *mfold* (sequence: AAAAATTTACACGGGTGCCTCGGCTGTCC).

Chapter 7: Application of electrochemically synthesised neutral and P-doped PANI-PSSA for the determination of tetrodotoxin

The thermodynamic data of tetrodotoxin-aptamer obtained from RNA Institution mfold are:

$\Delta G = -0.62$ kcal/mol at 25 °C Standard errors are roughly $\pm 5\%$, $\pm 10\%$, $\pm 11\%$ and 2 -

$\Delta G = \Delta H - T\Delta S$ 4 °C for free energy, enthalpy, entropy and T_m ,

$\Delta H = -16.00$ kcal mol⁻¹ respectively

$\Delta S = -49.5$ cal K⁻¹·mol⁻¹ Ionic conditions: [Na⁺] = 1.0 M, [Mg⁺⁺] = 0.0 M.

$T_m = 49.5$ °C assuming a 2 state model.

Table 7.23: The Gibbs free energy of five bases involved on the binding active site of the aptamer

Structural element	δG	Information
External loop	-0.38	13 ss bases & 1 closing helices
Stack	-1.26	External closing pair is A ₁₂ -T ₂₈
Stack	-0.29	External closing pair is C ₁₃ -G ₂₇
Stack	-0.14	External closing pair is G ₁₄ -T ₂₆
Helix	-1.69	4 base pairs
Interior loop	-0.85	External closing pair is G ₁₅ -C ₂₅
Hairpin loop	2.30	Closing pair is T ₁₇ -G ₂₃

7.18 UV/Vis absorption of the composite obtained for each detection step dispersed in DMF and DMSO

A comparison between the UV-Vis spectra of each modification step of biosensor (Fig.7.39) shows basically the same trend. The spectra show that in each step, four characteristic absorptions (a, b, c, and d) bands are observed. The (d) band can be

Chapter 7: Application of electrochemically synthesised neutral and P-doped PANI-PSSA for the determination of tetrodotoxin

attributed to the absorption of chromophores present in MDF. The purpose of this chapter was to develop a sensor based on p-doped PANI-PSSA composites for a TTX sensor. Therefore, the discussion of this analysis is focused on the three main absorption peaks appearing at (a), (b), and (c). As saying in paragraph 7.7, the band between 275.5 and 294.9 nm is due to the $\pi \rightarrow \pi^*$ transition of benzenoid ring of aniline and PSSA. It is deduced that this absorbance band increases When the aptamer is immobilised on the Glu/PANI-PSSA which explains the increase of C=C concentration from the aptamer into the system. Unlike the aptamer, the binding of TTX decreases the absorbance about 24 % can be explained by the delocalisation of electron along the Apt/Glu/PANI-PSSA composites chain. This delocalisation destabilises the C=C chromophores and the hydrogen bonds formed between the oxygen of DNA and the hydrogen of TTX (Fig. 7.40). The absorption peak at 327.4 nm (b) corresponds to the transition $n \rightarrow \sigma^*$ for the chromophores N-C for PANI chains.

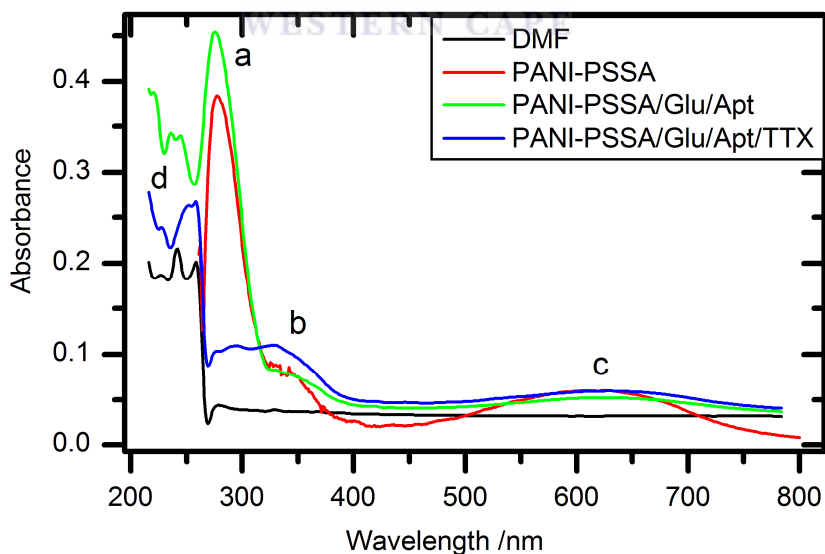


Figure 7.39: UV-Vis spectra of TTX biosensor in DMF.

Chapter 7: Application of electrochemically synthesised neutral and P-doped PANI–PSSA for the determination of tetrodotoxin

When the TTX is attached, this absorption (b) is more pronounced which indicates the reactivity of the aptamer vis-à-vis TTX. A broad peak (c) at 623.9 is observed on each modified step as said above corresponding to the shift of electron from benzenoid ring to quinone ring which involves the $\pi \rightarrow \pi^*$ electronic transition.

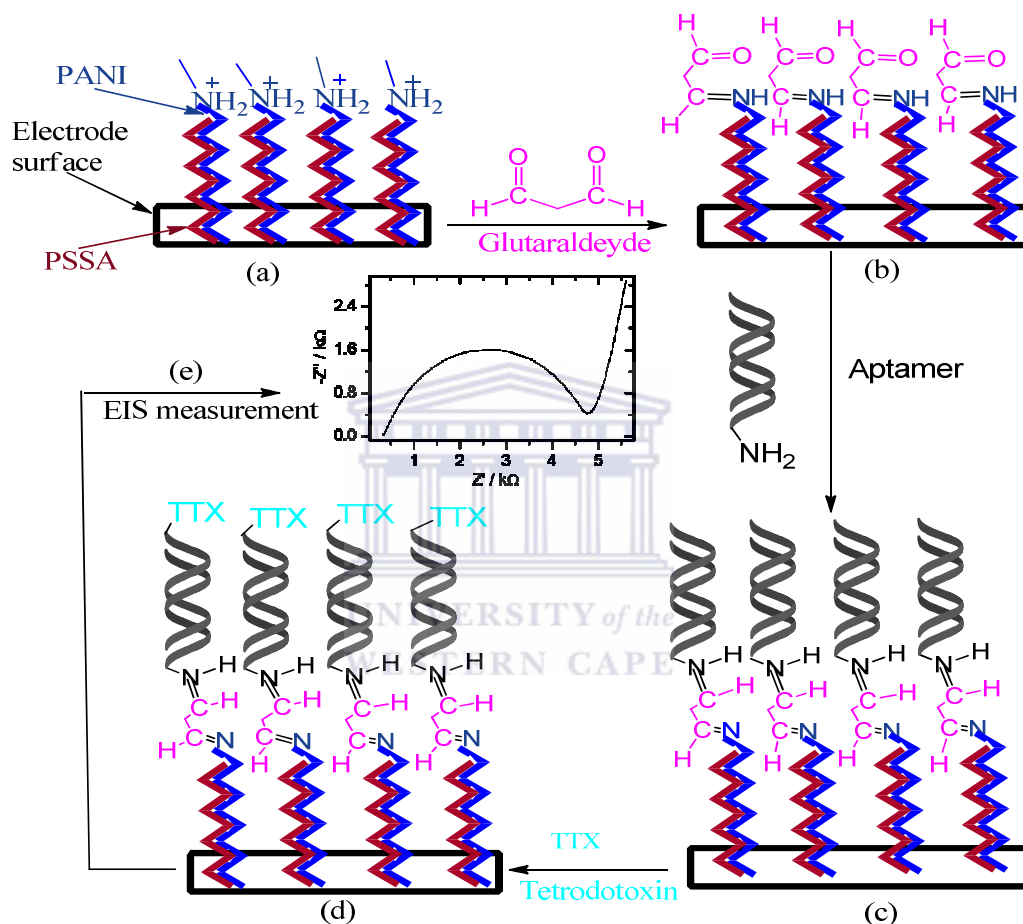


Figure 7.40: Scheme of the aptasensors: (a) electropolymerisation of PSSA doped aniline, (b) binding of glutaraldehyde on the modified-PANI–PSSA/GC surface, (c) immobilisation of NH_2 -Aptamer on Glu/PANI–PSSA/GC, (d), binding of tetrodotoxin to aptamer, (e) Route for label-free TTX detection

7.19 Scanning electron microscopy of each detection step on screen-printed electrode

Chapter 7: Application of electrochemically synthesised neutral and P-doped PANI–PSSA for the determination of tetrodotoxin

Figure 7.42 shows the field-emission scanning electron microscopy (FE-SEM) images of the surface appearance of Glu/PANI–PSSA, Apt/Glu/PANI–PSSA and TTX/Apt/Glu/PANI–PSSA. The SEM micrograph of Glu/PANI–PSSA (Fig. 7.41) shows an aggregation of 80 nm Glu/PANI–PSSA composites spherical bowls. When the aptamer is immobilised onto the Glu/PANI–PSSA, the SEM micrograph (Fig.7.42) shows the white spherical bowls with small diameter between 22 to 44 nm distributed over the glutaraldehyde. After the TTX has bound to the aptamer (Fig.7.43), an independent group of composites are formed.

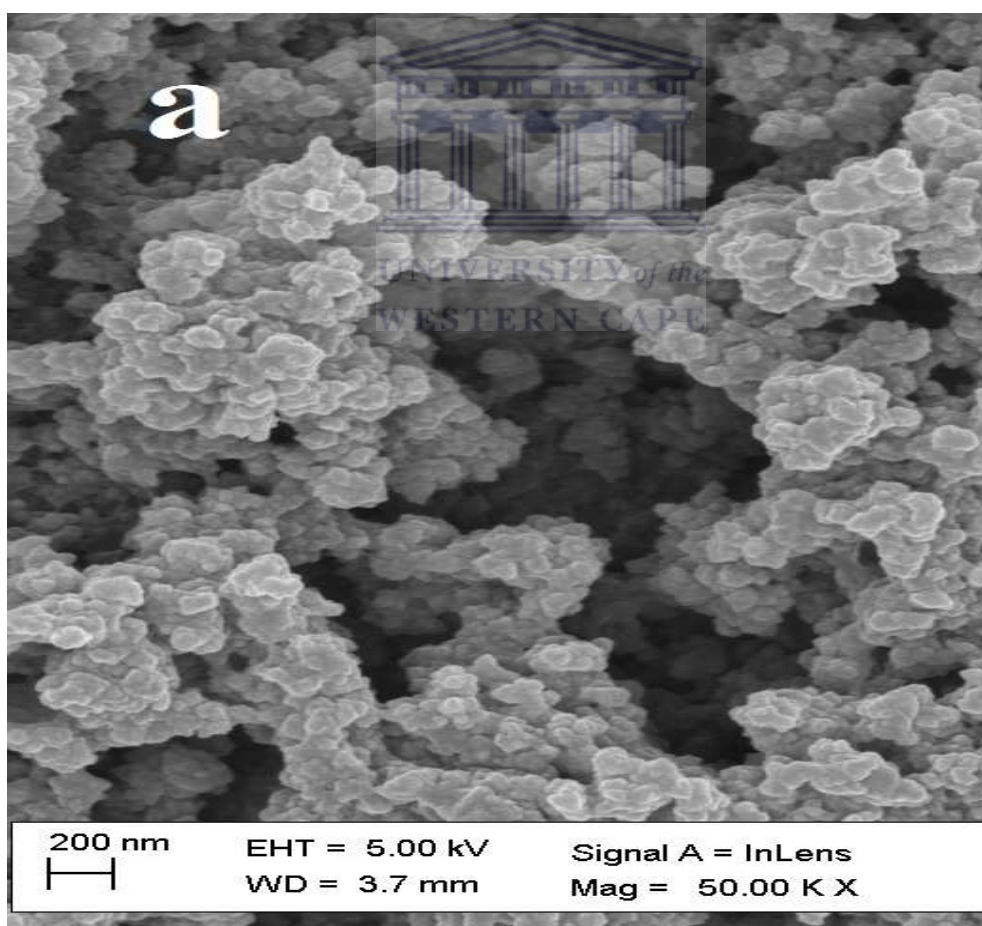


Figure 7.41: Scanning electron micrographs of Glu/PANI–PSSA.

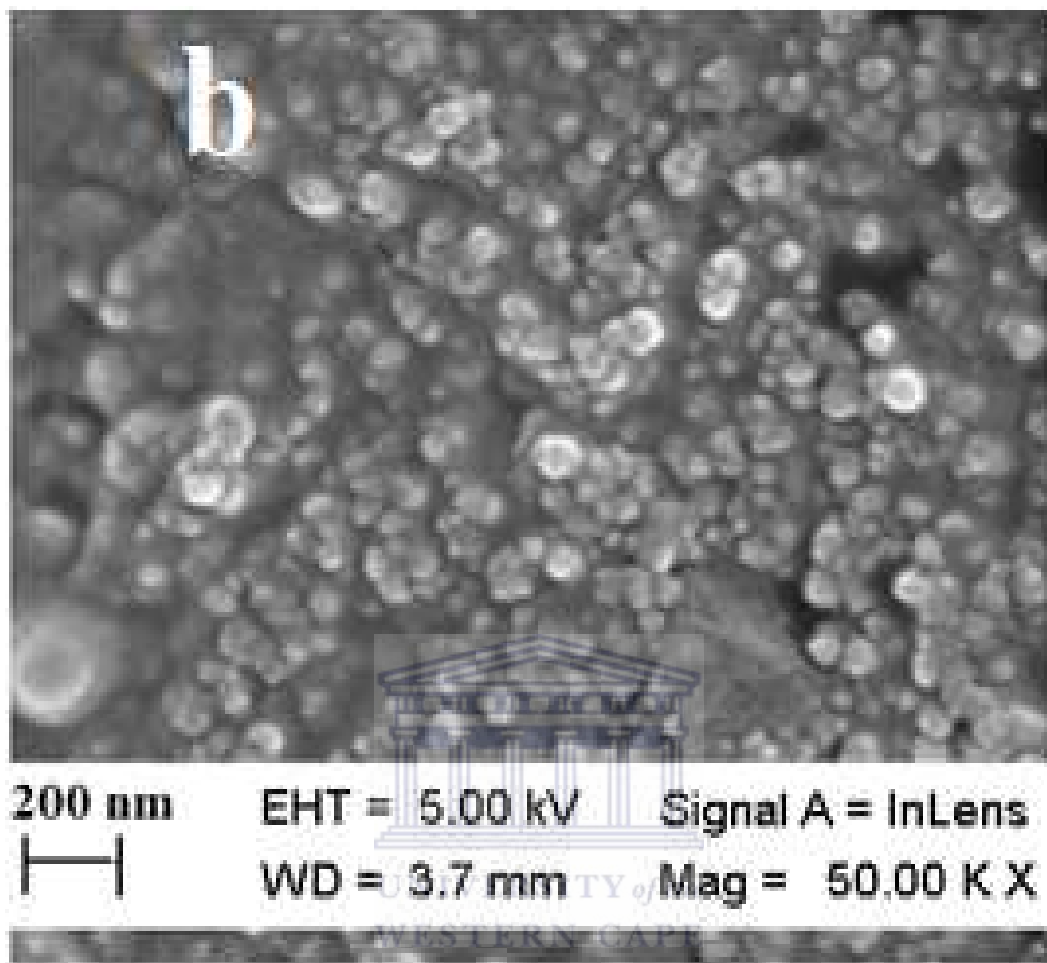


Figure 7.42: Scanning electron micrographs of Apt/Glu/PANI-PSSA.

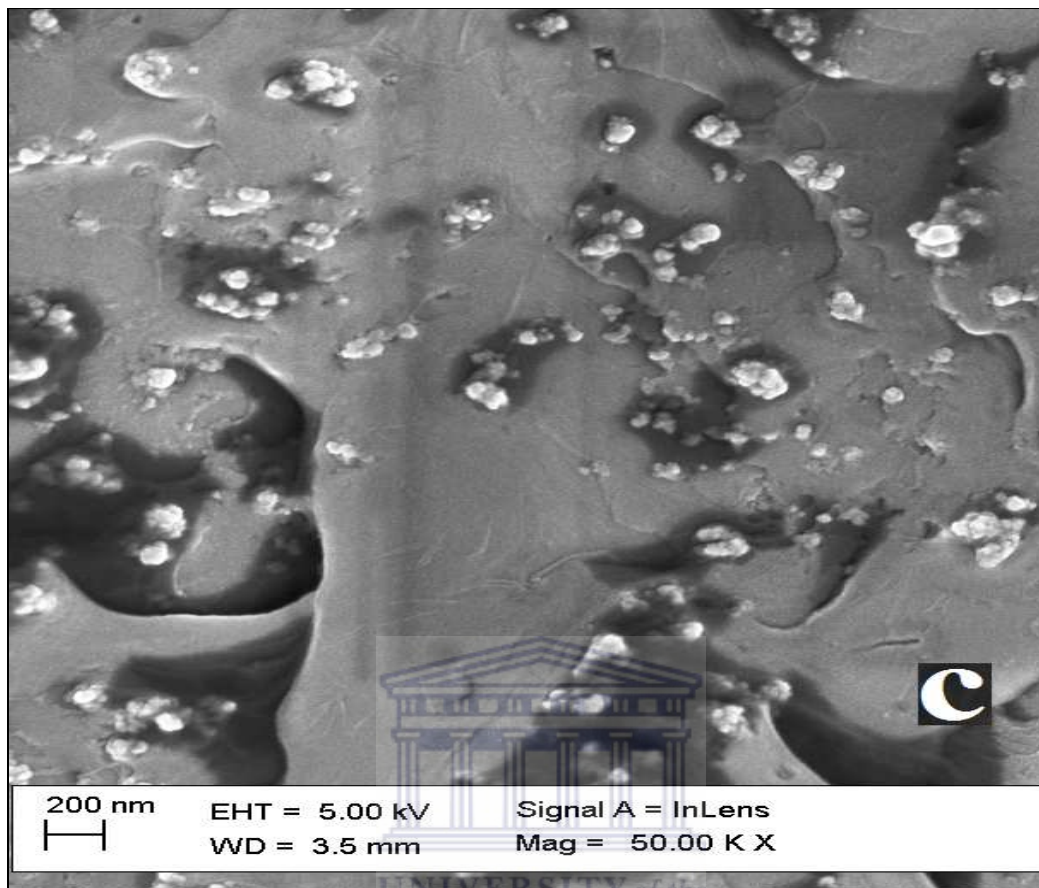


Figure 7.43: Scanning electron micrographs of TTX/Apt/Glu/PANI-PSSA.

This shows that a clear agglutination has taken place between the aptamer and TTX on the surface appearance of TTX/Apt/Glu/PANI-PSSA. This proved that there is a strong affinity between the aptamer and TTX as the aptamer successfully detects the tetrodotoxin.

7.20 Optimisation of aptasensor response

Impedimetry sensor was used to optimise the concentration of TTX by measuring the changes in charge-transfer resistance (R_{ct}) values in order to determine the linear range, the sensitivity and the detection limit of the tetrodotoxin-aptasensor. These three properties of

Chapter 7: Application of electrochemically synthesised neutral and P-doped PANI–PSSA for the determination of tetrodotoxin

aptasensor developed were investigated focusing on different adsorption isotherms used in analytical chemistry. As the tetrodotoxin concentration increases from 0 to 10 ng ml⁻¹, the electron transfer resistance increases respectively from 60 ± 1 to 355 ± 2 Ω (Fig 7.44). The PANI film introduces a barrier for electron transfer at the electrode interface and an enhanced electron transfer resistance is obtained. Figure 7.44 shows the charge transfer resistance response again the concentration of tetrodotoxin. When the concentration of TTX is optimised from 0 to 10 ng ml⁻¹, the curve obtained follows the adsorption isotherms of BET (Brunauer, Emmett and Teller). Therefore, one active site of aptamer can take not only one but several molecules of TTX. The increase of R_{ct} with an increasing of the concentration of TTX explains the occupation of active site of aptamer as more TTX are attaching.

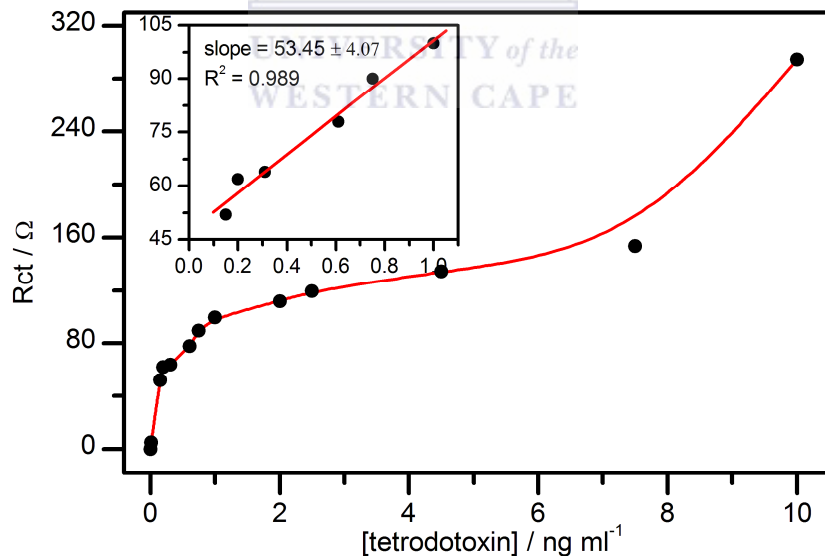


Figure 7.44: Calibration curve for the PSSA–PANI/Glu/Aptamer biosensor response to different concentrations of tetrodotoxin. Inset analytical linear range of the biosensor from 0.3 to 1.0 ng ml⁻¹.

Chapter 7: Application of electrochemically synthesised neutral and P-doped PANI-PSSA for the determination of tetrodotoxin

This experiment was repeated three times from 0 to 0.2 ng ml⁻¹ of tetrodotoxin but the detection on this range was not consistent (Fig.7.45).

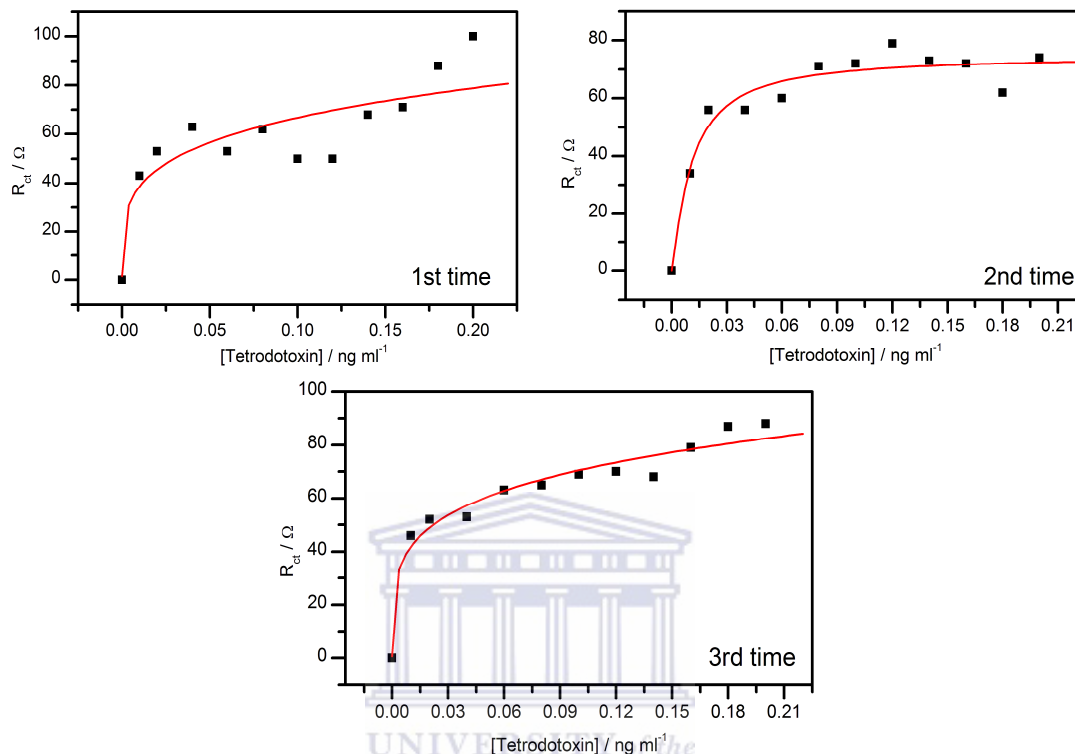


Figure 7.45: Calibration curve for the PSSA–PANI/Glu/Aptamer biosensor response to different concentrations of tetrodotoxin repeated three times at the range 0 to 0.2 ng ml⁻¹.

The optimisation was repeated at the concentration range between 0 to 2.5 ng ml⁻¹. By applying the isotherm adsorption of BET as explained earlier, the data characteristics of aptasensor for detection of tetrodotoxin were determined.

Chapter 7: Application of electrochemically synthesised neutral and P-doped PANI-PSSA for the determination of tetrodotoxin

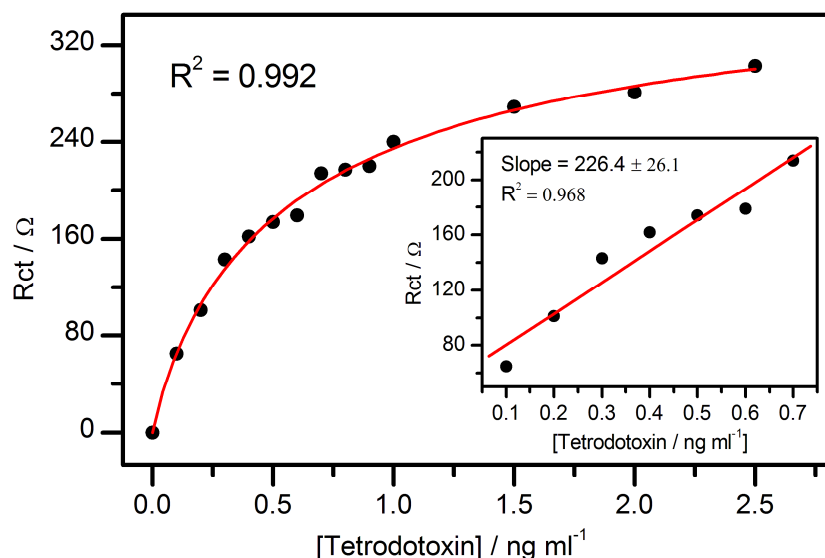


Figure 7.46: Calibration curve for the PSSA–PANI/Glu/Aptamer biosensor response to different concentrations of tetrodotoxin. Inset analytical linear range of the biosensor from 0 to 0.5 ng ml⁻¹.

The estimated linear range for the PSSA–PANI/Glu/Aptamer based biosensors were 0.064 to 0.736 ng ml⁻¹ tetrodotoxin. The linear ranges obtained were smaller than the range obtained for tetrodotoxin by [79, 81-82, 271] using ELISA and SPR method. The slope of the calibration curves were used to estimate the sensitivities of the aptasensor. The estimated sensitivity of the biosensor was 226.4 ± 26.1 Ω ml ng⁻¹. The limit of detection (LOD), for the p-doped PSSA–PANI/Glu/Aptamer biosensor was relatively low compare to the one reported by Taylor *et al.* (0.3 ng ml⁻¹) [271] and Neagu *et al.* (2 ng ml⁻¹, R² = 0.924) [73]. The value of the detection limit was calculated to be 0.119 ng ml⁻¹ and the limit of quantification was 0.357 ng ml⁻¹.

Table 7.24 compares the linear range and the limit of detection of some analytical technique used to determine TTX. It was found that the biosensor developed in this study

Chapter 7: Application of electrochemically synthesised neutral and P-doped PANI-PSSA for the determination of tetrodotoxin

has the small linear range amongst other techniques. The limit of detection was also lower compare to the one getting with other method. The LC-MS/MS, GC/MS, ELISA and biosensor are more relevant for the detection of tetrodotoxin.

Table 7.24: Comparison of different method of determination of tetrodotoxin

Method	Linear range [ng ml ⁻¹]	Limit of detection [ng ml ⁻¹]	References
LC-MS	93.75 – 9375	15.6	[54]
LC-MS/MS	1 – 10	0.1	[272]
HPLC	30 – 600	1.0	[86]
SPE and GC/MS	0.5 – 10.0	0.1	[52]
SPR	0.01 – 10.00	0.3	[79]
ELISA	2 – 50	1.0	[47]
	5 – 500	0.1	[74]
	40 – 8000	40	[76]
Biosensor	0.1 – 0.7	0.1	This study

CONCLUSION AND PERSPECTIVES

8.0 Conclusions

The electrochemical tetrodotoxin sensor developed on modified electrode based on neutral selective ionophores using ion transfer voltammetry and characterised using UV-Vis absorption analysis was investigated for the first time in this study. Using the ion-selective electrode and UV-Vis absorption spectroscopy, it was found that the electrochemical TTX sensor cannot be developed on neutral NaX and B18C6 selective ionophore. It is important to note that this was the first investigation of selective NaX and B18C6 ionophore complexation of TTX using ion transfer voltammetry and UV-Vis absorption spectroscopy. Selective ionophores immobilised on solid modified PANI-PSSA/electrode platform or applied in ion transfer electrode indicated that no electrochemical TTX sensor can be developed based on NaX and B18C6 ionophores as specific agent. UV-Vis of NaX, B18C6, the mixture of TTX/NaX and TTX/B18C6 was also investigated for the first time to check on the possible reaction which can occur between TTX and both ionophores in the respect of developing TTX sensor based on both ionophores. No electrochemical sensor can be developed for the determination of TTX based on NaX and B18C6 ionophores

On the other hand, the neutral and p-doped PANI-PSSA film polymers were electrochemically synthesized on Au, GC, PG, and Pt electrodes in phosphoric acid. These PANI-PSSA modified electrodes were characterised using CV, EIS, UV-Vis, FT-RI, FL, TEM and SEM analysis in order to find which of this composite is more indicated to be

Chapter 8: Conclusion and perspectives

applied on electrochemical TTX biosensors. The kinetic study of neutral and p-doped PANI–PSSA in phosphate and acetate buffer solutions on different electrodes lead this study to conclude that: Acetate buffer is more appropriate to study both polymers film than phosphate buffer for their applications in electrochemical sensor or biosensor; Au and PG electrodes are more indicated for the electrochemical synthesis of neutral PANI–PSSA while GC and Pt electrodes are more indicated for the electropolymerisation of p-doped PANI–PSSA. After characterisation of both polymer films using UV/Vis, FL, FT-IR, SEM and TEM techniques, it was found that the way of electrochemically synthesise (anodically or cathodically) the PANI films influence the nature of the polymer formed on the electrode surface. Regarding the characterization results, neutral PANI and p-doped PANI are two compounds totally different explained with their solubility medium, their absorption and emission bands (see UV/Vis and FL results) even in terms of the vibration bands as well (see FT-IR results). The kinetic parameters are summarized in the Table 8.1. In addition, p-doped PANI–PSSA modified glassy carbon was applied in the electrochemical aptasensor for the detection of TTX using cyclic voltammetry and electrochemical impedance spectroscopy analysis and some other techniques such as UV/Vis, FL emission, FT-IR and SEM were used to characterise each biosensor step. It was found that P-doped is a good mediator for tetrodotoxin biosensor and used as the probe molecule for electrode surface enhancing the production of electrons into the system.

Finally, the electrochemical tetrodotoxin aptasensor was developed for the first time and displayed typical sensor behaviour. The linear range of the biosensor exhibited an upper limit of approximately 0.065 to 1.085 ng ml⁻¹ ($R^2 = 0.989$). The sensitivity for the tetrodotoxin sensor was 53.45 Ω ml ng⁻¹ and detection limit was found to be 0.31 ng ml.

Chapter 8: Conclusion and perspectives

The estimated constant of BET (c) of 1.72 ng ml^{-1} and a concentration of tetrodotoxin adsorbed by a monolayer of 0.002 ng ml^{-1} were obtained. The p-doped PANI-PSSA films have great potential as electromediators in construction of biosensors for different analytes

8.1 Perspectives

One of the main challenges face in this study, on the construction of electrochemical TTX sensor based on ionophore using liquid-liquid interface (ion transfer voltammetry) was the negative charge of TTX. Since ionophores are cheaper and the technique used is easy, the possible answer to solve this problem can be to block the negative charge of oxygen of TTX by reacting the latter with inorganic groups like acyl chloride via acylation reaction to form the TTX with positive charge of guanidinium group only. After the TTX⁺ ion formed, the guanidinium sensor can be used to develop the TTX⁺ ion sensor based on the selective guanidinium ionophore using ion transfer voltammetry.

The application of PANI-PSSA in large scale processes has been limited by its insolubility and intractability. It is thus suggested that the substitution of alkyl (methyl, ethyl) or sulphonic groups in ortho-position could provide a solution to this problem.

One of the major problems encountered was the lack of licence to apply a new tetrodotoxin aptasensor on real sample. The application of biosensor developed in this study would be useful for health as well as for quality control purposes in food industries.

REFERENCES

1. Jal, S.; Khora, S. S.; Mandal, N.; Kanagaraj, M., *Marine toxicity and its implication on human health*. International Research journal of pharmacy, 2012. **3** (3): p. 39 - 42.
2. Gallacher, K.; Whittle, S., *Marine toxins*. British Medical Bulletin, 2000. **56**(1): p. 236-253.
3. Front, M., *Chemical Weapons Convention Chemicals Analysis* 2006: John Wiley & Sons, Ltd. i-xiii.
4. Patrick, W.; Scott, W. M.; Jaime, A.; Michael, A.; Corey, J.; Hilmas, M. D., *Medical Aspects of Chemical Warfare.*, in *Chapter 19 Toxins: Established and Emergent Threats*. 2008.
5. Nateghi, M. R.; Zahedi, M.; Mosslemin, M.H.; Hashemian, S.; Behzad, S.; Minnai, A., *Autoacceleration/degradation of electrochemical polymerization of substituted anilines*. Polymer, 2005. **46**(25): p. 11476-11483.
6. Gallacher, K. ; Whittle, S., *Marine toxins*. British Medical Bulletin, 2000. **56**(1).
7. Patrick, W.; Scott, W.M.; Jaime, A.M.; Michael, A.; Corey, J.; Hilmas, M.D. (2008) *Medical Aspects of Chemical Warfare*. Chapter 19 Toxins: Established and Emergent Threats, 613-644.
8. Shuyi, Louisa Quek, *Tetrodotoxin*, in *Chemical properties*. 2001.
9. Isbister, G. K.; Kiernan, M. C., *Neurotoxic marine poisoning*. The Lancet Neurology, 2005. **4**(4): p. 219-228.
10. Noguchi, T.; Ebesu, J. M., *Puffer poisoning: epidemiology and treatment*. Toxin Reviews, 2001. **20**(1): p. 1-10.

References

11. Arakawa, Tamao Noguchi & and Osamu, *Tetrodotoxin – Distribution and Accumulation in Aquatic Organisms, and Cases of Human Intoxication*. *Mar. Drugs* 2008. **6**: p. 220-242.
12. Matsumura, K., *Reexamination of tetrodotoxin production by bacteria*. *Applied and environmental microbiology*, 1995. **61**(9): p. 3468-3470.
13. Matsumura, K., *No ability to produce tetrodotoxin in bacteria*. *Applied and environmental microbiology*, 2001. **67**(5): p. 2393-2394.
14. Yu, CF.; Yu, P. HF.; Chan, PL.; Yan, Q.; Wong, PK., *Two novel species of tetrodotoxin-producing bacteria isolated from toxic marine puffer fishes*. *Toxicon*, 2004. **44**(6): p. 641-647.
15. Noguch, T.; Arakawa, O., *Tetrodotoxin–distribution and accumulation in aquatic organisms, and cases of human intoxication*. *Marine drugs*, 2008. **6**(2): p. 220-242.
16. Landsberg , J. H.; Hall, S.; Johannessen, J.N.; White ,K. D.; Conrad, S. M.; Abbott,J. P.; Flewelling, L. J.; Richardson, R. W.; Dickey, R. W.; Jester, E. L.; Etheridge, S. M.; Deeds, J. R.; Van Dolah, F. M.; Leighfield, T. A.; Zou, Y.; Beaudry, C. G.; Benner, R. A.; Rogers, P. L.; Scott, P .S.; Kawabata, K.; Wolny, J .L.; Steidinger ,K. A., *Saxitoxin Puffer Fish Poisoning in the United States, with the First Report of Pyrodinium bahamense as the Putative Toxin Source*. . *Environmental Health Perspectives*, 2006. **114**(10): p. 1502-1507.
17. Noguchi, T. and Ebesu, J.S.M. , *J.Toxicol.-Toxin Rev.*, (2001). **20**: p. 1–10.
18. Ribeiro, A. S.; de O Ribeiro, L. M.; Silva, J. G.; Navarro, M.; Tonholo, J., *Characterization by atomic force microscopy of electrodeposited films of polypyrrole dinitrobenzoyl-derivative*. *Microscopy and Microanalysis*, 2005. **11**(S03): p. 146-149.

References

19. Åslund, A.; Sigurdson, C. J.; Klingstedt, T.; Grathwohl, S.; Bolmont, T.; Dickstein, D. L.; Glimsdal, E.; Prokop, S.; Lindgren, M.; Konradsson, P., *Novel pentameric thiophene derivatives for in vitro and in vivo optical imaging of a plethora of protein aggregates in cerebral amyloidoses*. ACS chemical biology, 2009. **4**(8): p. 673-684.
20. Kong, H.; Chung, D. S.; Kang, I.; Lim, E.; Jung, Y. K.; Park, J.; Park, C. E.; Shim, H., *Fluorene-based conjugated copolymers containing hexyl-thiophene derivatives for organic thin film transistors*. BULLETIN-KOREAN CHEMICAL SOCIETY, 2007. **28**(11): p. 1945.
21. Cataldo, F.; Maltese, P., *Synthesis of alkyl and *N*-alkyl-substituted polyanilines: A study on their spectral properties and thermal stability*. European polymer journal, 2002. **38**(9): p. 1791-1803.
22. Yáñez-Heras, J.; Planes, G. A.; Williams, F.; Barbero, C. A.; Battaglini, F., *Sequential electrochemical polymerization of aniline and their derivatives showing electrochemical activity at neutral pH*. Electroanalysis, 2010. **22**(23): p. 2801-2808.
23. Brodie III, E. D.; Feldman, C. R.; Hanifin, C.T; Motychak, J. E.; Mulcahy, D. G.; Williams, B. L.; Brodie Jr, E. D., *Parallel arms races between garter snakes and newts involving tetrodotoxin as the phenotypic interface of coevolution*. Journal of Chemical Ecology, 2005. **31**(2): p. 343-356.
24. Asakawa, M.; Toyoshima, T.; Shida, Y.; Noguchi, T.; Miyazawa, K., *Paralytic toxins in a ribbon worm *Cephalothrix* species (Nemertean) adherent to cultured oysters in Hiroshima Bay, Hiroshima Prefecture, Japan*. Toxicon, 2000. **38**(6): p. 763-773.

References

25. Asakawa, M.; Toyoshima, T.; Ito, K.; Bessho, K.; Yamaguchi, C.; Tsunetsugu, S.; Shida, Y.; Kajihara, H.; Mawatari, S.F.; Noguchi, T.; Miyazawa, K., *Paralytic toxicity in the ribbon worm Cephalothrix species (Nemertea) in Hiroshima Bay, Hiroshima Prefecture, Japan and the isolation of tetrodotoxin as a main component of its toxins*. *Toxicon*, 2003. **41**(7): p. 747–753.
26. Mebs, D., *Toxicity in animals. Trends in evolution?* *Toxicon*, 2001. **39**(1): p. 87–96.
27. Miyazawa, K.; Noguchi, T., *Distribution and origin of tetrodotoxin*. *Journal of toxicology-toxin reviews*, 2001. **20**(1): p. 11–33.
28. Hanifin, C.T.; Brodie III, E.D.; Brodie, E.D., *Tetrodotoxin levels of the rough-skin newt, Taricha granulose, increase in long-term captivity*. *Toxicon* 2002. **40**(8): p. 1149–1153.
29. Narahashi, Toshio, *Pharmacology of tetrodotoxin*. *Toxin Reviews*, 2001. **20**(1): p. 67-84.
30. Nishikawa, T.; Asai, M.; Isobe, M., *Asymmetric total synthesis of 11-deoxytetrodotoxin, a naturally occurring congener* *Journal of the American Chemical Society* 2002. **124**(26): p. 7847-7852.
31. Nishikawa, T.; Isobe, M., *Synthesis of Tetrodotoxin, a Classic but Still Fascinating Natural Product*. *The Chemical Record*, 2013. **13**(3): p. 286-302.
32. Ohyabu, N.; Nishikawa, T.; Isobe, M.; Nishikawa, T., *First asymmetric total synthesis of tetrodotoxin*. *Journal of the American Chemical Society*, 2003. **125**(29): p. 8798-8805.
33. Hinman, A.; Du Bois, J., *A stereoselective synthesis of (-)-tetrodotoxin*. *Journal of the American Chemical Society*, 2003. **125**(38): p. 11510-11511.

References

34. Sato, K.; Akai, S.; Shoji, H.; Yoshida, S.; Nagai, Y.; Suzuki, K.; Nakamura, Y.; Kajihara, Y.; Funabashi, M.; Yoshimura, J., *Stereoselective and efficient total synthesis of optically active tetrodotoxin from D-glucose*. The Journal of Organic Chemistry, 2008. **73**(4): p. 1234-1242.
35. Sato, K.; Akai, S.; Sugita, N.; Ohsawa, T.; Kogure, T.; Shoji, H.; Yoshimura, J., *Novel and Stereocontrolled Synthesis of (\pm)-Tetrodotoxin from m yo-Inositol*. The Journal of Organic Chemistry, 2005. **70**(19): p. 7496-7504.
36. Umezawa, T.; Hayashi, T.; Sakai, H.; Teramoto, H. Yoshikawa, T. Izumida, M.; Tamatani, Y.; Hirose, T. Ohfuné, Y.; Shinada, T., *Total synthesis of (-)-5, 6, 11-trideoxytetrodotoxin and its 4-epime*. Organic Letters 2006. **8**(21): p. 4971-4974.
37. Rodriguez, P.; Alfonso, A.; Vale, C.; Alfonso, C.; Vale, P.; Tellez, A.; Botana, L. M., *First toxicity report of tetrodotoxin and 5, 6, 11-trideoxyTTX in the trumpet shell Charonia lampas lampas in Europe*. Analytical Chemistry, 2008. **80**(14): p. 5622-5629.
38. Yotsu-Yamashita, M.; Nishimori, K.; Nitani, Y.; Isemura, M.; Sugimoto, A.; Yasumoto, T., *Binding Properties of 3H -PbTx-3 and 3H -Saxitoxin to Brain Membranes and to Skeletal Muscle Membranes of Puffer Fish *Fugu pardalis* and the Primary Structure of a Voltage-Gated Na⁺ Channel α -Subunit (fMNa1) from Skeletal Muscle of *F. pardalis**. Biochemical and Biophysical Research Communications, 2000. **267** (1): p. 403-412.
39. Paula Rodríguez , Amparo Alfonso , Paz Otero , Panagiota Katikou , Dimitrios Georgantelis , Luis M. Botana *Liquid chromatography–mass spectrometry method*

References

- to detect Tetrodotoxin and Its analogues in the puffer fish Lagocephalus sceleratus (Gmelin, 1789) from European waters.* Food Chemistry 2012. **132**: p. 1103–1111.
40. Yotsu-Yamashita, M.; Schimmele, B.; Yasumoto, T., *Isolation and structural assignment of 5-deoxytetrodotoxin from the puffer fish Fugu poecilonotus.* Bioscience, Biotechnology, and Biochemistry, 1999. **63**(5): p. 961-963.
41. Pires Jr, O. R.; Sebben, A.; Schwartz, E. F.; Morales, R. V.; Bloch Jr, C.; Schwartz, C. A., *Further report of the occurrence of tetrodotoxin and new analogues in the Anuran family Brachycephalidae.* SourceToxicon, 2005. **45**(1): p. 73-79.
42. Jang, Jun-Ho; Yotsu-Yamashita, Mari, *6,11-Dideoxytetrodotoxin from the puffer fish, Fugu pardalis.* Toxicon, 2007. **50**(7): p. 947-951.
43. Endo, A., Khora, S. S., Murata, M., & Yasumoto, T. , *Isolation of 11-nortetrodotoxin- 6(R)-ol and other tetrodotoxin derivatives from the puffer. Fugu niphobles* Tetrahedron Letter, (1988). **29**: p. 4127–4128.
44. Shoji, Y.; Yotsu-Yamashita, M.; Miyazawa, T.; Yasumoto, T., *Electrospray ionization mass spectrometry of tetrodotoxin and its analogs: liquid Chromatography/mass spectrometry, tandem mass spectrometry, and liquid chromatography/tandem mass spectrometry.* Analytical Biochemistry, 2001. **290** (1): p. 10-17.
45. Yotsu, Mari., Hayashi, Yotsu., Khora, Samanta., Sato, Shin'ichi., & Yasumoto, Takeshi, *Isolation and structural assignment of 11-nortetrodotoxin-6(S)-ol from the puffer Arothron nigropunctatus.* . Bioscience, Biotechnology, and Biochemistry,, 1992. **56**(2): p. 370-371.

References

46. Yotsu-Yamashita, M.; Mebs, D., *The levels of tetrodotoxin and its analogue 6-*epi* tetrodotoxin in the red-spotted newt, *Notophthalmus viridescens**. *Toxicon*, 2001. **39**(8): p. 1261-1263.
47. O'Leary, M.A.; Schneider, J.J.; Isbister, G.K., *Use of high performance liquid chromatography to measure tetrodotoxin in serum and urine of poisoned patients*. *Toxicon*, 2004. **44**: p. 549–553.
48. Kawatsu, K.; Hamano, Y.; Yoda, T.; Terano, Y.; Shibata, T., *Rapid and highly sensitive enzyme immunoassay for quantitative determination of tetrodotoxin*. *Japanese journal of medical science & biology*, 1997. **50**(3): p. 133-150.
49. Neagu, D.; Micheli, L.; Palleschi, G., *Study of a toxin–alkaline phosphatase conjugate for the development of an immunosensor for tetrodotoxin determination*. *Analytical and bioanalytical chemistry*, 2006. **385**(6): p. 1068-1074.
50. Jan H. Landsberg, Sherwood Hall, Jan N. Johannessen, Kevin D. White, Stephen M. Conrad, Jay P. Abbott, Leanne J. Flewelling, R. William Richardson, Robert W. Dickey, Edward L.E. Jester, Stacey M. Etheridge, Jonathan R. Deeds, Frances M. Van Dolah, Tod A. Leighfield, Yinglin Zou, Clarke G. Beaudry, Ronald A. Benner, Patricia L. Rogers, Paula S. Scott, Kenji Kawabata, Jennifer L. Wolny, and Karen A. Steidinger, *Saxitoxin Puffer Fish Poisoning in the United States, with the First Report of *Pyrodinium bahamense* as the Putative Toxin Source*. *Environmental Health Perspectives*, 2006. **114** (10): p. 1502 - 1507.
51. Leung, K. S-Y.; Fong, B. M-W.; Tsoi, Y-K., *Analytical challenges: determination of tetrodotoxin in human urine and plasma by LC-MS/MS*. *Marine drugs*, 2011. **9**(11): p. 2291-2303.

References

52. Kurono, Shunsuke; Hattori, Hideki; Suzuki, Osamu; Yamada, Takamichi; Seno, Hiroshi, *Sensitive analysis of tetrodotoxin in human plasma by solid-phase extractions and gas chromatography/mass spectrometry*. Analytical Letters., 2001. **34, 14**: p. 2439-2446.
53. Yu, Chung-Him; Yu, Chun-Fai; Tam, Sidney; Hoi-Fu Yu, Peter, *Rapid screening of tetrodotoxin in urine and plasma of patients with puffer fish poisoning by HPLC with creatinine correction*. Food Additives & Contaminants, 2010. **27**(1): p. 89-96.
54. Tsai, Y. H.; Hwang, D. F.; Cheng, C.A.; Hwang, C. C.; Deng, J. F., *Determination of tetrodotoxin in human urine and blood using C18 cartridge column, ultrafiltration and LC-MS*. Journal of Chromatography B, 2006. **832**(1): p. 75-80.
55. Horie, M.; Kobayashi, S.; Shimizu, N.; Nakazawa, H., *Determination of tetrodotoxin in puffer-fish by liquid chromatography-electrospray ionization mass spectrometry*. Analyst, 2002. **127**(6): p. 755 -759.
56. Leung, K. S.; Fong, B. W.; Tsoi, Y. K., *Analytical Challenges: Determination of Tetrodotoxin in Human Urine and Plasma by LC-MS/MS*. Marine Drugs, 2011. **9**(11): p. 2291-2303.
57. Pattnaik, P.; Srivastav, A., *Surface plasmon resonance-applications in food science research: A review*. Journal of Food Science and Technology-Mysore, 2006. **43**(4): p. 329-336.
58. Homola, J., *Present and future of surface plasmon resonance biosensors*. Analytical and bioanalytical chemistry, 2003. **377**(3): p. 528-539.
59. Horie, M.; Ishii, R.; Kobayashi, S.; Nakazawa, H., *Analysis of tetrodotoxin in puffer-fish by LC/MS*. Shokuhin Eiseigaku Zasshi, 2002. **43**(4): p. 234-238.

References

60. Hsiao-Chin Jena, Shin-Jung Linb, Yung-Hsiang Tsaic, Chun-Hsiang Chend, Zu-Chun Line, Deng-Fwu Hwang,, *Tetrodotoxin poisoning evidenced by solid-phase extraction combining with liquid Chromatography–tandem mass spectrometry*. Journal of Chromatography B, 2008. **871**: p. 95-100.
61. Akaki, K.; Hatano, K., *Determination of tetrodotoxin in puffer-fish tissues, and in serum and urine of intoxicated humans by liquid chromatography with tandem mass spectrometry*. Shokuhin Eiseigaku Zasshi, 2006. **47**(2): p. 46-50.
62. Yotsu-Yamashita, M.; Jang, J-H.; Cho, Y.; Konoki, K., *Optimization of simultaneous analysis of tetrodotoxin, 4-epitetrodotoxin, 4, 9-anhydrotetrodotoxin, and 5, 6, 11-trideoxytetrodotoxin by hydrophilic interaction liquid chromatography–tandem mass spectrometry*. Forensic Toxicology, 2011. **29**(1): p. 61-64.
63. Chih-Yu, C.; Hong-Nong, C., *Detection of tetrodotoxin by high performance liquid chromatography in lined-moon shell and puffer fish* Acta Zoologica Taiwanica, 1998. **9**(41): p. 41-48.
64. Hwang , P. A.; Tsai, Y. H.; Deng, J.H.; Cheng, C.A.; Ho, P. H.; wang, D. F.,, *Identification of Tetrodotoxin in a Marine Gastropod (Nassarius glans) Responsible for Human Morbidity and Mortality in Taiwan*. Journal of Food Protection, 2005. **8**: p. 1556-1775.
65. Hwang , Pai-An, Tsai, Yung-Hsiang; Deng, Jou-Fang; Cheng, Chao-An; Ho, Ping-Ho; wang, Deng-Fwu, *Identification of Tetrodotoxin in a Marine Gastropod (Nassarius glans) Responsible for Human Morbidity and Mortality in Taiwan*. Journal of Food Protection 2005. **8**: p. 1556-1775

References

66. Fong, B. MW.; Tam, S.; Tsui, SH.; Leung, K. SY., *Development and validation of a high-throughput double solid phase extraction–liquid chromatography–tandem mass spectrometry method for the determination of tetrodotoxin in human urine and plasma*. *Talanta*, 2011. **83**(3): p. 1030-1036.
67. Nishikawa, T., Isobe, M., *Synthesis of Tetrodotoxin, a Classic but Still Fascinating Natural Product*. *The Chemical Record*, , 2013. **13**: p. 286-302.
68. Peng, K.; Shu, Q.; Liu, Z.; Liang, S., *Function and Solution Structure of Huwentoxin-IV, a Potent Neuronal Tetrodotoxin (TTX)-sensitive Sodium Channel Antagonist from Chinese Bird Spider *Selenocosmia huwena**. *Journal of Biological Chemistry*, 2002. **277**(49): p. 47564 - 47571.
69. Taber, D. F.; Storck, P. H., *Synthesis of (-)-tetrodotoxin: Preparation of an advanced cyclohexenone intermediate*. *Journal of Organic Chemistry* 2003. **68**(29): p. 7768-7771.
70. Shoji, Yuki; Yotsu-Yamashita, Mari; Miyazawa, Teruo; Yasumoto, Takeshi, *Electrospray ionization mass spectrometry of tetrodotoxin and its analogs: liquid chromatography/mass spectrometry, tandem mass spectrometry, and liquid chromatography/tandem mass spectrometry*. *Analytical Biochemistry*, 2001. **290**(1): p. 10-17.
71. Yotsu-Yamashita, Mari; Yamagishi, Yuki; Yasumoto, Takeshi, *5,6,11-Trideoxytetrodotoxin from the puffer fish, *Fugu poecilonotus**. *Tetrahedron Letters*, 1995. **36**(51): p. 9329–9332.
72. Marr, J. C.; Hu, T.; Pleasance, S.; Quilliam, M. A.; Wright, J. C., *Detection of new 7-*O*-acyl derivatives of diarrhetic shellfish poisoning toxins by liquid chromatography-mass spectrometry*. *Toxicon*, 1992. **30**(12): p. 1621-1630.

References

73. G., Neagu D.; Micheli L.; Palleschi, *Study of a toxin-alkaline phosphatase conjugate for the development of an immunosensor for tetrodotoxin determination.* Analytical and bioanalytical chemistry, 2006. **385**(6): p. 1068-1074.
74. Rong, J.; Jianwei, W.; Xueyun, L., *Determination of tetrodotoxin in puffer fishes using monoclonal antibody-based direct competitive inhibition enzyme-linked immunosorbent assay [J].* Chinese Journal of Food Hygiene, 2002. **5**: p. 003.
75. Li, S.; Xin-an, J.; Huang, J.; Pan, Z.; Wang, L.; He, R., *Comparison of Two Methods of Quantitatively Detecting Tetrodotoxin.* Journal of Yangzhou University 2004. **2**: p. 013.
76. Yu Zhou, Yansong Li, Shiyong Lu, Honglin Ren, Zhaohui Li, Yuanyuan Zhang, Fengguang Pan, Wensen Liu, Junhui Zhang, Zengshan Liu., *Gold nanoparticle probe-based immunoassay as a new tool for tetrodotoxin detection in puffer fish tissues.* Sensors and Actuators B: Chemical 2010. **146**: p. 368-372.
77. Kao, C.Y., *Tetrodotoxin, saxitoxin and their significance in the study of excitation phenomena.* Pharmacological reviews, 1966. **18**(2): p. 997-1049.
78. Terlau, H.; Stühmer, W., *Structure and function of voltage-gated ion channel.* Naturwissenschaften, 1998. **85**(9): p. 437-444.
79. Kawatsu, K.; Shibata, T.; Yonekazu, H., *Application of immunoaffinity chromatography for detection of tetrodotoxin from urine samples of poisoned patients.* Toxicon, 1999. **37**(2): p. 325-333.
80. Chou, J.C.; Chen, C.C.; Lee, C.C., *Development of Microcontroller Applied to Chlorine Ion Measurement System.* Sensors Journal, 2012. **12**(6): p. 2215-2221.
81. Cho, H. E.; Ahn, S. Y.; Son, I. S.; In, S.; Hong, R. S.; Kim, D. W.; Woo, S. H.; Moon, D. C.; Kim, S., *Determination and validation of tetrodotoxin in human*

References

- whole blood using hydrophilic interaction liquid chromatography–tandem mass spectroscopy and its application*. Forensic Science International, 2012. **217**(1): p. 76-80.
82. Chou, J. C.; Chen, C. C.; Lee, C. C. , *Development of Microcontroller Applied to Chlorine Ion Measurement System*. Sensors Journal, IEEE, 2012. **12**(6): p. 2215-2221.
83. Yu, C.H.; Yu, C.F.; Tam, S.; Yu, P.H.F., *Rapid screening of tetrodotoxin in urine and plasma of patients with puffer fish poisoning by HPLC with creatinine correction*. Food Addit. Contam, 2010. **27**: p. 89–96.
84. Fukushima, S.; Ohtsuka, Y. , *Tetrodotoxin*. 2005: Springer.
85. Fong, Bonnie Mei-Wah; Tam, Sidney; Tsui, Sik-Hon; Leung, Kelvin Sze-Yin, *Development and validation of a high-throughput double solid phase extraction–liquid chromatography–tandem mass spectrometry method for the determination of tetrodotoxin in human urine and plasma*. Talanta, 2011. **83**, **3**: p. 1030-1036.
86. Hwang, PA.; Tsai, YH.; Deng, JF.; Cheng, C-A.; Ho, PH.; Hwang, DF., *Identification of tetrodotoxin in a marine gastropod (Nassarius glans) responsible for human morbidity and mortality in Taiwan*. Journal of Food Protection, 2005. **68**(8): p. 1696-1701.
87. Wallace, GG.; Smyth, M.; Zhao, H., *Conducting electroactive polymer-based biosensors*. TrAC Trends in Analytical Chemistry, 1999. **18**(4): p. 245-251.
88. Gaihre, B.; Alici, G.; Spinks, G. M.; Cairney, J. M., *Synthesis and performance evaluation of thin film PPy-PVDF multilayer electroactive polymer actuators*. Sensors and Actuators A 2011. **165**(2): p. 321-328.

References

89. Spinks, G. M.; Dominis, A. J.; Wallace, G. G.; Tallman, D. E., *Electroactive conducting polymers for corrosion control*. Journal of Solid State Electrochemistry, 2002. **6**(2): p. 85-100.
90. Gelling, V. J.; Wiest, M. M.; Tallman, D. E.; Bierwagen, G. P.; Wallace, G. G., *Electroactive-conducting polymers for corrosion control: 4. Studies of poly (3-octyl pyrrole) and poly (3-octadecyl pyrrole) on aluminum 2024-T3 alloy*. Progress in organic coatings, 2001. **43**(1): p. 149-157.
91. Lira-Cantú, M.; Gómez-Romero, P., *The Organic-Inorganic Polyaniline/V₂O₅ System. Application as a High-Capacity Hybrid Cathode for Rechargeable Lithium Batteries*. Journal of Electrochemical Society, 1999. **146**(6): p. 2029-2033.
92. Abia, Atogho Jude, *Polyaniline and its Derivatives for Environmental Analysis*, in *The faculty of the Department of Chemistry*. 2006, East Tennessee State University: Johnson City. p. 69.
93. Shahinpoor, M.; Kim, K. J., *Ionic polymer-metal composites: IV. Industrial and medical applications*. Smart Materials and Structures, 2005. **14**(1): p. 197.
94. Toi, Y.; Kang, S. S., *Finite element analysis of two-dimensional electrochemical-mechanical response of ionic conducting polymer-metal composite beams*. Computers & Structures, 2005. **83**(31): p. 2573-2583.
95. Mano, N.; Mao, F.; Heller, A., *Characteristics of a miniature compartment-less glucose-O₂ biofuel cell and its operation in a living plant*. Journal of the American Chemical 2003. **125**(21): p. 6588-6594.
96. Manju, G.; Chaubey, A.; Malhotra, B.D., *Application of conducting polymers to biosensors*. biosensors and Bionelectronics, 2002. **17**(5): p. 345-359.

References

97. Saxena, V.; Malhotra, B.D., *Prospects of conducting polymers in molecular electronics*. Current Applied Physics, 2003. **3**, **2**: p. 293-305.
98. Palys, B., Kudelski, A., Stankiewicz, A. & Jackowska, K., *Influence of anions on formation and electroactivity of poly-2,5-dimethoxyaniline*. Synthetic Metals, (2000). **108**: p. 111–119.
99. Saxena, V.; Malhotra, B.D., *Prospects of conducting polymers in molecular electronics*. Current Applied Physics, 2003. **3** p. 293-305.
100. Lee, Myung Sub; Lee, Sung Bum; Lee, Jun Young; Kang, Han Saem; Kang, Hyun Suk; Joo, Jinsoo; Epstein, Arthur J, *All-polymer FET based on simple photolithographic micro-patterning of electrically conducting polymer*. Molecular Crystals and Liquid Crystals, 2003. **405**, **1**: p. 171-178.
101. Wallace, G. G.; Teasdale, P. R.; Spinks, G. M.; Kane-Maguire, L. P., *Introduction: Academic research in conducting polymers*. Conductive electroactive polymers: intelligent polymer systems. 2008, London New york: CRC press.
102. Immaculate, M., *Synthesis, Electrostatics and Biosensor Applications of Novel Sulphonated Polyaniline Nanocomposites*, in *Chemistry*. 2007, University of the Western Cape Town: cape Town. p. 223.
103. Yanyan, W., Kalle, L., *Influence of Dopant on Electroactivity of Polyaniline*. Macromolecular Symposia, 2012. **317**, **318**: p. 240–247.
104. Lindfors, T.; Ivaska, A., *Potentiometric and UV–vis characterisation of N-substituted polyanilines*. Journal of Electroanalytical Chemistry, 2002. **535**(1): p. 65-74.
105. Shu-Hua, C.; Sheng-Huei, H.; Tzy-Hsiang, S.; Guey-Sheng, L., *Novel aromatic poly (amine-imide) s bearing a pendent triphenylamine group: synthesis, thermal,*

References

- photophysical, electrochemical, and electrochromic characteristics.* Macromolecules, 2005. **38**, **2**: p. 307-316.
106. Gemeay, A. H.; El-Sharkawy, R. G.; Mansour, I. A.; Zaki, A. B., *Catalytic activity of polyaniline/MnO₂ composites towards the oxidative decolorization of organic dyes.* Applied Catalysis B: Environmental, 2008. **80**(1): p. 106-115.
107. Niu, L.; Li, Q.; Wei, F.; Wu, S.; Liu, P.; Cao, X., *Electrocatalytic behavior of Pt-modified polyaniline electrode for methanol oxidation: effect of Pt deposition modes.* Journal of Electroanalytical Chemistry, 2005. **578**(2): p. 331-337.
108. Li, X.; Wang, D.; Cheng, G.; Luo, Q.; An, J.; Wang, Y., *Preparation of polyaniline-modified TiO₂ nanoparticles and their photocatalytic activity under visible light illumination.* Applied Catalysis B: Environmental I, 2008. **81**(3): p. 267-273.
109. MacDiarmid, A. G., "Synthetic metals": A novel role for organic polymers (Nobel lecture). Angewandte Chemie International Edition, 2001. **40**(14): p. 2581-2590.
110. Pud, A.; Ogurtsov, N.; Korzhenko, A.; Shapoval, G., *Some aspects of preparation methods and properties of polyaniline blends and composites with organic polymers.* Progress in Polymer Science, 2003. **28**(12): p. 1701-1753.
111. Chen, C. H., *Thermal and morphological studies of chemically prepared emeraldine-base-form polyaniline powder.* Journal of Applied Polymer Science, 2003. **89**(8): p. 2142-2148.
112. Koh, J. K.; Kim, J.; Kim, B.; Kim, J. H.; Kim, E., *Highly Efficient, Iodine-Free Dye-Sensitized Solar Cells with Solid-State Synthesis of Conducting Polymers.* Advanced Materials, 2011. **23**(14): p. 1641-1646.

References

113. Delvaux, M.; Duchet, J.; Stavaux, P. Y.; Legras, R.; Demoustier-Champagne, S., *Chemical and electrochemical synthesis of polyaniline micro-and nano-tubules*. *Synthetic Metals*, 2000. **113**(3): p. 275-280.
114. Kinyanjui, J. M.; Hatchett, D. W.; Smith, J. A.; Josowicz, M., *Chemical synthesis of a polyaniline/gold composite using tetrachloroaurate*. *Chemistry of materials*, 2004. **16**(17): p. 3390-3398.
115. Magnuson, M.; Guo, J. H.; Butorin, S. M.; Agui, A.; Sâthe, C.; Nordgren, J.; Monkman, A. P., *The electronic structure of polyaniline and doped phases studied by soft x-ray absorption and emission spectroscopies*. *Journal of Chemical Physics*, 1999. **111**(10): p. 4756-4761.
116. Pruneanu, S., Veress, E., Marian, I. & Oniciu, L., *Characterization of polyaniline by cyclic voltammetry and UV-Vis absorption spectroscopy*. *Journal of Materials Science*, (1999). **34**: p. 2733–2739.
117. Mathebe, N.G.R., Morrin, A. & Iwuoha, E.I., *Electrochemistry and scanning electron microscopy of polyaniline/peroxidase-based biosensor*. *Talanta*, (2004). **64**: p. 115–120.
118. Reemts, J., Parisi, J. & Schlettwein, D., *Electrochemical growth of gas-sensitive polyaniline thin films across an insulating gap*. *Thin Solid Films*, (2004). **466**: p. 320– 325.
119. Pruneanu, S.; Veress, E.; Marian, I.; Oniciu, L., *Characterization of polyaniline by cyclic voltammetry and UV-Vis absorption spectroscopy*. *Journal of Materials Science*, 1999. **34**: p. 2733-2739.

References

120. Abdolahi, A.; Hamzah, E.; Ibrahim, Z.; Hashim, S., *Synthesis of uniform polyaniline nanofibers through interfacial polymerization*. *Materials*, 2012. **5**(8): p. 1487-1494.
121. Lukachova, Lilia V; Shkerin, Egor A; Puganova, Elena A; Karyakina, Elena E; Kiseleva, Svetlana G; Orlov, Andrey V; Karpacheva, Galina P; Karyakin, Arkady A, *Electroactivity of chemically synthesized polyaniline in neutral and alkaline aqueous solutions: Role of self-doping and external doping*. *Journal of Electroanalytical Chemistry*, 2003. **544**: p. 59-63.
122. Bhadra, S.; Singha, N. K.; Khastgir, D., *Electrochemical synthesis of polyaniline and its comparison with chemically synthesized polyaniline*. *Journal of Applied Polymer Science*, 2007. **104** (3): p. 1900-1904.
123. Eftekhari, A., *Electropolymerization of aniline onto passivated substrate and its application for preparation of enzyme-modified electrode*. *Synthetic Metals*, 2004. **145**(2): p. 211-216.
124. Pournaghi-Azar, M. H.; Habibi, B., *Electropolymerization of aniline in acid media on the bare and chemically pre-treated aluminum electrodes: A comparative characterization of the polyaniline deposited electrodes*. *Electrochimica Acta*, 2007. **52**(12): p. 4222-4230.
125. Eftekhari, A.; Yazdani, B., *Morphological effects of Ni nanostructures on electropolymerization of aniline*. *Journal of Applied Polymer Science*, 2011. **122**(3): p. 1579-1586.
126. Zhang, G.; Li, X.; Jia, H.; Pang, X.; Yang, H.; Wang, Y.; Ding, K., *Preparation and Characterization of Polyaniline (PANI) doped-Li₃V₂ (PO₄)₃*. *International Journal of Electrochemical Science*, 2012. **7**: p. 830-843.

References

127. Le, T. H.; Trinh, N. T.; Nguyen, L. H.; Nguyen, H. B.; Nguyen, V. A.; Nguyen, T. D., *Electrosynthesis of polyaniline–mutilwalled carbon nanotube nanocomposite films in the presence of sodium dodecyl sulfate for glucose biosensing*. *Advances in Natural Sciences: Nanoscience and Nanotechnology*, 2013. **4**(2): p. 025014.
128. Saraswat, A.; Sharma, L. K.; Singh, S.; Singh, R. P., *Electrochemical assisted synthesis and characterization of perchloric acid-doped aniline-functionalized copolymers*. *Synthetic Metals*, 2013. **167**: p. 31-36.
129. Mallick, K.; Witcomb, M. J.; Scurrall, M. S., *In situ synthesis of copper nanoparticles and poly (*o*-toluidine): A metal–polymer composite material*. *European polymer journal*, 2006. **42**(3): p. 670-675.
130. Bicak, N.; Karagoz, B., *Polymerization of aniline by copper-catalyzed air oxidation*. *Journal of Polymer Science Part A: Polymer Chemistry*, 2006. **44**(20): p. 6025-6031.
131. Lee, Y.; Chen, S.; Tu, H.; Yau, S.; Fan, L.; Yang, Y.; Dow, WP., *In Situ STM Revelation of the Adsorption and Polymerization of Aniline on Au (111) Electrode in Perchloric Acid and Benzenesulfonic Acid*. *Langmuir*, 2010. **26**(8): p. 5576-5582.
132. Stejskal, J.; Gilbert, R. G., *Polyaniline. Preparation of a conducting polymer (IUPAC technical report)*. *Pure and Applied Chemistry*, 2002. **74**(5): p. 857-867.
133. Lu, W.; Fadeev, A. G.; Qi, B.; Smela, E.; Mattes, B. R.; Ding, J.; Spinks, G. M.; Mazurkiewicz, J.; Zhou, D.; Wallace, G. G.; MacFarlane, D. R.; Forsyth, S. A.; Forsyth, M., *Use of ionic liquids for pi-conjugated polymer electrochemical devices*. *Science*, 2002. **297**(5583): p. 983-987.

References

134. Jiang, Y.; Wang, A.; Kan, J., *Selective uricase biosensor based on polyaniline synthesized in ionic liquid*. *Sensors Actuators B: Chemical*, 2007. **124**(2): p. 529-534.
135. Innis, P. C.; Mazurkiewicz, J.; Nguyen, T.; Wallace, G. G.; MacFarlane, D., *Enhanced electrochemical stability of polyaniline in ionic liquids*. *Current Applied Physics*, 2004. **4**(2): p. 389-393.
136. Can, M.; Özçiçek, P. N.; Yildiz, A., *Theoretical investigation of the proton effect on electropolymerization of aniline*. *Polymer*, 2003. **44** (8): p. 2585-2588.
137. Gok, A.; Omastova, M.; Prokes, J. , *Synthesis and characterization of red mud/polyaniline composites: electrical properties and thermal stability*. *European polymer journal*, 2007. **43**: p. 2471-2480.
138. Brožová, L.; Holler, P.; Kovářová, J.; Stejskal, J.; Trchová, M., *The stability of polyaniline in strongly alkaline or acidic aqueous media*. *Polymer Degradation and Stability*, 2008. **93**(3): p. 592-600.
139. Gaihre, B.; Alici, G.; Spinks, G. M.; Cairney, J. M., *Synthesis and performance evaluation of thin film PPy-PVDF multilayer electroactive polymer actuators*. *Sensors and Actuators A: Physical*, 2011. **165**(2): p. 321-328.
140. Millner, P. A.; Hays, H. CW.; Vakurov, A.; Pchelintsev, N. A.; Billah, M. M.; Rodgers, M. A., *Nanostructured transducer surfaces for electrochemical biosensor construction—Interfacing the sensing component with the electrode*, in *Seminars in Cell & Developmental Biology*. 2009: University of Leed. p. 34-40.
141. Paczosa-Bator, B.; Piech, R.; Cabaj, L., *The influence of an intermediate layer on the composition stability of a polymeric ion-selective membrane*. *Electrochimica Acta*, 2012. **85**: p. 104-109.

References

142. Chulanetra, M.; Bangphoomi, K.; Sookrung, N.; Thanongsaksrikul, J.; Srimanote, P.; Sakolvarvaree, Y.; Choowongkomon, K.; Chaicumpa, W., *Human ScFv that block sodium ion channel activity of tetrodotoxin*. *Toxicon*, 2012. **59**(2): p. 272-282.
143. Zacharias, G.; Marie-Line, L.; Rosario, S.; Kay, S., *Selective Complexation of Li⁺ in Water at Neutral pH Using a Self-Assembled Ionophore*. *Journal of the American Chemical Society* 2003. **125**(45): p. 13638-13639.
144. Bühlmann, P.; Pretsch, E.; Bakker, E., *Carrier-based ion-selective electrodes and bulk optodes. 2. Ionophores for potentiometric and optical sensors*. *Chemical Reviews*, 1998. **98**(4): p. 1593-1688.
145. Pandey, P. C.; Singh, G., *Electrochemical synthesis of tetraphenylborate-doped polypyrrole: Dependence of zinc ion sensing on the polymeric microstructure*. *Sensors Actuators B: Chemical*, 2002. **85**(3): p. 256-262.
146. Teixeira, M. F.; Bergamini, M. F.; Bocchi, N., *Application of the potentiometric stripping analysis with constant current for the determination of lithium ions using a spinel-type manganese (IV) oxide-modified carbon paste electrode*. *Current Analytical Chemistry*, 2010. **6**(2): p. 161-165.
147. Khayatian, G.; Shariati, S.; Salimi, A., *Thallium (I)-selective membrane potentiometric sensor based on dibenzylidiazacrown-6*. *Bulletin-Korean Chemical Society*, 2003. **24**(4): p. 421-425.
148. Malon, A.; Maj-Zurawska, M., *The new methods of determination of Mg²⁺, Ca²⁺, Na⁺ and K⁺ ions in erythrocytes by ion selective electrodes*. *Sensors Actuators B: Chemical*, 2005. **108**(1): p. 828-831.

References

149. Ni, X.; Castanares, M.; Mukherjee, A.; Lupold, S.E., *Nucleic acid aptamers: clinical applications and promising new horizons*. Current Medicinal Chemistry, 2011. **18**(27): p. 4206-4214.
150. Liss, M.; Petersen, B.; Wolf, H.; Prohaska, E., *An aptamer-based quartz crystal protein biosensor*. Analytical Chemistry, 2002. **74**(17): p. 4488-4495.
151. Kim, Y. S.; Gu, M. B., *Advances in aptamer screening and small molecule aptasensors*. Biosensors Based on Aptamers and Enzymes, 2014. **140**: p. 29-67.
152. Proske, D.; Blank, M.; Buhmann, R.; Resch, A., *Aptamers-basic research, drug development, and clinical applications*. Applied Microbiology and Biotechnology, 2005. **69**(4): p. 367-374.
153. McKeague, M.; DeRosa, M. C., *Challenges and opportunities for small molecule aptamer development*. Journal of nucleic acids, 2012. **2012**(2012): p. 1-20.
154. Silverman, S. K., *Artificial functional nucleic acids: aptamers, ribozymes, and deoxyribozymes identified by in vitro selection*. Functional Nucleic Acids For Analytical Applications, 2009. **1**: p. 47-108.
155. Shimada, T.; Fujita, N.; Maeda, M.; Ishihama, A., *Systematic search for the Cr-binding promoters using genomic SELEX system*. Genes to Cells, 2005. **10**(9): p. 907-918.
156. White, R.; Rusconi, C.; Scardino, E.; Wolberg, A.; Lawson, J.; Hoffman, M.; Sullenger, B., *Generation of species cross-reactive aptamers using "toggle" SELEX*. Molecular Therapy, 2001. **4**(6): p. 567-573.
157. Sefah, K.; Shangguan, D.; Xiong, X.; O'Donoghue, M. B.; Tan, W., *Development of DNA aptamers using cell-SELEX*. Nat Protocol, 2010. **5**(6): p. 1169-1185.

References

158. Devor, E. J.; Behlke, M. A., *Strategies for attaching oligonucleotides to solid supports*. IDTutorial: DNA Replication., 2005: p. 1-24.
159. Peelen, D.; Smith, L. M., *Immobilization of amine-modified oligonucleotides on aldehyde-terminated alkanethiol monolayers on gold*. Langmuir, 2005. **21**(1): p. 266-271.
160. DeChancie, J.; Houk, K. N., *The origins of femtomolar protein-ligand binding: hydrogen-bond cooperativity and desolvation energetics in the biotin-(strept) avidin binding site*. Journal of the American Chemical 2007. **129**(17): p. 5419-5429.
161. Maryanski, J. L.; Verdini, A. S.; Weber, P. C.; Salemme, F. R.; Corradin, G., *Competitor analogs for defined T cell antigens: peptides incorporating a putative binding motif and polyproline or polyglycine spacers*. Cell, 1990. **60**(1): p. 63-72.
162. Balamurugan, S.; Obubuafo, A.; Soper, S. A.; Spivak, D.A., *Surface immobilization methods for aptamer diagnostic applications*. Analytical and bioanalytical chemistry, 2008. **390**(4): p. 1009-1021.
163. Elnashar, M. M., *Review article: Immobilized molecules using biomaterials and nanobiotechnology*. Journal of Biomaterials and Nanobiotechnology, 2010. **1**(01): p. 61-77.
164. Çetinus, Ş. A.; Şahin, E.; Saraydin, D., *Preparation of Cu(II) Adsorbed Chitosan Beads for Catalase Immobilization* Food Chemistry, 2009. **114**(3): p. 962- 969.
165. Shousha, G. H., *Novel Application of Luffa cylindrica In Production of Fructose*. Australian Journal of Basic and Applied Sciences, 2011. **5**(12): p. 2127-2137.
166. Hirsh, S. L.; Bilek, M.M.; Nosworthy, N. J.; Kondyurin, A.; Dos Remedios, C. G.; McKenzie, D. R., *A comparison of covalent immobilization and physical*

References

- adsorption of a cellulase enzyme mixture*. Langmuir, 2010. **26**(17): p. 14380-14388.
167. Xie, T.; Wang, A.; Huang, L.; Li, H.; Chen, Z.; Wang, Q.; Yin, X., *Recent advance in the support and technology used in enzyme immobilization*. Journal of Biotechnology, 2009. **8**(19): p. 4724- 4733.
168. Cho, E. J.; Collett, J. R.; Szafranska, A. E.; Ellington, A. D., *Optimization of aptamer microarray technology for multiple protein targets*. Analytica Chimica Acta, 2006. **564**(1): p. 82-90.
169. Velasco-Garcia, M.; Missailidis, S., *New trends in aptamer-based electrochemical biosensors*. Gene Therapy and Molecular Biology, 2009. **13**(1): p. 1-10.
170. Hianik, T.; Ostatná, V.; Sonlajtnerova, M.; Grman, I., *Influence of ionic strength, pH and aptamer configuration for binding affinity to thrombin*. Bioelectrochemistry, 2007. **70**(1): p. 127-133.
171. Huang, C. C.; Cao, Z.; Chang, H. T.; Tan, W., *Protein-protein interaction studies based on molecular aptamers by affinity capillary electrophoresis*. Analytical Chemistry, 2004. **76**(23): p. 6973-6981.
172. Hwang, J.; Nishikawa, S., *Novel approach to analyzing RNA aptamer-protein interactions: toward further applications of aptamers*. Journal of Biomolecular Screening, 2006. **11**(6): p. 599-605.
173. González-Garcia, M. B.; Fernandez-Sanchez, C.; Costa-Garcia, A., *Colloidal gold as an electrochemical label of streptavidin-biotin interaction*. Biosensors and Bioelectronics, 2000. **15**(5): p. 315-321.
174. Castañeda, M.; Alegret, S.; Merkoci, A., *Electrochemical sensing of DNA using gold nanoparticles*. Electroanalysis, 2007. **19**(7-8): p. 743-753.

References

175. Brockstedt, U.; Uzaroeska, A.; Montpetit, A.; Pfau, W.; Labuda, D., *In vitro evolution of RNA aptamers recognizing carcinogenic aromatic amines*. Biochemical and Biophysical Research Communications, 2003. **313**(4): p. 1004-1008.
176. Tombelli, S.; Minunni, M.; Mascini, M., *Aptamers-based assays for diagnostics, environmental and food analysis*. Biomolecular Engineering, 2007. **24**(2): p. 191-200.
177. Fan, L.; Zhao, G.; Shi, H.; Liu, M.; Li, Z., *A highly selective electrochemical impedance spectroscopy-based aptasensor for sensitive detection of acetamiprid*. Biosensors and Bioelectronics, 2013. **43**: p. 12-18.
178. Chen, Z.; Li, L.; Zhao, H.; Guo, L.; Mu, X., *Electrochemical impedance spectroscopy detection of lysozyme based on electrodeposited gold nanoparticles*. Talanta, 2011. **83**(5): p. 1501-1506.
179. Özkan, S. A.; Uslu, B.; Aboul-Enein, H. Y., *Analysis of pharmaceuticals and biological fluids using modern electroanalytical techniques*. Critical Reviews in Analytical Chemistry, 2003. **33**(3): p. 155-181.
180. Vielstich, W., *Cyclic voltammetry*. Handbook of Fuel Cells. 2010: Wiley Online Library.
181. Chevion, S.; Roberts, M. A.; Chevion, M., *The use of cyclic voltammetry for the evaluation of antioxidant capacity*. Free Radical Biology and Medicine, 2000. **28**(6): p. 860-870.
182. DuVall, S. H.; McCreery, R. L., *Self-catalysis by catechols and quinones during heterogeneous electron transfer at carbon electrodes*. Journal of the American Chemical Society, 2000. **122**(28): p. 6759-6764.

References

183. Zare, H. R.; Nasirizadeh, N.; Mazloun, A. M., *Electrochemical properties of a tetrabromo-*p*-benzoquinone modified carbon paste electrode. Application to the simultaneous determination of ascorbic acid, dopamine and uric acid.* Journal of Electroanalytical Chemistry, 2005. **577**(1): p. 25-33.
184. Liu, B.; Mirkin, M. V., *Charge Transfer Reactions at the Liquid / Liquid Interface.* Analytical Chemistry, 2001. **73**(23): p. 670-677.
185. Reymond, F.; Fermin, D.; Lee, J.; Girault, H., *Potential applications in molecular biology of the electrochemistry of liquid/liquid interfaces.* . Electrochimical Acta, 2000. **45**(14): p. 2647-2662.
186. Osborne, M. C.; Shao, Y.; Pereira, C. M.; Girault, H. H., *Micro-hole interface for the amperometric determination of ionic species in aqueous solutions.* Journal of Electroanalytical Chemistry 1994. **364**(1): p. 155-161.
187. Osborne, M. D., Girault, H. H., *The liquid-liquid micro-interface for the amperometric detection of urea.* Electroanalysis, 1995. **7**: p. 714-721.
188. Silva, F.; Sousa, M. J.; Pereira, C. M., *Electrochemical study of aqueous-organic gel micro-interfaces.* Electrochimical Acta, 1997. **42**(20): p. 3095-3103.
189. Ohkouchi, T.; Kakutani, T.; Osakai, T.; Senda, M., *Voltammetry with an ion-selective microelectrode based on polarizable oil/water interface.* Analytical Sciences, 1991. **7**(3): p. 371-376.
190. Lee, H. J.; Beattie, P. D.; Seddon, B. J.; Osborne, M. D.; Girault, H. H., *Amperometric ion sensors based on laser-patterned composite polymer membranes.* Journal of Electroanalytical Chemistry, 1997. **440**(1): p. 73-82.

References

191. Hossain, M. M.; Girault, H. H.; Lee, H. J., *Voltammetric Studies of Anion Transfer Reactions Across a Microhole Array-Water/PVC-NPOE Gel Interface*. Bulletin-Korean Chemical Society, 2012. **33**(5): p. 1735.
192. Lee, H. J.; Beriet, C.; Girault, H. H. , *Amperometric detection of alkali metal ions on micro-fabricated composite polymer membranes*. Journal of Electroanalytical Chemistry, 1998. **453**(1): p. 211-219.
193. Lee, H. J.; Girault, H. H., *Amperometric ion detector for ion chromatography*. Analytical Chemistry, 1998. **70**(20): p. 4280-4285.
194. Lee, H. J.; Pereira, C. M.; Silva, A. F.; Girault, H. H. , *Pulse amperometric detection of salt concentrations by flow injection analysis using ionodes*. Analytical Chemistry, 2000. **72**(5): p. 562-5566.
195. Wilke, S.; Schürz, R.; Wang, H. , *Amperometric ion detection in capillary zone electrophoresis by ion transfer across a liquid-liquid microinterface*. Analytical Chemistry, 2001. **73**(6): p. 1146-1154.
196. Liu, B.; Shao, Y.; Mirkin, M. V. , *Dual-pipet techniques for probing ionic reactions*. Analytical Chemistry, 2000. **72**(3): p. 510-519.
197. Liu, B.; Mirkin, M. V., *Charge Transfer Reactions at the Liquid / Liquid Interface*. Analytical Chemistry, 2001. **73**: p. 670-677.
198. Vanysek, P., *in*. Mod. Electroanal. Tech. Chem. Anal. Ser., (John Wiley: New York, 1996). **139**: p. 337-364 .
199. Norouzi, P., *Electrochemical determination of surface active compounds at noble metal ultramicroelectrodes in flowing solutions*. 1999.
200. Barsoukov, E.; Macdonald, J., *Impedance spectroscopy: theory, experiment, and applications*. Second Edition ed ed. 2005: John, Wiley and Sons, Inc.: Hoboken.

References

201. Edwards, J. C., *Principles of NMR*. Process NMR Associates LLC, 87A Sand Pit Rd, Danbury CT, 2009. **200**: p. 1999-2005.
202. Wade, J.G., *Organic Chemistry I*. Pearson Education, Editor. 2003, New Jersey.
203. Chang, R., *Physical Chemistry for the Biosciences*. 2005: USA: University Science Books.
204. Atkins, P.; Julio, D. P., *Physical Chemistry for the Life Sciences*. 2006, Freeman and Company: New York, NY: W.H. p. 550-555.
205. Vollhardt, K.; Peter, C.; Schore, N., *Organic chemistry structure and function*. 2007: New York: W.H. Freeman.
206. Scheer, A. M.; Welz, O.; Sasaki, D. Y.; Osborn, D. L.; Taatjes, C. A., *Facile Rearrangement of 3-Oxoalkyl Radicals is Evident in Low-Temperature Gas-Phase Oxidation of Ketones*. Journal of the American Chemical Society, 2013. **135**(38): p. 14256-14265.
207. Dong, J.; Solntsev, K.M.; Tolbert, L. M., *Solvatochromism of the green fluorescence protein chromophore and its derivatives*. Journal of the American Chemical Society, 2006. **128**(37): p. 12038-12039.
208. M. Sauer, J. Hofkens, and J. Enderlein, *Handbook of Fluorescence Spectroscopy and Imaging.*, in *Basic Principles of Fluorescence Spectroscopy*. 2011, WILEY-VCH Verlag GmbH & Co. KGaA Weinheim.
209. Lakowicz, J. R. , *Principles of Fluorescence Spectroscopy*. 3rd edition ed. 2006, Baltimore, Maryland, USA. 518.
210. Lysetska, M.; Knoll, A.; Boehringer, D.; Hey, T.; Krauss, G.; Krausch, G., *UV light-damaged DNA and its interaction with human replication protein A: an*

References

- atomic force microscopy study*. Nucleic Acids Research, 2002. **30**(12): p. 2686-2691.
211. Barth, C.; Hynninen, T.; Bielecki, M.; Henry, C. R.; Foster, A. S.; Esch, F.; Heiz, U., *AFM tip characterization by Kelvin probe force microscopy*. New Journal of Physics, 2010. **12**(9): p. 093024.
212. Glatzel, T.; Hoppe, H.; Sariciftci, N.S.; Lux-Steiner, M.C.; Komiyama, M., *Kelvin probe force microscopy study of conjugated polymer/fullerene organic solar cells*. Japanese journal of applied physics, 2005. **44**(7S): p. 5370.
213. Stoiljković, Z. Ž.; Avramov, M. L.; Petrović, S. D.; Mijin, D. Ž.; Stevanović, S. I.; Lačnjevac, U. Č.; Marinković, A. D., *Voltammetric and Square Wave Anodic Stripping Determination of Amlodipine Besylate on Gold Electrode*. International Journal of Electrochemical Science, 2012. **7**(3): p. 2288 - 2303.
214. Spătaru, T.; Spătaru, N.; Fujishima, A., *Detection of aniline at boron-doped diamond electrodes with cathodic stripping voltammetry*. Talanta, 2007. **73**(2): p. 404-406.
215. Obaid, A.Y.; El-Mossalamy, E. H.; Al-Thabaiti, S. A.; El-Hallag, I. S.; Hermas, A. A.; Asiri, A. M., *Electrodeposition and Characterization of Polyaniline on Stainless Steel Surface via Cyclic, Convulsive Voltammetry and SEM in Aqueous Acidic Solutions*. International Journal of Electrochemical Science, 2014. **9**: p. 1003-1015.
216. Darowicki, K.; Kawula, J., *Impedance characterization of the process of polyaniline first redox transformation after aniline electropolymerization*. Electrochimica Acta, 2004. **49** (27): p. 4829-4839.

References

217. Bhatti, N. K.; Subhani, M. S.; Khan, A. Y.; Qureshi, R.; Rahman, A., *Heterogeneous Electron Transfer Rate Constants of Viologen Monocations at a Platinum Disk Electrode*. Turkish Journal of Chemistry, 2006. **30**(2): p. 165-180.
218. Rangel-Vázquez, N. A.; Salgado-Delgado, R.; García-Hernández, E.; Mendoza-Martínez, A. M., *Characterization of Copolymer Based in Polyurethane and Polyaniline (PU/PANI)*. Journal of the Mexican Chemical Society, 2009. **53**(4): p. 248-252.
219. Iwuoha, I.E.; Mavundla, S. E.; Somerset, V. S.; Petrik, L. F.; Klink, M. J.; Sekota, M.; Bakers, P., *Electrochemical and Spectroscopic Properties of Fly Ash–Polyaniline Matrix Nanorod Composites*. Microchimica Acta, 2006. **155**(3-4): p. 453-458.
220. Sun, X.; Cao, Y.; Gong, Z.; Wang, X.; Zhang, Y.; Gao, J., *An Amperometric Immunosensor Based on Multi-Walled Carbon Nanotubes-Thionine-Chitosan Nanocomposite Film for Chlorpyrifos Detection*. Sensors 2012. **12**(12): p. 17247-17261.
221. Chira, A.; Covaci, O. I.; Radu, G. L., *A comparative study of gold electrodes modification methods with aromatic compounds based on diazonium and thiol chemistry*. UPB Buletin Stiintific, Series B: Chemistry and Materials Science, 2012. **74**(1): p. 183-192.
222. Zhao, Y.; Zhang, W.; Chen, H.; Luo, Q. M.; Li, S. Y., *Direct electrochemistry of horseradish peroxidase at carbon nanotube powder microelectrodes*. Sensors Actuators B: Chemical, 2002. **87**(1): p. 168-172.

References

223. Wang, Z.; Liu, S.; Wu, P.; Cai, C., *Detection of glucose based on direct electron transfer reaction of glucose oxidase immobilized on highly ordered polyaniline nanotubes*. Analytical Chemistry, 2009. **81**(4): p. 1638-1645.
224. Joo, J.; Song, H. G.; Chung, Y. C.; Baeck, J. S.; Jeong, S. K.; Suh, J. S.; Oh, E. J., *The effects of dopant and solvent on charge transport of doped polyanilines*. Journal-Korean Physical Society, 1997. **30**: p. 230-236.
225. Polk, Brian J; Potje-Kamloth, Karin; Josowicz, Mira; Janata, Jiri, *Role of protonic and charge transfer doping in solid-state polyaniline*. The Journal of Physical Chemistry B, 2002. **106, 44**: p. 11457-11462.
226. Sinha, S.; Bhadra, S.; Khastgir, D., *Effect of dopant type on the properties of polyaniline*. Journal of Applied Polymer Science, 2009. **112**(5): p. 3135-3140.
227. Hamilton, P. J.; Pollet, B. G., *Effect of dopant type on the properties of polyaniline*. Journal of Applied Polymer Science, 2009. **112** (5): p. 3135-3140.
228. Catedral, MD; Tapia, AKG; Sarmago, RV; Tamayo, JP; del Rosario, EJ, *Effect of Dopant Ions on the Electrical Conductivity and Microstructure of Polyaniline (Emeraldine Salt)*. Science Diliman, 2007. **16**(2): p. 41-46.
229. Chen, Y. H.; Wu, J. Y.; Chung, Y. C., *Preparation of polyaniline modified electrodes containing sulfonated polyelectrolytes using layer-by-layer techniques*. Biosensor and Bioelectronics, 2006. **22**(4): p. 489-494.
230. Kaplan, E. H., *Sensuous Seas: Tales of a Marine Biologist*. 2006: Princeton University Press.
231. Johnson, Jim, *Tetrodotoxin*, T.F.S. University, Editor. 2002: Tallahassee, Florida, USA.

References

232. Ulmeanu, S.; Lee, H. J.; Fermin, D. J.; Girault, H. H.; Shao, Y., *Voltammetry at a liquid-liquid interface supported on a metallic electrode*. *Electrochemistry communications*, 2001. **3**(5): p. 219-223.
233. Zhang, J.; Harris, A. R.; Cattrall, R. W.; Bond, A. M., *Voltammetric ion-selective electrodes for the selective determination of cations and anions*. *Analytical chemistry*, 2010. **82**(5): p. 1624-1633.
234. Vázquez, M.; Danielsson, P.; Bobacka, J.; Lewenstam, A.; Ivaska, A., *Solution-cast films of poly (3, 4-ethylenedioxythiophene) as ion-to-electron transducers in all-solid-state ion-selective electrodes*. *Sensors Actuators B: Chemical*, 2004. **97**(2): p. 182-189.
235. Gupta, V. K.; Goyal, R. N.; Agarwal, S.; Kumar, P.; Bachheti, N., *Nickel (II)-selective sensor based on dibenzo-18-crown-6 in PVC matrix*. *Talanta*, 2007. **71**(2): p. 795-800.
236. Hayvalı, M.; Hayvalı, Z., *The Synthesis of Some New Mono and bis (Crown Ether)s and Their Sodium Complexes. Tautomerism in o-Hydroxybenzo-15-crown-5 Schiff Bases as Studied by UV-VIS Spectrophotometry*. *Synthesis and Reactivity in Inorganic and Metal-Organic Chemistry*, 2004. **34**(4): p. 713-732.
237. Kim, S. D.; Lee, H. W., *Fluorometric Quantitative Analysis of Al (III) Ion Using 5-Methoxy-2-phenyliminomethylphenol*. *Bulletin of the Korean Chemical Society*, 2009. **30**(5): p. 1027.
238. Asakawa, M.; Shida, Y.; Miyazawa, K.; Noguchi, T., *Instrumental Analysis of Tetrodotoxin* 2012: InTech. 245 - 270.
239. Katritzky, A, *Physical methods in heterocyclic chemistry*. Vol. 3. 2012: Elsevier.

References

240. Kaminow, I.; Li, T.; Willner, A. E., *Optical Fiber Telecommunications Volume VIA: Components and Subsystems*. 2013: Academic press.
241. Tauc, J; Grigorovici, R; Vancu, A, *Optical properties and electronic structure of amorphous germanium*. *physica status solidi (b)*, 1966. **15**(2): p. 627-637.
242. Xing, S. G.; Tingyu, Y. F.; Chen W. M.; Juan, P., *Screening and Structure Analysis of the Aptamer Against Tetrodotoxin*. *Journal of Chinese Institute of Food Science and Technology*, 2012. **2**(032): p. 347-351.
243. Yuan, G. L.; Kuramoto, N.; Su, S. J., *Template synthesis of polyaniline in the presence of phosphomannan*. *Synthetic metals*, 2002. **129**(2): p. 173-178.
244. Saxena, V.; Malhotra, B. D., *Prospects of conducting polymers in molecular electronics*. *Current Applied Physics*, 2003. **3**(2): p. 293-305.
245. Cho, M. S.; Park, S. Y.; Hwang, J. Y.; Choi, H. J., *Synthesis and electrical properties of polymer composites with polyaniline nanoparticles*. *Materials Science and Engineering: C*, 2004. **24**(1): p. 15-18.
246. Bai, J., Guo, L., Ndamanisha, J. C., Qi, B., *Electrochemical properties and simultaneous determination of dihydroxybenzene isomers at ordered mesoporous carbon-modified electrode*. *Journal of Applied Electrochemistry*, 2009. **39**, **12**: p. 2497-2503.
247. Bai, J.; Guo, L.; Ndamanisha, J. C.; Qi, B., *Electrochemical properties and simultaneous determination of dihydroxybenzene isomers at ordered mesoporous carbon-modified electrode*. *Journal of Applied Electrochemistry*, 2009. **39**(12): p. 2497-2503.
248. Nilsson, A.; Pettersson, L. M.; Norskov, J., *Chemical bonding at surfaces and interfaces*. First edition ed. 2011: Elsevier.

References

249. Ndangili, P. M.; Olowu, R. A.; Mailu, S. N.; Ngece, R. F.; Jijana, A.; Williams, A.; Iftikhar, F.; Baker, P. G.; Iwuoha, E. I., *Impedimetric Response of a Label-Free Genosensor Prepared on a 3-Mercaptopropionic Acid Capped Gallium Selenide Nanocrystal Modified Gold Electrode*. International Journal of Electrochemical Science, 2011. **6**: p. 1438-1453.
250. Klink, M. J.; Iwuoha, E. I.; Ebenso, E. E., *Electrochemical Properties of Nanotubes and Nanomicelles from Novel Polyaniline and Derivative*. International Journal of Electrochemical Science, 2012. **7**: p. 3031-3046.
251. Njomo, N.; Waryo, T.; Masikini, M.; Ikpo, C. O.; Mailu, S.; Tovide, O.; Ross, N.; Williams, A.; Matinise, N.; Sunday, C. E., *Graphenated tantalum (IV) oxide and poly (4-styrene sulphonic acid)-doped polyaniline nanocomposite as cathode material in an electrochemical capacitor*. Electrochimica Acta, 2014. **128**: p. 226-237.
252. Luo, H.; Shi, Z.; Li, N.; Gu, Z.; Zhuang, Q., *Investigation of the electrochemical and electrocatalytic behavior of single-wall carbon nanotube film on a glassy carbon electrode*. Analytical Chemistry, 2001. **73**(5): p. 915-920.
253. Girija, T. C.; Sangaranarayanan, M. V., *Analysis of polyaniline-based nickel electrodes for electrochemical supercapacitors*. Journal of Power Sources, 2006. **156**(2): p. 705-711.
254. Umeda, M.; Dokko, K.; Fujita, Y.; Mohamedi, M.; Uchida, I.; Selman, J. R., *Electrochemical impedance study of Li-ion insertion into mesocarbon microbead single particle electrode: Part I. Graphitized carbon*. Electrochimica Acta, 2001. **47**(6): p. 885-890.

References

255. Meyers, J. P.; Doyle, M.; Darling, R. M.; Newman, J., *The impedance response of a porous electrode composed of intercalation particles*. Journal of The Electroanalytical Society, 2000. **147**(8): p. 2930-2940.
256. Komura, T.; Yamaguchi, T.; Shimatani, H.; Okushio, R., *Interfacial charge-transfer resistance at ionizable thiol monolayer-modified gold electrodes as studied by impedance spectroscopy*. Electrochimica Acta, 2004. **49**(4): p. 597-606.
257. Lupu, S., *Electrochemical impedance measurements on prussian blue films deposited on platinum electrode*. UPB Scientific Bulletin, Series B: Chemistry and Materials Science, 2011. **73**(1): p. 85-96.
258. Qakala, S., *Towards rapide electrochemical test system of polyaniline-laccase-on-gold enzyme nanobiosensor for water estrogens*, in Chemistry. 2013, University of the Western Cape: Cape Town.
259. Nateghi M. R., Zahedi M., Mosslemin M. H., Hachemian S., Behzad S., Minnai A., *Autoacceleration/degradation of Electrochemical Polymerisation of Substituted Polyanilines*. Polymer, 2005. **46**: p. 11476-11483.
260. Komsiyiska L., Tsacheva Ts., Tsakova V., *Electrochemical formation and Copper Modification of Poly-o-methoxyaniline*. Thin Solid Films, 2005. **493**: p. 88-95.
261. Gopalakrishnan, K.; Elango, M.; Thamilselvan, M., *Optical studies on nano-structured conducting polyaniline prepared by chemical oxidation method*. Archives of Physical Medicine and Rehabilitation, 2012. **3**(4): p. 315-319.
262. Yan, J.; Zhang, Y.; Kim, P.; Pinczuk, A., *Electric field effect tuning of electron-phonon coupling in graphene*. Physical review letters, 2007. **98**(16): p. 29-32.

References

263. Neetika, G.; Kumar, D.; Tomar, S. K., *Thermal Behaviour of Chemically Synthesized Polyanilines/Polystyrene Sulphonic Acid Composites*. International Journal of Materials and Chemistry, 2012. **2**(2): p. 79-85.
264. Lin, D. S., *Measurement of the electrochemical response time and electron paramagnetic resonance behavior of poly (o-phenetidine)–poly (styrene sulfonic acid) and poly (2-ethyl-aniline)–poly (styrene sulfonic acid) complexes*. Journal of Applied Polymer Science, 2005. **96**(4): p. 1211-1221.
265. Mavundla, S. E.; Malgas, G. F.; Baker, P.; Iwuoha, E., *Synthesis and Characterization of Novel Nanophase Hexagonal Poly (2, 5-dimethoxyaniline)*. Electroanalysis, 2008. **20**(21): p. 2347-2353.
266. Guimard, N. K.; Gomez, N.; Schmidt, C. E., *Conducting polymers in biomedical engineering*. Progress in Polymer Science, 2007. **32**(8): p. 876-921.
267. Prabhakar, N.; Matharu, Z.; Malhotra, B. D., *Polyaniline Langmuir–Blodgett film based aptasensor for ochratoxin A detection*. Biosensors and Bioelectronics, 2011. **26**(10): p. 4006-4011.
268. Prabhakar, N.; Arora, K.; Singh, H.; Malhotra, B. D., *Polyaniline based nucleic acid sensor*. The Journal of Physical Chemistry B, 2008. **112**(15): p. 4808-4816.
269. Katz, E.; Willner, I., *Probing Biomolecular Interactions at Conductive and Semiconductive Surfaces by Impedance Spectroscopy: Routes to Impedimetric Immunosensors, DNA-Sensors, and Enzyme Biosensors*. . Electroanalysis, 2003. **15**(11): p. 913-947.
270. Ladbury, J. E.; Klebe, G.; Freire, E., *Adding calorimetric data to decision making in lead discovery: a hot tip*. Nature Reviews Drug Discovery, 2009. **9**(1): p. 23-27.

References

271. Taylor, A.D.; Ladd, J.; Etheridge, S.; Deeds, J.; Hall, S.; Jiang, S., *Quantitative detection of tetrodotoxin (TTX) by a surface plasmon resonance (SPR) sensor*. *Sensors and Actuators B: Chemical*, 2008. **130**(1): p. 120-128.
272. Matsui, T.; Ohtsuka, Y.; Sakai, J., *Recent advance of studies on fugu toxin*. *Yakugaku Zasshi*, 2000. **10**: p. 825–837.



ANNEX

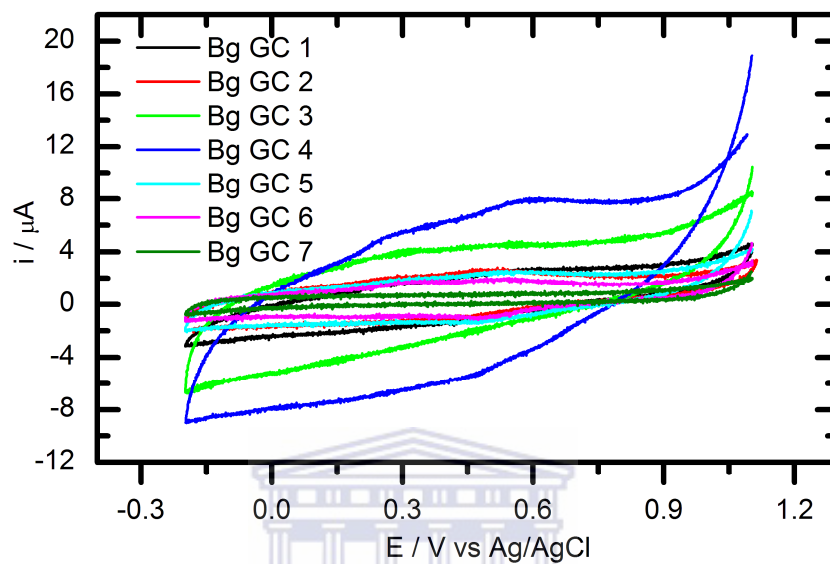


Figure A1: Background CVs of seven different glassy carbon electrodes used to optimise the glutaraldehyde and aptamer concentration.

Annex

Table A1: Data for characteristic peaks of PANI-PSSA/GC obtained when optimising the glutaraldehyde concentration

Modified electrode	E_{pa1} (V)	E_{pa2} (V)	E_{pc1} (V)	E_{pc2} (V)	ΔE_{p1} (V)	ΔE_{p2} (V)	$E^{o}1$ (V)	$E^{o}2$ (V)	i_{pa} (μ A)	i_{pa2} (μ A)	i_{pc1} (μ A)	i_{pc2} (μ A)	i_{pa1}/i_{pc1}	i_{pa2}/i_{pc2}
GC1	-0.003	0.261	-0.128	0.202	0.125	0.059	-0.066	0.232	14.59	24.46	-14.56	-21.93	-1.00	-1.12
GC2	0.008	0.272	-0.106	0.180	0.114	0.092	-0.049	0.226	14.94	26.05	-15.88	-23.92	-0.94	-1.09
GC3	-0.003	0.272	-0.128	0.202	0.125	0.070	-0.060	0.237	16.35	26.08	-15.24	-24.72	-1.07	-1.06
GC4	-0.003	0.272	-0.117	0.202	0.114	0.070	-0.060	0.237	15.92	24.81	-17.05	-23.82	-0.93	-1.04
GC5	-0.003	0.261	-0.117	0.202	0.114	0.059	-0.060	0.237	13.16	22.31	-13.19	-22.27	-0.99	-1.00
GC6	-0.014	0.261	-0.128	0.202	0.114	0.059	-0.071	0.232	15.36	24.73	-14.55	-23.00	-1.06	-1.07
GC7	-0.003	0.261	-0.117	0.202	0.114	0.059	-0.060	0.232	11.87	20.53	-11.32	-19.05	1.05	-1.07

Annex

Table A2: Data for characteristic peaks of Glu/PANI–PSSA/GC obtained when optimising the glutaraldehyde concentration

Modified electrode [Glu] mM	E_{pa1} (V)	E_{pa2} (V)	E_{pc1} (V)	E_{pc2} (V)	ΔE_{p1} (V)	ΔE_{p2} (V)	E^{01} (V)	E^{02} (V)	i_{pa} (μ A)	i_{pa2} (μ A)	i_{pc1} (μ A)	i_{pc2} (μ A)	i_{pa1}/i_{pc1}	i_{pa2}/i_{pc2}
0.00	-0.003	0.261	-0.106	0.191	0.103	0.07	-0.055	0.226	14.64	24.94	-14.83	-24.86	-0.98	-1.00
0.02	0.019	0.283	-0.084	0.224	0.125	0.059	-0.033	0.254	14.00	24.56	-14.68	-55.94	-0.95	-0.44
0.05	0.008	0.294	-0.106	0.235	0.114	0.059	-0.049	0.265	16.02	25.35	-15.6	-61.93	-1.03	-0.41
0.2	0.008	0.261	-0.106	0.246	0.114	0.015	-0.049	0.254	16.51	25.11	-17.46	-57.5	-0.95	-0.44
0.5	0.019	0.283	-0.106	0.235	0.125	0.048	-0.044	0.259	12.27	19.98	-12.13	-57.07	-1.01	-0.35
0.10	0.019	0.294	-0.106	0.235	0.125	0.059	-0.044	0.265	14.16	22.93	-13.89	-66.1	-1.02	-0.35
0.20	0.008	0.283	-0.106	0.246	0.114	0.037	-0.049	0.265	11.16	18.86	-10.81	-55.57	-1.03	-0.34

Annex

Table A3: Data for characteristic peaks of Apt/Glu/PANI–PSSA/GC obtained when optimising the glutaraldehyde concentration

Modified electrode	E_{pa1} (V)	E_{pa2} (V)	E_{pc1} (V)	E_{pc2} (V)	ΔE_{p1} (V)	ΔE_{p2} (V)	$E^{o}1$ (V)	$E^{o}2$ (V)	i_{pa} (μ A)	i_{pa2} (μ A)	i_{pc1} (μ A)	i_{pc2} (μ A)	i_{pa1}/i_{pc1}	i_{pa2}/i_{pc2}
GC1	0.019	0.261	-0.095	0.235	0.114	0.026	-0.038	0.048	15.27	25.38	-15.49	-54.16	-0.98	-0.47-
GC2	0.030	0.261	-0.073	0.180	0.103	0.081	-0.022	0.221	14.36	23.94	-15.5	-55.5	-0.93	0.43
GC3	0.019	0.272	-0.095	0.202	0.114	0.059	-0.038	0.237	15.73	24.58	-15.32	-59.79	-1.03	-0.41
GC4	0.019	0.261	-0.095	0.235	0.114	0.026	-0.038	0.248	16.58	25.1	-17.28	-52.08	-0.96	-0.48
GC5	0.019	0.261	-0.084	0.202	0.103	0.059	-0.033	0.237	12.31	19.57	-12.39	-61.86	-0.99	-0.32
GC6	0.019	0.272	-0.084	0.202	0.103	0.070	-0.033	0.237	14.2	22.37	-13.93	-68.79	-1.02	-0.33
GC7	0.030	0.261	-0.084	0.213	0.114	0.048	-0.027	0.237	11.05	18.35	-10.77	-53.55	-1.03	-0.34

Annex

Table A4: Data for characteristic peaks of TTX/Apt/Glu/PANI-PSSA/GC obtained when optimising the glutaraldehyde concentration

Modified electrode	E_{pa1} (V)	E_{pa2} (V)	E_{pc1} (V)	E_{pc2} (V)	ΔE_{p1} (V)	ΔE_{p2} (V)	E^{01} (V)	E^{02} (V)	i_{pa} (μ A)	i_{pa2} (μ A)	i_{pc1} (μ A)	i_{pc2} (μ A)	i_{pa1}/i_{pc1}	i_{pa2}/i_{pc2}
GC1	0.030	0.261	-0.084	0.213	0.114	0.048	-0.027	0.237	14.97	24.1	-15.22	-50.34	-0.98	-0.49
GC2	0.041	0.261	-0.062	0.180	0.103	0.081	-0.021	0.221	14.32	20.04	-15.09	-51.11	-0.95	-0.39
GC3	0.030	0.261	-0.084	0.191	0.114	0.070	-0.027	0.226	15.51	23.73	-14.97	-55.39	-1.04	-0.43
GC4	0.030	0.261	-0.084	0.224	0.114	0.037	-0.027	0.243	16.41	24.46	-17.03	-52.31	-0.96	-0.47
GC5	0.030	0.261	-0.084	0.191	0.114	0.070	-0.027	0.226	12.19	18.87	-12.00	-52.52	-1.02	-0.36
GC6	0.030	0.261	-0.084	0.191	0.114	0.070	-0.027	0.226	14.06	21.69	-13.61	-59.22	-1.03	-0.37
GC7	0.030	0.261	-0.084	0.202	0.114	0.059	-0.027	0.232	10.79	17.72	-10.55	-49.37	-1.02	-0.36

Annex

Table A5: Data for characteristic peaks of PANI–PSSA/GC obtained when optimising the aptamer concentration

Modified electrode	E_{pa1} (V)	E_{pa2} (V)	E_{pc1} (V)	E_{pc2} (V)	ΔE_{p1} (V)	ΔE_{p2} (V)	E^{01} (V)	E^{02} (V)	i_{pa} (μ A)	i_{pa2} (μ A)	i_{pc1} (μ A)	i_{pc2} (μ A)	i_{pa1}/i_{pc1}	i_{pa2}/i_{pc2}
GC1	0.052	0.284	-0.109	0.172	0.161	0.112	-0.038	0.342	82.55	103.1	-75.10	-142.0	-1.09	-0.73
GC2	0.008	0.284	-0.111	0.166	0.119	0.118	-0.050	0.152	60.53	76.24	-49.62	-115.9	-1.21	-0.66
GC3	0.041	0.382	-0.172	0.202	0.213	0.180	-0.066	0.292	95.33	120.5	-90.66	-170.6	-1.05	-0.71
GC4	0.041	0.393	-0.183	0.202	0.224	0.191	-0.071	0.298	93.67	117.5	-86.20	-173.6	-1.08	-0.68
GC5	0.019	0.371	-0.161	0.246	0.180	0.125	-0.071	0.309	82.51	100.4	-73.91	-152.1	-1.12	-0.73
GC6	0.019	0.349	-0.161	0.224	0.180	0.125	-0.071	0.287	81.04	95.31	-69.62	-146.8	-1.16	-0.65
GC7	0.019	0.349	-0.161	0.246	0.180	0.103	-0.071	0.298	80.68	97.61	-72.00	-152.0	-1.12	-0.64

Annex

Table A6: Data for characteristic peaks of Glu/PANI–PSSA/GC obtained when optimising the aptamer concentration

Modified electrode	E_{pa1} (V)	E_{pa2} (V)	E_{pc1} (V)	E_{pc2} (V)	ΔE_{p1} (V)	ΔE_{p2} (V)	$E^{0}1$ (V)	$E^{0}2$ (V)	i_{pa} (μ A)	i_{pa2} (μ A)	i_{pc1} (μ A)	i_{pc2} (μ A)	i_{pa1}/i_{pc1}	i_{pa2}/i_{pc2}
GC1	0.030	0.360	-0.150	0.191	0.180	0.169	-0.060	0.276	82.15	105.9	-75.48	-168.8	-1.09	-0.62
GC2	0.129	0.305	-0.029	0.059	0.158	0.246	0.050	0.182	89.68	71.01	-85.64	-165.9	-1.05	-0.43
GC3	0.041	0.382	-0.161	0.180	0.202	0.202	-0.060	0.281	97.14	122.2	-90.47	-90.40	-1.07	-1.35
GC4	0.052	0.382	-0.150	0.158	0.202	0.224	-0.049	0.270	94.18	116.6	-86.49	-175.0	-1.09	-0.66
GC5	0.030	0.360	-0.139	0.213	0.169	0.147	-0.055	0.287	82.02	101.7	-73.45	-145.9	-1.12	-0.69
GC6	0.030	0.349	-0.139	0.169	0.169	0.180	-0.055	0.259	79.84	91.97	-67.47	-148.4	-1.18	-0.62
GC7	0.030	0.349	-0.128	0.180	0.158	0.169	-0.049	0.265	77.78	96.00	-68.97	-154.2	-1.12	-0.62

Annex

Table A7: Data for characteristic peaks of Apt/Glu/PANI–PSSA/GC obtained when optimising the aptamer concentration

[Aptamer] /μM	E_{pa1} (V)	E_{pa2} (V)	E_{pc1} (V)	E_{pc2} (V)	ΔE_{p1} (V)	ΔE_{p2} (V)	$E^{o}1$ (V)	$E^{o}2$ (V)	i_{pa} (μA)	i_{pa2} (μA)	i_{pc1} (μA)	i_{pc2} (μA)	i_{pa1}/i_{pc1}	i_{pa2}/i_{pc2}
0.5	0.041	0.338	-0.128	0.169	0.169	0.169	-0.044	0.254	84.26	104.3	-76.74	-149.0	-11.09	-0.7
0.2	0.151	0.294	-0.040	0.037	0.191	0.257	-0.056	0.166	86.08	66.9	-82.05	-84.68	-1.05	-0.79
0.1	0.041	0.360	-0.139	0.136	0.180	0.224	-0.049	0.248	98.82	120.7	-94.09	-166.2	-1.05	0.73
0.05	0.063	0.360	-0.139	0.125	0.202	0.235	-0.038	0.243	95.84	113.9	-87.85	-160.8	-1.09	-0.71
0.02	0.041	0.338	-0.117	0.158	0.158	0.180	-0.038	0.248	84.16	99.8	-74.56	-145.0	-1.13	-0.69
0.01	0.041	0.327	-0.128	0.125	0.169	0.202	-0.044	0.226	82.05	88.63	-66.55	-142.6	-1.23	-0.62
0μ	0.030	0.327	-0.117	0.147	0.147	0.180	-0.044	0.237	79.6	92.04	-68.38	-142.1	-1.16	-0.74

Annex

Table A8: Data for characteristic peaks of TTX/Apt/Glu/PANI-PSSA/GC obtained when optimising the aptamer concentration

Electrode	E_{pa1}	E_{pa2}	E_{pc1}	E_{pc2}	ΔE_{p1}	ΔE_{p2}	E^{01}	E^{02}	i_{pa}	i_{pa2}	i_{pc1}	i_{pc2}	i_{pa1}/i_{pc1}	i_{pa2}/i_{pc2}
after TTX	(V)	(V)	(V)	(V)	(V)	(V)	(V)	(V)	(μ A)	(μ A)	(μ A)	(μ A)		
GC1	0.041	0.327	-0.117	0.125	0.158	0.202	-0.038	0.226	86.09	101.8	-80.2	-147.7	-1.07	-0.69
GC2	0.162	0.328	-0.062	0.004	0.224	0.324	-0.050	0.166	82.51	59.76	-79.3	-81.37	-1.04	-0.73
GC3	0.052	0.349	-0.139	0.103	0.191	0.246	-0.044	0.226	100.4	118.4	-99.71	-157.7	-1.00	-0.75
GC4	0.063	0.349	-0.139	0.092	0.202	0.257	-0.038	0.221	97.46	110.8	-89.47	-154.9	-1.08	0.72
GC5	0.041	0.327	-0.128	0.125	0.166	0.202	-0.044	0.226	85.71	97.28	-75.4	-142.5	-1.13	-0.68
GC6	0.052	0.316	-0.117	0.114	0.169	0.202	-0.033	0.215	82.7	85.78	-66.37	-139.3	-1.25	-0.62
GC7	0.041	0.305	-0.117	0.114	0.158	0.191	-0.038	0.210	80.55	88.47	-68.46	-137.5	-1.29	-0.64



UNIVERSITY *of the*
WESTERN CAPE